



2013-06-17

# Comparison of Performance-Based Liquefaction Initiation Analyses Between Multiple Probabilistic Liquefaction Models Using the Standard Penetration Test

Alexander David Wright  
*Brigham Young University - Provo*

Follow this and additional works at: <https://scholarsarchive.byu.edu/etd>

 Part of the [Civil and Environmental Engineering Commons](#)

---

## BYU ScholarsArchive Citation

Wright, Alexander David, "Comparison of Performance-Based Liquefaction Initiation Analyses Between Multiple Probabilistic Liquefaction Models Using the Standard Penetration Test" (2013). *All Theses and Dissertations*. 3710.  
<https://scholarsarchive.byu.edu/etd/3710>

This Thesis is brought to you for free and open access by BYU ScholarsArchive. It has been accepted for inclusion in All Theses and Dissertations by an authorized administrator of BYU ScholarsArchive. For more information, please contact [scholarsarchive@byu.edu](mailto:scholarsarchive@byu.edu), [ellen\\_amatangelo@byu.edu](mailto:ellen_amatangelo@byu.edu).

Comparison of Performance-Based Liquefaction Initiation Analyses  
Between Multiple Probabilistic Liquefaction Models  
Using the Standard Penetration Test

Alexander D. Wright

A thesis submitted to the faculty of  
Brigham Young University  
in partial fulfillment of the requirements for the degree of  
Master of Science

Kevin W. Franke, Chair  
Kyle M. Rollins  
Norman L. Jones

Department of Civil and Environmental Engineering  
Brigham Young University

June 2013

Copyright © 2013 Alexander D. Wright

All Rights Reserved

## ABSTRACT

### Comparison of Performance-Based Liquefaction Initiation Analyses Between Multiple Probabilistic Liquefaction Models Using the Standard Penetration Test

Alexander D. Wright  
Department of Civil and Environmental Engineering, BYU  
Master of Science

This study examines the use of performance-based approaches in liquefaction hazard analysis. Two new methods of performance-based liquefaction initiation analysis are proposed which use the works of Juang et al. (2012) and Boulanger and Idriss (2012). Further advances are made by incorporating the performance-based magnitude scaling factors as proposed by Cetin et al. (2012). Using these new equations a comparative study is made between the three methods. Further comparisons are made between the performance-based approaches and the more widely used deterministic approaches. The comparisons reveal that on average for the 11 sites used in this study, the performance-based approaches tend to be slightly less conservative than deterministic approaches overall, with large differences possible for some locations in the country. They also reveal that the newer performance-based approaches are generally less conservative than the approach proposed by Kramer and Mayfield (2007). Some cases where this relationship does not hold true and the new relationships are more conservative are outlined.

Keywords: Alexander D. Wright, Kevin W. Franke, probabilistic, performance-based, liquefaction, standard penetration test, SPT, factor of safety, induced stress, initiation, triggering, earthquake, seismic, hazard, magnitude scaling factor, probability, fragility curve, deterministic

## ACKNOWLEDGMENTS

This thesis was only made possible by the efforts of a group, and I would have been unable to finish it alone; as such I wish to offer specific thanks to a few people, without whom I would not have finished. I would like to especially thank Dr. Kevin W. Franke for the time and effort taken to help a young student to understand a complex topic. His help over the course of this project was invaluable; indeed he spent countless hours working to help teach me what I needed to know to finish this project. I would like to also thank Dr. Kyle M. Rollins for his inspired assistance to a young engineer in helping him to become passionate about the field of geotechnical engineering, and teaching him the joy that comes from research. I would like to thank Dr. Norman L. Jones whose help and comments on programming helped to make the program better than I could have done alone. I would also like to recognize Aaron Marsh and Brian Franke for constructive comments on programming and other topics.

In addition to those mentioned above, the work of Cody Hatch was essential in the completion of this research. His assistance with the auto download feature in PB LiquefY made this research much quicker and facilitated other research in which he was involved.

Finally, I would be ungrateful if I did not mention my wife. Her patience as I worked on this research was very great, and without her support I would not have been able to finish. She further assisted with the design of the program logo and editing of the grammar and punctuation of the body of the thesis. On top of all this, her support helped keep the project on track and moving forward. Katherine, thank you.

## TABLE OF CONTENTS

<b>LIST OF TABLES</b> .....	<b>xi</b>
<b>LIST OF FIGURES</b> .....	<b>xiv</b>
<b>1 Introduction</b> .....	<b>1</b>
<b>2 Review of Liquefaction</b> .....	<b>3</b>
2.1 Susceptibility .....	4
2.1.1 Historical Criteria.....	4
2.1.2 Geologic Criteria.....	5
2.1.3 Compositional Criteria.....	6
2.1.4 State Criteria .....	8
2.2 Initiation.....	11
2.2.1 Causes .....	11
2.2.2 Flow Liquefaction.....	12
2.2.3 Cyclic Mobility .....	16
2.3 Effects .....	18
2.3.1 Settlement .....	18
2.3.2 Lateral Spread .....	20
2.3.3 Flow Failure .....	22
2.3.4 Loss of Bearing Capacity .....	24
2.3.5 Other Effects .....	25
<b>3 Characterization of Seismic Loading</b> .....	<b>28</b>
3.1 Earthquakes.....	28
3.2 Modifying Effects .....	29
3.2.1 Near Source, Basin, and Topographic Effects .....	29

3.2.2	Site Amplification.....	31
3.3	Seismic Hazard Analysis .....	33
3.3.1	Deterministic Seismic Hazard Analysis.....	34
3.3.2	Probabilistic Seismic Hazard Analysis .....	34
3.4	Seismic Hazard Curves.....	41
<b>4</b>	<b>Assessment of Liquefaction Initiation Potential.....</b>	<b>43</b>
4.1	Laboratory Testing.....	43
4.2	Numerical Modeling and Simulation.....	45
4.3	Empirical Deterministic Methods.....	46
4.3.1	Seed and Idriss Simplified Procedure.....	47
4.3.2	NCEER Procedure .....	49
4.3.3	Cetin and Seed et al. Procedure .....	56
4.3.4	Idriss and Boulanger Procedure .....	61
4.4	Empirical Probabilistic Methods .....	68
4.4.1	Early Procedures .....	68
4.4.2	Cetin and Seed et al. Procedure .....	70
4.4.3	Boulanger and Idriss Procedure .....	71
4.4.4	Juang and Ching et al. Procedure.....	72
<b>5</b>	<b>Performance-Based Earthquake Engineering .....</b>	<b>74</b>
5.1	PEER Performance-Based Framework.....	74
5.1.1	Framework Parameters .....	76
5.1.2	Hazard and Fragility Curves .....	77
5.2	Performance-Based Liquefaction Initiation.....	78
5.2.1	Cetin et al. Performance-Based Procedure .....	79
5.2.2	Incorporation of Boulanger and Idriss Probabilistic Model.....	82

5.2.3	Incorporation of Juang et al. Modal .....	86
5.2.4	Incorporation of Performance-Based Magnitude Scaling Factors .....	87
<b>6</b>	<b>Comparative Analysis Evaluation Set Up.....</b>	<b>91</b>
6.1	PB LiquefY .....	91
6.2	Site Locations .....	94
6.3	Soil Profiles.....	97
<b>7</b>	<b>Performance-Based Analysis and Results .....</b>	<b>101</b>
7.1	Statistical Analysis of Performance-Based Data .....	103
7.2	SPT Blow Count Variation .....	105
7.3	Shear Wave Velocity Variation .....	107
7.3.1	Shear Wave Velocity Epistemic Uncertainty and its Effects.....	112
7.4	Fines Content Variation .....	123
7.5	Depth Variation.....	129
7.5.1	K Sigma Limit.....	134
7.6	Return Period Variation .....	137
7.7	Parameter Uncertainty Error Term .....	140
7.8	Applying Performance-Based Magnitude Scaling Factors.....	142
7.9	Factor of Safety Prediction Differences.....	144
7.10	Summary of Performance-Based Results .....	146
<b>8</b>	<b>Comparison of Conventional and Performance-Based Results.....</b>	<b>148</b>
8.1	SPT Blow Count and Shear Wave Velocity .....	149
8.2	Depth and Return Period.....	151
8.3	Direct Comparison of Methods.....	152
8.4	Statistical Comparison of Conventional and Performance-Based Procedures .....	156
8.5	Summary of Comparison of Conventional and Performance-Based Procedures .....	158

<b>9</b>	<b>Conclusions.....</b>	<b>159</b>
	<b>References.....</b>	<b>164</b>
	<b>Appendix A.....</b>	<b>171</b>
	A.1 Detailed Discussion –Development of Constant Error Terms.....	171
	A.2 Detailed Discussion – Standard Deviation for Andrus and Stokoe .....	173
	A.3 Detailed Discussion – Sensitivity Analysis of Cetin et al.....	178
	A.4 Detailed Discussion – Performance-Based Magnitude Scaling Factors.....	183
	A.5 Detailed Discussion – Liquefaction Initiation Current State of the Practice and State of the Art.....	184
	A.6 Detailed Discussion – Comparison between Deterministic Methods, Past Research ...	190
	<b>Appendix B.....</b>	<b>192</b>
	B.1 Analysis Details - Soil Profiles .....	192
	B.1 Analysis Details – Sample Output .....	211
	<b>Appendix C.....</b>	<b>220</b>
	C.1 PBliquefY – Overview.....	220
	C.1.1 Basic Analysis.....	221
	C.1.1.1 Opening the Program .....	221
	C.1.1.2 Step 1: Soil Profile Details Page .....	223
	C.1.1.3 Step 2: Loading Data Input Page.....	229
	C.1.1.4 Step 3a: Analysis Options Page; Deterministic.....	235
	C.1.1.5 Step 4a: Viewing Deterministic Results.....	237
	C.1.1.6 Step 3b: Analysis Options Page; Performance-Based.....	240
	C.1.1.7 Step 4b: Viewing Performance-Based Analysis .....	241
	C.1.2 Using Applied Loadings and $K_{\alpha}$ .....	248
	C.1.2.1 User Defined Load Case .....	248
	C.1.2.2 Uniform Load Case .....	252



C.1.2.3 Embankment Load Case.....	253
C.1.2.4 Detailed Discussion – Applied Loadings and $K_{\alpha}$ .....	255
C.1.2.5 Detailed Discussion – Multiple Analysis Run .....	257
C.1.3 Using Amplification Factors .....	261
C.1.4 Using Other Loading File Types.....	263
C.1.5 Using Performance-Based and Deterministic Advanced Options .....	265
C.1.6 Using Graphs.....	271
C.1.7 Analysis Options for Factor of Safety and $(N_1)_{60cs}$ Required .....	273
C.1.7.1 Analysis by Return Period.....	273
C.1.7.2 Analysis by Sub Layer .....	275
C.1.8 Analysis Options for Ground Improvement.....	280
C.1.9 Using and Understanding the Performance-Based Summary Page .....	284
C.1.10 PBliquefY – Theory, Assumptions, and Code .....	286
C.1.11 PBliquefY – Soils Profile Input Page.....	287
C.1.12 PBliquefY – Loading Data Input Page.....	288
C.1.13 PBliquefY – Liquefaction Analysis Options Page.....	290
C.1.14 PBliquefY – $FS_{liq}$ and $N_{req}$ Analysis Options Page.....	291

## LIST OF TABLES

Table 2-1: Youd, Hansen et al. (2002) lateral spread coefficients.....	21
Table 4-1: Correction factors (Youd, Idriss et al. 2001).....	51
Table 4-2: Model parameters (Cetin 2002).....	59
Table 5-1: Boulanger and Idriss total standard deviation with and without parameter estimation error included.....	85
Table 5-2: Juang and Ching et al. (2012) model parameters with and without parameter estimation error included for use in probability equation shown. ....	86
Table 5-3: Comparison of MSF to magnitude specific MSF (PB MSF) after Cetin and Bilge (2012).....	90
Table 6-1: Site locations used in study. ....	95
Table 6-2: Mean magnitude and acceleration from PSHA corresponding to $T_R=2475$ years. (Bold values – High, Italicized – Medium, Underlined - Low).....	97
Table 6-3: Assumed properties of soil profile. ....	98
Table 6-4: Soil profiles used in study. ....	98
Table 7-1: Tables of quantile values (Top) and means for one way analysis of variance (bottom). ....	104
Table 7-2: Range of values in sensitivity analysis.....	117
Table 7-3: Results of analysis of liquefaction triggering using a $FS=1.2$ .....	145
Table 7-4: Summary of effects of variables on value of $\Delta N_{req}$ . ....	146
Table 8-1: Soil profile used in site specific liquefaction analyses.....	155
Table 0-1: Values found using Monte Carlo simulation.....	177
Table 0-2: Statistical results of regression of standard deviation. ....	178
Table 0-3: Range of input parameters used sensitivity analysis. ....	179
Table 0-4: Sample of data used in sensitivity analysis of Cetin et al. (2004) method. ....	181

Table 0-5: Soil properties used in comparative analyses (input from PB LiquefY).....	187
Table 0-6: Performance-based.....	189
Table 0-7: Scenario based.....	189
Table 0-8: Mean pseudo probabilistic.....	189
Table 0-9: Modal pseudo probabilistic.....	189
Table 0-1: List of abbreviations.....	192
Table 0-2: Soil profiles 1 and 2.....	193
Table 0-3: Soil profiles 3 and 4.....	194
Table 0-4: Soil profiles 5 and 6.....	195
Table 0-5: Soil profiles 7 and 8.....	196
Table 0-6: Soil profiles 9 and 10.....	197
Table 0-7: Soil profiles 11 and 12.....	198
Table 0-8: Soil profiles 13 and 14.....	199
Table 0-9: Soil profiles 15 and 16.....	200
Table 0-10: Soil profiles 17 and 18.....	201
Table 0-11: Soil profiles 19 and 20.....	202
Table 0-12: Soil profiles 21 and 22.....	203
Table 0-13: Soil profiles 23 and 24.....	204
Table 0-14: Soil profiles 25 and 26.....	205
Table 0-15: Soil profiles 27 and 28.....	206
Table 0-16: Soil profiles 29 and 30.....	207
Table 0-17: Soil profiles 31 and 32.....	208
Table 0-18: Soil profiles 33 and 34.....	209
Table 0-19: Soil profiles 35 and 36.....	210
Table 0-1: Site soil profile details for a single soil column.....	224

Table 0-2: Probability of exceedance for 8 deaggregation files to be uploaded.....	233
Table 0-3: Approximate values for Q. ....	251
Table 0-4: Values for a and b table after Stewart, Liu et al. (2003). ....	262
Table 0-5: Default values for Boulanger and Idriss (2012) $\sigma_{tot}$ equation. ....	270
Table 0-6: Typical values of $C_d$ from Idriss and Boulanger (2008). ....	288

## LIST OF FIGURES

Figure 2-1: Bray and Sancio Criteria represented graphically in comparison to data from other studies. (Bray and Sancio 2006).....	7
Figure 2-2: Atterberg limit chart showing representative values for each soil that exhibited clay - like, sand - like or intermediate behavior (Boulanger and Idriss 2006).....	8
Figure 2-3: Behavior of soil given a set of starting conditions plotted against a) arithmetic effective stress scale and b) logarithmic effective stress scale (Kramer 1996).....	9
Figure 2-4: Liquefaction susceptibility of soil with dilative and contractive tendencies (Kramer 1996).....	10
Figure 2-5: Flow failure paths; bottom path C represents flow liquefaction.....	14
Figure 2-6: Plot of soils experiencing flow liquefaction in $p' - q$ space (above) and starting point of soil with respect to the SSL. (Kramer 1996).....	16
Figure 2-7: Cyclic mobility before (a) and after (b).....	17
Figure 2-8: Differential settlement in Iran 1990 after NOAA/NGDC - M. Mehrain, Dames and Moore.....	20
Figure 2-9: Plot showing normalized strength vs. $N_{160cs}$ (Idriss and Boulanger 2008).....	23
Figure 2-10: Flow failure at lower San Fernando Dam 1971 after NOAA/NGDC - E.V. Leyendecker, U.S. Geological Survey.....	24
Figure 2-11: Bearing capacity failure after NOAA/NGDC - NOAA National Geophysical Data Center.....	25
Figure 2-12: Sand boil in El Centro, CA 1979 after NOAA/NGDC – University of Colorado at Boulder.....	26
Figure 2-13: Retaining wall failure due to liquefaction after <a href="http://mceer.buffalo.edu/publications/bulletin/07/21-03/images/05embankmentlg.jpg">http://mceer.buffalo.edu/publications/bulletin/07/21-03/images/05embankmentlg.jpg</a> .....	27
Figure 3-1: Pulse from Lander 1992 earthquake (top). No pulse from Landers 1992 earthquake (not in direction of fault rupture) (bottom).....	30

Figure 3-2: Spatial uncertainty bin techniques for a) a source of known location and b) a source whose location is somewhat unknown or which covers a wider area. ....	35
Figure 3-3: NGA results created using NGA equations worksheet created by Linda Al Atik 2009. ....	39
Figure 3-4: Deaggregation for Seattle site for 1039 year return period. ....	40
Figure 4-1: Stress curves used to evaluate liquefaction potential for given factor of safety after Seed and Idriss (1971). ....	45
Figure 4-2: CSR ( $\tau/\sigma'$ ) vs. $N_{160}$ for sand from (Seed, Tokimatsu et al. 1985). ....	49
Figure 4-3: CRR curves for fines content of 35, 15, and 5 % (Youd, Idriss et al. 2001). ....	52
Figure 4-4: Comparison of depth reduction factors (Youd, Idriss et al. 2001). ....	53
Figure 4-5: Range of magnitude scaling factors (MSF). ....	55
Figure 4-6: range of values for $K_\sigma$ using the NCEER equation (Youd, Idriss et al. 2001). ....	56
Figure 4-7: Comparison of Seed and Idriss 1971 (solid black lines) to Cetin and Seed et al. 2004 (grey lines) after Cetin, Seed et al. (2004). ....	58
Figure 4-8: $CSR_{eq}^*$ vs. $N_{160}$ according to Cetin, Seed et al. (2004). ....	60
Figure 4-9: $C_N$ for Idriss and Boulanger compared to Liao and Whitman (Idriss and Boulanger 2010). ....	62
Figure 4-10: Comparison of $r_d$ Idriss and Boulanger to average $r_d$ from Seed and Idriss 1971 (Idriss and Boulanger 2010). ....	64
Figure 4-11: CRR curve for Idriss and Boulanger (Idriss and Boulanger 2010). ....	65
Figure 4-12: MSF comparison of Idriss relationship to other relationships. (Idriss and Boulanger 2010). ....	66
Figure 4-13: Idriss and Boulanger $K_\sigma$ relationship (Idriss and Boulanger 2010). ....	67
Figure 5-1: Fragility curves for liquefaction initiation ( $M_w = 6.5$ ; $a_{max} = 0.15$ g). ....	77
Figure 5-2: Hazard curve FS vs. mean annual rate of nonexceedance. ....	78
Figure 5-3: Process of developing hazard curves for liquefaction initiation. ....	81
Figure 5-4: Boulanger and Idriss (2012) total standard deviation curve. ....	83

Figure 5-5: Typical performance-based hazard curve developed using Boulanger and Idriss equations with and without $N=30$ cap. ....	84
Figure 5-6: Fragility curves with and without cap ( $M_w = 6.5$ ; $a_{max} = 0.15$ ). ....	85
Figure 6-1: PB LiquefY program organization. ....	93
Figure 6-2: Performance-based procedure loop. ....	94
Figure 6-3: Location of 11 sites (red) used in study in relation to USGS quaternary fault database (light blue). ....	96
Figure 7-1: Distribution of input data (counts) within study. ....	102
Figure 7-2: Density plot of $\Delta N_{req}$ values. ....	103
Figure 7-3: Box plot showing distribution of $\Delta N_{req}$ for three methods. ....	104
Figure 7-4: Average $\Delta N_{req}$ for 11 sites using soil profiles 1-24 and all $T_R$ 's. ....	105
Figure 7-5: Average variation in $\Delta N_{req}$ by site. ....	107
Figure 7-6: Shear wave velocity ( $V_{s12}$ ) vs. average $\Delta N_{req}$ ....	109
Figure 7-7: Shear wave velocity ( $V_{s12}$ ) vs. average $\Delta N_{req}$ with fines content. ....	110
Figure 7-8: Shear wave velocity vs. $\Delta N_{req}$ by location. ....	110
Figure 7-9: Shear wave velocity data points. ....	111
Figure 7-10: Comparison with varying shear wave velocity by return period. ....	112
Figure 7-11: Epistemic uncertainty in $V_{s12}$ and its overall effect on $\Delta N_{req}$ . ....	115
Figure 7-12: Variations in $\Delta N_{req}$ by return period. ....	116
Figure 7-13: Plot of probability of liquefaction by acceleration. ....	119
Figure 7-14: Plot of probability of liquefaction by magnitude and SPT blow count. ....	119
Figure 7-15: Probability of liquefaction by depth. ....	121
Figure 7-16: Probability of liquefaction by fines content. ....	121
Figure 7-17: Probability of liquefaction by average shear wave velocity ( $V_{s12}$ ). ....	122
Figure 7-18: Comparison of effect of SPT resistance and $V_{s12}$ on Probability of liquefaction. ....	122

Figure 7-19: Comparison of effect of shear wave velocity and SPT blow count. ....	123
Figure 7-20: Graph showing changes in fines content and the effects. ....	124
Figure 7-21: Effects of fines content by location. ....	125
Figure 7-22: Comparison of effects of fines content by location and uncorrected SPT blow count. (Blue N=5, Red N=15, Green N=25, Purple N=35). ....	126
Figure 7-23: Differences in $\Delta N_{req}$ with fines content, return period and N value. (Blue N=5, Red N=15, Green N=25, Purple N=35). ....	127
Figure 7-24: Fines content by depth and its effect on $\Delta N_{req}$ . ....	127
Figure 7-25: Comparison of fines content correction at FC = 10 (left) and FC = 30 (right). ....	128
Figure 7-26: Difference between new methods and Cetin et al method. ....	129
Figure 7-27: $\Delta N_{req}$ vs. depth at N=25 and RP = 2475. ....	130
Figure 7-28: Comparison by depth and location (Blue N=5, Red N=15, Green N=25, Purple N=35). ....	131
Figure 7-29: Changes in $\Delta N_{req}$ by depth and $T_R$ . ....	132
Figure 7-30: Comparison of Cetin and Seed and Boulanger and Idriss depth reduction factors. ....	133
Figure 7-31: $K_\sigma$ limit effect (red without limit, blue with limit). ....	134
Figure 7-32: Effect of $K_\sigma$ limit with varying return periods. (Red without limit, Blue with limit). ....	135
Figure 7-33: Effect of the $K_\sigma$ limit by return period and uncorrected SPT blow count. (Red without limit, Blue with limit). ....	136
Figure 7-34: Return Period vs. Mean $\Delta N_{req}$ . ....	137
Figure 7-35: Return Period vs. Mean $\Delta N_{req}$ . ....	138
Figure 7-36: Effect of return period on $\Delta N_{req}$ by location (Blue N=5, Red N=15, Green N=25, Purple N=35). ....	139
Figure 7-37: Hazard curve developed for N=15 excluding parameter uncertainty for a soil layer at a depth of 8 meters located at latitude 40.671 North longitude 111.791 West. ....	139



Figure 7-38: Comparison of three methods for fines content of 0 and various ways of accounting for parameter error.....	141
Figure 7-39: Variation caused by uncertainty term in equations. (Blue N=5, Red N=15, Green N=25, Purple N=35).....	142
Figure 7-40: Effect of performance-based magnitude scaling factors San Francisco. ....	143
Figure 7-41: Effect of performance-based magnitude scaling factors Butte. ....	144
Figure 7-42: MSF <sub>PB</sub> using $r_u$ definition after Cetin and Bilge (2012). ....	144
Figure 8-1: Comparison of approaches by SPT blow count. ....	150
Figure 8-2: Comparison of approaches by $V_{s12}$ . ....	150
Figure 8-3: Comparison of conventional and performance-based procedures by depth. ....	151
Figure 8-4: Comparison of procedures by return period. ....	152
Figure 8-5: Comparison of Cetin et al. conventional and performance-based approaches. ....	153
Figure 8-6: Comparison of Boulanger and Idriss (performance-based) and Idriss and Boulanger (conventional). ....	154
Figure 8-7 Two site specific analyses for 475 year return period comparing conventional and performance-based analyses. ....	155
Figure 8-8: Comparison of Conventional and Performance-Based Results. ....	157
Figure 0-1: Normal distribution for $(N_1)_{60\text{mean}} = 5$ using 5,000 points. ....	174
Figure 0-2: Normal distribution of shear wave velocity using 5,000 data points. ....	175
Figure 0-3: Standard deviation in shear wave velocity due to parameter uncertainty. ....	177
Figure 0-4: Data and regression line for standard deviation of shear wave velocity. ....	178
Figure 0-5: Summary of sensitivity analysis results. ....	182
Figure 0-6: m values plot after Cetin and Bilge (2012). ....	184
Figure 0-7: Bi modal event for site located in Cincinnati. ....	187
Figure 0-8: Comparison of pseudo probabilistic, scenario based, and performance-based analyses for Cincinnati site with $T_R = 2475$ years and uniform SPT of 10 blows/ft. ....	188

Figure 0-1: Title page and flow chart. ....	222
Figure 0-2: Soil profile details page.....	223
Figure 0-3: Soil profile information entered on Soil Info Page.....	225
Figure 0-4: Applied loading section. ....	226
Figure 0-5: Soil profile details table and figure. ....	227
Figure 0-6: Stresses calculated using PB LiquefY. ....	228
Figure 0-7: Loading data page. ....	230
Figure 0-8: USGS interactive deaggregations website. ....	231
Figure 0-9: Deaggregation produced using the USGS 2008 interactive deaggregation website. ....	232
Figure 0-10: Uploading file for 50% in 75 years.....	233
Figure 0-11: Loading data page after data and graphs are generated. ....	234
Figure 0-12: Liquefaction analysis options page. ....	236
Figure 0-13: Specify return period user form. ....	236
Figure 0-14: Deterministic $M_w$ and $a_{max}$ .....	237
Figure 0-15: Deterministic Summary Page.....	238
Figure 0-16: Deterministic graphs a) by sample depth b) by layer depth.....	239
Figure 0-17: Performance-Based Analysis Options. ....	240
Figure 0-18: $FS_{liq}$ and $N_{req}$ Analysis Options Page.....	241
Figure 0-19: $FS_{liq}$ and $N_{req}$ graphs developed from performance-based analysis.....	242
Figure 0-20: Hazard curves developed using PB LiquefY. ....	243
Figure 0-21: Deaggregation charts developed using PB LiquefY.....	244
Figure 0-22: Ground improvement analysis options page.....	245
Figure 0-23: Ground improvement for tutorial. ....	246
Figure 0-24: Performance-based summary page. ....	247
Figure 0-25: Applied loads and fills section. ....	248

Figure 0-26: User defined controls. ....	249
Figure 0-27: $K_{\alpha}$ options. ....	250
Figure 0-28: $K_o$ options box.....	251
Figure 0-29: User input portion of table. ....	252
Figure 0-30: Uniform load controls. ....	252
Figure 0-31: Loading after application of uniform load. ....	253
Figure 0-32: Embankment loading options.....	255
Figure 0-33: Flow chart for calculations in the presence of an embankment. ....	256
Figure 0-34: Input text file creator page. ....	257
Figure 0-35: Multiple run options for use in multi analysis. ....	258
Figure 0-36: Selection of auto run analysis type. ....	259
Figure 0-37: Loading data page, soil amplification factor section. ....	261
Figure 0-38: Amplification factor menu. ....	261
Figure 0-39: Deaggregation data file uploading section a) buttons for uploading data (left of image) and b) file type selector drop box (right of image).....	263
Figure 0-40: File creator page.....	264
Figure 0-41: Deterministic and performance-based analysis options page. ....	266
Figure 0-42: Number of runs box. ....	268
Figure 0-43: Example hazard curve with variables for calculating n. ....	268
Figure 0-44: Advanced Boulanger and Idriss (2012) error options input box.....	270
Figure 0-45: Normal curve from Wikipedia. ....	271
Figure 0-46: Deterministic graph controls.....	272
Figure 0-47: Graphing and analysis options by return period. ....	273
Figure 0-48: $FS_{liq}$ vs. depth at a return period of 475 years (left); $N_{req}$ vs. Depth graph (right).....	275
Figure 0-49: Analysis by sub layer. ....	276

Figure 0-50: Hazard curve for $(N_1)_{60cs}$ required. ....	277
Figure 0-51: Hazard curve for factor of safety. ....	278
Figure 0-52: Deaggregation plots for Cetin et al (2004) and Boulanger and Idriss (2012). ....	279
Figure 0-53: Ground improvement analysis page.....	281
Figure 0-54: Ground improvement vs. depth in terms of $\Delta(N_1)_{60cs}$ . ....	282
Figure 0-55: Performance-based summary page. ....	285
Figure 0-56: Summary data table.....	286
Figure 0-57: Bin A intersects the line in one place as the line is of a normal form; Bin B intersects the line in three locations as the hazard curve is not of a normal form. ....	289

## **1 INTRODUCTION**

Liquefaction and its prediction are of vital importance in the field of civil engineering. Predicting the likelihood of seismic-related hazards such as liquefaction and their associated damage will help to save lives, reduce losses, and improve the standard of living for people throughout the world. In order to understand and predict hazards, it is important to understand what causes them and under what conditions they will exist. Predicting the occurrence of liquefaction has been difficult, in large measure due to our lack of understanding of the phenomenon. Recent advances in our understanding of what causes liquefaction to occur and in the amount of data available to researchers has led to the development of new and improved empirical models for predicting liquefaction and its probability of occurrence (Cetin, Seed et al. 2004; Boulanger and Idriss 2012; Juang, Ching et al. 2012).

Another recent development in engineering is the use of performance-based approaches to analysis and design. The Pacific Earthquake Engineering Research (PEER) center has developed and advanced performance-based earthquake engineering (PBEE). Performance-based approaches are advantageous over the more traditional deterministic approaches to engineering because they allow the engineer to account for uncertainty in a systematic and compartmentalized way. When coupled with the deterministic approaches they can provide a good maximum limit and risk analysis tool. Risk and hazard can be assessed in a systematic

way, which allows engineers to understand in a more comprehensive manner the results of the analysis they are performing.

This thesis will develop two new performance-based liquefaction initiation models using the framework developed by Kramer and Mayfield (2007). The new models will incorporate the Juang, Ching et al. (2012) probabilistic model and the Boulanger and Idriss (2012) probabilistic model. These two models will then be compared with the existing model proposed by Kramer and Mayfield (2007) which uses the Cetin, Seed et al. (2004) probabilistic model and the differences between the models will be identified and examined. A brief comparison of the deterministic procedures commonly used in practice to the performance-based approaches will also be made.

The comparison of the different models will reveal how and where they differ. Such knowledge will enable engineers to better understand the limitations and uses of each of the different models and will help advance the field of performance-based design in the area of liquefaction initiation. The equations and evaluation tools developed in the course of this study will allow engineers to more fully and completely analyze liquefaction initiation and will give future researchers in earthquake engineering a platform from which to develop further research into the area of performance-based engineering, specifically with respect to liquefaction and its effects.

## 2 REVIEW OF LIQUEFACTION

Liquefaction has posed a serious risk to infrastructure throughout time. It was not until recently that this earthquake phenomenon was recognized and began to be studied. The extensive liquefaction which occurred during the 1964 Portage, Alaska and 1964 Niigata, Japan earthquakes helped the engineering community recognize the problems and hazards liquefaction posed. These earthquakes and others have shown the need to predict the occurrence of liquefaction and to mitigate its effects.

Liquefaction has been difficult to define due to the confusion regarding what should and should not be classified as liquefaction. Lateral spreads, settlements, flow failures, and other events are all the result of liquefaction. Most agree that liquefaction occurs when there is a dramatic decrease in the soil strength. Liquefaction was defined in the simplified method to be “a phenomenon in which a cohesionless soil loses strength during an earthquake and acquires a degree of mobility sufficient to permit movements ranging from several feet to several thousand feet” (Seed and Idriss 1971). More recently, the National Center for Earthquake Engineering Research (NCEER) in their report published by Youd, Idriss et al. (2001) stated that, “liquefaction is defined as the transformation of a granular material from a solid to a liquefied state as a consequence of increased pore-water pressure and reduced effective stress.”

To understand the hazards posed by liquefaction as defined above, the liquefaction hazard must be analyzed. Liquefaction analysis is important because it enables the engineer to mitigate hazards and design to the existing conditions at the site. Liquefaction analysis can be divided into three distinct parts: susceptibility, initiation, and effects (Kramer 1996).

## **2.1 Susceptibility**

A soil is considered susceptible if it is able to liquefy. Some soils will not liquefy under almost any circumstances and others cannot liquefy due to the conditions and environment in which they are found. To understand which soils are susceptible to liquefaction and which soils are not, it is constructive to examine some of the criteria that affect liquefaction. These criteria include historical, geological, compositional, and state criteria (Kramer 1996).

### **2.1.1 Historical Criteria**

Historical criteria are defined by whether liquefaction has occurred in the past or not. Examining the effects of past earthquakes on a site shows what sorts of effects we can expect in the future. A site that shows evidence of past liquefaction is more likely to liquefy again. Evidence can include sand boils, lateral spread, and other liquefaction effects. Historical records are used to determine if liquefaction has occurred at a site in the recorded past. A site with no historical evidence of liquefaction cannot, however, be safely ruled out as being unable to liquefy (Kramer 1996). Sites might experience different seismic conditions in the future and liquefy in a previously safe area. Historical criteria can be of assistance in showing whether liquefaction is possible, but should not be used in isolation to determine the susceptibility of a site or soil type.



### **2.1.2 Geologic Criteria**

The underlying existing geologic conditions can have a very large impact on a sites susceptibility to liquefaction. Geologic age and depositional environment have been shown to play a large role in whether a soil profile is susceptible (Youd and Hoose 1977).

Geologic age has been shown to decrease liquefaction susceptibility. The older soils, such as soils from the Pleistocene epoch or soils that are pre-Pleistocene in age are much less susceptible to liquefaction. In general the older a deposit is, the greater its resistance to liquefaction. The depositional environment of a deposit also plays a role. Depositional environments such as deltaic or fluvial environments will often be more susceptible. Poorly compacted fill is also considered to be more susceptible (Youd and Hoose 1977).

The location of the groundwater table can affect a soils capacity to liquefy. If a soil is above the water table and unsaturated, current practice considers it to be unsusceptible to liquefaction because it is considered impossible for the necessary pore water pressure to build up if little or no pore water is present (Kramer 1996). Recent research has proposed that unsaturated soil may liquefy (Unno, Kazama et al. 2008) when the air and water are unable to drain away during cyclic loading. When this occurs both are placed under increased pressure causing the soils to reach a zero effective stress in spite of being in an unsaturated state. This increased pressure is caused in part by a change in volume which occurs in the soil as it is subjected to cyclic loading. This phenomenon has been proposed as a mechanism that would allow soils that are unsaturated, and typically thought of as not susceptible, to liquefy.

### 2.1.3 Compositional Criteria

The composition of a soil profile can play a major role in determining if a site is susceptible to liquefaction. Sites that have a high percentage of fines are much less likely to liquefy than areas that are composed of sands or gravels. Most researchers agree that sands are susceptible to liquefaction when saturated. An area of ongoing research is whether fine grained soils can liquefy. Recent advances in this area have shown that there are certain types of fine grained soils which can undergo liquefaction. These fine grained soils have been shown to react with sand like behavior and liquefy if the soil meets certain bounding criteria (Boulanger and Idriss 2006; Bray and Sancio 2006). These bounding criteria are discussed below.

The Chinese Criteria has been used for years by geotechnical professionals to determine the susceptibility of fine grained soils. The Chinese criteria as reported by Kramer is defined as (Kramer 1996):

$$\text{Fraction finer than } 0.005 \text{ mm} \leq 15\%$$

$$\text{Liquid Limit (LL)} < 35\%$$

$$\text{Natural water content (} w_c \text{)} \geq 0.9\text{LL}$$

$$\text{Liquidity Index (LI)} \leq 0.75$$

However, the Chinese Criteria has come to be viewed as obsolete (Bray and Sancio 2006), and newer criteria have been developed. Bray and Sancio in their paper on liquefaction susceptibility (Bray and Sancio 2006) state that a soil may be liquefiable if:

$$\text{Plastic Index (PI)} < 12$$

$$\text{Water content (} w_c \text{)} / \text{LL} > 0.85$$

This is consistent with the data they examined and is a good measure of the susceptibility of fine grained soils (Figure 2-1).

Boulanger and Idriss (2006) also studied the phenomena of liquefaction susceptibility. They state that a soil will exhibit clay like behavior if the PI is greater than or equal to 7 and may exhibit clay like behavior in soil with a PI as low as 5 if the soil is a CL-ML. Soils with a PI less than these may exhibit sand like behavior, and thus may liquefy. The transition zone between clay like and sand like behavior ranges from a PI of 5 to a PI of 7 and is slightly nonlinear. The range of the transition zone as outlined by Boulanger and Idriss is shown in Figure 2-2. These two liquefaction susceptibility criteria differ slightly in the details and are essentially reporting the same thing; soils that behave as sands are susceptible to liquefaction and soils that behave as clays are not.

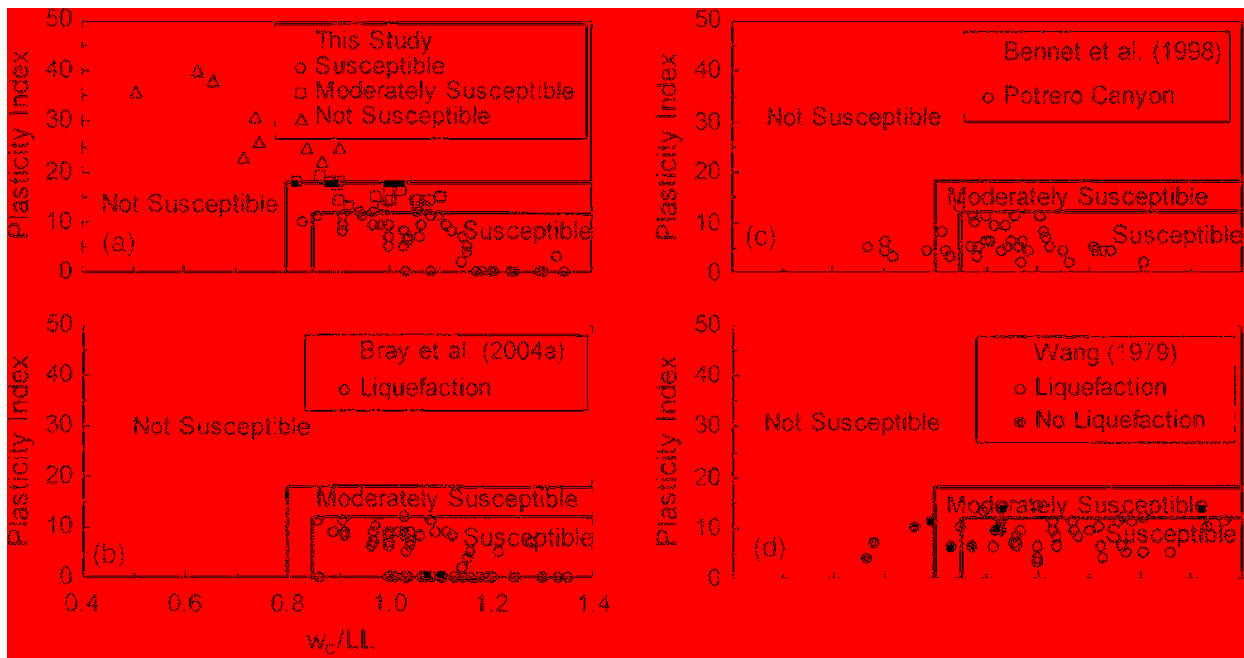


**Figure 2-1: Bray and Sancio Criteria represented graphically in comparison to data from other studies. (Bray and Sancio 2006).**

Although reporting similar results, it is important in doing a liquefaction analysis to determine which set of criteria the author(s) of a particular method used. The criteria for liquefaction susceptibility will affect the outcome of the results and if a different set of

susceptibility criteria are used inconsistent answers may be computed. The assumptions about susceptibility made by the author(s) of a particular method should be followed in order to be consistent with the author(s) intent and the relationships they have developed.

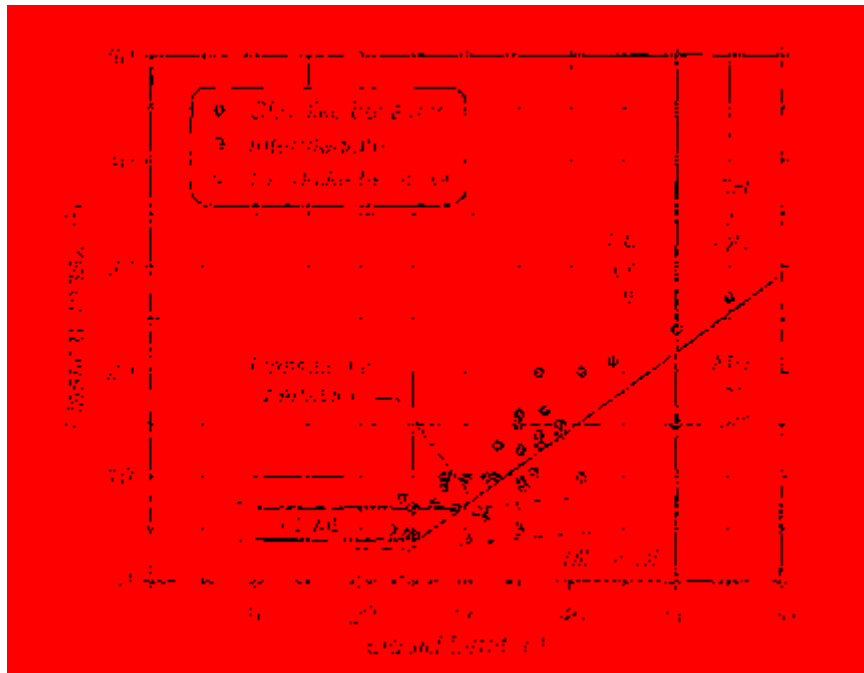


**Figure 2-2: Atterberg limit chart showing representative values for each soil that exhibited clay - like, sand - like or intermediate behavior (Boulanger and Idriss 2006).**

#### 2.1.4 State Criteria

State criteria are so named because they look at the liquefaction susceptibility with respect to the current state of the soil. The current state can be determined by examining the current effective stress and void ratio (or density) of the soil. Casagrande was the first to examine how these state criteria affected soil and postulated that there was a critical void ratio (CVR) to which all drained soils converged (Figure 2-3). This CVR line defines the boundary between contractive and dilative soils (Casagrande 1936).

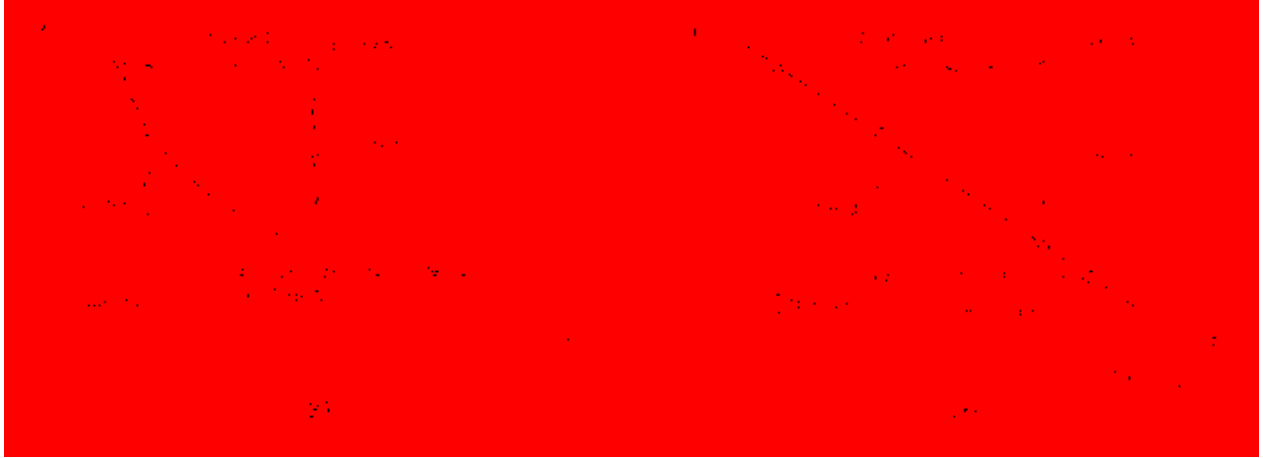


**Figure 2-3: Behavior of soil given a set of starting conditions plotted against a) arithmetic effective stress scale and b) logarithmic effective stress scale (Kramer 1996).**

Casagrande was later shown to be partially incorrect when Fort Peck Dam suffered a failure due to liquefaction. He had limited data for drained conditions and had not accounted for what came to be known as a flow structure. Casagrande’s student, Castro, examined these phenomena in detail using undrained tests (Castro 1969) and accounted for the formation of a flow structure (Figure 2-4). His results showed that a line called the steady state line (SSL) existed, which was almost parallel to but slightly lower than the CVR line. This new line represented the true boundary between contractive and dilative soil under undrained conditions, and as such is a good indication of whether a soil can liquefy. In turn, this is a good indication of whether a soil is susceptible to flow liquefaction or not (Kramer 1996). Seed and Idriss recognized flow liquefaction and cyclic mobility as different types of liquefaction as early as 1971.

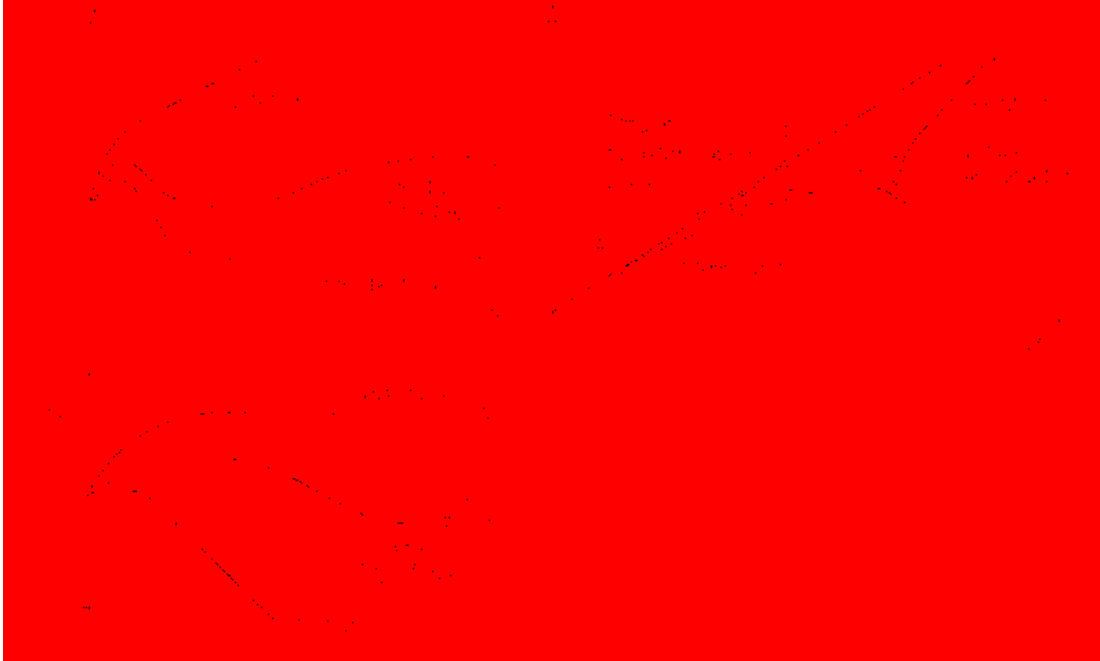


**Figure 2-4: Liquefaction susceptibility of soil with dilative and contractive tendencies (Kramer 1996).**

Been and Jeffries (1985) used this idea to develop a state parameter, so called because it is based on the steady state line. This state parameter could be used to determine if a soil was susceptible to flow liquefaction or not. The state parameter is in effect a measure of the distance in void ratio space to the SSL line. This parameter can be used to quantify this distance between the soils current state and the SSL. The equation for the state parameter is shown below.

$$\Psi = e - e_{ss} \quad (1)$$

In this equation  $e$  is the void ratio at a given effective confining pressure,  $e_{ss}$  is the void ratio that corresponds to the steady state line at that confining pressure, and  $\Psi$  is the state parameter (Been and Jeffries 1985). If the state parameter is positive the soil exhibits contractive behavior; if it is negative the soil exhibits dilative behavior. This helps identify soils susceptible to liquefaction as contractive soils are generally susceptible to flow liquefaction and dilative soils are not.

## 2.2 Initiation

Liquefaction initiation occurs when a soil is susceptible and the right conditions occur. Many different models have been proposed to evaluate liquefaction initiation, which is sometimes called liquefaction triggering. In order to understand how these models work, it is important to understand under what conditions liquefaction is likely to occur and to characterize how this will happen.

Simply because a soil has been shown to be able to liquefy (it is susceptible) does not mean that it will. Some soils are only liquefiable under very high accelerations or very long durations of shaking. A soil profile's susceptibility does not show its liquefaction hazard; it simply states whether it is possible for a soil to liquefy or not. In order to assess liquefaction hazard, both the possibility and probability of liquefaction under a given set of circumstances must be assessed.

Understanding both the soils susceptibility to liquefaction and whether liquefaction will initiate/trigger are important and even critical issues. The way a soil will react to different loading conditions and how a soil will respond when it liquefies will vary from soil to soil. The causes of liquefaction initiation are much better understood today and two different types of liquefaction are now recognized: flow liquefaction, and cyclic mobility.

### 2.2.1 Causes

In general liquefaction triggers when the pore water pressure builds up and equals the effective confining stress; however, different definitions of that point exist. In a review of the existing literature, Cetin and Bilge (2012) showed that a range of definitions exist for the triggering of liquefaction with respect to the pore pressure ratio ( $r_u$ ) and the cyclic strain ( $\gamma$ ). They showed that in the existing literature, definitions range from 0.8 to 1.0 for the pore pressure

ratio and from 3% to 20% for the cyclic strain. They further state that a partial reason for this variation of definitions is due to the fact that the onset of liquefaction varies from soil type to soil type, with soils that are more contractive liquefying at smaller shear strains.

As liquefaction initiates, the strength of a soil will decrease. In basic terms, this can be seen by examining the general behavior of a saturated soil. A soil can be dilative or contractive when subject to shear stresses. A contractive soil, as stated above, can develop increased pore pressure which leads to a decrease in the overall strength of the soil. A dilative soil can develop negative pore pressures, which lead to an overall increase in the strength of the soil; thus, a dilative soil will not typically liquefy. In a contractive soil, once the pore pressure equals the effective confining stress of the soil, initial liquefaction will occur.

Although Casagrande and Castro helped the engineering community to understand more details about liquefaction, the susceptibility criteria do not give enough details about whether a soil will liquefy. Vaid and Chern (1985) observed that the work of Castro and his student Casagrande did not adequately consider the stress conditions associated with the onset of liquefaction (i.e. loading). An understanding of the conditions that cause liquefaction to initiate is as important as understanding if it is susceptible. The initiation of flow liquefaction and cyclic mobility will be discussed in greater detail in the sections that follow.

### **2.2.2 Flow Liquefaction**

Flow liquefaction is a phenomenon which occurs as a result of an earthquake. Flow liquefaction occurs when the residual shear strength of the liquefied soil is not sufficient to resist the static shear stresses existing in the soil due to gravity. This type of liquefaction can be highly dangerous and can cause the failure of dams, slopes, and other similar geologic or engineered structures.



Flow liquefaction was one of the first types of liquefaction recognized. Seed and Idriss (1971) said that, “When the term [liquefaction] was originally introduced it was intended to describe a phenomenon in which a soil could undergo large movements, as in flow slides...”. This type of liquefaction known as flow liquefaction occurs when pore pressures build up during an earthquake. As pore water pressures increase, they can cause a soil to reach some residual strength that is much less than the maximum soil strength. Due to this loss of strength, a cascade effect may occur where a portion of a slope’s shear strength is exceeded by the shear stresses caused by the slope. Once a small section reaches this point it will fail and other areas of the slope experience higher stress, which in turn can cause them to fail. This can lead to catastrophic failures as failure surfaces propagate through the slope. It is important to note that these types of flow failures are not unique to flow liquefaction, but can occur any time the soil undergoes a loss of shear strength.

To illustrate, Figure 2-5 shows a soil under seismic and monotonic loading. Both eventually cause the soils strength to drop and approach the residual strength of the soil. This occurs as the strain increases and eventually the stress on the soil exceeds the maximum allowable stress the soil can sustain. However, this does not occur for all points in the soil at once, rather a single point passes the peak and drops to some residual strength, which can cause the next point to feel increased stress and also exceed its maximum capacity. As a result failure occurs.

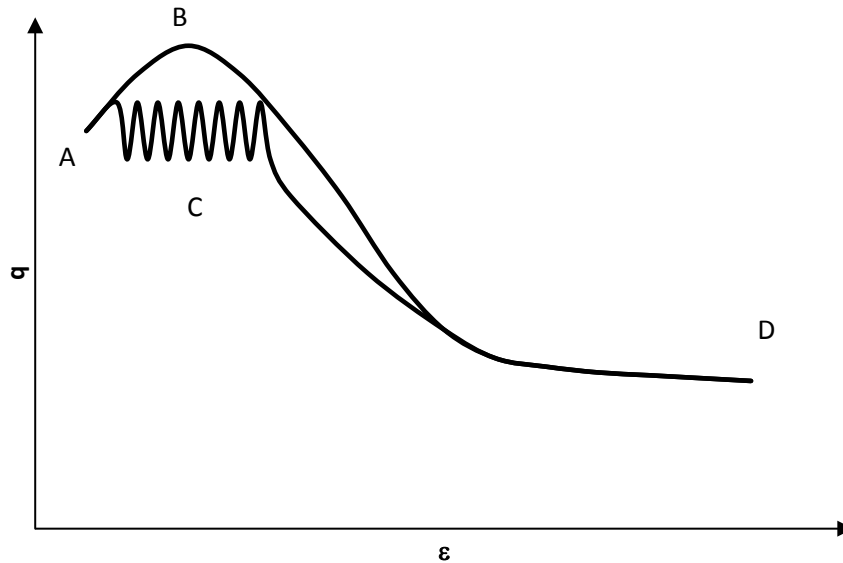


**Figure 2-5: Flow failure paths; bottom path C represents flow liquefaction.**

Figure 2-5 shows that to get from A to D, there are two paths. Seismic loading causes a path that runs through C as repeated cyclic loading increases the strain, while another scenario without cyclic loading is shown passing through B. Both scenarios lead to catastrophic failure of the slope.

Flow liquefaction is a phenomenon that occurs only under certain initial stress and state conditions. The starting conditions must be such that the pore water pressures can increase as the soil shears. This means that the soil must contract as it is sheared. In a static state the boundary between dilative and contractive soils is the critical void ratio (CVR) line. This line represents the static boundary between contractive and dilative soils at small strains. However, in a steady state of deformation, such as exists under very large strains, a steady state line (SSL) is reached whose boundary is slightly below the CVR line (Kramer 1996).

Vaid and Chern (1985) studied these concepts of liquefaction using pluviated laboratory samples. Their work led them to introduce the idea of the flow liquefaction surface (FLS). The FLS is a line in  $q - p'$  space that helps differentiate between regions of flow liquefaction and cyclic mobility. Vaid and Chern refer to this line as the CSR line but to avoid confusion this paper will not follow similar notation but will instead refer to it as the FLS.

The SSL and the FLS are both explanations of a piece of the process that leads to flow liquefaction. To illustrate the concepts of the SSL and the FLS a series of imaginary soils is presented as seen in Figure 2-6. In this figure, soils A and B are to the left of the SSL and will be unable to experience flow liquefaction as they are dilative. Soils C, D, and E are to the right of the SSL, and are thus contractive and can undergo flow liquefaction. The point at which flow liquefaction can be considered to trigger (and where the soil's shear strength drops off dramatically) is shown by the dashed line representing the FLS. Soils A and B are unable to reach this surface and will never undergo flow liquefaction (although they can experience cyclic mobility) while soils C, D, and E are able to reach the FLS and can undergo flow liquefaction.

When a soil reaches the FLS then flow liquefaction triggers and the soil quickly drops to the steady state point causing flow liquefaction to occur. As the soil drops to the steady state point the soil loses strength, eventually falling to its residual strength. The soil's strength, being reduced to this residual value, will be unable to support the slope or embankment which will cause the slope to fail. This can cause large motions that we associate with flow failures to occur. Often these failures take the form of landslides and other large soil movements. It should be noted that liquefaction failures can occur even after the earthquake is concluded depending on the soil structure and geologic setting of the site (Malvick, Kutter et al. 2006).

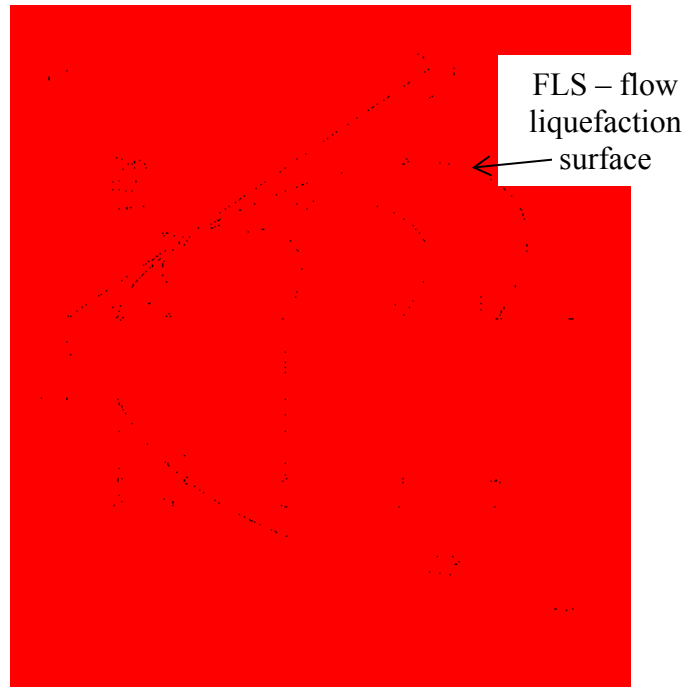


**Figure 2-6: Plot of soils experiencing flow liquefaction in  $p'$  -  $q$  space (above) and starting point of soil with respect to the SSL. (Kramer 1996).**

### 2.2.3 Cyclic Mobility

Even though not all soils are susceptible to flow liquefaction, this does not mean that repeated cyclic loading will not have any effect on the soil. Soils whose initial conditions are such that flow liquefaction cannot occur may still liquefy and undergo what is known as cyclic mobility. Cyclic mobility occurs when the shear strength of the soil is greater than the required static shear strength, resulting in smaller movements. The term cyclic mobility was defined by Seed and Idriss (1971), although they used a broader definition for liquefaction in their paper. They were some of the first to recognize the difference between flow liquefaction and cyclic mobility. By defining cyclic mobility and flow liquefaction as individual and different they enabled ideas about liquefaction to be more easily communicated. Castro, in his experiments,

also showed that there was a difference between flow failure and cyclic mobility in sands, although he didn't recognize and define the different types of liquefaction at the time (Castro 1975). Some years later Vaid and Chern (1985) defined cyclic mobility as an "...accumulation of deformations which are limited in magnitude" that occur due to the cyclic loading causing the effective stresses to repeatedly pass through zero.

Repeated cyclic loading of the soil profile will result in the soil slowly and permanently straining and deforming from a few inches to a few feet. Cyclic mobility will always occur in sands that are cyclically loaded (Vaid and Chern 1985), and has been observed in both contractive and dilative soils.

Cyclic mobility can result in lateral spread, settlement, sand boils, and other liquefaction effects (Figure 2-7). Many of the effects of cyclic mobility occur only after the dissipation of the pore water pressure. For example, seismic settlement cannot occur until the pore water pressure dissipates, and as such, visible effects may not show on the surface until sometime after the earthquake has finished when the pore water pressure has had time to dissipate.

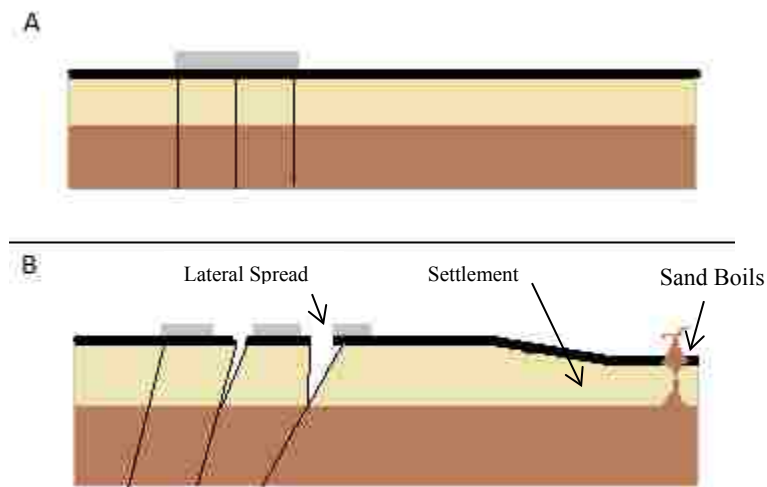


**Figure 2-7: Cyclic mobility before (a) and after (b).**

## **2.3 Effects**

Liquefaction effects pose significant hazards to many critical aspects of modern infrastructure including transportation networks, bridges, port facilities, lifelines, and structures. There are many different types of liquefaction effects. However not all of these effects cause damage. In order to understand the hazard to engineered structures and the risk to life, an understanding of what liquefaction will do is needful. Effects can be wide ranging and their impacts can be as well. Some effects include: sand boils, lateral spreading, landslides, settlement, toppling of buildings, failure of retaining walls, floating of subterranean structures, and many other possible problems.

The extent of the damage these effects cause is well illustrated by such events as the 2011 Christchurch earthquakes in New Zealand and the 2011 Tohoku earthquake in Japan. Both events teach us important things about the need to understand and mitigate the hazard posed by liquefaction and earthquakes in general. In Urayasu, Japan the Tohoku earthquake caused enough damage that a reported \$500 million US dollars was spent to restore sewer, water, and roads. In Christchurch, the repeated earthquakes in 2011 caused massive liquefaction damage. This resulted in the decision of the city of Christchurch to make entire areas of their city unbuildable or red zoned to prevent such massive damage in the future (Boulanger 2013).

### **2.3.1 Settlement**

Settlement during earthquakes occurs as a result of liquefaction. During the process of shaking, pore water pressures build up causing the soil to become partially suspended. As the pore water pressures dissipate, the soil particles often will realign in a denser configuration as they come back into more direct contact with each other, resulting in settlement. Note that seismic settlement may also occur in dry non liquefied sand layers above the water table.

Tokimatsu and Seed (1987) proposed a procedure for evaluating the potential seismic settlements from a single event. In their procedure, the volumetric strain of a soil layer was evaluated based on the duration of an earthquake, the cyclic shear strain, and other factors. It was later noted that in order to account for multi dimension shaking in the free field, the strain needed to be multiplied by a parameter between 2 and 3 depending on whether it was accounting for two or three dimensional shaking (Pyke, Seed et al. 1975). In general practice, it is common to multiply these strains by a factor of two. These strains are then used to calculate the settlement from the layer and the settlements of the entire profile are cumulatively added together to determine the total settlement of a soil profile. The total settlement of the soil profile can be found using the equation shown below.

$$\text{Total Settlement} = \sum_{n=1}^{n=\# \text{ sublayers}} \varepsilon_n * \text{thickness}_n \quad (2)$$

In this equation, thickness is the thickness of the sub layer, n is the sub layer number, and  $\varepsilon$  is the strain that occurs in the layer as a result of the loading caused by the earthquake.

As a result of the seismically induced settlements, large deformations can occur during or even after the earthquake, depending on the time it takes for the pore water pressure to dissipate. Seismic settlements can also induce quite large differential settlements that can cause damage to buildings (Figure 2-8). More recently, several advances in this area have led to newer methods being developed (Stewart and Whang 2003; Kramer 2008; Cetin, Bilge et al. 2009).



**Figure 2-8: Differential settlement in Iran 1990 after NOAA/NGDC - M. Mehrain, Dames and Moore.**

### **2.3.2 Lateral Spread**

Lateral spread can occur during an earthquake as a result of cyclic mobility. The cyclic mobility must occur as a result of liquefaction in an area where there is a slope or a free face. The soil profile in these conditions has driving forces acting on it that can slowly move the soil mass under repeated cyclic loads, such as during an earthquake. As the earthquake progresses, the soil gradually moves downslope, or towards the free face, causing soil deformation, cracks, fissures, and scarps (Youd and Bartlett 1995).

A hypothetical example of lateral spread is shown in Figure 2-7. In this figure a foundation is shown before (A) and after (B) lateral spread has occurred. Soil thus mobilized can cause severe damage to buildings, underground lifelines, bridges, and other structures as it moves and shifts. The magnitude of the motion is not generally large when compared to flow



failures, although displacements of 18 feet or greater have been observed. Due to the large areas involved and the relatively large displacements the costs to repair damage caused by cyclic mobility can be significant.

Youd and Bartlett (1995), in their paper on lateral spread, proposed an empirical equation based on a case history database for use in prediction of the magnitude of lateral spread which a scenario event would cause. This was later updated to the current form which is given in equations 3 and 4 (Youd, Hansen et al. 2002).

$$\log D_H = b_0 + b_1 M_w + b_2 \log R^* + b_3 R + b_4 \log W + b_5 \log S + b_6 \log T_{15} + b_7 \log(100 - F_{15}) + b_8 \log(D50_{15} + 0.1) \quad (3)$$

$$R^* = R + 10^{0.89M - 5.64} \quad (4)$$

Where  $b_0$ - $b_8$  are coefficients specified by Bartlett and Youd (Table 2-1),  $M$  is the moment magnitude,  $R$  is the horizontal distance to the seismic source in km,  $R^*$  is the distance parameter to account for near field effects,  $W$  is the free face ratio (%),  $S$  is the slope (%), and  $T_{15}$ ,  $F_{15}$ , and  $D50_{15}$  are parameters describing the soil conditions. The values associated with each of the coefficients  $b_0$  through  $b_8$  can be seen in Table 2-1.

**Table 2-1: Youd, Hansen et al. (2002) lateral spread coefficients**

Case:	$b_0$	$b_1$	$b_2$	$b_3$	$b_4$	$b_5$	$b_6$	$b_7$	$b_8$
Ground Slope	-16.213	1.532	-1.406	-0.012	0	0.338	0.54	3.413	-0.795
Free Face	-16.713	1.532	-1.406	-0.012	0.592	0	0.54	3.413	-0.795

This formulation is based on a deterministic single scenario approach. Recently, semi-empirical forms of lateral spread calculations have also become available (Faris 2004; Kramer 2008). These equations are somewhat complex and are not discussed here.

### **2.3.3 Flow Failure**

Flow failures occur when there is a dramatic decrease in the available strength of the soil. Flow failure effects are the result of either flow liquefaction or a loss of strength (see Figure 2-5). They can lead to landslides and other large quick movements of soil. This type of liquefaction was described by Seed and Idriss in their paper as flow liquefaction (Seed and Idriss 1971). These types of failures generally pose a major risk to life and can cause large and costly damage to infrastructure. They occur when the available resisting forces are exceeded by the driving forces in a soil.

To find the available resisting forces in a soil requires an understanding of the soils strength after liquefaction has occurred. Soils that liquefy will generally retain some strength even after liquefaction has occurred. Determining the magnitude of this residual strength can be difficult to do and contains large uncertainty. According to Franke (2011) several methods exist for estimating this residual strength and include laboratory testing, in situ testing and correlations, and normalized strength techniques. Laboratory testing is difficult to perform properly as well as expensive and is not used routinely. One of the cheapest ways to obtain the residual shear strength is to use the normalized strength techniques. Several normalized shear strength techniques exist and can be used in practice (Seed, Cetin et al. 2003; Idriss and Boulanger 2008).

Normalized strength techniques rely on charts and equations that have been developed from case histories and laboratory testing. Using these techniques it is possible to estimate the residual strength of the soil (Figure 2-9) although with a great deal of uncertainty involved. There is also some difficulty in estimating residual strengths with these methods at higher SPT

blow counts and shallower depths, with further research needed in this area (Franke 2011; Youd 2013).

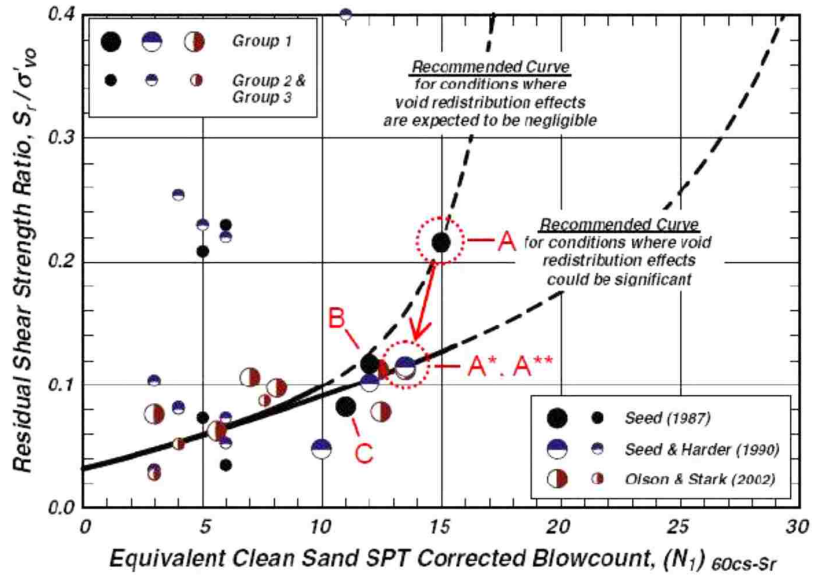


**Figure 2-9: Plot showing normalized strength vs.  $N_{160cs}$  (Idriss and Boulanger 2008).**

Once the residual strength of a soil has been estimated it is possible to determine whether a flow failure will occur. Flow failures occur when the resisting forces in the slope are exceeded by the driving forces acting on the slope. If liquefaction has occurred and the resisting forces are much smaller than the driving forces flow liquefaction and failure of the slope will occur. Flow failures can pose a very real hazard when they are not prevented. A case history that illustrates this point occurred when the lower San Fernando dam nearly failed because flow liquefaction occurred on the upstream slope of the dam (Figure 2-10).



**Figure 2-10: Flow failure at lower San Fernando Dam 1971 after NOAA/NGDC - E.V. Leyendecker, U.S. Geological Survey.**

### **2.3.4 Loss of Bearing Capacity**

Another affect commonly associated with liquefaction is a loss of bearing capacity. This effect can cause major damage to buildings as it can result in failure of the foundations (Figure 2-11). The bearing capacity of the soil is reduced due to the buildup of pore pressures, which causes the strength of the soil to approach its residual strength. This can decrease the ability of the soil to resist loads and can result in a bearing capacity failure, which can ultimately lead to collapse, failure of structures, and possible loss of life. Many of the approaches mentioned above for estimating residual strengths of soils can be used to estimate the residual strengths associated with this type of failure as well.



**Figure 2-11: Bearing capacity failure after NOAA/NGDC - NOAA National Geophysical Data Center.**

### **2.3.5 Other Effects**

Other effects of liquefaction include sand boils, ground motion attenuation, and deformation flow failures. Sand boils (Figure 2-12) are the result of a buildup of and release of pore water pressure.

As the pore water pressure finds cracks and weak planes in the soil, the pressure that has built up during a seismic event is released. During this process, sand can be forced to the surface and create what are known as sand boils as the pressure escapes.

As a result of liquefaction, ground motions can be attenuated. This occurs because the waves that are traveling up through the soil must pass through a semiliquid portion of soil that is undergoing liquefaction. When this occurs, some of the higher frequency waves are filtered due to the sudden change in impedance in the soil layering. Liquefaction in effect ‘liquefies’ the soil and modifies the ability of the soil to transfer energy and shear waves through the soil.

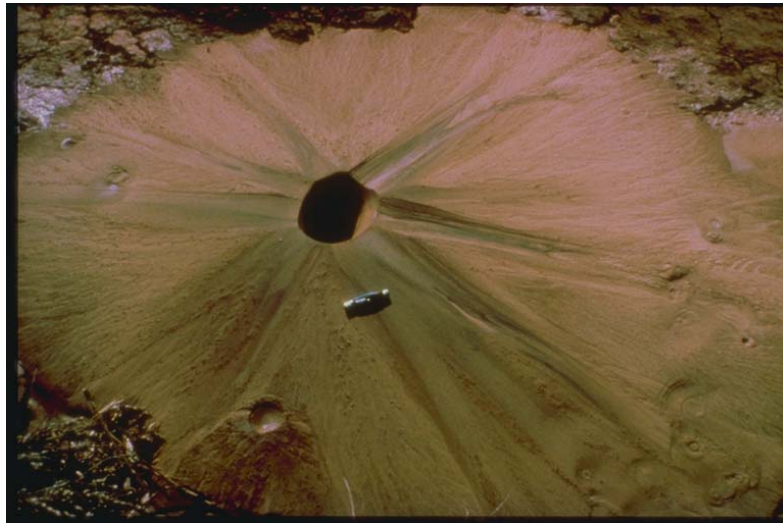


**Figure 2-12: Sand boil in El Centro, CA 1979 after NOAA/NGDC – University of Colorado at Boulder.**

Several other effects can also increase the hazard posed by liquefaction. It is important to understand these other effects as they can potentially harm structures and infrastructure in the area. These other effects include changes in the soil which can lead to failure of retaining walls and changes in the soil which can lead to floatation of lifelines.

Liquefaction can cause the failure of retaining walls (Figure 2-13). This is especially true in areas where hydraulic fill has been used. This can occur for several reasons, including the increase in pore water pressure and the effect liquefaction has on the failure wedge. When liquefaction occurs, it leads to the development of a much larger failure area than is normally assumed in the design of retaining walls. Most retaining walls are designed to retain the active case. When liquefaction occurs, the assumption of an active case is no longer valid as the shape of the failure changes from the active case to a “hydrostatic” case and the resulting pressures on

the retaining wall can increase dramatically. Failure often results as few retaining structures are designed to hold up under the “hydrostatic” case. Liquefaction has resulted in the failure or partial failure of many retaining walls (Day 2002).



**Figure 2-13: Retaining wall failure due to liquefaction after**  
<http://mceer.buffalo.edu/publications/bulletin/07/21-03/images/05embankmentlg.jpg>.

Lifelines exposed to liquefaction can also be adversely affected. When liquefaction occurs, the changes in the soil cause the buoyant force of the lifelines to exceed the available ability of the soil to resist. Lifelines are often found “floating” above the ground surface after an earthquake occurs and can be expensive to fix. Lateral spread caused by liquefaction can also sever or destroy existing lifelines and can make emergency response and recovery after the earthquake difficult and expensive.

### **3 CHARACTERIZATION OF SEISMIC LOADING**

Liquefaction is strongly affected by the amplitude and duration of shaking to which the ground is exposed. Soil might not liquefy during one earthquake, but might liquefy during the next due to the differences in the seismic loading. To be able to predict whether liquefaction will occur the engineer must first understand the types and frequency of seismic loading expected to occur at a site. To understand these loadings an understanding of earthquakes in general and of site specific seismic hazard analysis is beneficial.

#### **3.1 Earthquakes**

When an earthquake occurs, it usually releases its energy along a fault over a very short period. An earthquake can also release the energy in several separate bursts along a single fault or along several separated fault segments in an area. The energy that is released by an earthquake can be amplified or changed by near source and directivity effects, basin effects, and other effects that can occur (Kramer 1996). Ground motions will also tend to be larger in the fault normal direction. These general rules have been observed using accelerometers and other measuring equipment which record ground motions during an earthquake. The ground motion measurements and other results can be used to help understand future events, and thus narrow the uncertainty associated with the possible range of input parameters for a liquefaction analysis.



The relationships that are made using these measurements are known as attenuation relationships or ground motion prediction equations (GMPEs).

### **3.2 Modifying Effects**

Ground motions developed using modern GMPEs do not take into account some of the other effects that have been observed and are known to cause changes in the ground motions. These effects must be accounted for separately by an experienced engineer. These effects include near source and directivity effects, basin effects, soil amplification, and topographic effects.

#### **3.2.1 Near Source, Basin, and Topographic Effects**

Near source, basin, and topographic effects cause changes in ground motions at a site. Near source and directivity effects can modify ground motions and affect the way in which they interact with a site. These effects occur due to the pulse created during the initial instance of the earthquake. Usually near source and directivity effects will affect buildings within about 10-15 km of a fault; with the distance of these effects depending on the soil type and the geologic setting at a site (Kramer 1996). The occurrence of these effects is based on whether the earthquake occurs towards or away from a site as well as whether the site is located in the fault normal or fault parallel position. If the fault ruptures toward a site it will often exhibit a pulse in the time history data (Figure 3-1). This will result in local effects and damage that can be much greater than the damage to surrounding areas or areas in the opposite direction from the fault rupture.

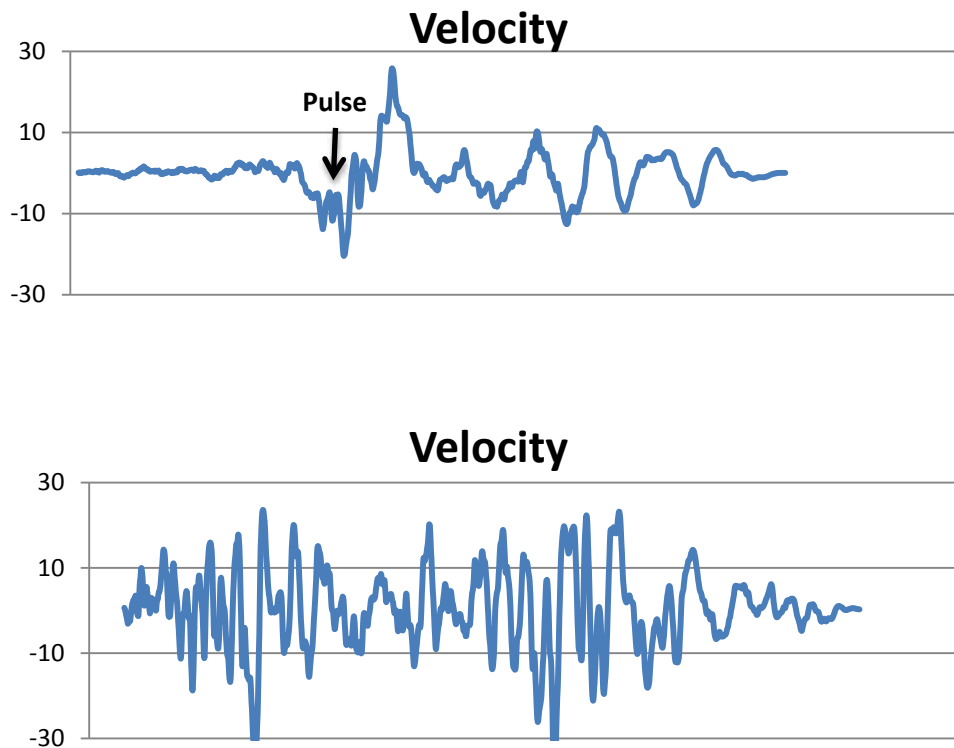


**Figure 3-1: Pulse from Lander 1992 earthquake (top). No pulse from Landers 1992 earthquake (not in direction of fault rupture) (bottom).**

Basin effects are common within the mountain west. These can amplify and change ground motions extensively. Basin effects occur due to the reflective nature of the exposed bedrock in the mountains surrounding a basin. As ground waves approach the edge of the basin they interact with the rock and reflect and refract off the edges of the basin creating complex patterns and interference. These reflections and refractions can make it difficult or impossible to fully predict the ground motions within a basin.

Topography effects will also have an effect on the types of ground motions and their prediction. Topography effects occur when there is local narrowing or concentration points in

the geology which concentrate seismic waves and energy. These can lead to locally large displacements and accelerations while the earthquake regionally may not be as large.

### 3.2.2 Site Amplification

Determining the amount of acceleration at the surface caused by the peak ground acceleration (PGA) at bedrock of a site can be difficult due to the effect of the soil overlying the rock. The change in acceleration caused by the overlaying soil is known as soil amplification. To account for this effect there are several different methods available to researchers. Stewart et al. looked at soil amplification statistically and determined that for a given age of soil, average values could be used to find the peak surface or maximum surface acceleration ( $a_{max}$ ) using the PGA of rock (Stewart, Liu et al. 2003). This is important because many of the measurements are made and recorded for values corresponding to bedrock.

Using the Stewart, Liu et al. (2003) relationships allows the  $PGA_{rock}$  to be converted to a surface acceleration  $a_{max}$  (5).

$$F_a = \frac{a_{max}}{PGA} = \exp[a + b * \ln(PGA)] \quad (5)$$

where  $F$  is the amplification factor,  $a_{max}$  is the acceleration at the surface,  $a$  and  $b$  are factors derived from the statistical analysis performed by Stewart et al., and  $PGA$  is the peak ground acceleration of bedrock. Quaternary age values specified by Stewart et al. are  $a = -0.15$  and  $b = -0.13$ . Quaternary values should often be used as most soil layers at or near the surface in the regions of concern are soils that have been laid down geologically recently. Further, most liquefiable soils are younger in age, and will fall into the Quaternary period.

Alternatively, to find  $a_{max}$  from the  $PGA$ , a numerical site response analysis can be performed. This is more site specific than using the Stewart et al. or other relationships might

be, but can be expensive due to the need to characterize the soil located at the site through in situ testing and lab testing. Numerical modeling can be run using equivalent linear or nonlinear analysis. Equivalent linear models tend to be much cheaper to run, and may be appropriate for sites where there is not a large enough budget to quantify the soils at the site sufficient to run a nonlinear analysis. Kramer (1996) observed, however, that equivalent linear analyses tend to have “spurious resonances...[and] can lead to an oversoftened and overdamped...[or] undersoftened and underdamped system...” The nonlinear analysis is generally more sophisticated and thus more time consuming, but can sometimes lead to a more accurate representation of what is occurring. It is difficult to implement due to the need to have a reliable constitutive model. The development of such a model is difficult and costly and is only performed for a few very critical sites.

The equivalent linear analysis can be used to model a soil profile. This allows the engineer to determine amplification and modification of the ground motions as they travel from bedrock to the ground surface. Equivalent linear models assume a shear modulus ( $G$ ) and an equivalent linear damping ratio ( $\xi$ ) value and use these values to calculate the ground response. The effective shear strain from the ground response is used to calculate new values for  $G$  and  $\xi$ . This sets up an iterative process which continues until some minimum change between iterations is reached (Kramer 1996).

The nonlinear analyses is more sophisticated than the equivalent linear analyses because it takes into account the changes that occur in a soil layer with time and the fact that soils do not react linearly under large strains. For example, during an earthquake, soil amplification will not be as high by the end of the earthquake as it was at the beginning when liquefaction occurred, as the liquefaction will attenuate the ground motions. Other similar nonlinear relationships exist.

As researchers develop better constitutive models, the results of nonlinear analyses become more accurate. Developing those constitutive models is currently one of the major problems with nonlinear analyses. Another major problem can be the need for much larger computing power, although this is decreasing with time as computers become more powerful. One major advantage of nonlinear analyses over equivalent linear analyses is the ability of the nonlinear analyses to develop models of pore pressure development.

The benefits of running these analyses are that they allow the engineer to develop a site specific amplification factor as well as other site specific values and can lead an engineer to have more confidence in the results than can be achieved with some of the more generalized relationships. It can also allow the development of plots of different properties, such as pore pressure and surface acceleration, with time.

The simpler of these two approaches is the correlations developed by Stewart, Liu et al. (2003). In order to use these relationships, however, a predicted value for  $PGA_{rock}$  is required. The development of the PGA can be done using a seismic hazard analysis. Such analyses will be discussed in detail in the following sections.

### **3.3 Seismic Hazard Analysis**

A seismic hazard analysis is a complex process that evaluates seismic hazards in a region. It requires extensive knowledge about the nature of the seismic sources in the region. Generally there are two basic approaches to evaluating seismic hazards, namely, deterministic seismic hazard analysis (DSHA) and probabilistic seismic hazard analysis (PSHA). Each type of analysis will be discussed in detail as both can be used to evaluate liquefaction hazards at a site or across a region.

### **3.3.1 Deterministic Seismic Hazard Analysis**

A deterministic seismic hazard analysis (DSHA) is the easiest form of seismic hazard analysis. It takes all of the sources of hazard and analyzes them based on the possibility of an earthquake occurring. To perform a DSHA four steps are usually taken:

1. Identify the active sources and magnitude – This can be quite difficult due to the fact that not all seismic sources have been identified, and some have been identified but the data for the fault is insufficient to allow characterization of the size of earthquake it can generate.
2. Compute the closest source to site distance – Some error can occur here due to either lack of data or lack of exact measurements for the fault location.
3. Compute ground motion values – Computation of the ground motions using some form of relationship is common. NGA equations are often used in the western US, and updated GMPEs are currently being developed for other areas in the US.
4. Identify governing ground motions for scenario earthquake – This is usually the earthquake that will have the largest ground motions at the site.

Once these steps are taken, the governing ground motions are used in design. This process has some disadvantages however, as it does not account for the likelihood of the governing earthquake occurring, only the possibility that it will occur. It also does not explicitly deal with uncertainty in attenuation relationships or seismic source characterization. These weaknesses have recently begun to be addressed by using Probabilistic Seismic Hazard Analyses.

### **3.3.2 Probabilistic Seismic Hazard Analysis**

Probabilistic seismic hazard analysis (PSHA) is becoming more prevalent in the engineering community. A PSHA looks at all sources of hazard and the likelihoods and

uncertainties associated with a given seismic source. By accounting for this uncertainty a PSHA can be used to more fully account for all the possible types of seismic hazard associated with a site. A PSHA deals directly with the spatial, temporal, size, and attenuation uncertainty. A detailed discussion of each of these types of uncertainty and how they are accounted for follows.

### 3.3.2.1 Spatial Uncertainty

Spatial uncertainty is the uncertainty associated with the location of the earthquake. Spatial uncertainty occurs because prior to the seismic event, it is currently impossible to predict exactly where the epicenter of the earthquake will be. Spatial uncertainty can be accounted for by dividing a fault into bins along a line or grid (Figure 3-2) and assigning a probability to each section (which represent the likelihood of the earthquake occurring in that section). Typically, unless there is evidence to the contrary such as evidence of seismic gap behavior, a uniform distribution of likelihood is assumed for all portions of the grid or line.

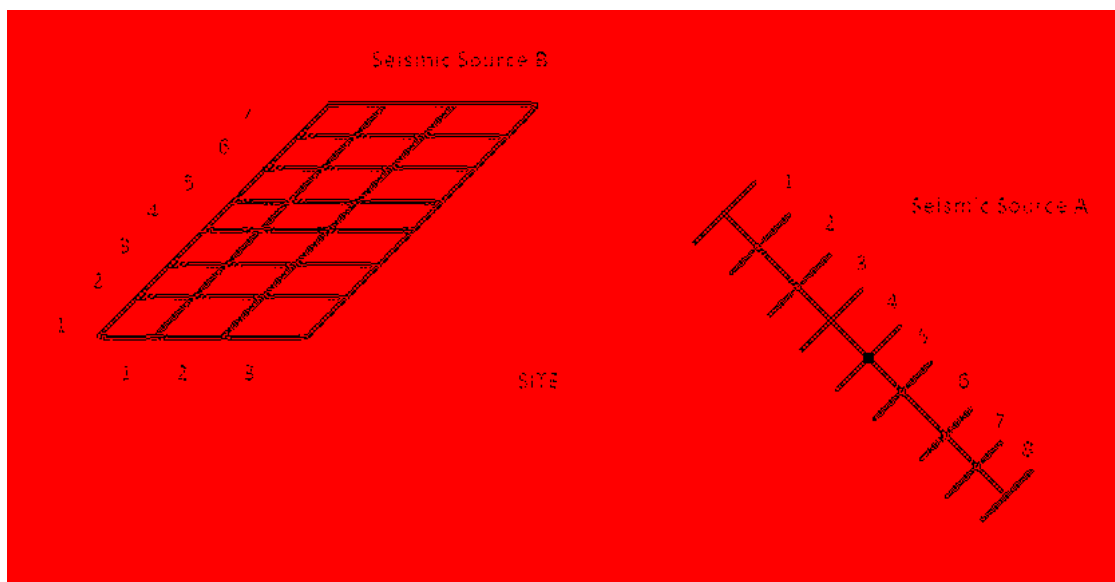


**Figure 3-2: Spatial uncertainty bin techniques for a) a source of known location and b) a source whose location is somewhat unknown or which covers a wider area.**

A grid is used in cases where the location of a fault is unknown. This occurs most often when the fault does not surface but is known to exist due to earthquake records. Line source is used when the exact location of the source is known. A fault that has been mapped through seismic and geological studies can be represented as a line source.

### **3.3.2.2 Temporal Uncertainty**

Temporal uncertainty occurs because the actual time an earthquake will occur is unknown. This leads to uncertainty in how often the event will occur, or even if it will occur. This is handled by applying the Poisson probability model, since the time it will occur is often widely distributed and relatively unknown, making it an almost random event. A Poisson probability model assigns all times the same uncertainty, or in other words they are considered to occur at completely random times. More recently time dependent models have been developed (Wong 2012). These time dependent models take into account the fact that earthquakes do not occur independently of each other, but in fact have a time dependent relationship. Currently time dependent models are not widely used due to the difficulty in gaining a large enough data set to develop the necessary relationships in a region. Obtaining a large data set is made difficult due to the time periods over which most earthquakes occur.

### **3.3.2.3 Size Uncertainty**

Size uncertainty occurs because faults can produce earthquakes of varying sizes and durations. The size of an earthquake is vital to understanding the effects from the earthquake, but it remains unknown until the earthquake occurs. To account for this, engineers have developed what are known as recurrence laws. A recurrence law is a relationship between the return period of an earthquake and its magnitude. The relationships show that larger earthquakes



tend to occur less often than smaller earthquakes. One of the first papers to recognize this pattern was written by Gutenberg and Richter (1944).

There are many different types of recurrence laws; some of which include slip-dependent recurrence laws (Slemmons 1982), bounded Gutenberg-Richter recurrence laws (Gutenberg and Richter 1944), and recurrence laws based on the characteristic earthquake (Youngs and Coppersmith 1985; Wells and Coppersmith 1994). These recurrence laws can be used to determine the mean annual rate of exceedance and thus the return period for a given ground motion parameter. The return period is usually given in years (i.e. the average number of years before a ground motion parameter exceeds a specified value) and is the inverse of the mean annual rate of exceedance where the mean annual rate of exceedance is the probability that the average value will exceed a given value annually. For example a return period of 500 years would correspond to a mean annual rate of exceedance of  $1/500 = 0.002$ .

#### **3.3.2.4 Attenuation Uncertainty**

Attenuation uncertainty occurs because the attenuation models used in probabilistic seismic hazard analysis are not always exactly correct. The variation between the different models is known as epistemic uncertainty. This epistemic uncertainty is often dealt with by assigning probabilities to different relationships and then incorporating several different relationships into the PSHA. For example, if an engineer has two different relationships they feel are equally likely, the relationships would each be weighted accordingly with equal probabilities of 50% and the results of each relationship would in effect be averaged to obtain the final value. In this way multiple GMPE's can be used to account for epistemic uncertainty associated with ground motion prediction.

There are many different types of GMPE's. PSHA's tend to use several models as explained above. Different approaches to developing these types of models with varying levels of complexity and success have been developed. Often in the development of GMPE's the Ergodic assumption is used. The Ergodic assumption states that an Ergodic process is a process which "is random process in which the distribution of a random variable in space is the same as the distribution of that same random process at a single point when sampled as a function of time."(Anderson and Brune 2000) Application of the Ergodic assumption allowed the combination of geographically dissimilar events into one data set and is necessary due to the limited ground motion data available for statistical analysis.

Recently the USGS worked with 5 teams of researchers to develop the next generation attenuation relationships (NGA) (Power, Chiou et al. 2008). These models tend to be more complex than some of the earlier models. The NGA models allow the determination of the types of ground motions that will occur at a site given a seismic event's magnitude and the fault geometry of the fault generating the event. The NGA equations are valid in most of the United States, as they are valid where there are strike slip, normal, and reverse faults. A sample of the type of output obtained from these relationships is shown below in Figure 3-3.

The NGA relationships are only valid for normal, reverse, and strike slip type faulting mechanisms. Other GMPE's have been developed for use in areas with subduction zones. These areas require a different set of equations as the ground motions and magnitudes associated with subduction zones are different than those associated with other faulting types. Several relationships exist for classification of these ground motions including Zhao, Zhang et al. (2006), and Atkinson and Boore (2003).

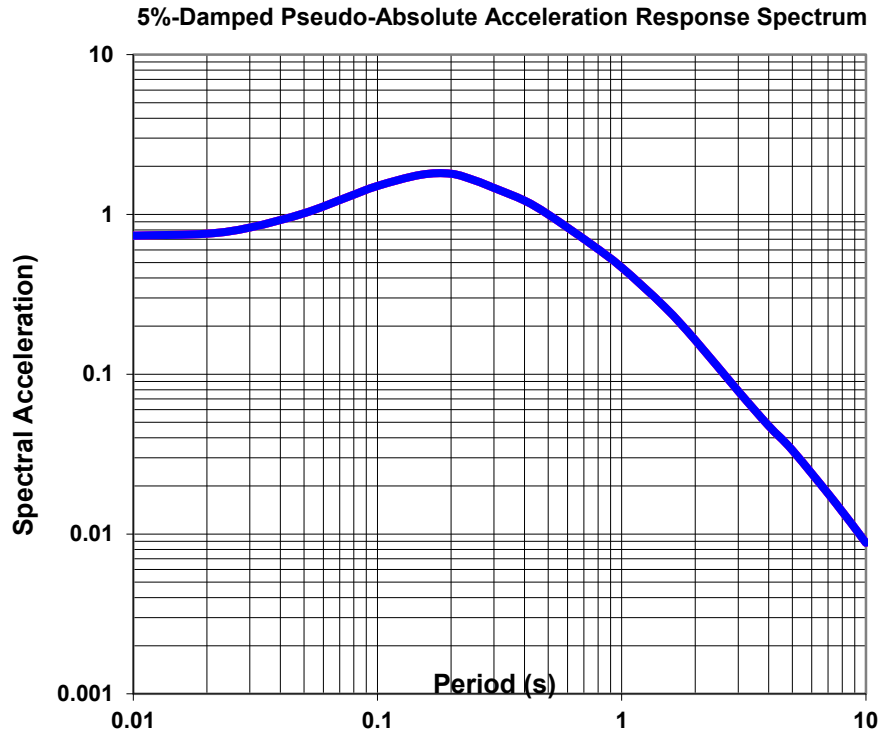


**Figure 3-3: NGA results created using NGA equations worksheet created by Linda Al Atik 2009.**

The USGS and other open source models use the aforementioned relationships as well as other relationships in their seismic source models to determine the peak ground acceleration and other parameters. The incorporation of multiple models allows epistemic uncertainty to at least be limited in the final output of the PSHA.

### **3.3.2.5 Seismic Source Model Development**

Open source seismic source models have been developed for public use for most of the continental United States by the USGS and others (Petersen, Frenkel et al. 2008) . A seismic source model looks at all the possible sources of seismic activity and their respective return

periods as well as the type and size of earthquakes that can be expected. The geophysicist will then develop a model showing the sources that can contribute to seismic hazard which incorporates the uncertainties associated with those sources. The development of seismic source models is a complex topic which will not be covered in detail here as it is mainly pertinent to the realms of seismology and geophysics.

The way these uncertainties are accounted for can most easily be seen in a deaggregation plot. The deaggregation plot showing the contributions towards the ground motions of interest can be deaggregated to show the amount of contribution towards that hazard incurred as a function of distance and magnitude (Figure 3-4). These deaggregated contributions can be used to determine which seismic sources contribute most to the ground motion. For example, Figure 3-4 shows that there is a seismic source with a moment magnitude ( $M_w$ ) between 6.4 and 7.1 that is located within about 3 km of the site and a second source located about 48 km from the site, which contributes to the total probabilistic seismic hazard.

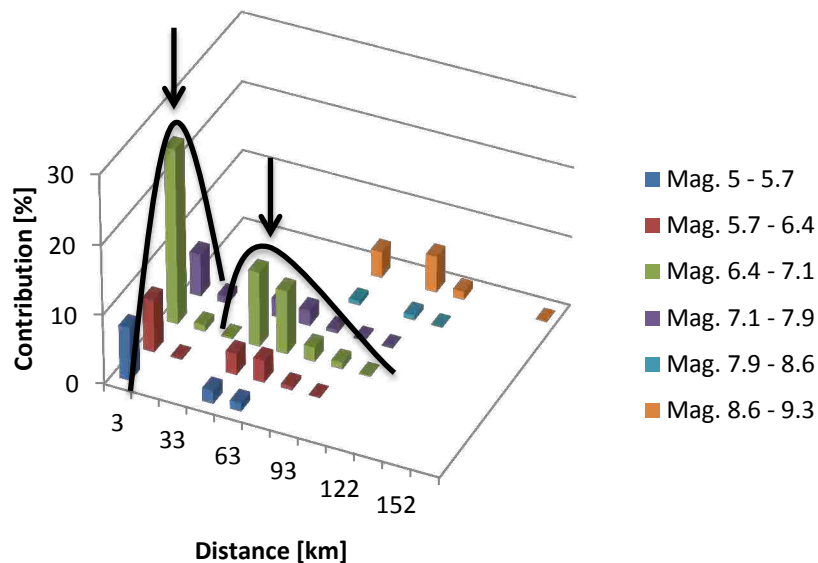


**Figure 3-4: Deaggregation for Seattle site for 1039 year return period.**

Uncertainties in the location and magnitude of the events are also apparent in the deaggregation. For example, the fault system located at a distance of roughly 3 km has some uncertainty in its magnitude ( $M_w$  from 5.0 – 7.9), and thus has varying contributions for several magnitude bins. The deaggregation also shows distance uncertainty which can be most easily seen with the source at 48 km which has contributions toward the total hazard starting at about 33 km and ranging up to 93 km.

Understanding and characterizing seismic sources and ground motion parameters is important in an analysis of liquefaction. If the seismic loading input into the liquefaction analysis is erroneous, then the liquefaction analysis will carry forward those same errors. To understand if liquefaction will initiate, a thorough deterministic and/or probabilistic analysis must be performed, and the possible sources of error in those analyses understood and accounted for.

### 3.4 Seismic Hazard Curves

Once all of the sources of uncertainty have been examined and uncertainty accounted for, the total probability theorem can be used to develop a seismic hazard curve associated with a particular ground motion parameter or outcome. The total probability theorem states that the probability of a given event is the sum of the probabilities of the contributing events. In terms of seismic modeling this is done by taking the probabilities from the seismic source and determining the probability of a given event using equation 6.

$$\lambda_{y^*} = \sum_{i=1}^{N_s} v_i \sum_{j=1}^{N_m} \sum_{k=1}^{N_R} P[Y > y^* | m_j, r_k] P[M = m_j] P[R = r_k] \quad (6)$$

where  $\lambda_{y^*}$  is the mean annual rate of exceedance for a given magnitude.  $P[Y > y^* | m_j, r_k]$  is the probability of the actual ground motion exceeding the specified ground motion given a

magnitude  $m_j$ , a source to site distance  $r_k$ , and a contribution from each of the seismic sources  $v_i$ . This equation is used to develop values from which a seismic hazard curve can be developed for a given ground motion parameter such as PGA or PGV. The development of these hazard curves is useful in engineering practice as it facilitates the development of hazard curves for other parameters. This can be done using the PEER triple integral in conjunction with equations which predict the probability of liquefaction which will be discussed in more detail later.

## **4 ASSESSMENT OF LIQUEFACTION INITIATION POTENTIAL**

Three different types of assessment of liquefaction initiation potential have been developed. These methods are laboratory testing, numerical modeling and simulation, and empirical deterministic methods. These methods enable the engineer to gain an understanding of whether or not a soil will liquefy. Once initiation is understood, the effects of that liquefaction can be examined and a decision reached on the types of mitigating measures needed. These three methods range in price and accuracy and a knowledge of all three is beneficial when making decision about how to analyze a site.

### **4.1 Laboratory Testing**

Laboratory testing can be used to evaluate liquefaction initiation potential. Several different methods exist for obtaining samples from the field in order to perform lab testing on them. A tube sampler can be used to obtain field samples in cohesive soils; however, granular material is not sampled well using this technique. As most liquefaction occurs in samples which are granular another method must be used. An alternative sampling method is to freeze the samples and collect data in this manner. This has the advantage of producing much less sample disturbance, but can be expensive and in some cases cost prohibitive.

Many different laboratory tests have been developed over the years to allow for the testing of soil liquefaction potential. These tests include the cyclic triaxial test, resonant column test, cyclic direct simple shear test, and the cyclic torsional shear test (Kramer 1996). Bhatia, Schwab et al. (1985) conducted a comparative study between three of the available tests at the time and found that stress and strain controlled tests yielded significantly different results. Despite the inconsistency of the tests, the use of soil samples in liquefaction initiation can still be beneficial to the engineer. Yoshimi, Tokimatsu et al. (1994) looked at the use of frozen samples in a review of their previous work. They also conducted testing of additional frozen samples which showed that frozen samples produce good results in sands.

More recent studies into liquefaction using laboratory testing include the works of Cetin and Bilge (2012). They collected data from laboratory testing and examined the results of stress controlled triaxial tests (CTXT) and simple shear tests (SST). Cetin and Bilge (2012) developed models to help predict the cyclic strain and pore pressure ratio that soils would undergo during cyclic loading. The tests showed that corrections were needed to bring laboratory testing results in line with values consistent with field conditions.

Seed and Idriss (1971) describe the general process for evaluating liquefaction potential using lab samples. The process uses laboratory testing to determine the number of stress cycles needed to trigger liquefaction for various depths and confining pressures. They recommend the use of cyclic load triaxial or cyclic load simple shear tests for this purpose. In general there are four steps to evaluating liquefaction initiation using laboratory samples:

1. Establish soil conditions, ground motion parameters, and design earthquake.
2. Convert stress history into equivalent number of uniform stress cycles. Plot stress level as a function of depth.



3. Determine cyclic shear stresses that would need to be developed to induce liquefaction. Plot stresses required to cause failure as a function of depth.
4. Determine where liquefaction will occur by examining stress level and comparing it to stresses required to cause liquefaction.

Using this procedure with field testing it is possible to assess a soil's liquefaction potential given the design ground motions. The zone of liquefaction can be identified based on the cyclic stress developed by the earthquake and the cyclic stress it would take to cause a given soil to liquefy (Figure 4-1).

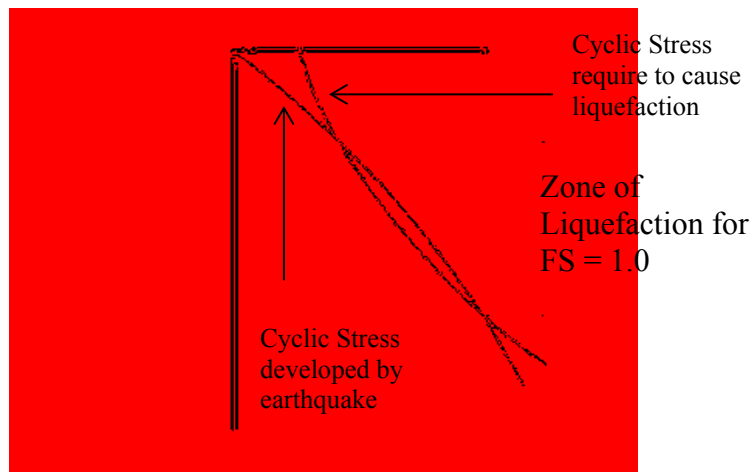


**Figure 4-1: Stress curves used to evaluate liquefaction potential for given factor of safety after Seed and Idriss (1971).**

#### 4.2 Numerical Modeling and Simulation

Numerical models in general yield results that are more detailed than generic correlations. Numerical models can be made for the one, two, and three dimensional case. The process of modeling is complicated by the difficulty in achieving a good constitutive model with valid soil parameter inputs. To build a good numerical model of a site requires extensive testing

and analysis which can be exceedingly difficult. Constitutive models which yield accurate results that are well validated are also difficult to find (Vytiniotis 2012).

If a good numerical model is developed then numerical simulations can be run with some confidence in the results. The results have the advantage of yielding time dependent output for a soil profile. Numerical models are helpful when modeling soil profiles because they allow the engineer to model nonlinear behavior. Output can also be made site specific. Nonlinear models have added potential due to their ability to model soil as it is in motion, including its changing pore pressure. Nonlinear models can be useful in our understanding of liquefaction as it is through nonlinear models that we are able to model pore pressure generation and liquefaction initiation under cyclic loads (Kramer 1996).

#### **4.3 Empirical Deterministic Methods**

Empirical deterministic methods have the advantage of using in situ conditions of the soil profile which removes the need to accurately characterize the soil dynamic properties and strength properties in a laboratory. This means that the uncertainties inherent in laboratory testing are mostly eliminated, although they are partly replaced by uncertainties in the relationships used with the in situ methods. Empirical deterministic methods allow for an engineer to calculate the possibility of liquefaction occurring for a scenario earthquake at the site of interest. Deterministic methods are limited to evaluating a scenario earthquake. The following sections will discuss the simplified method in detail, as well as looking at different techniques for assessing liquefaction initiation that have been developed over time.

### 4.3.1 Seed and Idriss Simplified Procedure

Prior to the development of the simplified method, liquefaction analysis was usually conducted solely on the basis of lab testing and field data. The lab tests were used to determine if a soil was liquefiable. Seed and Idriss (1971) developed a simplified procedure for the evaluation of a soil profile to determine if it was susceptible to liquefaction. In their paper, they outlined several key points that needed to be examined to understand if a soil profile would liquefy. These were soil type, relative density or void ratio, initial confining pressure, intensity of ground shaking, and the duration of ground shaking.

However evaluation of many different parameters using lab testing was expensive and often difficult to implement. In that light, Seed and Idriss proposed a different method for the evaluation of liquefaction potential (Seed and Idriss 1971). This method has become known as the simplified method and has since gained wide acceptance in engineering practice.

The simplified method as developed by Seed and Idriss takes into account the stress on the soil, the maximum surface acceleration experienced by the soil, and a depth reduction factor (referred to as a stress reduction coefficient) used to account for the change in shear stress with depth. Their equation was of the form shown in equation 7.

$$\tau_{av} = 0.65 * \frac{\gamma * h}{g} * a_{max} * r_d \quad (7)$$

where  $\tau_{av}$  is the shear stress,  $\gamma$  is the unit weight,  $h$  is the depth,  $a_{max}$  is the maximum acceleration at the surface, and  $r_d$  is the depth reduction factor. The depth reduction factor is important because it accounts for variations in cyclic stress with depth. Using this equation, it was possible to calculate the average shear stress by depth in a soil profile and compare it to the induced shear stress. It is possible to modify this equation by dividing both sides by the effective vertical stress at that depth. Doing so results in an equation for the cyclic stress ratio, CSR, which is the ratio

of shear stress to the effective vertical stress in the soil (Seed, Tokimatsu et al. 1985). The equation for CSR is given as,

$$CSR = \frac{\tau_{av}}{\sigma'_v} = 0.65 * \frac{\sigma_v}{\sigma'_v} * \frac{a_{max}}{g} * r_d \quad (8)$$

where  $\sigma'_v$  is the effective vertical stress in a soil layer and  $\sigma_v$  is the total vertical stress in a layer.

The CSR can be used to evaluate liquefaction potential using the figure provided by Seed, Tokimatsu et al. (1985) (Figure 4-2). In this figure the point at which liquefaction triggers is correlated to a standard penetration test (SPT) blow count. The blow count is a measure of the number of blows required to push 12 inches. SPT blow counts are correlated to many of the different factors associated with liquefaction such as relative density.

To evaluate whether liquefaction will trigger two things must be determined. One is the cyclic stress ratio at the site which can be found using equation 8. The other is the resistance a soil can provide against liquefaction. This resistance is known as the cyclic resistance ratio (CRR) and can also be found using Figure 4-2.

For example suppose we have calculated a CSR value of 0.20 using a scenario earthquake. We can find the CRR for a soil profile with a blow count of 10 to be 0.115. Using these values we would say that liquefaction will trigger as the cyclic stress is greater than the cyclic resistance of the soil.

In modern practice the CSR is used in conjunction with the CRR to develop a factor of safety against liquefaction initiation ( $FS_{liq}$ ).

$$FS_{liq} = \frac{CRR}{CSR} \quad (9)$$

The factor of safety provided using this simplified procedure is much easier to find than could be done using the previous methods. This simplified procedure for evaluation of liquefaction initiation has been updated and is used widely in practice to evaluate liquefaction potential.

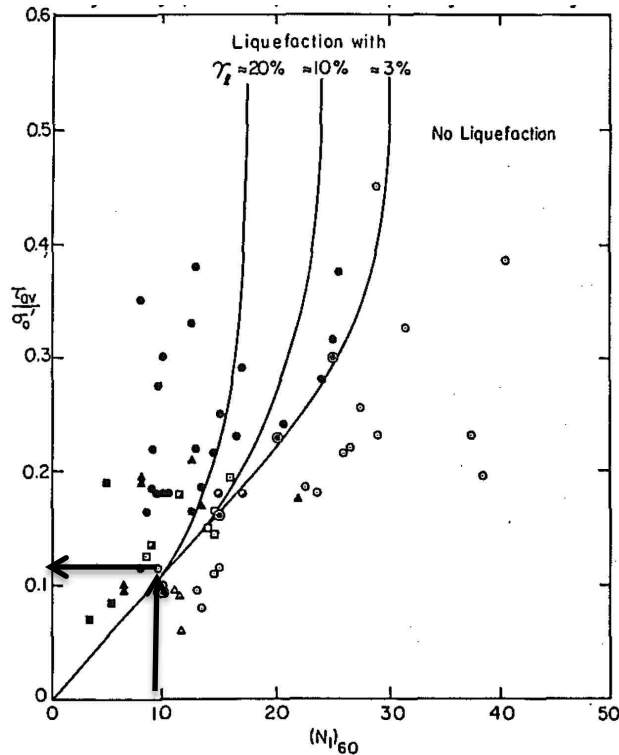


Figure 4-2: CSR ( $\tau/\sigma'$ ) vs.  $N_{160}$  for sand from (Seed, Tokimatsu et al. 1985).

#### 4.3.2 NCEER Procedure

As more data on liquefaction was collected, new methods began to emerge for evaluating liquefaction initiation. This resulted in some confusion among practicing engineers about how to evaluate liquefaction initiation. In order to help the civil engineering community to have consistent practice and to help engineers to better understand how liquefaction analysis should be conducted, a workshop was organized to resolve these differences. In 2001 a report was published of the 1996 NCEER and 1998 NCEER/NSF workshops (Youd, Idriss et al. 2001) and the findings of the workshops became common practice throughout the engineering profession. The updates to the original simplified procedure consisted of updates to the SPT blow count corrections, updates to the evaluation of CRR, and updates to the correction factors and depth reduction factor used.

#### 4.3.2.1 Updated SPT Blow Count Corrections

One of the updates made by the workshop consisted of updating the SPT blow count standardizations. These standardizations are necessary due to variations in the SPT measuring equipment. These standardizations correct the SPT blow counts from the field ( $N_{field}$ ) to a standardized clean sand corrected value known as  $(N_1)_{60cs}$ . Several correction factors are applied to correct the SPT blow count value for fines content, overburden pressure, hammer energy, rod length, and sampler type. The value of  $(N_1)_{60}$  can be found by multiplying a  $N_{field}$  value by correction factors such that,

$$(N_1)_{60} = C_N C_E C_R C_B C_S N_{field} \quad (10)$$

where  $C_N$  is the correction factor for overburden pressure,  $C_E$  is the correction for hammer energy delivered,  $C_R$  is the correction for rod length, and  $C_S$  is the correction factor for sampler type. These corrections give standardized values for the SPT which can be used in relationships and correlations. Values for the different correction factors can be obtained in Table 4-1. These standardized values correspond to standardizations made based off of standard practice in the United States.

Values for computing  $C_N$  can be obtained using:

$$C_N = \left( \frac{P_a}{\sigma_v'} \right)^{0.5} \leq 1.7 \quad (11)$$

where  $P_a$  is atmospheric pressure and  $\sigma_v'$  is the initial vertical effective stress. The workshop participants noted that this equation seems to have some problems handling overburden pressures greater than 200 kPa.

Further standardization is needed for  $(N_1)_{60}$  to correct the value to a clean sand equivalent for use in the liquefaction initiation procedures.

**Table 4-1: Correction factors (Youd, Idriss et al. 2001)**

Factor	Equipment Variable	Term	Correction
Overburden pressure	-	C <sub>N</sub>	See Equation 11
Energy ratio	Donut Hammer	C <sub>E</sub>	0.5-1.0
Energy ratio	Safety Hammer	C <sub>E</sub>	0.7-1.2
Energy ratio	Automatic-tip Donut-type Hammer	C <sub>E</sub>	0.8-1.3
Borehole Diameter	65-115mm	C <sub>B</sub>	1
Borehole Diameter	150mm	C <sub>B</sub>	1.05
Borehole Diameter	200mm	C <sub>B</sub>	1.15
Rod length	<3m	C <sub>R</sub>	0.75
Rod length	3-4m	C <sub>R</sub>	0.8
Rod length	4-6m	C <sub>R</sub>	0.85
Rod length	6-10m	C <sub>R</sub>	0.95
Rod length	10-30m	C <sub>R</sub>	1
Sampling method	Standard Sampler	C <sub>S</sub>	1
Sampling method	Sampler without Liners	C <sub>S</sub>	1.1-1.3

The NCEER report recommended the use of R.B. Seed's formulation of the clean sand correction (Youd, Idriss et al. 2001) shown below.

$$(N_1)_{60cs} = \alpha + \beta * (N_1)_{60} \quad (12)$$

where alpha and beta are coefficients that correct the SPT blow count for fines content. The values of  $\alpha$  and  $\beta$  can be obtained using the relationships shown below.

$$\alpha = \begin{cases} 0.0 & \text{for } FC \leq 5\% \\ \exp\left[1.76 - \left(\frac{190}{FC^2}\right)\right] & \text{for } 5\% < FC < 35\% \\ 5.0 & \text{for } FC \geq 35\% \end{cases} \quad (13)$$

$$\beta = \begin{cases} 1.0 & \text{for } FC \leq 5\% \\ \left[0.99 + \left(\frac{FC^5}{1000}\right)\right] & \text{for } 5\% < FC < 35\% \\ 1.2 & \text{for } FC \geq 35\% \end{cases} \quad (14)$$

where FC is fines content in percent.

#### 4.3.2.2 Updated Cyclic Resistance Ratio

The workshop recommended some updates to the simplified procedure proposed by Seed and Idriss. These updates took into account the larger data sets that were available and the additional research which had been performed. The workshop recommended calculating the CRR using an  $(N_1)_{60cs}$  value corresponding to a magnitude 7.5 event (Youd, Idriss et al. 2001). The equation that was recommended by the workshop is shown below in Equation 15.

$$CRR_{M=7.5} = \frac{1}{34-(N_1)_{60cs}} + \frac{(N_1)_{60cs}}{135} + \frac{50}{(10*(N_1)_{60cs}+45)^2} - \frac{1}{200} \text{ for } (N_1)_{60cs} \leq 30 \quad (15)$$

This form of the equation for the CRR was developed as an approximation of the CRR line seen in Figure 4-3.



**Figure 4-3: CRR curves for fines content of 35, 15, and 5 % (Youd, Idriss et al. 2001).**



### 4.3.2.3 Other Updates and Changes

Several other factors were also updated by the NCEER workshop participants and recommended for use. These updates included a new equation for the depth reduction factor ( $r_d$ ), and discussion of the magnitude scaling factor (MSF), and the factors  $K_\sigma$  and  $K_\alpha$ .

The new equation for the depth reduction factor,  $r_d$ , was made to better encompass the changes in  $r_d$  with depth. The equations for  $r_d$  are shown below.

$$r_d = [1 - 0.00765 * z] \text{ for } z \leq 9.15m \quad (16)$$

$$r_d = [1.174 - 0.0267 * z] \text{ for } 9.15m \leq z \leq 23m \quad (17)$$

where  $z$  is the depth in meters. A graphical representation of the values of  $r_d$  with depth is shown in Figure 4-4.

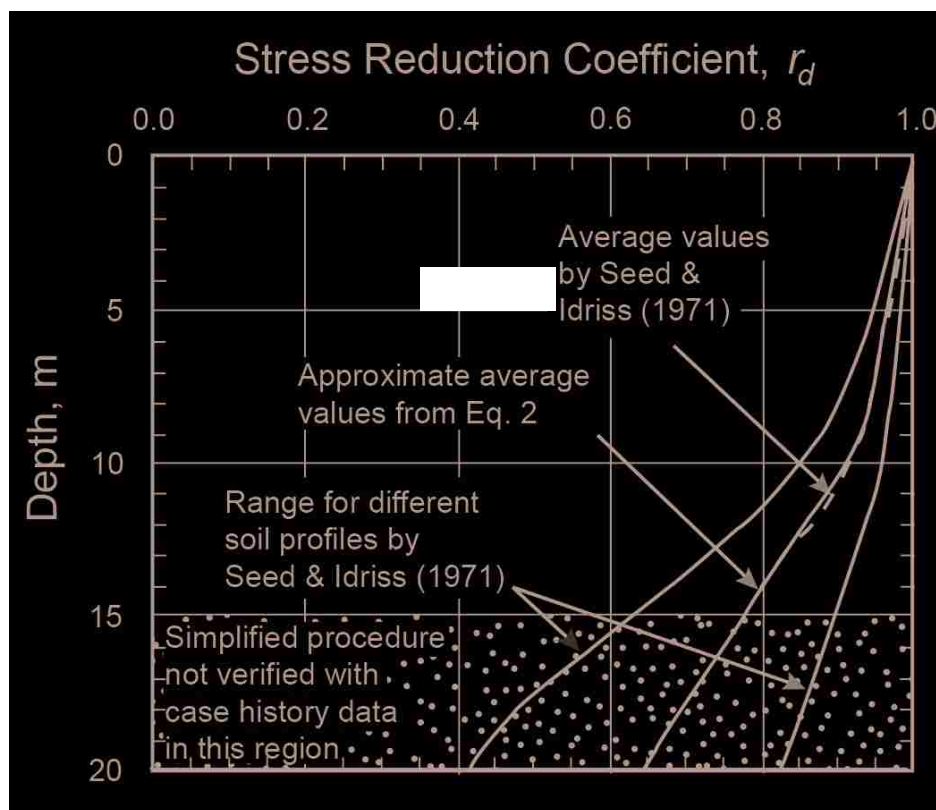


Figure 4-4: Comparison of depth reduction factors (Youd, Idriss et al. 2001).

The magnitude scaling factor, and the  $K_\sigma$  and  $K_\alpha$  factors were introduced to correct the value of CRR to a magnitude 7.5 earthquake and for overburden effects and in place static pressure affects that exist in the soil. The correction of CRR for these effects can be incorporated into the equation for the factor of safety against liquefaction. The new equation is shown below in Equation 18.

$$FS_{liq} = \frac{CRR_{M=7.5}}{CSR} * MSF * K_\sigma * K_\alpha \quad (18)$$

where MSF can be calculated using Equation (19),  $K_\sigma$  is a correction factor used to allow for nonlinear correction of the overburden pressure at depth which can be calculated using Equation(20), and  $K_\alpha$  is a correction factor used to correct for static stresses.

The magnitude scaling factor mentioned above can be found using several different equations in the NCEER procedure. Equation (20) was selected for this study because it is recommended by the workshop participants as the lower bound for MSF.

$$MSF = \frac{10^{2.24}}{M_w^{2.56}} \quad (19)$$

In this equation  $M_w$  is the moment magnitude of the scenario earthquake. Equation (19) was chosen for use in this study (Figure 4-5). It can be seen to more closely follow values from more recent studies (Cetin, Seed et al. 2004; Idriss and Boulanger 2010).

The factor,  $K_\sigma$ , was recommended for use by the workshop. The equation they recommended was given as:

$$K_\sigma = \sigma_v'^{(f-1)} \quad (20)$$

where the effective stress is raised to the f-1 power where f is a value dependent on relative density. For relative density values from 40 – 60%,  $f = 0.7-0.8$ .

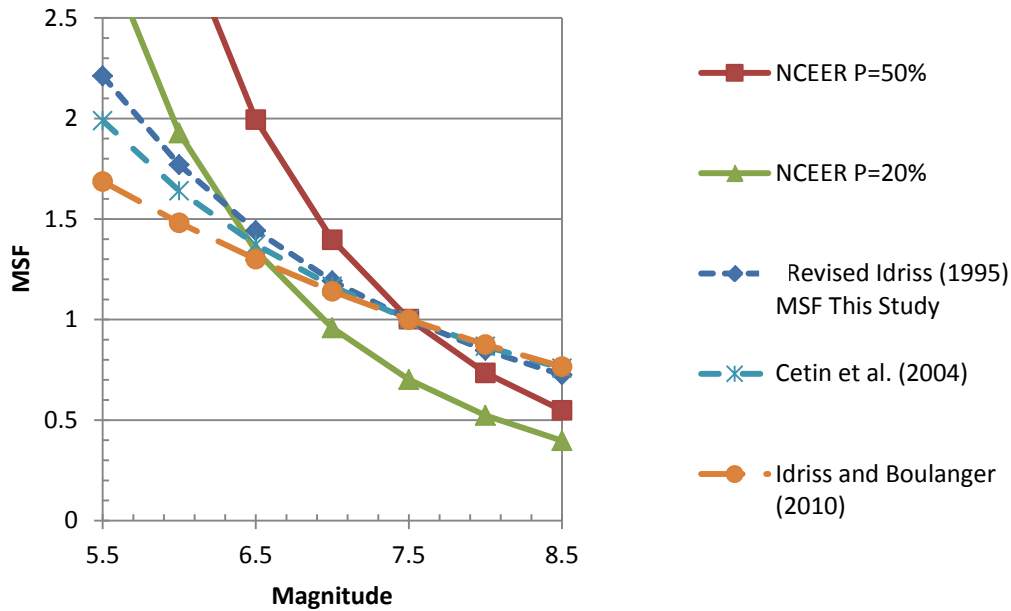


**Figure 4-5: Range of magnitude scaling factors (MSF).**

For relative density values from 60 – 80%,  $f = 0.6-0.7$ . Figure 4-6 shows the range of values that the NCEER formulation of this equation will yield using various  $f$  values.

The  $K_\alpha$  factor was originally meant to account for the fact that most of the data used in developing the liquefaction correlations came from level case histories. The NCEER workshop noted that this factor was “not to be used by non-specialists in geotechnical earthquake engineering or in routine engineering practice.” This recommendation came because of the wide range of published values available at that time. The workshop members felt that more research was needed before these factors could be routinely used by engineering practitioners.

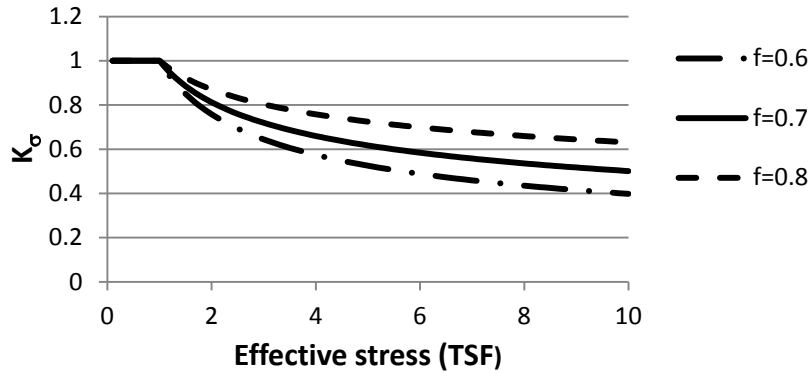


**Figure 4-6: range of values for  $K_\sigma$  using the NCEER equation (Youd, Idriss et al. 2001).**

### 4.3.3 Cetin and Seed et al. Procedure

Since the NCEER workshop there have been several advances that have led to the development of new relationships. One major advance was the development of statistical models that allowed engineers to develop more statistically sound relationships for the variables involved in a liquefaction analysis. The advancement of computational power in computing has also lent itself to the development of more robust relationships.

Cetin and Seed et al. (2004) developed a method that could be applied to deterministic analysis, although originally developed to allow the calculation of the probability of liquefaction. They made some changes to the previous work using statistical analysis to develop updated relationships. Their method also had the advantage of using a much larger data base than had been used in previous analysis, and this allowed for a more comprehensive statistical analysis. Some of the updates that were made included updates to the existing depth reduction factor relationships, updates to the way the cyclic resistance ratio is calculated, and updates to the scaling factors.

### 4.3.3.1 Updated Depth Reduction Factor

A new relationship for  $r_d$  was created using an updated database (Cetin and Seed 2004). This new  $r_d$  factor was of a more complex form. Some of the major changes that were made in this update were to incorporate the use of magnitude, acceleration, and shear wave velocity.

The shear wave velocity was incorporated into the equations using a term  $V_{s12}$ , which is the average shear wave velocity over the top 12 meters of the soil profile. This value can be found using the equation:

$$V_{s12m}^* = \frac{\sum_{i=1}^N t_i}{\sum_{i=1}^N t_i/V_{s_i}} = \frac{12m}{\sum_{i=1}^N \frac{t_i}{V_{s_i}}} \quad (21)$$

where  $t$  is the thickness of layer  $i$ , and  $V_{s,t}$  is the shear wave velocity of the given layer. This equation results in the geometric mean of the shear wave velocity for the upper 12 meters of the soil profile for layers  $i$  to  $N$ .

Using this new term, a new equation for the depth reduction factor was regressed. The regressions were performed on a data set created using a suite of synthesized values generated with computer models. The value of the depth reduction factor can be calculated using equation 22 for  $d < 20$  meters, and equation 23 for  $d$  values greater than or equal to 20m.

$$r_d = \left( \frac{\left( 1 + \frac{(-23.013 - 2.949a_{max} + 0.999M_w + 0.0525V_{s12})}{(16.258 + 0.201 \exp(0.341(-d + 0.0785V_{s12} + 7.586)))} \right)}{\left( 1 + \frac{(-23.013 - 2.949a_{max} + 0.999M_w + 0.0525V_{s12})}{(16.258 + 0.201 \exp(0.341(0.0785V_{s12} + 7.586)))} \right)} \right) \pm \sigma_{\epsilon_{r_d}} \quad (22)$$

$$r_d = \left( \frac{\left( 1 + \frac{(-23.013 - 2.949a_{max} + 0.999M_w + 0.0525V_{s12})}{(16.258 + 0.201\exp(0.341(-20 + 0.0785V_{s12} + 7.586)))} \right)}{\left( 1 + \frac{(-23.013 - 2.949a_{max} + 0.999M_w + 0.0525V_s)}{(16.258 + 0.201\exp(0.341(0.0785V_{s12} + 7.586)))} \right)} \right) - 0.0046$$

\* (d - 20) ± σ<sub>ε<sub>r<sub>d</sub></sub></sub>

(23)

where  $a_{max}$  is the maximum surface acceleration,  $M_w$  is the moment magnitude, and  $V_{s12}$  is the average shear wave velocity as found by Equation 22. It should be noted that  $V_{s12}$  is limited to a range from 120 m/s to 250 m/s.

A comparison of these relationships to those proposed by Seed and Idriss (1971) shows how the two relationships differ (Figure 4-7). The shapes of the depth reduction factor curve for the Seed and Idriss and the Cetin and Seed relationships are very different at shallower depths. Cetin and Seed et al. (2004) felt that the newer updated depth reduction factor was a more conservative relationship. Cetin and Seed et al. also felt that it was a better representation of what actually occurs in nature.

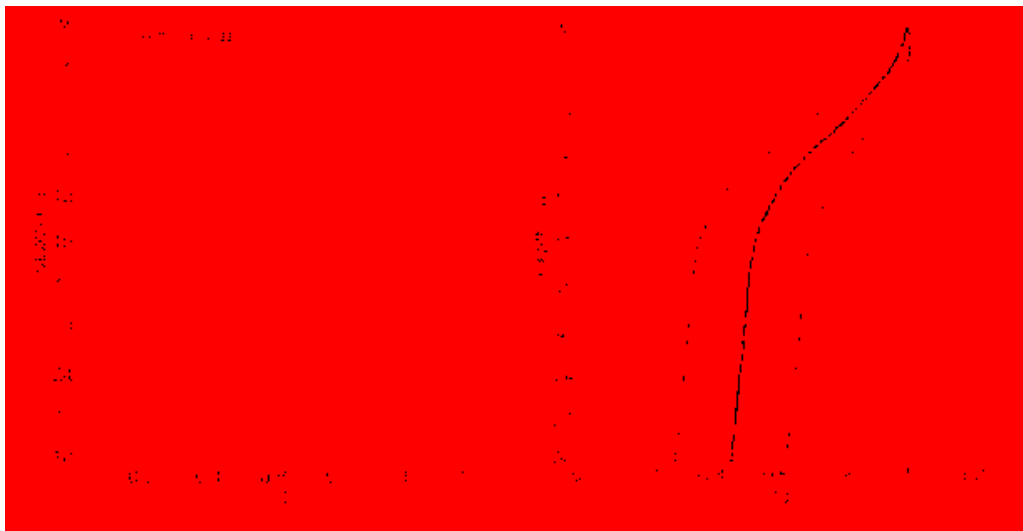


**Figure 4-7: Comparison of Seed and Idriss 1971 (solid black lines) to Cetin and Seed et al. 2004 (grey lines) afterCetin, Seed et al. (2004).**

### 4.3.3.2 Updated Cyclic Resistance Ratio

These new  $r_d$  relationships were used in conjunction with other parameters and an enlarged database to develop a new CRR equation using a bayesian updating analysis. The new equation for CRR is shown below:

$$CRR = \exp\left(\frac{(N_1)_{60}(1+\theta_1 FC) - \theta_2 \ln(M_w) - \theta_3 \ln\left(\frac{\sigma'_v}{P_a}\right) + \theta_4 FC + \theta_5 + \theta_6 \Phi^{-1}(P_L)}{13.32}\right) \quad (24)$$

where FC is fines content in percent,  $M_w$  is moment magnitude,  $\sigma'_v$  is the initial vertical effective stress,  $P_a$  is atmospheric pressure, and  $P_L$  is the probability of liquefaction which is set at 15% for a deterministic analysis. The measurement estimation error can be either included or removed by changing the values of  $\theta_1$ – $\theta_6$  (Table 4-2).

The CRR equation uses a standard cumulative normal distribution( $\Phi$ ) function of the probability which can be estimated in EXCEL© using a norm.s.dist function. A graph showing the location of this curve is shown below (Figure 4-8). The top portion of the graph (values of CSR greater than 0.4) was drawn in by hand and was recommended for use in deterministic analyses.

**Table 4-2: Model parameters (Cetin 2002)**

Case	Measurement/Estimation errors	$\theta_1$	$\theta_2$	$\theta_3$	$\theta_4$	$\theta_5$	$\theta_6$	$\sigma_\varepsilon$
I	Included	0.00	13.79	29.06	3.82	0.06	15.25	4.21
II	Removed	0.00	13.32	29.53	3.70	0.05	16.85	2.70

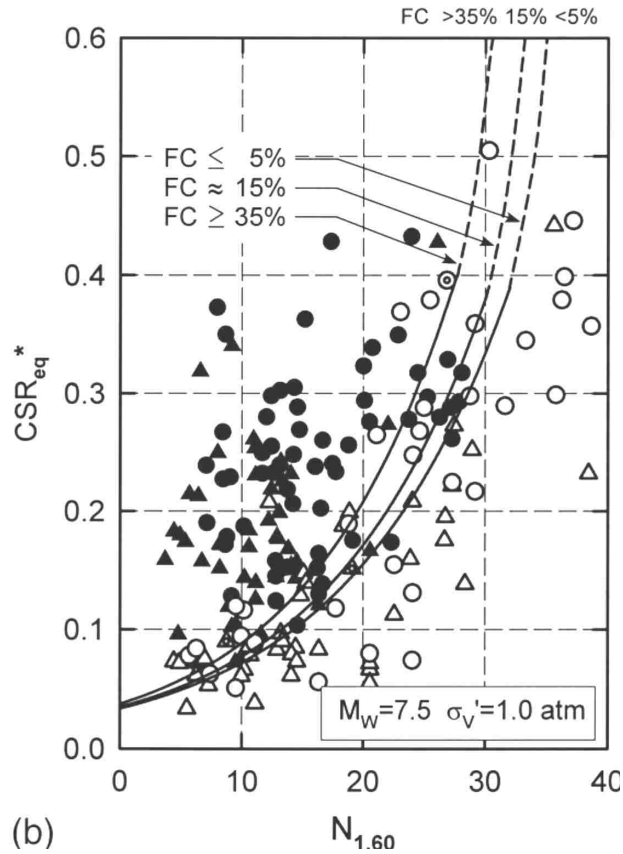


Figure 4-8:  $CSR_{eq}^*$  vs.  $N_{160}$  according to Cetin, Seed et al. (2004).

#### 4.3.3.3 Other Updates and Changes

The new relationships proposed by Cetin, Seed et al. (2004) has an assumed MSF built into it. The new MSF build into the CRR equation can be calculated seperatly for comparison and use. The MSF equation was found (Kramer 2008) to be,

$$DWF = MSF = \left(\frac{7.5}{M_w}\right)^{2.217} \quad (25)$$

where  $M_w$  is the moment magnitude, and DWF is the duration weighting factor which corresponds to the MSF in other procedures.



The new equation for CRR also has a built in fines correction for  $(N_1)_{60}$  to correct these values for clean sand. The form of this relationship can be found to be (Mayfield, Kramer et al. 2010):

$$(N_1)_{60cs} = (N_1)_{60} * C_{Fines} \quad (26)$$

$$C_{Fines} = (1 + \theta_1 FC) + \theta_5 \left( \frac{FC}{(N_1)_{60}} \right) \quad (27)$$

where FC is fines content in percent and  $\theta_1$  and  $\theta_5$  are both coefficients found through statistical regression as shown in Table 4-2.

#### 4.3.4 Idriss and Boulanger Procedure

An alternative update to the procedure proposed by Cetin, Seed et al. (2004) was presented by Boulanger and Idriss (2006). Their procedure was regressed using a slightly different database yielding a different set of changes. The changes proposed by Idriss and Boulanger were newer correction factors for the SPT, updates to the depth reduction factor, updates to the CRR equation, and other updates and changes.

##### 4.3.4.1 Updated SPT Blow Count Corrections

Idriss and Boulanger updated many of the correction factors used to correct  $N_{field}$  to the value for  $(N_1)_{60cs}$ . One of their updates was to the  $C_N$  coefficient. The new correction term as proposed by Idriss and Boulanger can be obtained from,

$$C_N = \left( \frac{P_a}{\sigma_v'} \right)^m \leq 1.7 \quad (28)$$

$$m = 0.784 - 0.0768 \sqrt{(N_1)_{60cs}} \quad (29)$$

where  $P_a$  is atmospheric pressure,  $\sigma_v'$  is the vertical effective stress,  $m$  is a parameter estimated using Equation 31, and  $(N_1)_{60cs}$  is the corrected clean sands value for  $N$ . Figure 4-4 shows the

relationship of  $C_N$  to Liao and Whitman's relationship. These graphs show that as effective stress increases, the value of  $C_N$  decreases, and as the value of  $(N_1)_{60cs}$  increases  $C_N$  increases. It is also of note that the values proposed by Idriss and Boulanger are bound on either side of the mean value proposed by Liao and Whitman in 1986 (Idriss and Boulanger 2010).

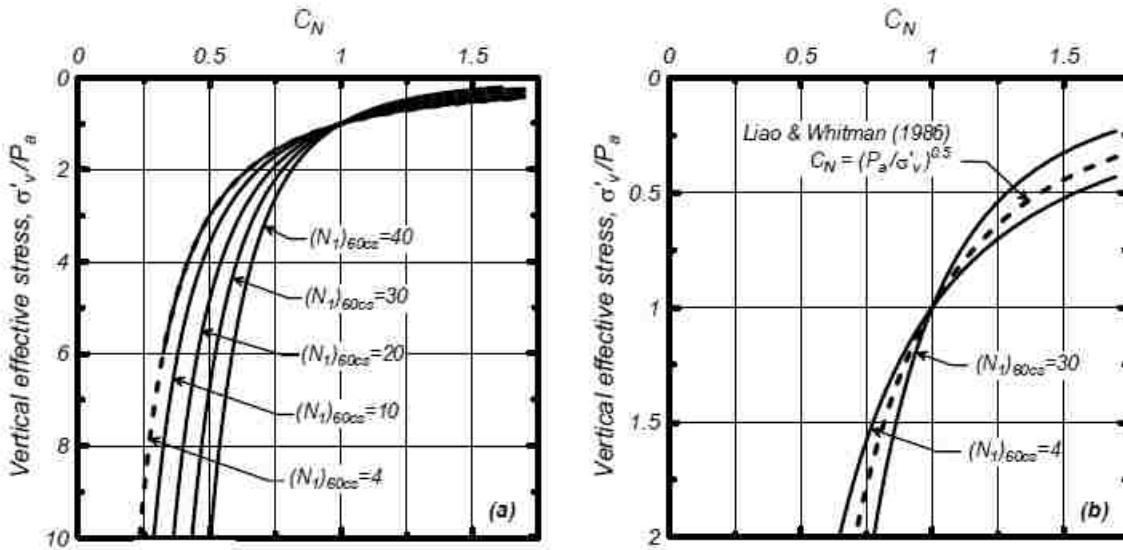


**Figure 4-9:  $C_N$  for Idriss and Boulanger compared to Liao and Whitman (Idriss and Boulanger 2010).**

Further updates were made to the equation used to determine the value of  $(N_1)_{60cs}$ . The new equations used are iterative in nature and are most easily solved in a spreadsheet or computer program. The new equation for the fines content correction is given as:

$$(N_1)_{60cs} = (N_1)_{60} + \Delta(N_1)_{60} \quad (30)$$

$$(N_1)_{60} = C_N C_E C_R C_B C_S N_{field} \quad (31)$$

$$\Delta(N_1)_{60} = \exp\left(1.63 + \frac{9.7}{FC+0.01} - \left(\frac{15.7}{FC+0.01}\right)^2\right) \quad (32)$$

where  $\Delta(N_1)_{60}$  is a term used to correct for fines content. The other factors include the energy correction factor ( $C_E$ ), the rod correction factor ( $C_R$ ), the borehole correction factor ( $C_B$ ), and the sampler type correction factor ( $C_S$ ). Except for the  $C_N$  value, these factors were not updated from the original NCEER procedure.

#### 4.3.4.2 Updated Depth Reduction Factor

Idriss and Boulanger developed an updated version of the depth reduction factor. The updated relationship took into account the effect of magnitude as well as depth. The new relationship for  $r_d$  is given as:

$$r_d = \exp(\alpha(z) + \beta(z)M_w) \quad (33)$$

$$\alpha(z) = -1.012 - 1.126 \sin\left(\frac{z}{11.73} + 5.133\right) \quad (34)$$

$$\beta(z) = 0.106 + 0.118 \sin\left(\frac{z}{11.28} + 5.142\right) \text{ for } z \leq 34m \quad (35)$$

where  $\alpha$  and  $\beta$  are coefficients that are dependent on depth ( $z$ ), and  $M_w$  is the moment magnitude. The results of this relationship are seen to be comparable to the relationship used by Idriss and Seed in 1971 (Figure 4-10).

Idriss and Boulanger used this simpler formulation for calculating  $r_d$  - which is dependent on magnitude and depth only - rather than the more complex formulation given by Cetin and Seed et al (2004) as they felt that the use of shear wave velocity, “adds another degree of complication and implied accuracy that is not warranted at this time.” (Idriss and Boulanger 2006).

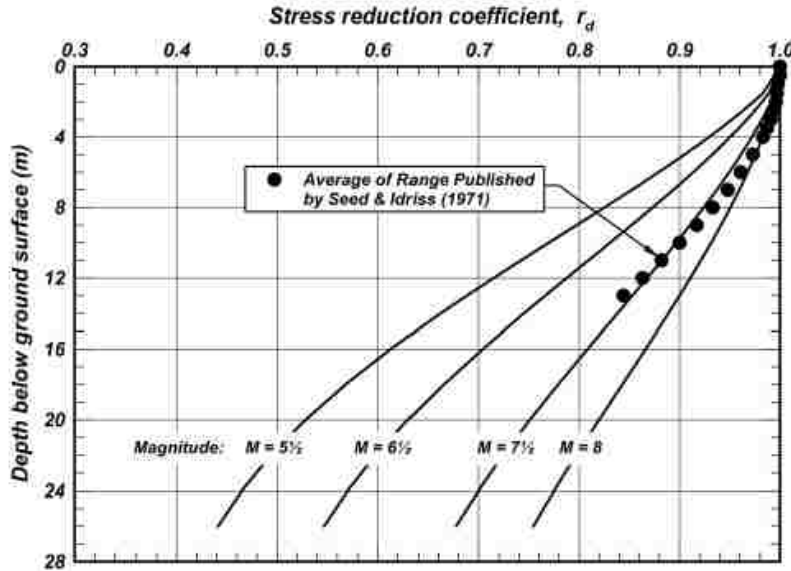


**Figure 4-10: Comparison of  $r_d$  Idriss and Boulanger to average  $r_d$  from Seed and Idriss 1971 (Idriss and Boulanger 2010).**

#### 4.3.4.3 Updated Cyclic Resistance Ratio

Idriss and Boulanger (2006) proposed a new form for the CRR equation. Their new equation was a polynomial of the form:

$$CRR_{M=7.5, \sigma'_v=1atm} = \exp\left(\frac{(N_1)_{60cs}}{14.1} + \left(\frac{(N_1)_{60cs}}{126}\right)^2 - \left(\frac{(N_1)_{60cs}}{23.6}\right)^3 + \left(\frac{(N_1)_{60cs}}{25.4}\right)^4 - 2.8\right) \quad (36)$$

where this equation uses CRR that corresponds to 1 atmosphere of overburden pressure and a magnitude of 7.5. The CRR calculated using this equation will need to be corrected for magnitude and overburden pressure using the MSF and  $K_\sigma$  correction factors. This will give the value of the CRR at the given value for  $(N_1)_{60cs}$  (Figure 4-11).

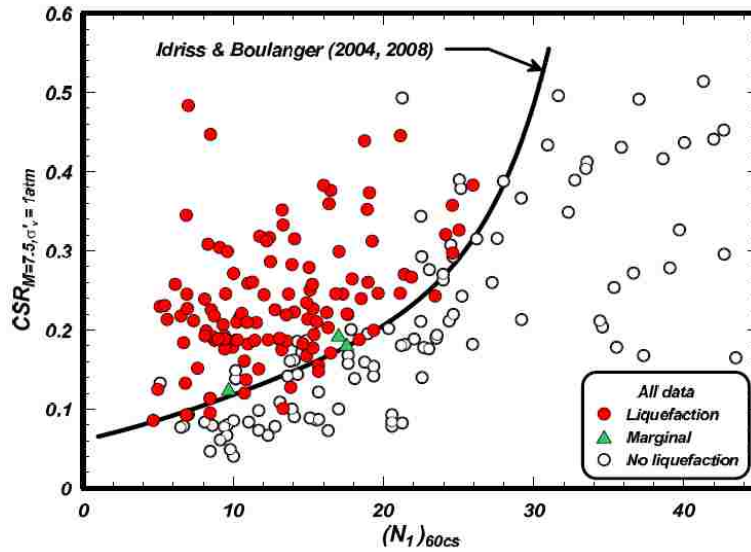


Figure 4-11: CRR curve for Idriss and Boulanger (Idriss and Boulanger 2010).

#### 4.3.4.4 Other Updates and Changes

Further modifications of the simplified procedure were made by Idriss and Boulanger to incorporate changes warranted by increased understanding and increased data sets. These other updates and changes included changes to the MSF,  $K_\sigma$ , and  $K_\alpha$ .

An update to the magnitude scaling factor was made as a result of a reevaluation by Idriss. The updated MSF equation was given as:

$$MSF = 6.9 \exp\left(-\frac{M_w}{4}\right) - 0.058 \leq 1.8 \quad (37)$$

This magnitude scaling factor was developed by Idriss in 1999 (Idriss and Boulanger 2006). It can be seen in Figure 4-12 to be in essentially the same range as several previous relationships and is close to the median values of the range defined by the relationships proposed by Seed and Idriss, and Cetin and Seed et al.

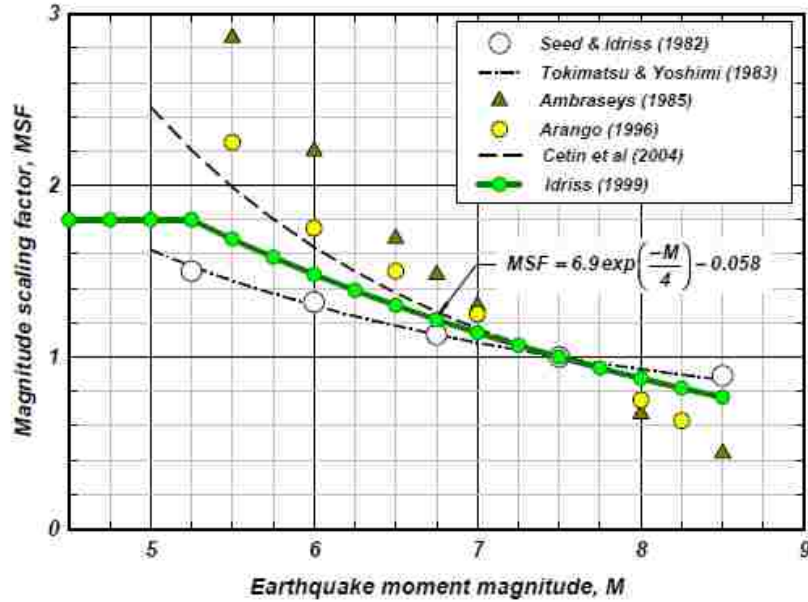


**Figure 4-12: MSF comparison of Idriss relationship to other relationships. (Idriss and Boulanger 2010).**

$K_{\sigma}$ , another important correction factor which must be applied, was updated and can be calculated by Idriss and Boulanger using the following equations (Idriss and Boulanger 2010).

$$K_{\sigma} = 1 - C_{\sigma} \ln \left( \frac{\sigma'_v}{P_a} \right) \leq 1.1 \quad (38)$$

$$C_{\sigma} = \frac{1}{18.9 - 2.55 \sqrt{((N_1)_{60cs})}} \leq 0.3 \quad (39)$$

In these equations  $\sigma'_v$  is the initial effective vertical stress of the layer,  $P_a$  is the atmospheric pressure, and  $C_{\sigma}$  is a factor which incorporates the effect of SPT blow count. The equations yield a relationship that can be seen in Figure 4-13 where the values are shown to decrease with increasing  $(N_1)_{60cs}$  and increasing effective stress. Thus, as we move deeper into the soil profile, the  $K_{\sigma}$  value will decrease the value of the CRR.

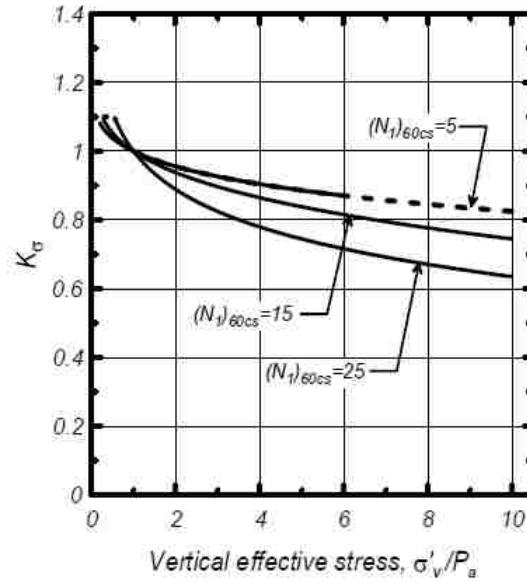


**Figure 4-13: Idriss and Boulanger  $K_G$  relationship (Idriss and Boulanger 2010).**

Idriss and Boulanger's continued research into liquefaction resulted in a new set of relationships for  $K_\alpha$  (Boulanger 2003) as well. The new relationship uses the following equations:

$$K_\alpha = a + b * \exp\left(-\frac{\xi_R}{c}\right)$$

$$\xi = \frac{1}{Q - \ln\left(\frac{100\sigma'}{P_a}\right)} - D_R$$

$$\alpha = \frac{\tau}{\sigma'}$$

$$a = 1267 + 636\alpha^2 - 634 \exp(\alpha) - 632 \exp(-\alpha)$$

$$b = \exp[-1.11 + 12.3\alpha^2 + 1.31 \ln(\alpha + 0.0001)]$$

$$c = 0.128 + 0.126\alpha + 2.52\alpha^3$$

$$\text{limits: } \alpha \leq 0.35 ; -0.6 \leq \xi_R \leq 0.1$$

(40)

where  $\alpha$  is initial shear stress over the initial effective consolidation stress,  $\xi$  is the state parameter which is a function of relative density ( $D_R$ ), and material type index number ( $Q$ ) used to represent the mineralogy of the soil (see for details), and  $a$ ,  $b$ , and  $c$  are coefficients found using the equations shown. It is important to note in these equations the limits that apply to  $\alpha$  and  $\xi$ . These limits represent the range over which the equation is valid.

#### 4.4 Empirical Probabilistic Methods

Probabilistic methods are valuable because they tell you more about how the data is spread and allow an engineer to more systematically handle error than can be done using deterministic methods alone. Several different methods exist for performing such an empirical probabilistic analysis including Cetin and Seed et al. (2004), Boulanger and Idriss (2012), and Juang, Ching et al. (2012).

##### 4.4.1 Early Procedures

Early efforts to quantify the probability of liquefaction were made by several researchers (Liao, Veneziano et al. 1988; Youd and Noble 1997; Toprak, Holzer et al. 1999). These early analysis used much smaller data sets, as there was less data available at the time.

Liao et al (1988) used a small data set and developed statistical relationships which would give the probability of liquefaction occurring. One model proposed (Liao, Veneziano et al. 1988) gave the probability of liquefaction as follows.

$$P_L = \frac{1}{1 + \exp[-\beta_0 + \beta_1 * \ln(CSR) + \beta_2 * (N_1)_{60}]} \quad (41)$$

In this equation  $P_L$  is the probability of liquefaction and  $\beta_0 - \beta_2$  are coefficients determined by the analysis.



This form of the equation was notable in that it was one of the first attempts to quantify probability in this manner. Youd and Noble further advanced this work by adding magnitude as a parameter in their analysis. They proposed a liquefaction relationship of the form,

$$\ln(CRR) = 2.466 - 0.7289M_w + 0.0834(N_1)_{60cs} + 0.3231 * \ln\left(\frac{P_L}{1-P_L}\right) \quad (42)$$

where  $P_L$  is the probability of liquefaction occurring and  $(1-P_L)$  is the probability of liquefaction not occurring (Youd and Noble 1997). In other words, if liquefaction is predicted to occur, there is a  $(1-P_L)$  probability that liquefaction will not occur. Although not widely used in practice, this relationship shows the first attempt to quantify liquefaction in terms of Magnitude,  $(N_1)_{60cs}$ , and  $P_L$ . This is a notable improvement of the initial work of Liao (1988).

Further work was conducted in this area by Toprak, Holzer et al. (1999). The form of the equation used was,

$$\text{Logit}(P_L) = \ln\left(\frac{P_L}{1-P_L}\right) = 10.4459 - 0.2295(N_1)_{60cs} + 4.0573 * \ln\left(\frac{CSR}{MSF}\right) \quad (43)$$

This work was notable in that this form of the equation was more accurate for the data set used by Toprak et al which was a larger data set than had been used previously and included the data set that had been used by Youd et al (Toprak, Holzer et al. 1999).

More recently, researchers have used newer and larger databases, an increased understanding of statistical analysis, and the greater computing power available to develop more robust relationships for use in engineering practice (Cetin, Seed et al. 2004; Boulanger and Idriss 2012; Juang, Ching et al. 2012).

#### 4.4.2 Cetin and Seed et al. Procedure

Progress was made when a much larger database was used with a Bayesian model assessment technique to develop new equations for use in probabilistic liquefaction triggering analysis (Cetin 2002).

$$P_L = \Phi \left( -\frac{N_{1,60}(1+\theta_1 FC) - \theta_2 \ln(CSR_{eq}) - \theta_3 \ln(M_w) - \theta_4 \ln\left(\frac{\sigma'_v}{P_a}\right) + \theta_5 FC + \theta_6}{\sigma_\epsilon} \right) \quad (44)$$

This equation is of a similar form to the CRR equation used in the deterministic analysis. The equation was modeled both with and without parameter uncertainty with values obtained as given above in the deterministic section. This was a notable advance over previous studies, both deterministic and probabilistic, as it enabled an engineer to arrive at a value for either  $CSR_{eq}$  or  $P_L$  directly instead of requiring multiple calculations. Built into this equation are both the MSF and FC corrections.

Cetin and Seed et al. (2004) felt that the new relationship was improved over previous relationships for several reasons. Older relationships had used a smaller, and in some cases, less robust database for their analysis. The new database used by Cetin and Seed et al. was larger than previous databases. Most other regressions had used a basic binary regression and left some values such as FC and MSF as a priori (meaning they were not regressed as a part of the relationship, but instead found FC and MSF values from previously developed relationships).

Finally, in the case of Juang and Ching et al. (2002) which had used more robust statistical methods, the relationships used data which Cetin et al. felt had “some questionable cases included” in the analysis (Cetin, Seed et al. 2004). Cetin and Seed et al. (2004) further improved their data quality by taking into account the bias in the collected data toward liquefied sites. They found a bias had been created by the fact that researchers had focused more on sites

that liquefied when gathering data. The magnitude of this bias was felt to probably be about 1.5 to 1 for liquefied to non-liquefied sites (Cetin 2002) .

The Cetin and Seed et al. probabilistic analysis has been widely used in literature to further the field of earthquake engineering and liquefaction analysis. In areas such as settlement, liquefaction initiation, and performance-based design, the Cetin and Seed et al. probabilistic model and the database developed in the process of the development of that method have been used successfully by several researchers as a basis from which to expand earthquake engineering (Kramer and Mayfield 2007; Kramer 2008; Mayfield, Kramer et al. 2010).

#### 4.4.3 Boulanger and Idriss Procedure

The Boulanger and Idriss (2012) procedure has recently been published as an alternative to the Cetin, Seed et al. (2004) model. This new model uses a database similar to the one used by the Cetin, Seed et al. (2004) model with a few key differences which they felt better represented the data. Boulanger and Idriss felt that these differences were critical to the formulation of an accurate equation.

The new model proposed by Boulanger and Idriss was similar in form to their deterministic model. The formulation of the equation chosen by Boulanger and Idriss is,

$$P_L = \Phi \left( - \frac{\left( \frac{(N_1)_{60cs}}{14.1} + \left( \frac{(N_1)_{60cs}}{126} \right)^2 - \left( \frac{(N_1)_{60cs}}{23.6} \right)^3 + \left( \frac{(N_1)_{60cs}}{25.4} \right)^4 - 2.67 - \ln(CSR_{M=7.5, \sigma'_v=1atm}) \right)}{\sigma_{\ln(R)}} \right) \quad (45)$$

where  $\sigma_{\ln(R)}$  is the standard deviation with respect to the CRR, CSR is corrected for magnitude and overburden, and  $(N_1)_{60cs}$  is the SPT blow count value corrected to a clean sand value using the equations from the deterministic approach.

Boulanger and Idriss in their paper, proposed an equation for dealing with the standard deviation for their analysis. Their equation allows the engineer to break up the standard deviations from CSR, CRR and the SPT (N) value. Using their equation it is possible to find a total overall standard deviation.

$$\sigma_{tot}^2 = \left( \frac{1}{14.1} + \frac{2N}{126^2} - \frac{3N^2}{23.6^3} + \frac{4N^3}{25.4^4} \right)^2 (\sigma_N)^2 + (\sigma_{\ln(R)})^2 + (\sigma_{\ln(s)})^2 \quad (46)$$

The total standard deviation,  $\sigma_{tot}$ , is defined in terms of  $\sigma_N$  - the standard deviation with respect to N,  $\sigma_{\ln(R)}$  - the standard deviation with respect to CRR, and  $\sigma_{\ln(s)}$  - the standard deviation with respect to CSR. Using this equation it is possible to compute the standard deviation for the actual data used. Examples of values would be to use a  $COV_N = 0.2$ ;  $\sigma_{\ln(s)} = 0.2$ ;  $\sigma_{\ln(R)} = 0.15$ . The standard deviation of the SPT blow count ( $\sigma_N$ ) will equal  $COV_N * N$ . In this way, a systematic approach to the amount of variation in the equation for a specific site can be arrived at and used in the analysis, such that the parameter estimation error is included.

Boulanger and Idriss (2012) agreed with Cetin and Seed et al (2004) that the data should be weighted to account for a bias in the data towards liquefied sites. They accounted for this bias using the same values used by Cetin and Seed et al (2004). However, due to the differences in their databases, their equations yield substantially different curves for CRR.

#### 4.4.4 Juang and Ching et al. Procedure

Another model, recently put forth as an alternative to the Cetin et al (2004) probabilistic model, is the Juang and Ching et al. (2012) model. This model uses the same database as was used by Boulanger and Idriss (2012), but uses slightly different assumptions. Juang and Ching et al. used a variety of models in their regression of the data, and chose to not weight the data to account for the fact that the number of liquefied sites where data was collected might be greater

than the number of non-liquefied sites where data was collected. The form of the equation which they recommended for use in practice was (Juang, Ching et al. 2012),

$$P_L = \frac{1}{1 + \exp\left[-7.55\left(0.95 - \frac{CRR((N_1)_{60CS})}{CSR}\right)\right]} \quad (47)$$

where the CRR and CSR are calculated using the method proposed by Idriss and Boulanger (2010).

Juang and Ching et al. (2012) used a different set of starting assumptions and a different statistical method for regressing their equations. It has the disadvantage for comparison purposes of having used the Boulanger and Idriss data set, as well as their form of the CRR and CSR equations; and as such, any errors or advantages therein are inherently included. This model also did not remove parameter uncertainty from the final equation.

## **5 PERFORMANCE-BASED EARTHQUAKE ENGINEERING**

Performance-based engineering is a recent development in engineering that came about as researchers began to seek reliable standards to deal with increasing socio- economic risks posed by seismic events in urban areas (Franke 2011). Performance-based engineering allows the development of risk and hazard analyses which deal with risk in a much more consistent and systematic way. Deterministic approaches to analysis and design tend to yield a binary solution set: either it fails or it passes. These deterministic relationships can be inconsistent in the evaluation of hazard (Kramer and Mayfield 2007) and do not communicate risk adequately to all stakeholders. The communication of risks and evaluation of safety have often been dealt with by engineers in a haphazard and subjective manner in the past using factors of safety and other such methods of analysis. The introduction of the performance-based framework by the Pacific Earthquake Engineering Research center (PEER) has helped deal with these issues in a more systematic way and allowed increased communication among all stakeholders.

### **5.1 PEER Performance-Based Framework**

To change the way engineers deal with hazards, performance-based earthquake engineering (PBEE) is being developed and researched by the Pacific Earthquake Engineering Research center (PEER). By developing tools for performance-based design, engineers and owners are better able to communicate and understand the risks and hazards associated with a

projects. The performance-based framework focuses on a systems level approach, which allows an engineer to understand how the entire system will react with respect to loss of life, risk of failure, costs, and other parameters (Faris 2004; Franke 2011; Boulanger 2013).

Performance-based design is critical to the future of earthquake engineering. It is through performance-based design that the overall impact of an earthquake on society as a whole can be examined and questions of importance to engineers, owners, and society answered. It enables engineers and others to examine costs and risks in terms of impact and cost to society both short and long term. For example, society may feel that the risks posed by the failure of a hospital building or civic center justify the extra cost associated with increased safety. With performance-based design, such a goal is quantifiable, and the cost and benefits could be clearly calculated and understood. With deterministic design, it is difficult or impossible to quantify what the exact cost to benefit ratio might be and where the most improvement in safety might be achieved. Performance-based design enables design criteria to be shaped by needs and costs from all aspects of the project and community in a logical and quantifiable way.

The PEER framework was developed to meet the needs of both engineers and society as a whole. The PEER framework facilitates designing to such criteria as fully operational, operational, life safety, and near collapse (Faris 2004). This allows engineers to design to meet the needs of a project, rather than designing all buildings to meet the same criteria. For critical structures such as hospitals, fire stations, and police stations, an engineer can now design these buildings to be operational during an earthquake, rather than simply designing them to not collapse during an earthquake. Other structures which are less critical such as fast food places, malls, or other structures can be designed to life safety criteria. The PEER performance-based

framework gives the engineer flexibility in the design that is helpful in creating structures that meet the needs of the public.

### 5.1.1 Framework Parameters

The framework proposed by PEER consists of all the parameters associated with a project and the desired outcome. These parameters are the intensity measure (IM), the engineering demand parameter (EDP), the damage measure (DM), and the decision variables (DV) (Kramer and Mayfield 2007). These parameters can be combined together using the total probability theorem. This theory can be applied to engineering applications using,

$$\lambda_{dv} = \sum_{k=1}^{N_{DM}} \sum_{j=1}^{N_{EDP}} \sum_{i=1}^{N_{IM}} P[DV > dv^* | DM = dm_k] * P[DM = dm_k | EDP = edp_j] * P[EDP = edp_j | IM = im_i] \Delta \lambda_{im_i} \quad (48)$$

In this equation  $N_{DM}$  is the number of increments for DM,  $N_{EDP}$  is the number of increments for EDP,  $N_{IM}$  is the number of increments for IM,  $P[a|b]$  is the probability of a given b, and  $\lambda_{DV}$  is the mean annual rate of exceedance with respect to various levels of DV (Kramer and Mayfield 2007). This equation is a numerical approximation of the triple integral. The greater the number of iterations computed (i.e. the larger the values for  $N_{DM}$ ,  $N_{EDP}$ , and  $N_{IM}$ ), the more accurate the equation becomes (Franke 2011).

This equation can be used to create a hazard curve for the desired output as long as valid relationships are maintained. In the case of a liquefaction analysis, this framework allows for the creation of a hazard curve relating the EDP of liquefaction initiation ( or  $FS_{liq}$ ) to the IM of  $a_{max}$  and magnitude using a fragility relationship.



### 5.1.2 Hazard and Fragility Curves

A fragility curve is a curve developed based on the probability of an event. Fragility relationships are usually given in the form of an equation for probability. Relationships for liquefaction initiation have been developed by Cetin, Seed et al. (2004), Juang, Ching et al. (2012), and Boulanger and Idriss (2012) and a discussion of these probabilistic relationships was shown previously. A comparison of the three different fragility curves developed using these relationships is shown for a hypothetical site in Figure 5-1.

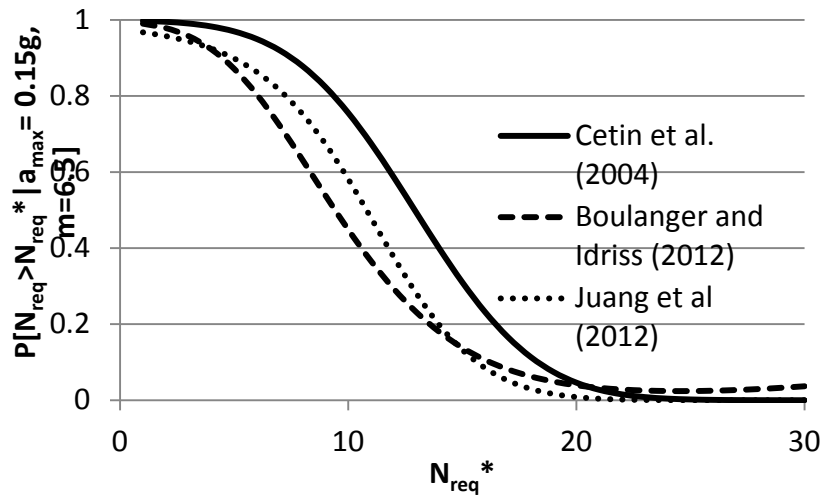


**Figure 5-1: Fragility curves for liquefaction initiation ( $M_w = 6.5$ ;  $a_{max} = 0.15$  g).**

Using these fragility curves within the framework of the PEER method, it is possible to develop a hazard curve that represents the liquefaction initiation hazard. This is done by using a numerical approximation of the integral over the hazard.

Hazard curves are useful because they allow an engineer to more fully grasp the risks involved with a selected level of hazard. They can also help the engineer determine if a little more investment will or will not increase the safety of the building dramatically, thus allowing a better assessment of where money should be spent.

A good example of this is shown below in Figure 5-2 for a theoretical location and soil profile. In this theoretical analysis, the hazard curve shows that very small change in the factor of safety can yield both large and small changes in the return period of liquefaction. In this example increasing the factor of safety from 0.75 to 1.00, an increase of 0.25, yields a change in the mean annual rate of NON exceedance of almost a factor of 10. A similar change, from 1.00 to 1.25, yields a much smaller increase in the mean annual rate of NON exceedance. Thus the cost effectiveness can be much smaller at larger factors of safety than at smaller factors of safety. Using a hazard curve, an engineer can see at what point the diminishing returns no longer justify the expense of increased safety. A more detailed discussion of the development of hazard curves for liquefaction is given later.

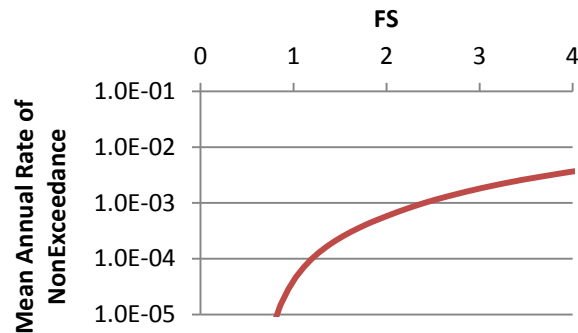


**Figure 5-2: Hazard curve FS vs. mean annual rate of nonexceedance.**

## 5.2 Performance-Based Liquefaction Initiation

The above principles can be applied to a liquefaction analysis. In the case of a liquefaction analysis, there are two intensity measures associated with the probability of liquefaction. These are  $a_{max}$  and magnitude, which are obtained from a PSHA and are dependent upon the GMPE's and seismic source models used to develop the PSHA. These can then be

related to the EDP which in this case is either the factor of safety against liquefaction ( $FS_{liq}$ ) or the SPT blow count required to prevent liquefaction ( $N_{req}$ ). This sort of application of the PEER PBEE framework to liquefaction initiation potential was first undertaken by Kramer and Mayfield (2007) and was considered by many to be a landmark effort.

### 5.2.1 Cetin et al. Performance-Based Procedure

Kramer and Mayfield (2007) recognized that the new framework proposed by PEER could be applied to the problem of liquefaction initiation. This was a considerable advantage over previously used deterministic methods as it was shown to allow for a more consistent comparison of liquefaction initiation potential across sites of varying seismicity (Kramer and Mayfield 2007).

In order to develop a performance-based liquefaction analysis, some modifications to the existing PEER PBEE framework had to be made. Kramer and Mayfield (2007) first modified the equation from a probability of exceedance to a probability of non-exceedance. This allows for the determination of the probability of  $FS_{liq}$  being less than  $FS_{liq}^*$  for a given IM.

$$\Lambda_{FS_L^*} = \sum_{i=1}^{N_{IM}} P(FS_L < FS_L^* | IM_i) \Delta \lambda_{IM_i} \quad (49)$$

They stated that this form of the equation was used, “because non-exceedance of a particular factor of safety represents an undesirable condition, just as exceedance of an intensity measure does” (Kramer and Mayfield 2007). This form of the equation uses the mean annual rate of nonexceedance ( $\Lambda$ ) instead of the mean annual rate of exceedance ( $\lambda$ ) (Kramer and Mayfield 2007).

Another modification by Kramer and Mayfield (2007) was made to address the issue of IM sufficiency. Kramer and Mayfield pointed out that IM sufficiency does not exist for liquefaction

initiation analysis and that the equation must be modified in order to address this problem. They were able to make these adjustments and incorporate both  $a_{max}$  and  $m_j$  into one equation for the assessment of liquefaction initiation, where  $\Delta\lambda_{a_{max},m_j}$  is a term understood to be the incremental mean annual rate of exceedance for a single value of  $a_{max}$  and  $m_j$  (Kramer and Mayfield 2007).

$$\Lambda_{FS_L^*} = \sum_{j=1}^{N_{m_j}} \sum_{i=1}^{N_{a_{max}}} P(FS_L < FS_L^* | a_{max_i}, m_j) \Delta\lambda_{a_{max_i}, m_j} \quad (50)$$

In this equation,  $P(FS_{liq} < FS_{liq}^* | a_{max}, m_j)$  can be replaced by the relationship proposed by Cetin and Seed et al. (2004) for the probability of liquefaction, modified such that it is in terms of  $FS_{liq}$ .

The equation can then be given as,

$$P[FS_{liq} < FS_{liq}^* | a_{max}, m_j] = \Phi \left[ -\frac{N^*(1+\theta_1 FC) - \theta_2 \ln(CSR_{eq} * FS_{liq}^*) - \theta_3 \ln(m_j) - \theta_4 \ln\left(\frac{\sigma'_v}{P_a}\right) + \theta_5 FC + \theta_6}{\sigma_\epsilon} \right] \quad (51)$$

where  $N^*$  is  $(N_1)_{60}$ ,  $CSR_{eq}$  is the cyclic stress ratio as given by Cetin and Seed et al. (2004), and  $m_j$  is the moment magnitude elsewhere shown as  $M_w$ . It is important to note that  $CSR_{eq}$  is calculated using a value of  $a_{max}$  corresponding to the event and  $m_j$  is the magnitude of that event. This allows for a performance-based approach to be applied over the entire range of possible  $a_{max}$  and  $m_j$  values for a set of events.

Equations 49 and 50 are useful in running a performance-based liquefaction initiation analysis. Kramer and Mayfield, however, were able to take it one step further and relate the return period of liquefaction to the  $N$  value.

$$\lambda_{N_{req}^*} = \sum_{j=1}^{N_{m_j}} \sum_{i=1}^{N_{a_{max}}} P(N > N_{req}^* | a_{max_i}, m_j) \Delta\lambda_{a_{max_i}, m_j} \quad (52)$$

where the term  $\lambda_{N_{req}^*}$  is the mean annual rate of exceedance for the  $N$  value, or in other words, the mean annual rate of liquefaction initiation.  $P(N_{req} > N_{req}^* | a_{max}, m_j)$  can be given by the

relationship shown in equation 52, and will be shown in equations hereafter as  $P_L$ . The probability of liquefaction ( $P_L$ ) is a function that represents the fragility curve. Thus the hazard curve with respect to magnitude and acceleration is used with the fragility function for the probability of liquefaction to determine the hazard curve of the mean annual rate of exceedance for liquefaction initiation. In this way the probability that any given value of SPT blow count being greater than the required blow count (i.e.  $N_{req} > N_{req}^*$ ) for the hazard can be found with a sum of probabilities. In this way a hazard curve for any value of SPT blow count can be developed (Figure 5-3).

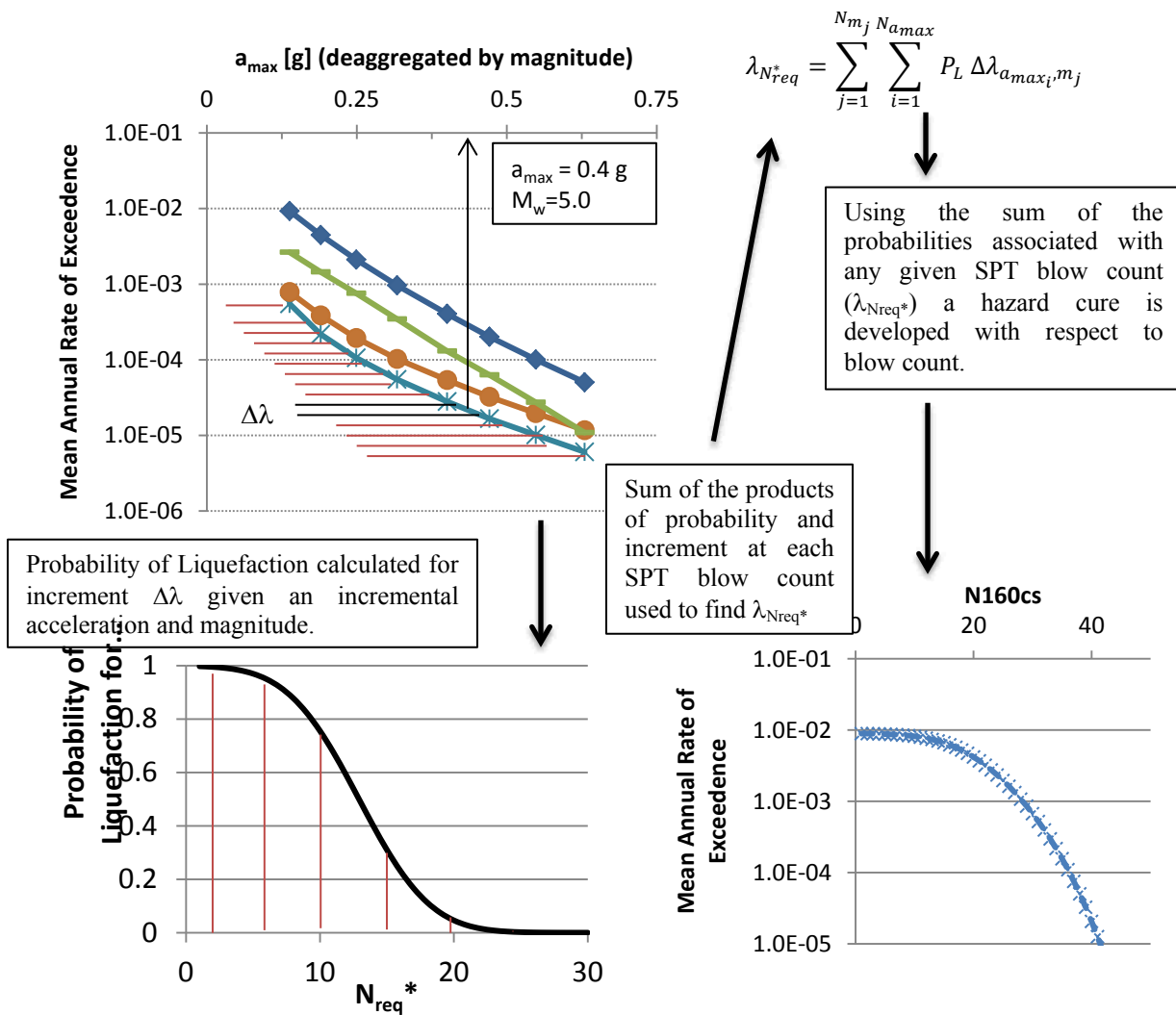


**Figure 5-3: Process of developing hazard curves for liquefaction initiation.**

$P_L$  can be found using a modification of the Cetin and Seed et al (2004) form of the equation as well. This modification can be made to obtain an equation in terms of  $(N_1)_{60cs}$  by removing the fines content correction from the equation (Mayfield, Kramer et al. 2010).

$$P_L = \Phi \left( -\frac{(N_1)_{60cs}^* - \theta_2 \ln(CSR_{eq}) - \theta_3 \ln(m_j) - \theta_4 \ln\left(\frac{\sigma'_v}{Pa}\right) + \theta_6}{\sigma_\epsilon} \right) \quad (53)$$

Since the time when this performance-based method was developed by Kramer and Mayfield (2007), other authors have called certain points of the database used by Cetin and Seed et al. (2004) into question (Idriss and Boulanger 2010). In order to allow for a more complete understanding of the problems or advantages of using the Cetin and Seed et al. model in the Kramer performance-based framework, two other recently published models (Boulanger and Idriss 2012; Juang, Ching et al. 2012) were used to develop a new set of performance-based liquefaction triggering relationships.

### 5.2.2 Incorporation of Boulanger and Idriss Probabilistic Model

In order to use the Boulanger and Idriss probabilistic model in the framework established by Kramer and Mayfield (2007), it is necessary to make some modifications to the proposed probabilistic relationship such that it will be in terms of  $a_{maxi}$ , and  $m_j$ . This form of the equation can be seen below in equation 53.

$$P_L = \Phi \left( -\frac{\frac{(N_1)_{60cs}^*}{14.1} + \left(\frac{(N_1)_{60cs}^*}{126}\right)^2 - \left(\frac{(N_1)_{60cs}^*}{23.6}\right)^3 + \left(\frac{(N_1)_{60cs}^*}{25.4}\right)^4 - 2.67 - \ln(CSR)}{\sigma_{tot}} \right) \quad (54)$$

In this equation CSR is in terms of  $a_{maxi}$ ,  $m_j$ , and  $(N_1)_{60cs}^*$ .  $(N_1)_{60cs}^*$  replaces  $(N_1)_{60cs}$  in this formulation of the equation to allow for computation of the required  $(N_1)_{60cs}^*$  to resist liquefaction.

The term for total standard deviation can be found using equation 54 (shown below for convenience).

$$\sigma_{tot} = \left( \left( \frac{1}{14.1} + \frac{2N}{126^2} - \frac{3N^2}{23.6^3} + \frac{4N^3}{25.4^4} \right)^2 (\sigma_N)^2 + \sigma_{lnR}^2 + \sigma_{lnS}^2 \right)^{.5} \quad (55)$$

A total error term can be solved for the equation both with and without parameter estimation error included (Table 5-1). Boulanger and Idriss felt that this form of the total standard deviation equation was useful as it allowed for the accounting of variations in N, CRR, and CSR.

The use of the equation provided by Boulanger and Idriss was found to provide reasonable values within the range of  $(N_1)_{60cs}$  from 1 – 20. However, outside of these bounds the equation begins to return unreasonably large values (Figure 5-4). This would not normally be a problem in the deterministic sense as soils with  $(N_1)_{60cs} > 30$  are not usually evaluated for liquefaction initiation and are often considered to be unable to liquefy.

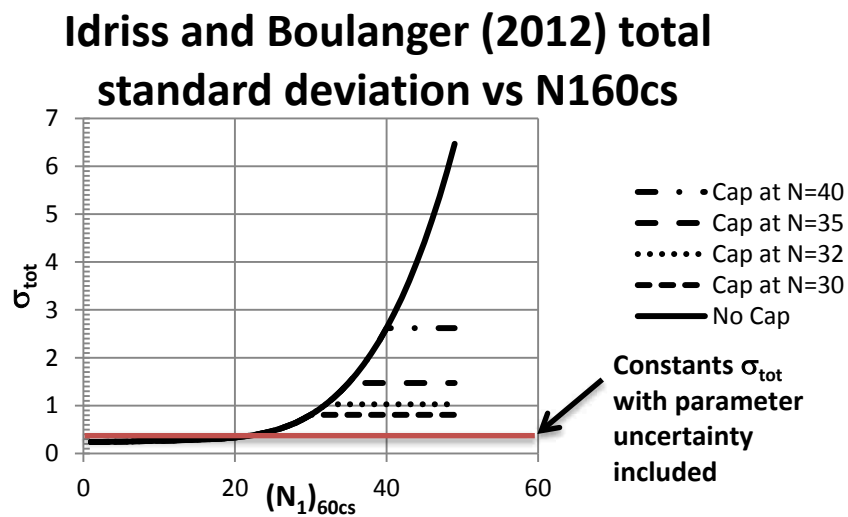


**Figure 5-4: Boulanger and Idriss (2012) total standard deviation curve.**

When using a performance-based approach, however, a range of values are applied and the incorporation of an overly large  $\sigma_{tot}$  causes the hazard curves developed from this calculation to be inaccurate (Figure 5-5). This is primarily due to the shape of the fragility curve which can be seen to increase at larger SPT blow counts (Figure 5-6).

In order to keep the values for the total standard deviation within a reasonable range when using the error calculation as originally proposed by Boulanger and Idriss a cap of  $(N_1)_{60cs} = 30$  was applied to the equation. The effect of the cap on the total standard deviation can be seen in Figure 30 with the effect of using caps other than 30 also shown.

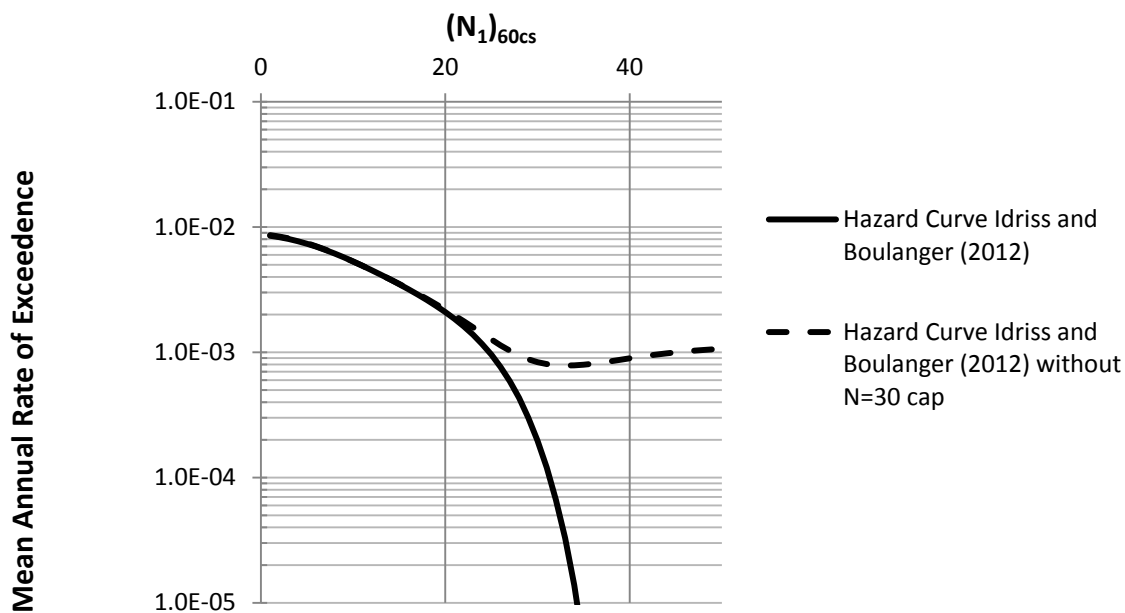


**Figure 5-5: Typical performance-based hazard curve developed using Boulanger and Idriss equations with and without  $N=30$  cap.**



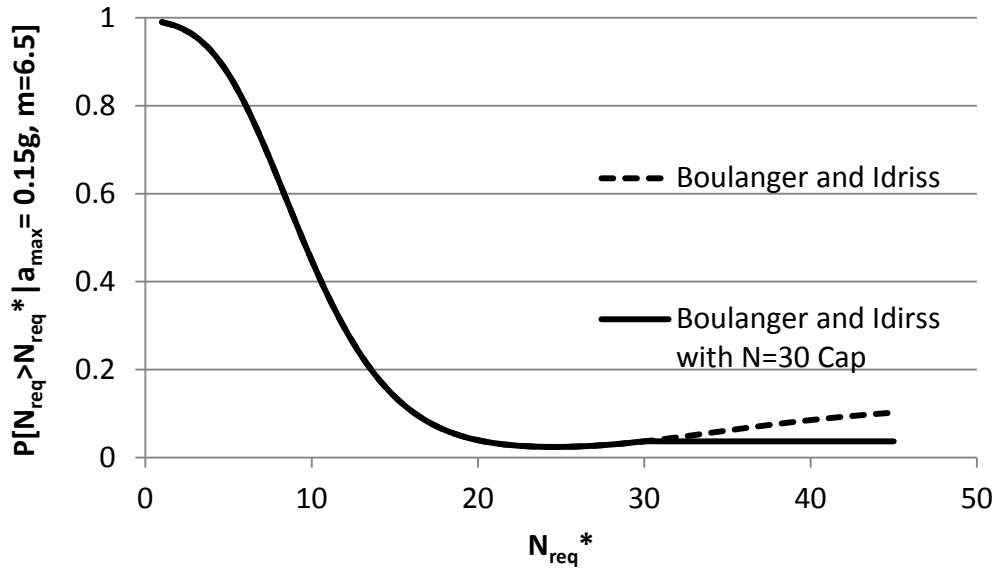


**Figure 5-6: Fragility curves with and without cap ( $M_w = 6.5$ ;  $a_{max} = 0.15$ ).**

Another approach to incorporating to account for the error in the equation is to generate a single total error term for the two possible cases (parameter uncertainty included and parameter uncertainty excluded). This single term includes uncertainty in CRR, CSR, and N. The computed values for this single term are provided in Table 5-1 and a detailed description of their development can be found in Appendix A.

**Table 5-1: Boulanger and Idriss total standard deviation with and without parameter estimation error included.**

	$\sigma_{tot}$
Parameter estimation error included (estimated value)	0.28
Parameter estimation error removed	0.13

### 5.2.3 Incorporation of Juang et al. Modal

Another alternative to the above mentioned equations is to use the Juang et al (2012) model in the performance-based analysis. This model was first proposed in 2012 and uses different assumptions than were used by the previous authors (Juang, Ching et al. 2012). This model does not include the correction of the data set for data bias that both of the previous models used. It also does not remove the parameter uncertainty from the model uncertainty, although an approximation of such can be made (see appendix).

The model that was recommended for use by Juang and Ching et al is shown below. There were several other models developed in their analysis as well, but for convenience they recommended the use of this single relationship.

$$P_L = \frac{1}{1 + \exp \left[ \theta_1 \left( \frac{\exp \left( \frac{(N_1)_{60CS}^*}{14.1} + \left( \frac{(N_1)_{60CS}^*}{126} \right)^2 - \left( \frac{(N_1)_{60CS}^*}{23.6} \right)^3 + \left( \frac{(N_1)_{60CS}^*}{25.4} \right)^4 - 2.8 \right)}{CSR_{amax_i, m_j, (N_1)_{60CS}^*}} \right) - \theta_2 \right]} \quad (56)$$

In this equation  $\theta_1$  and  $\theta_2$  are coefficients developed for the model for including or excluding parameter estimation error (Table 5-2).

**Table 5-2: Juang and Ching et al. (2012) model parameters with and without parameter estimation error included for use in probability equation shown.**

	$\theta_1$	$\theta_2$
Parameter estimation error removed	7.55	-0.95
Parameter estimation error included (estimated values)	14	-0.92

The coefficients developed for parameter uncertainty were found using the database used by Juang and Ching et al. (2012). This is the same database used by Boulanger and Idriss.

#### 5.2.4 Incorporation of Performance-Based Magnitude Scaling Factors

Another addition to the Kramer and Mayfield (2007) framework is the inclusion of performance-based magnitude scaling factors ( $MSF_{PB}$ ) which were first introduced by Cetin and Bilge (2012). This allows the engineer to change the point at which liquefaction is considered to trigger. Most liquefaction triggering correlations have the built in assumption of a liquefaction triggering definition of about a pore pressure ratio ( $r_u$ ) of 0.95 or strain ( $\gamma_{max}$ ) of about 5-6%. The use of  $MSF_{PB}$  allows the correction of the standard relationships which use these typical triggering definitions to a different triggering point such as  $r_u$  of 0.80. Such flexibility can be very useful in liquefaction analysis because it provides flexibility in the point of triggering which up until now has not been possible with the current relationships. The use of standard MSF can result in under prediction of CSR, and these under predictions may be as large as 60% for some cases when using traditional MSF (Cetin and Bilge 2012). Thus, the flexibility of the new  $MSF_{PB}$  is desired as it allows a much better prediction of whether liquefaction will initiate.

In order to use the new  $MSF_{PB}$  in the liquefaction triggering procedure correctly the engineer must be familiar with liquefaction triggering and how and at what point liquefaction triggers with different conditions and soils. The liquefaction triggering definitions for  $r_u$  and  $\gamma_{max}$  have been studied for some time and various researchers have arrived at a variety of definitions. Cetin and Bilge (2012) cite a number of authors and their definitions with  $\gamma_{max}$  ranging from values as small as 3% to as high as 20% and values for  $r_u$  ranging from 0.8 to 1.0.

Cetin and Bilge (2012) proposed a procedure for determining performance-based magnitude scaling factors. In order to do so, they first developed a set of relationships to predict the cyclic laboratory strain of saturated sands (Cetin and Bilge 2012). These equations were then

used to develop estimates of the magnitude scaling factors for values of  $\gamma_{max}$  and  $r_u$  (Cetin and Bilge 2012).

These estimates were used to develop relationships for the slope of the number of uniform stress cycles vs. CSR lines for  $\gamma_{max}$  and  $r_u$  respectively as shown below.

$$\ln(m_{\gamma_{max}}) = \ln\left(-\left(\gamma_{max}^{1.308}(1.952 \ln D_R - 6.719) + \gamma_{max}^{1.678}(0.529 * \ln \sigma'_{v,0} - 1.538) + 0.231\right) * 0.03\right) \pm 0.055 \quad (57)$$

$$\ln(m_{r_u}) = \ln\left(-\left(r_u^{4.803}(2.506 \ln D_R - 19.134) + r_u^{5.549}(0.645 \ln \sigma'_{v,0} + 7.798) + 0.621\right) * 0.612\right) \pm 0.107 \quad (58)$$

$$lim: 25 \text{ kPa} \leq \sigma'_{v,0} \leq 250 \text{ kPa} ; 30\% \leq D_R \leq 85\% ; 1\% \leq \gamma_{max} \leq 10\% ; r_u \leq 1.0$$

The slope of the line ( $m_{r_u}$  or  $m_{\gamma_{max}}$ ) is shown to be determined by a relationship dependent on the relative density ( $D_R$ ), initial vertical effective stress ( $\sigma'_{v,0}$ ), and either  $r_u$  or  $\gamma_{max}$ . These relationships were developed using limited datasets, and according to Cetin and Bilge (2012), only valid within the limits shown. The equations were found to be invalid in certain regions of the ‘valid’ range, and this necessitated a small modification to allow the equations to work (See appendix).

In their paper, Cetin and Bilge (2012) show that this value of  $m$  can be related to the performance-based magnitude scaling factor  $MSF_{PB}$  by the term  $c$  using  $N$ , the number of uniform stress cycles. The relationship between  $c$  and  $m$  is shown below.

$$MSF_{PB} = \left(\frac{N}{N_{M_w=7.5}}\right)^m = \left(\frac{M_w}{7.5}\right)^c \quad (59)$$

This equation required the use of a relationship for  $c$ . Cetin and Bilge (2012) extended the work of Liu, Stewart et al. (2001) in order to determine values for  $N$  (number of cycles). However,

they found that the relationship given by Liu, Steward et al. (2001) was significantly different than the values determined by the cycle counting scheme. They corrected this by normalizing the N values to  $N_{Mw=7.5}$  and found that by doing this the differences between the relationship and the cyclic counting scheme became insignificant. Cetin and Bilge (2012) then used this modified relationship to determine the relationship between c and m. They gave a simplified version of their relationship which excludes R, as the relationship was relatively insensitive to R, as

$$\ln(c) = \ln((-6.0591 + 0.3120 * S) * (-m)^{1.4391}) \pm 0.056 \quad (60)$$

where m is the slope given by equation 57 or 58 and S is a value for either soil or rock (S=1 for soil; S=0 for rock).

The above equations can then be applied to the performance-based method for estimating liquefaction initiation. In order to do this, the performance-based framework equation must also be in terms of the performance-based magnitude scaling factors given by  $MSF_{PB}$ .

$$\lambda_{N_{req}^*} = \sum_{j=1}^{N_{m_j}} \sum_{i=1}^{N_{a_{max}}} \sum_{k=1}^{N_{MSFPBk}} P(N > N_{req}^* | a_{max_i}, m_j, c) \Delta \lambda_{a_{max_i}, m_j} \quad (61)$$

where the term c is the value corresponding to MSF equations proposed by Cetin and Bilge. The c value is the slope of the line associated with Cetin and Bilge's Mw/7.5 to MSF plots. By incorporating Cetin and Bilge (2012) MSF equations into the overall equation for calculating the probability of liquefaction, it becomes possible to use performance-based magnitude scaling factors defined at different liquefaction triggering points using either  $r_u$  or  $g_{max}$ . This performance-based magnitude scaling factor is used in place of the magnitude scaling factors specified in the various methods for calculating the probability of liquefaction and is dependent on  $m_j$  and the specified definition of liquefaction triggering. A comparison of magnitude scaling factors to performance-based magnitude scaling factors was provided by Cetin and Bilge and is partially repeated here for the convenience of the reader (Table 5-3).

**Table 5-3: Comparison of MSF to magnitude specific MSF (PB MSF) after Cetin and Bilge (2012).**

Seed and Idriss 1982	Idriss 1995	Youd and Noble 1997	Andrus and Stokoe 1997		M <sub>w</sub>
0.72	0.47	0.23	0.37	$\gamma_{\max} = 1\%$	5.5
0.77	0.58	0.35	0.49		6
0.85	0.70	0.51	0.63		6.5
0.93	0.85	0.72	0.80		7
1.00	1.00	1.00	1.00		7.5
1.06	1.18	1.36	1.23		8
1.11	1.37	1.77	1.50		8.5
0.90	0.58	0.29	0.46	$\gamma_{\max} = 3\%$	5.5
0.91	0.68	0.41	0.57		6
0.94	0.78	0.56	0.70		6.5
0.98	0.89	0.76	0.84		7
1.00	1.00	1.00	1.00		7.5
1.01	1.13	1.30	1.17		8
1.02	1.26	1.62	1.37		8.5
1.45	0.94	0.47	0.74	$\gamma_{\max} = 5\%$	5.5
1.28	0.96	0.58	0.81		6
1.18	0.97	0.70	0.87		6.5
1.09	0.99	0.85	0.93		7
1.00	1.00	1.00	1.00		7.5
0.91	1.02	1.18	1.06		8
0.84	1.04	1.33	1.13		8.5
0.73	0.47	0.23	0.37	$r_u=0.50$	5.5
0.78	0.58	0.35	0.49		6
0.86	0.71	0.51	0.64		6.5
0.93	0.85	0.73	0.80		7
1.00	1.00	1.00	1.00		7.5
1.06	1.18	1.36	1.22		8
1.11	1.37	1.76	1.49		8.5
1.31	.085	0.42	0.67	$r_u=0.90$	5.5
1.19	0.89	0.54	0.75		6
1.12	0.93	0.67	0.84		6.5
1.06	0.97	0.83	0.91		7
1.00	1.00	1.00	1.00		7.5
0.93	1.04	1.20	1.08		8
0.87	1.08	1.39	1.18		8.5

## **6 COMPARATIVE ANALYSIS EVALUATION SET UP**

To more fully understand the differences between the proposed performance-based methods and the previously used Cetin and Seed et al (2004) procedure a comparative analysis was conducted. In order to determine the strengths and weaknesses of each analysis type, as well as the limitations and possible sources of difference between the models these comparative analyses had to be inclusive of a wider range of parameters and locations. A program was designed (PB LiquefY) to assist in the analysis of the models. Statistical analyses were conducted using a statistical software package called JMP Pro 10.

### **6.1 PB LiquefY**

To obtain valid performance-based results and have the ability to compare them it was necessary to construct a tool to perform the numerous probabilistic computations. Performance-based designs can require millions of iterations and would be impossible to do by hand. In order to facilitate the design of a program that would be both research friendly and have the potential for use by practicing engineers, the program was constructed in EXCEL© 2010 using Visual Basic for Applications. The use of EXCEL © to make the program facilitated a user friendly system that would be compatible with a wide range of programs and platforms. The desire was to create a tool that would allow engineers to integrate performance-based liquefaction initiation analyses into their current practice with ease and simplicity.

PBliquefY uses a range of equations and relationships to develop a powerful tool for use by the engineer or researcher (see ). It has a wide range of capabilities and allows engineers to perform as complex or simple of an analysis as the needs of the project dictate. It further has analysis software that permits calculation of multiple analyses with multiple soil profiles simpler, which facilitates the mapping and comparison of liquefaction initiation.

PBliquefY was designed to run both deterministic and performance-based empirical liquefaction analyses using models common to modern practice and two newer performance-based methods. The program allows the user to account for standard conditions as well as giving the user the capability to examine how the effects of embankments and other loads will affect liquefaction initiation. The use of these load cases is important because additional loads above the soil profile change the stresses within the profile and have a direct effect on the susceptibility of the soil profile to liquefaction. The program also allows the user to account for non-level conditions using  $K_{\alpha}$ . In addition to these capabilities, PB LiquefY has the capacity to run a large number of sites and soil profiles in a single run. The program organization is shown in Figure 6-1.

The first step is to select a location for the analysis. The selection of a location can be done for either a single location or a series of locations (see ). Following the selection of a location a soil profile is uploaded or chosen. Again, the selection can be automatically done for multiple pre-saved profiles. Finally, using the location selected, the program will download data from the USGS deaggregation website and run the analyses selected by the user. When finished, the program will loop through all of the desired return periods and pull the desired data from the program, saving the output to a text file. The calculation process requires the re-running of the deterministic analyses for each selected return period (Loop A). Once all of the data is collected for that soil profile, a new soil profile is either



uploaded by the user or uploaded automatically from a pre-selected list (Loop B). The analyses are run again with the new soil profile. Finally, the program moves to the next location (Loop C) and runs through the entire process again. The result when finished is a text file containing the specified output for all of the soil profiles, locations, and return periods specified by the user. An error file is also output showing any errors which occurred during the run.

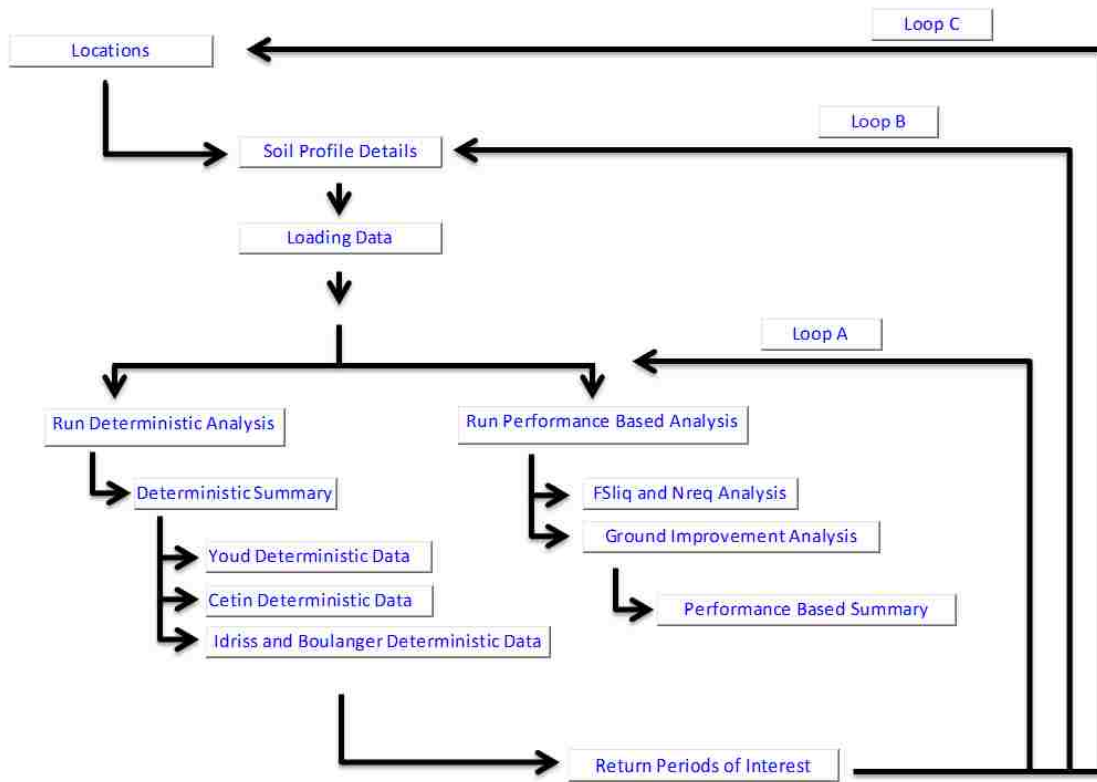


**Figure 6-1: PB Liquefy program organization.**

Each time the program runs through an iteration it needs to calculate the performance-based data corresponding to that run. To run this calculation the program loops through the performance-based procedure (Figure 6-2). This loop is used to calculate the contribution towards the hazard curve from each magnitude, acceleration, and  $N^*$  value as outlined in the proceeding sections regarding the incorporation of the different models. In general, one performance-based analyses will require between 900,000 and 1,100,000 iterations to complete resulting in over 3,000,000 iterations per analysis run if all of the performance-based methods are selected. For a detailed discussion of the Performance-based analysis and the mechanics of how it is performed see

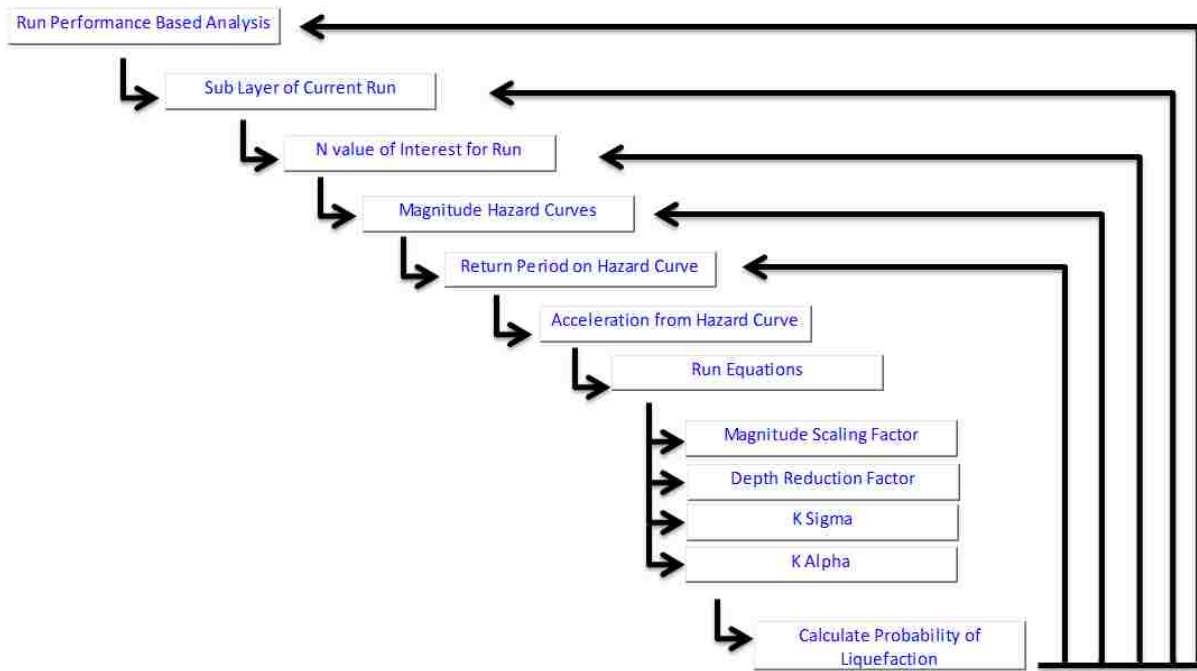


**Figure 6-2: Performance-based procedure loop.**

The procedures and equations associated with the analyses are complex, and their implementation is likewise complex. Some of the tools developed with PB LiquefY include deaggregated hazard plots, FS and  $N_{req}$  vs. depth plots, ground improvement plots, and other tools. A full discussion of PB LiquefY and these tools is included in

## 6.2 Site Locations

Site selection was one of the first necessary steps to make in collection of the data. The sites used in the comparative analyses of the liquefaction initiation methods were in general similar in nature to the sites used by Kramer and Mayfield (2010), with one additional site being added in Richmond, VA (Table 6-1). These sites were used as they are representative of a wide range of possible locations and allow comparison of the methods across many of the different seismic environments represented within the continental United States.

**Table 6-1: Site locations used in study.**

#	Site Name	Latitude	Longitude
1	Butte	45.983 N.	112.527 W.
2	Charleston	32.780 N.	79.930 W.
3	Eureka	40.800 N.	124.170 W.
4	Memphis	35.028 N.	90.009 W.
5	Portland	45.542 N.	122.649 W.
6	Richmond	37.637 N.	77.474 W.
7	Salt Lake City	40.671 N.	111.791 W.
8	San Francisco	37.781 N.	122.498 W.
9	San Jose	37.346 N.	121.885 W.
10	Santa Monica	34.035 N.	118.507 W.
11	Seattle	47.610 N.	122.330 W.

Of the 11 sites used, 4 of the sites were located on the west coast near the San Andreas Fault system, 2 were located in the North West near the Cascadia Subduction Zone and similarly located faults, 2 were along the Wasatch fault and Rocky Mountain areas, and 3 sites were located on the area of the New Madrid fault system and Charleston liquefaction features.

The USGS seismic source model was used in the analysis of these sites. A map showing the relationship between the site locations and the quaternary fault and fold database from the USGS (2013) is shown (Figure 6-3). The 2008 version of the USGS seismic source model was used to develop PSHA's for the analysis in this study. This seismic model uses the "source and attenuation models of the NSHMP" (Petersen, Frenkel et al. 2008). The USGS 2008 model is the most current version of the USGS National Seismic Hazard Mapping Project (NSHMP) available at this time. The results of this study are, strictly speaking, only valid with these source and attenuation models. Among geophysicist there is still a great deal of discussion about the development of these models and what methods are best (Wong 2012). Should new or different models be used the same general patterns seen in this study should remain true although individually calculated values may change in magnitude.



**Figure 6-3: Location of 11 sites (red) used in study in relation to USGS quaternary fault database (light blue).**

The data was broken into groups to facilitate discussion of the locations specified. For this purpose the mean maximum accelerations and magnitudes corresponding to a return period of 2475 years were used (Table 6-2). To divide the range of accelerations for these locations into three groups, the values within one standard deviation of the mean are designated as being the medium seismic environment group, those greater than one standard deviation from the mean are the high seismic environment group, and those lower than one standard deviation from the mean are the low seismic environment group. The mean value of these accelerations is 0.566 g with a standard deviation of 0.296 g. The breakup of the 11 sites into these categories gives 7 sites in

the medium category (San Jose, Santa Monica, Seattle, Charleston, Memphis, Portland, and Salt Lake City), 2 in the low category (Butte and Richmond), and 2 in the high category (San Francisco and Eureka). These definitions are specific to this data set and are designed to facilitate analysis and discussion of the data only.

**Table 6-2: Mean magnitude and acceleration from PSHA corresponding to  $T_R=2475$  years. (Bold values – High, Italicized – Medium, Underlined - Low).**

#	Site Name	$a_{max}[g]$	$M_w$
1	Butte	<u>0.19</u> (L)	6.04
2	Charleston	<i>0.65</i> (M)	7.00
3	Eureka	<b>1.17</b> (H)	7.44
4	Memphis	<i>0.44</i> (M)	7.19
5	Portland	<i>0.41</i> (M)	7.30
6	Richmond	<u>0.12</u> (L)	5.68
7	Salt Lake City	<i>0.49</i> (M)	6.84
8	San Francisco	<b>0.84</b> (H)	7.64
9	San Jose	<i>0.64</i> (M)	6.65
10	Santa Monica	<i>0.76</i> (M)	6.88
11	Seattle	<i>0.52</i> (M)	6.86

### 6.3 Soil Profiles

Soil profiles were developed to allow examination of different characteristics that affect liquefaction. The results were then examined to determine the effect that varying a given variable or set of variables had on the outcome of the analysis. To maintain consistency between the soil profiles, certain aspects of the soil profiles were held constant.

The values in the soil profile and analysis that were kept constant are shown in Table 6-3. These values were used for all of the analyses. These values were held constant to eliminate as many confounding factors in the analysis as possible. The exception to this being the water table depth, which was varied for one set of analyses (stress ratio analyses).

**Table 6-3: Assumed properties of soil profile.**

Hammer Energy	60%
Borehole Diameter	120 mm
Water Table Depth	0 m
Rod Stickup Length	1.5 m
Units	Metric

Soil profiles consisted of 10 layers equally divided over a 20 meter depth. Values for certain portions of the soil profile were then varied. Soil profiles and their corresponding values are shown in Table 6-4 and detailed soil profiles can be found in the appendix. Other analyses were also run to determine the effect of using performance-based magnitude scaling factors and the effect of the application of different standard deviations (either including or excluding the parameter estimation error).

Values were generally held constant while a single value was varied in order to eliminate confounding factors in the analysis. The exception to this occurs in the case of shear wave velocity, N value, and relative density. These factors are directly related to each other and correlations were used to allow these parameters to stay dependent on each other.

**Table 6-4: Soil profiles used in study.**

Soil Profile	N Value	Fines Content	Shear Wave Velocity	Soil Type	Susceptibility
1	5	0	Correlation Mean	Sand	Assume Yes
2	5	10	Correlation Mean	Sand	Assume Yes
3	5	20	Correlation Mean	Sand	Assume Yes
4	5	30	Correlation Mean	Sand	Assume Yes
5	5	40	Correlation Mean	Sand	Assume Yes
6	5	50	Correlation Mean	Sand	Assume Yes
7	15	0	Correlation Mean	Sand	Assume Yes
8	15	10	Correlation Mean	Sand	Assume Yes
9	15	20	Correlation Mean	Sand	Assume Yes
10	15	30	Correlation Mean	Sand	Assume Yes
11	15	40	Correlation Mean	Sand	Assume Yes

12	15	50	Correlation Mean	Sand	Assume Yes
13	25	0	Correlation Mean	Sand	Assume Yes
14	25	10	Correlation Mean	Sand	Assume Yes
15	25	20	Correlation Mean	Sand	Assume Yes
16	25	30	Correlation Mean	Sand	Assume Yes
17	25	40	Correlation Mean	Sand	Assume Yes
18	25	50	Correlation Mean	Sand	Assume Yes
19	35	0	Correlation Mean	Sand	Assume Yes
20	35	10	Correlation Mean	Sand	Assume Yes
21	35	20	Correlation Mean	Sand	Assume Yes
22	35	30	Correlation Mean	Sand	Assume Yes
23	35	40	Correlation Mean	Sand	Assume Yes
24	35	50	Correlation Mean	Sand	Assume Yes
25	5	0	Correlation Mean + 1 $\sigma$	Sand	Assume Yes
26	10	0	Correlation Mean + 1 $\sigma$	Sand	Assume Yes
27	20	0	Correlation Mean + 1 $\sigma$	Sand	Assume Yes
28	30	0	Correlation Mean + 1 $\sigma$	Sand	Assume Yes
29	5	0	Correlation Mean - 1 $\sigma$	Sand	Assume Yes
30	10	0	Correlation Mean - 1 $\sigma$	Sand	Assume Yes
31	20	0	Correlation Mean - 1 $\sigma$	Sand	Assume Yes
32	30	0	Correlation Mean - 1 $\sigma$	Sand	Assume Yes
33	5	0	Correlation Mean	Sand	Assume Yes
34	10	0	Correlation Mean	Sand	Assume Yes
35	20	0	Correlation Mean	Sand	Assume Yes
36	30	0	Correlation Mean	Sand	Assume Yes

To develop the needed value for the shear wave velocity of each layer, the correlation proposed by Andrus and Stokoe (2000) was used. This correlation was developed based on data collected for the NCEER workshop on liquefaction. The relationship between shear wave velocity and SPT blow count was given as a statistical relationship of the form,

$$V_{s1} = \beta_1 * [(N_1)_{60}]^{\beta_2} \quad (62)$$

In this equation  $V_{s1}$  is the shear wave velocity in meters per second,  $N_{160}$  is the SPT blow count of the sand layer, and  $\beta_1$  and  $\beta_2$  are statistically regressed coefficients. The values of the  $\beta_1$  and  $\beta_2$  are 93.2 and 0.231 respectively. The residual standard deviation ( $S_{res}$ ) of this equation is

given as 12 m/s. This equation was considered valid for use in clean sands. As such, a clean sand correction was applied using, for consistency, the NCEER methodology and the resulting SPT blow counts used to find reasonable values for shear wave velocity

Relative density was used in the performance-based magnitude scaling factor calculations. To obtain a value for relative density in a reasonable range, the correlation given by Marcuson and Bieganousky (1977) was used. The equation given for the clean sand correlation of SPT blow count is shown below.

$$D_R = 100 * \left[ \frac{(N_1)_{60}}{60} \right]^5 \quad (63)$$

Again, this correlation was used after correcting the SPT blow count for fines in order to make it consistent with clean sand. A cap of 100% was applied on this equation to prevent values from exceeding the maximum relative density possible in nature.



## 7 PERFORMANCE-BASED ANALYSIS AND RESULTS

In order to understand how the different methods – Cetin and Seed et al. (2004), Boulanger and Idriss (2012), and Juang and Ching et al. (2012) – vary from one another, a detailed comparative analysis was conducted. This analysis was done using theoretical soil profiles set up as explained previously. The soil profiles were analyzed for all 11 sites for return periods corresponding to 475, 1039, 2479, 4975, and 9950 years. The differences between the  $\Delta N_{\text{req}}$  were examined after varying SPT blow count, fines content, depth, return period, seismic environment, and shear wave velocity. Additional comparisons were made while looking at epistemic uncertainty in shear wave velocity, performance-based magnitude scaling factors, error from parameter uncertainty, and the optional  $K_{\sigma}$  limit imposed by Boulanger and Idriss. These analyses were conducted using the conditions listed above and in general, unless otherwise specified, using a constant value for the error term including parameter uncertainty. For convenience the Cetin and Seed et al. (2004) method is referred to as the Cetin et al. method, the Boulanger and Idriss (2012) method is referred to as the Boulanger and Idriss method, and the Juang and Ching et al. (2012) method is referred to as the Juang et al. method.

In the following graphs the axis labeled  $\Delta N_{\text{req}}$  is the difference between  $N_{\text{req}}$  and  $N_{\text{site}}$ . It can be thought of as the necessary ground improvement needed to prevent liquefaction. As such

it is limited to values greater than or equal to 0, as values less than this will result in no needed ground improvement.

After running the analysis on the 11 sites, it was noted that certain inconsistencies in the data needed to be removed. The inconsistencies resulted from the way in which data was calculated and interpolated in the program PB LiquefY. For low seismicity cities there were cases where the return period of liquefaction never became as low as the specified values desired (for example if 475 year return period was requested and the smallest possible return period calculated was 1020). For these cases the data returned corresponded to the smallest possible return period rather than the return period of interest. As such these data were removed. The two sites where this occurred were both from the low seismic category with the affected values corresponding to the return periods for 475, 1038 and 2475 years for Richmond and 475 years for Butte. The values corresponding to these return periods at these locations were removed to prevent them from artificially skewing the analysis. As all of the data for these return periods were thrown out, the data within each return period set remained balanced (Figure 7-1).

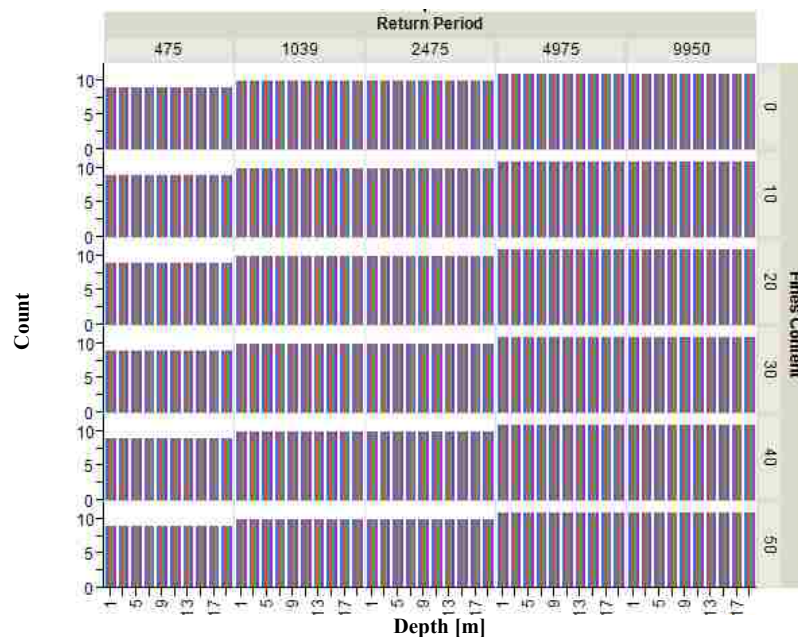


**Figure 7-1: Distribution of input data (counts) within study.**

## 7.1 Statistical Analysis of Performance-Based Data

A statistical analysis of the data set can help to narrow down how the data differs. An analysis of the data from soil profiles 1-24 was performed at the 11 sites mentioned above. The resulting data was analyzed to determine general trends in the data.

A density plot of the values illustrates how the average predictions vary for these three methods (Figure 7-2). For the three methods in this study, 2 of the methods namely the Juang et al and Boulanger and Idriss methods on average predict very similar values. These two methods tend to have a higher density of values at lower  $\Delta N_{req}$  values. The Cetin et al. method tends to have a higher density at higher  $\Delta N_{req}$  values. This means that the Cetin et al. method tends to be more conservative overall, while the Juang et al and the Boulanger and Idriss methods in general will predict less conservative, i. e. smaller, values for  $\Delta N_{req}$ .

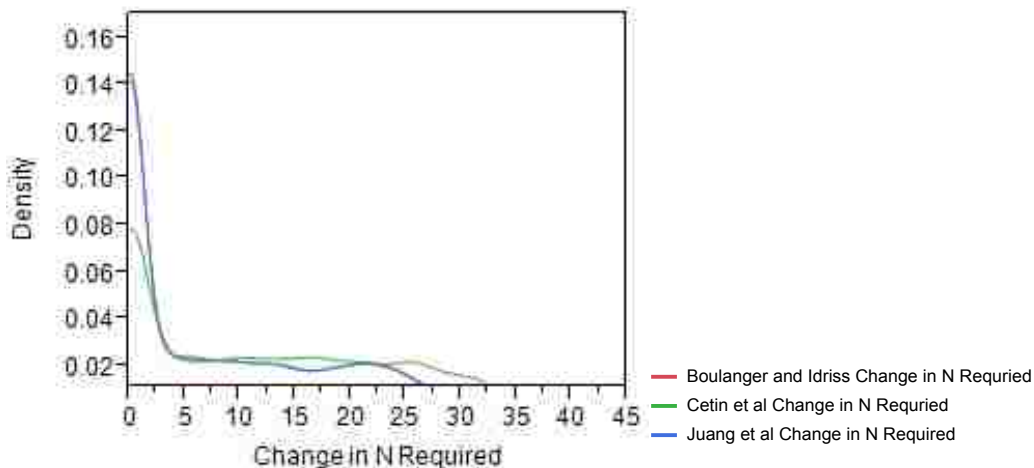


**Figure 7-2: Density plot of  $\Delta N_{req}$  values.**

A look at the distribution of the  $\Delta N_{req}$  values using box plots for the three methods confirms that the Cetin et al method is more conservative on average (Figure 7-3). The Cetin et al. method has a mean value of the results of 12.35 with a 95% confidence interval from 12.173

to 12.526. This is much greater than the Boulanger and Idriss method (mean value of results of 7.73 with 95% confidence interval from 7.56 to 7.91) and the Juang et al method (mean value of results of 7.88 with 95% confidence interval from 7.70 to 8.06) (Table 7-1). This means that on average the Cetin et al method is more conservative and will call for greater amounts of ground improvement than would be called for by the other two methods of analysis.

**Table 7-1: Tables of quantile values (Top) and means for one way analysis of variance (bottom).**

Level	Minimum	10%	25%	Median	75%	90%	Maximum
Boulanger and Idriss Change in N Required	0	0	0	3.249978	14.70497	22.53725	34.96574
Cetin et al Change in N Required	0	0	0	10.60362	21.60881	29.03091	43.33236
Juang et al Change in N Required	0	0	0	3.579066	14.93431	22.77257	35.07574

Level	Number	Mean	Std Error	Lower 95%	Upper 95%
Boulanger and Idriss Change in N Required	12240	7.7314	0.09026	7.555	7.908
Cetin et al Change in N Required	12240	12.3495	0.09026	12.173	12.526
Juang et al Change in N Required	12240	7.8793	0.09026	7.702	8.056

Std Error uses a pooled estimate of error variance

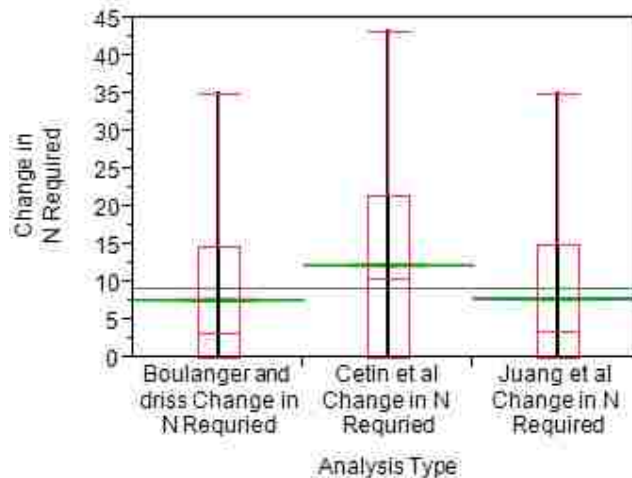


**Figure 7-3: Box plot showing distribution of  $\Delta N_{req}$  for three methods.**

The fact that the Cetin et al. method is more conservative than the other two methods is fairly widely known in the engineering profession. The fact that this trend holds for the performance-based approach is new, however, and useful in understanding the differences between these performance-based approaches. An in depth examination will now be conducted to determine if and where this relationship holds true, or if there are cases where the Cetin et al. methods becomes less conservative.

## 7.2 SPT Blow Count Variation

An examination of the variation due to the SPT blow count is beneficial and helps in an understanding of the characteristics of the different methods and how they change with blow count. For this analysis soil profiles 1-24 were used. The averages of the  $\Delta N_{req}$  values from the resulting analyses are shown below in Figure 7-4.

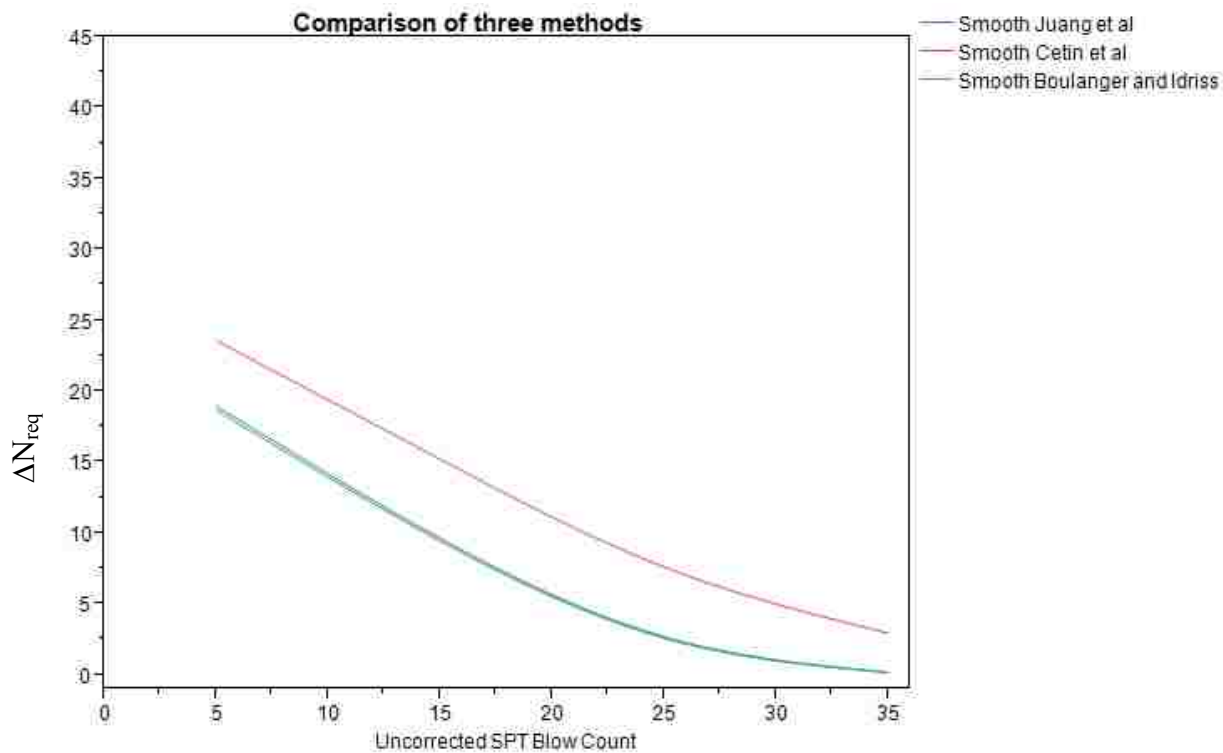
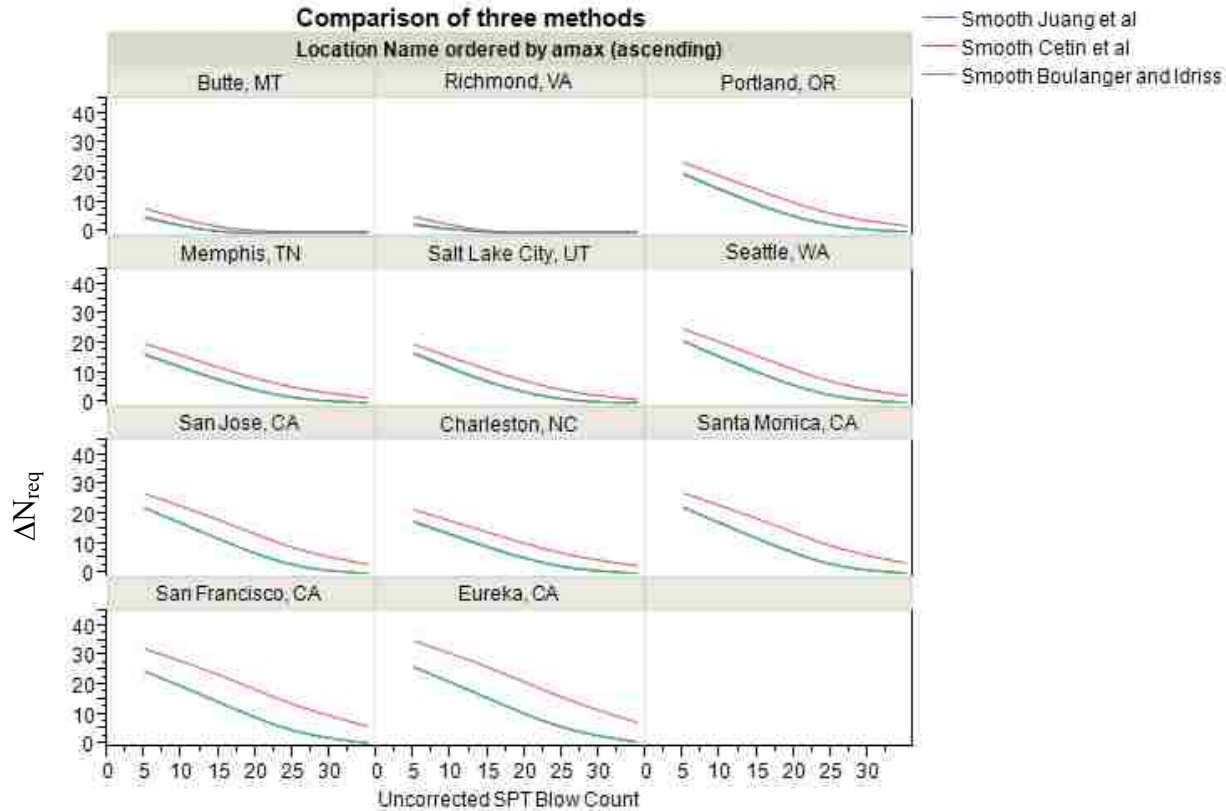


Figure 7-4: Average  $\Delta N_{req}$  for 11 sites using soil profiles 1-24 and all  $T_R$ 's.

Several things of interest were observed as N values were allowed to vary. These included the N value range past which liquefaction could be considered to no longer be occurring, as well as areas in which the methods differed from each other. When examining these differences it is important to keep in mind that as the N value was allowed to change, the shear wave velocity was also allowed to change according to the Andrus and Stokoe equation.

For both the Boulanger and Idriss and Juang et al. methods, the absolute maximum value past which no  $\Delta N_{req}$  is needed corresponds to an uncorrected SPT blow count of 35. Values of SPT blow count greater than 30 require an average of less than 1 blow increase to prevent liquefaction from occurring. The Cetin et al relationship however has no discernable maximum values past which liquefaction will not occur over the range of the study (SPT values from 5 to 35 blows per foot).

Looking at the SPT blow count graph and breaking it up by location (Figure 7-5), we can see a pattern in the data for the sites chosen. Both of the sites in the high seismic category exhibit larger differences between the Cetin et al. method and the Boulanger and Idriss and Juang et al. methods with the differences decreasing slightly at high SPT blow counts. Those in the medium category all exhibit smaller differences, with the differences still notable and also decreasing at high blow counts. Those in the low seismic category exhibit almost no difference between the methods with regard to  $\Delta N_{req}$ . This is interesting because it means that in areas of low seismicity the three methods, in general, predict similarly for these 11 sites.



**Figure 7-5: Average variation in  $\Delta N_{req}$  by site.**

A comparison of all three approaches shows how they vary from each other as well as how they are similar and allows examination of the ranges in which one or the other equations is more conservative. One pattern that is seen, and is in most ways obvious, is that as the SPT blow count increases, the value of  $\Delta N_{req}$  for each of the three methods will decrease. The Cetin et al. method is the most conservative of the three methods as it requires larger  $\Delta N_{req}$  for every value of SPT blow count and location.

### 7.3 Shear Wave Velocity Variation

Shear wave velocity is related to SPT blow count by the Andrus and Stokoe equation for these analyses; we will examine the differences between the methods here. It is important to

note that the 4 input N values resulted in a wider range of shear wave velocities due to the dependence of shear wave velocity on N value and fines content (Shear wave velocity is dependent on  $N_{160cs}$ ). However, in spite of these differences it would be expected that similar patterns would result from shear wave velocity as resulted from SPT blow count since they are correlated. A graph comparing the resulting  $\Delta N_{req}$  from the three methods with increasing  $V_{s12}$  is shown (Figure 7-6). The resulting oddly curved shape of the graph is the effect of the fines correction on the Andrus and Stokoe equation (used to determine shear wave velocity). If the effect of fines content is removed from the graph a much smoother line can be made (Figure 7-7). Similar relationships can be seen in these graphs with higher  $V_{s12}$  corresponding to lower  $\Delta N_{req}$  and with the Cetin et al. method overall requiring a higher  $\Delta N_{req}$  on average.

Looking at shear wave velocity by location, we see patterns similar to the patterns in the SPT blow count graphs. These patterns include: decreased  $\Delta N_{req}$  with increasing shear wave velocity/blow count (Figure 7-6), increasing differences between methods at larger seismicity sites (Figure 7-8 and Figure 7-9). A few new patterns are seen with the examination of the effect of return period and fines content.

One of the patterns that emerges with the analysis of the interaction between shear wave velocity fines content is the fact that increases in fines content generally result in an increased difference between the methods. The reasons behind this will be examined in more detail later. The interaction between shear wave velocity and return period shows a few cases where the Cetin et al. method requires less  $\Delta N_{req}$  than the other two methods (Figure 7-10). These cases only occur at low shear wave velocities and low return periods.



In summary, the shear wave velocity shows similar patterns to those seen in the graphs of  $\Delta N_{req}$ . Overall the Cetin et al. approach on average calls for larger  $\Delta N_{req}$  values except at very small shear wave velocities and return periods.

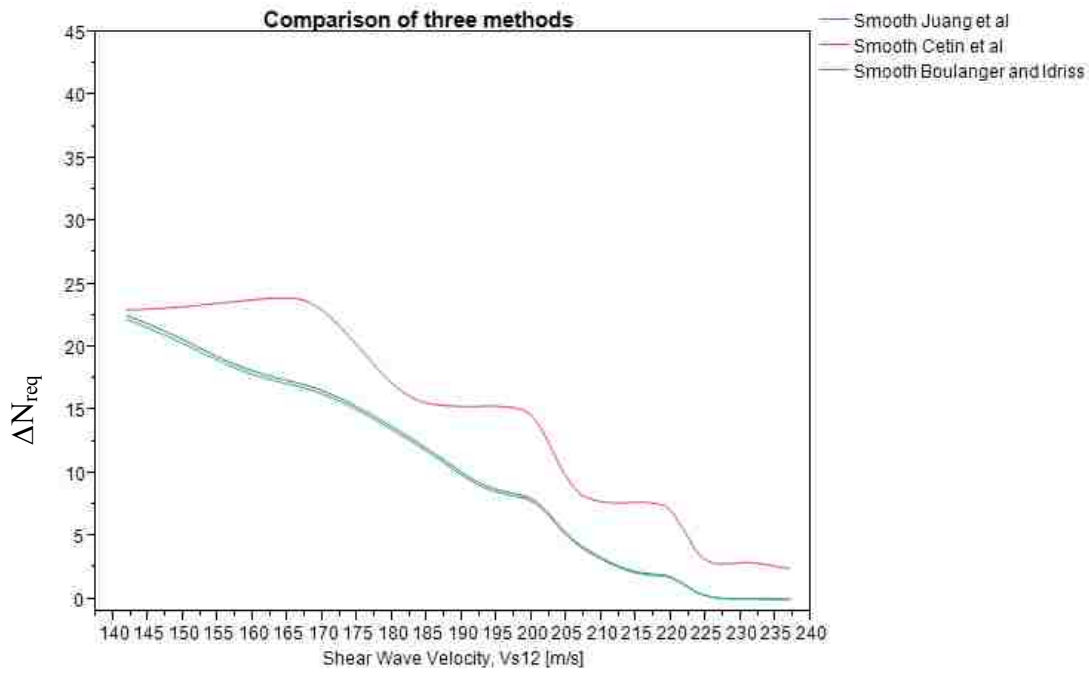


**Figure 7-6: Shear wave velocity ( $V_{s12}$ ) vs. average  $\Delta N_{req}$**

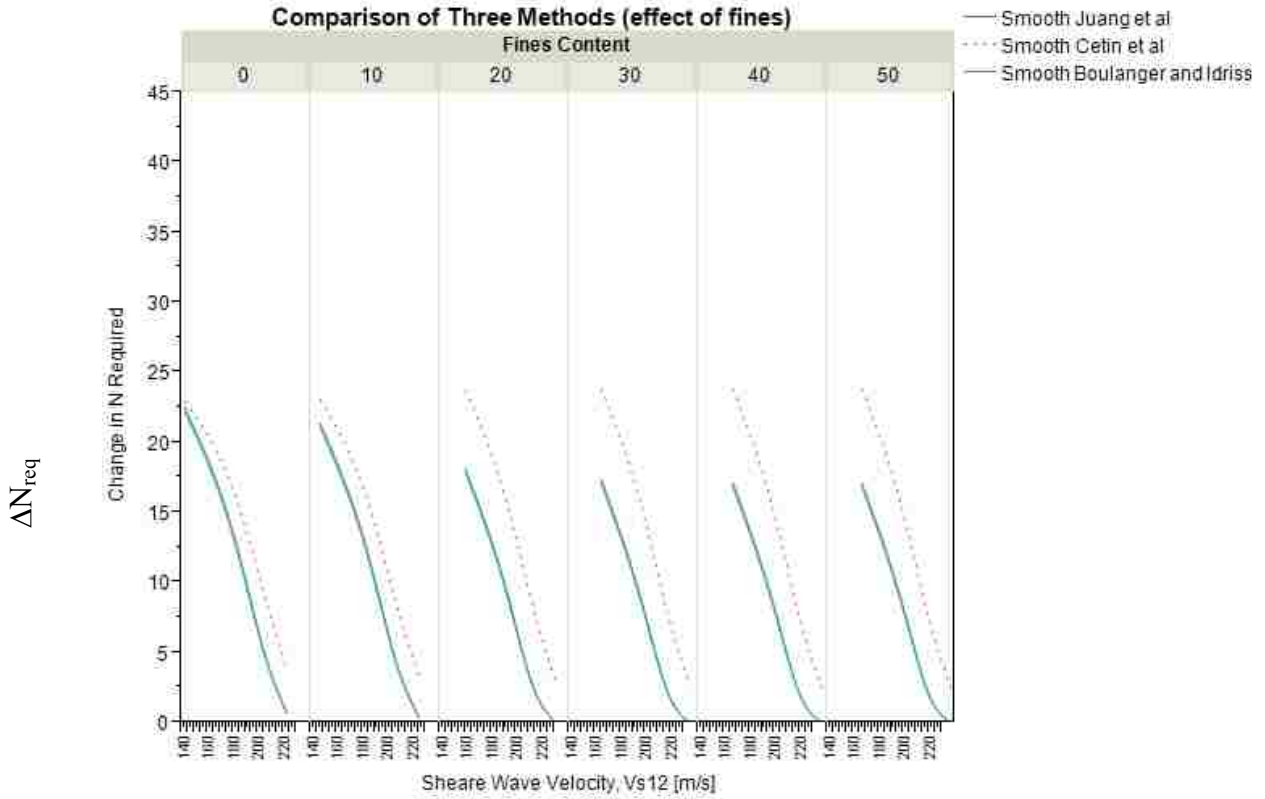


Figure 7-7: Shear wave velocity ( $V_{s12}$ ) vs. average  $\Delta N_{req}$  with fines content.

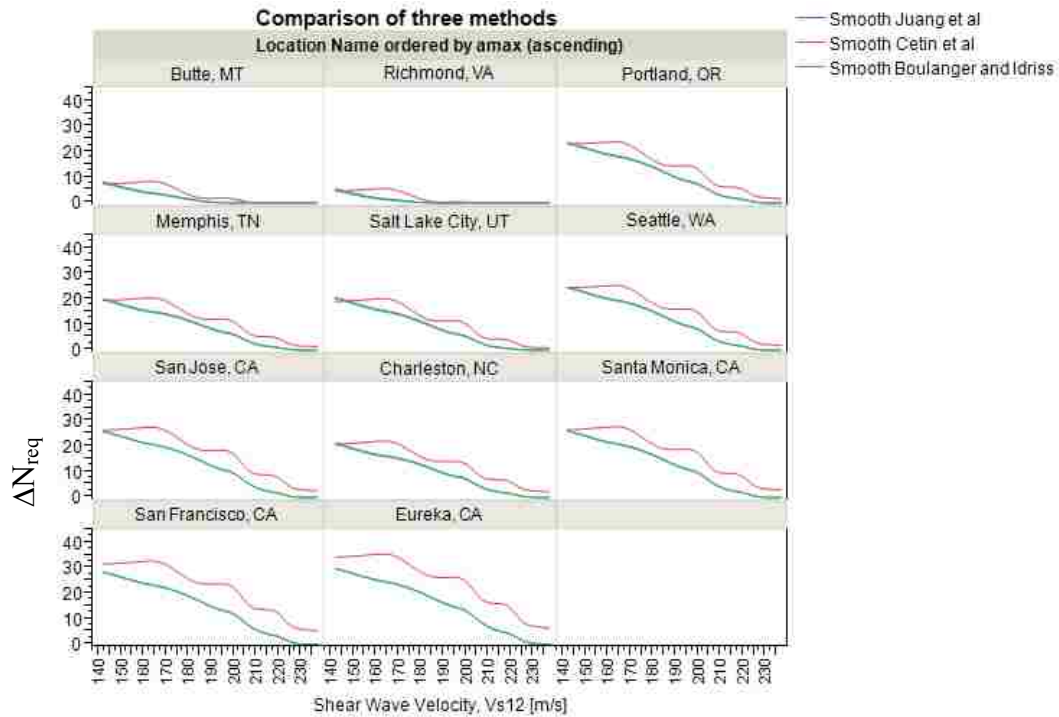
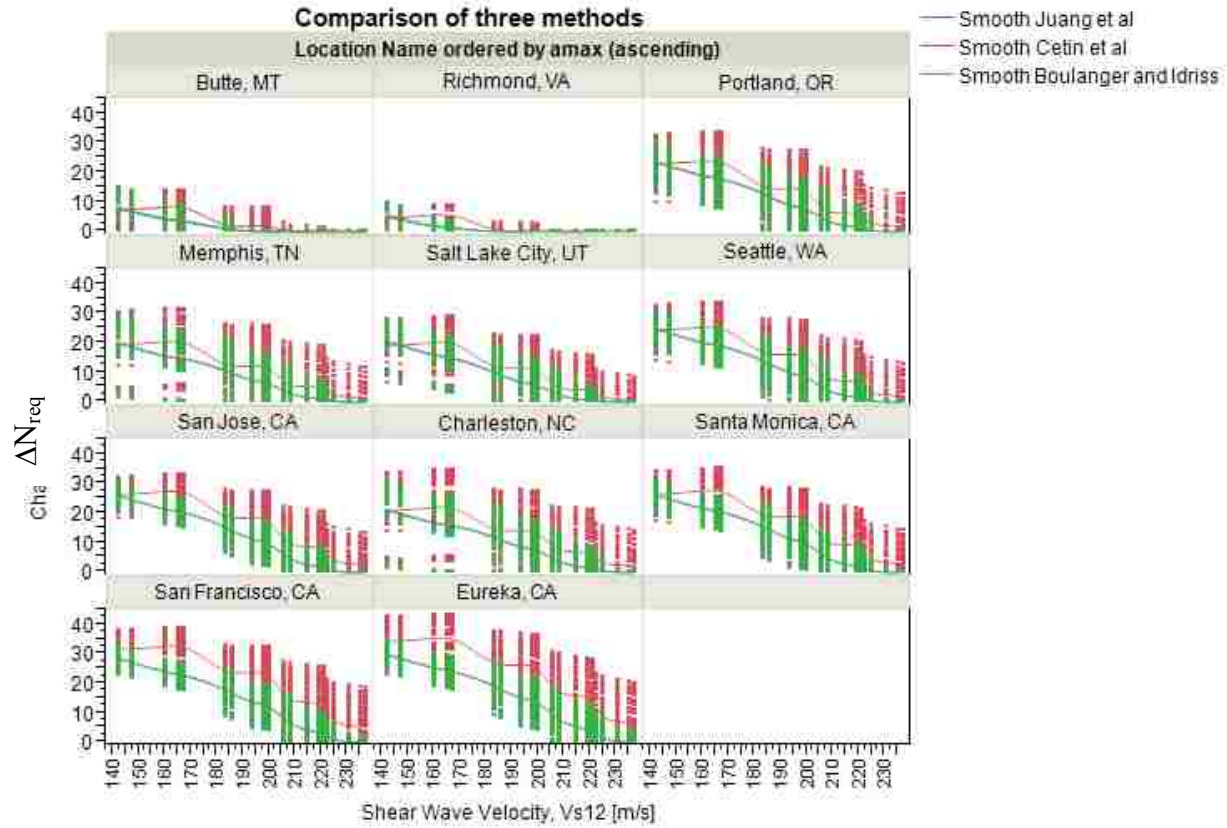
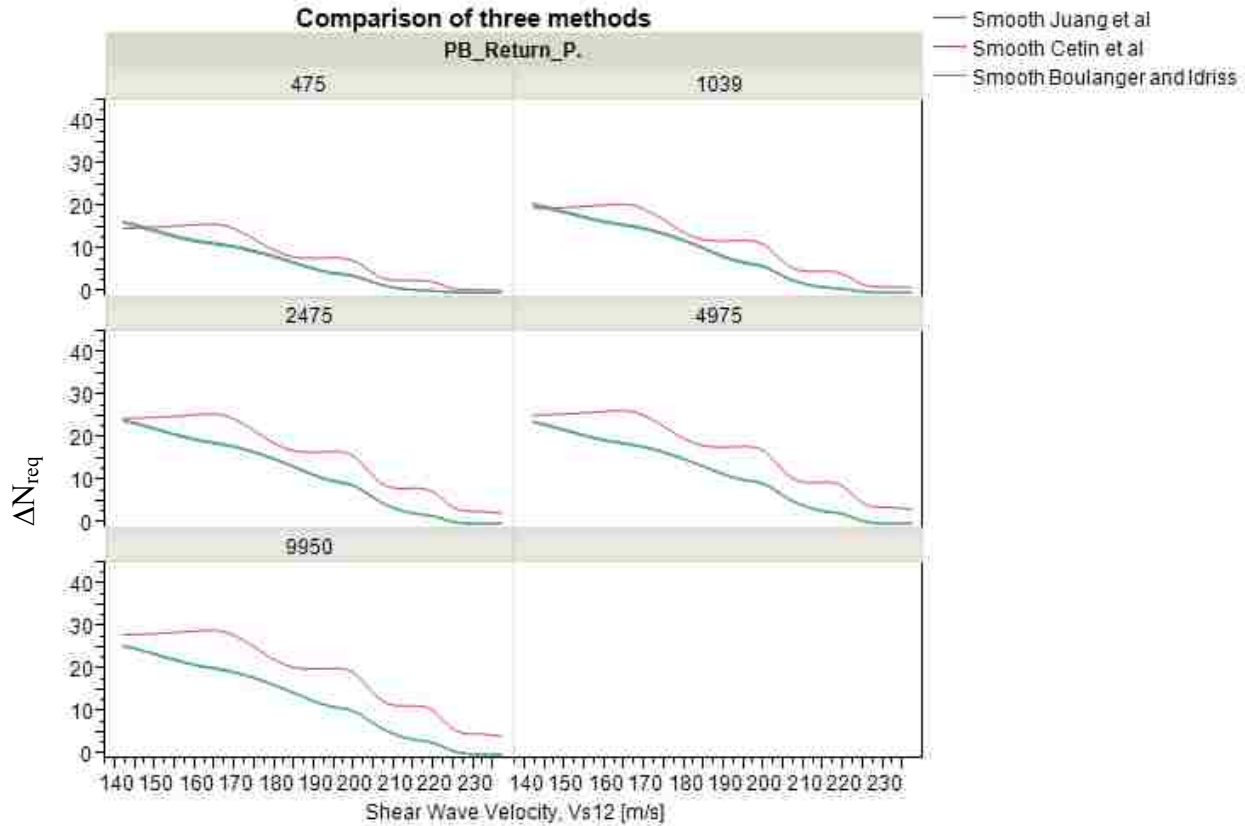


Figure 7-8: Shear wave velocity vs.  $\Delta N_{req}$  by location.



**Figure 7-9: Shear wave velocity data points.**



**Figure 7-10: Comparison with varying shear wave velocity by return period.**

### 7.3.1 Shear Wave Velocity Epistemic Uncertainty and its Effects

Since only one of the models uses  $V_{s12}$  (the Cetin et al. method), a possible cause of the difference between the models is the correlated values used for obtaining  $V_{s12}$ . The uncertainty inherent in shear wave velocity measurements and correlations may play a central role in the differences in the  $\Delta N_{req}$  from each of the methods. To understand how  $V_{s12}$  affects the outcome of the analysis, values were obtained representing typical epistemic uncertainty associated with shear wave velocity measurements. Moss (2008) showed that different measurement methods are associated with different coefficients of variation. He gave values ranging from 1-3% for invasive methods, and as high as 5%-6% for SASW. These values were stipulated to be tentative, and that further data was needed to more accurately estimate shear wave velocity

coefficients of variation. Dr. Brady R. Cox is of the opinion that where “good” measurements are taken the variability in the measurements is probably around 10%. He stipulated that many “poor” measurements have been taken in recent years due to the ease with which such measurements can be obtained with modern equipment. For these measurements Dr. Cox felt that the epistemic uncertainty is probably closer to 10%-20% and may be even higher in some cases (personal communication, December 19, 2012).

In this study, shear wave velocity was correlated with SPT resistance and values for  $V_{s12}$  were calculated based off of these correlated values. When correlated values are used instead of measurements the percent error may increase above the afore-mentioned values depending on which correlation is used. Many different correlations for shear wave velocity and SPT blow count have been developed over the years. Two such correlations were investigated during this study (IYISAN 1996; Andrus and Stokoe 2000); however, the relationship of Iyisan was ultimately not used because it is used less commonly in practice and lacks the necessary standard deviations on the correlation from which to develop an understanding of the variation in shear wave velocities. The Andrus and Stokoe relationship was used to develop all shear wave velocity values in this study. The standard deviation computed by Andrus and Stokoe was 12 m/s, which represents the standard deviation of the residuals. To better understand how the shear wave velocity might vary with variations in parameter, i.e. SPT blow count, a Monte Carlo simulation was performed. A detailed discussion of the Monte Carlo simulation can be found in the Appendix A.

The final standard deviation (including parametric and model uncertainty) was computed as:

$$S_{Parameter} = 4.686 \frac{m}{s} + 2.99 \frac{m}{s} * \ln(N_{160cs}) ; R^2 = 0.9874 \quad (64)$$

$$\sigma_{Vs}^2 = S_{parameter}^2 + S_{res}^2$$

where  $\sigma_{Vs}$  is the standard deviation,  $S_{res}$  is the residual standard deviation from the original Andrus and Stokoe equation given as 12 m/s,  $S_{parameter}$  is the standard deviation from the uncertainty in the SPT blow count, and  $N_{160cs}$  is the corrected SPT blow count. For a SPT blow count of 15,  $\sigma_{Vs}$  corresponds to a value of 17.533 m/s for a shear wave velocity of 174.218 m/s, or roughly 10% error. This is in agreement with the ranges of variation mentioned previously although dealing with a correlation rather than with direct measurements. Thus the standard deviation as found in equation 64 was considered to be valid and this standard deviation was used in this study for the Andrus and Stokoe equation to represent the wider band of possible variation. A detailed discussion of this topic is included in Appendix A.

To account for the effect of the  $V_{s12}$  on the Cetin et al method, values for SPT blow count were varied and the mean shear wave velocity was calculated from these values. For the purpose of this study these mean values were assumed as the baseline and values were then calculated plus or minus one standard deviation of the shear wave velocity. This resulted in three curves for the Cetin et al method: mean, mean + 1  $\sigma$ , mean – 1  $\sigma$ . The data for these curves comes from liquefaction analyses run using soil profiles 25 – 36 as shown in Table 6-4 and all 11 locations.

In general, when the mean - 1  $\sigma$  of shear wave velocity is used to calculate  $V_{s12}$  in the Cetin et al method, the resulting values will be less conservative than they would normally be, while the mean + 1 sigma results in values that are more conservative.

This is the opposite effect of what would be expected. Normally, the  $V_{s12}$  is thought to approximate density. As  $V_{s12}$  increases, the density of the soil should be increasing and the  $\Delta N_{req}$  should be smaller. We are seeing the opposite of this trend with larger  $\Delta N_{req}$  values occurring with larger  $V_{s12}$  (Figure 7-11).

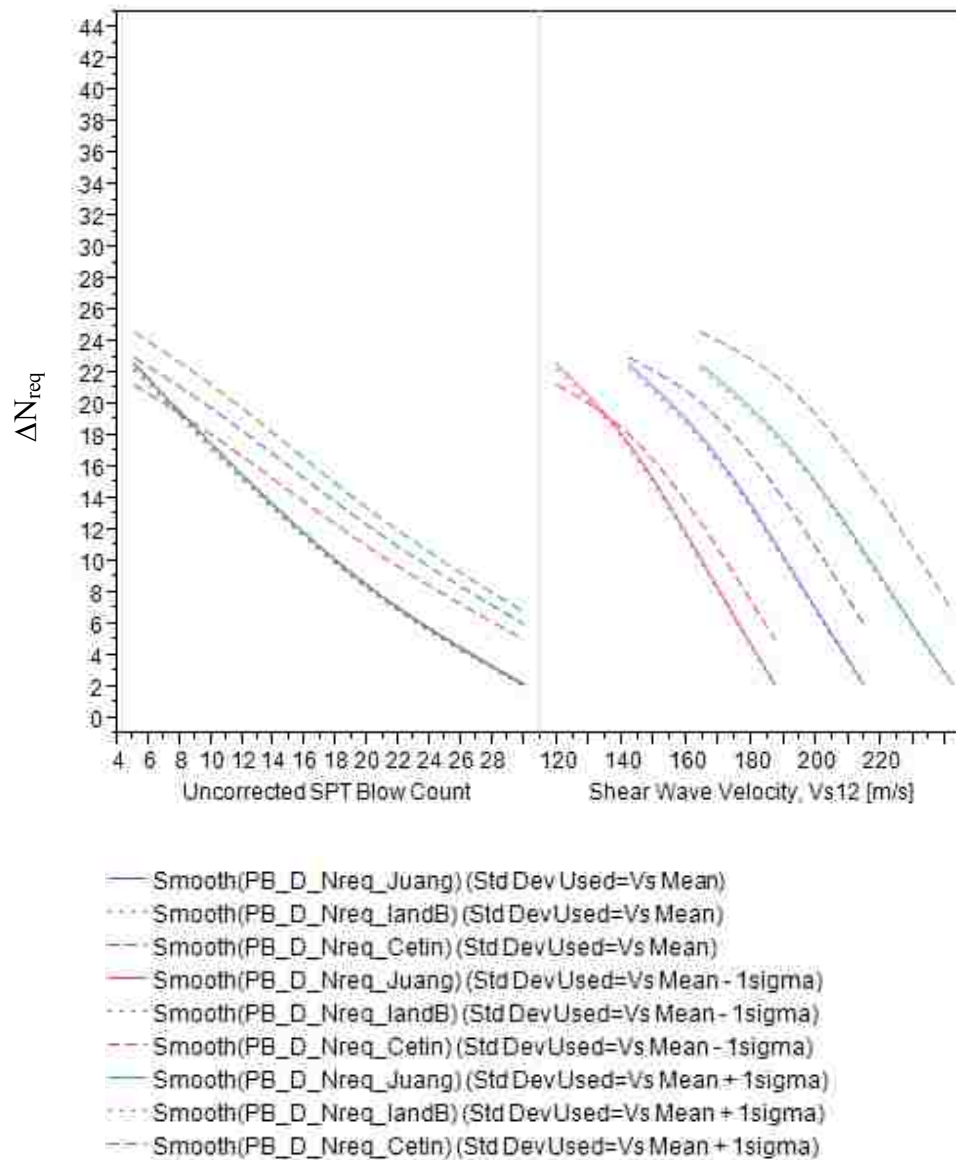


**Figure 7-11: Epistemic uncertainty in  $V_{s12}$  and its overall effect on  $\Delta N_{req}$ .**

A look at how this effect varies with return period reveals cases where the Cetin et al. method becomes less conservative. At lower return periods, as seen previously, the Cetin et al. method becomes less conservative than the Boulanger and Idriss and Juang et al methods (Figure 7-12). The effect of return period on the conservatism of the Cetin et al. method can be increased or decreased by using mean, mean + 1 $\sigma$ , or mean - 1 $\sigma$  values for  $V_{s12}$ .

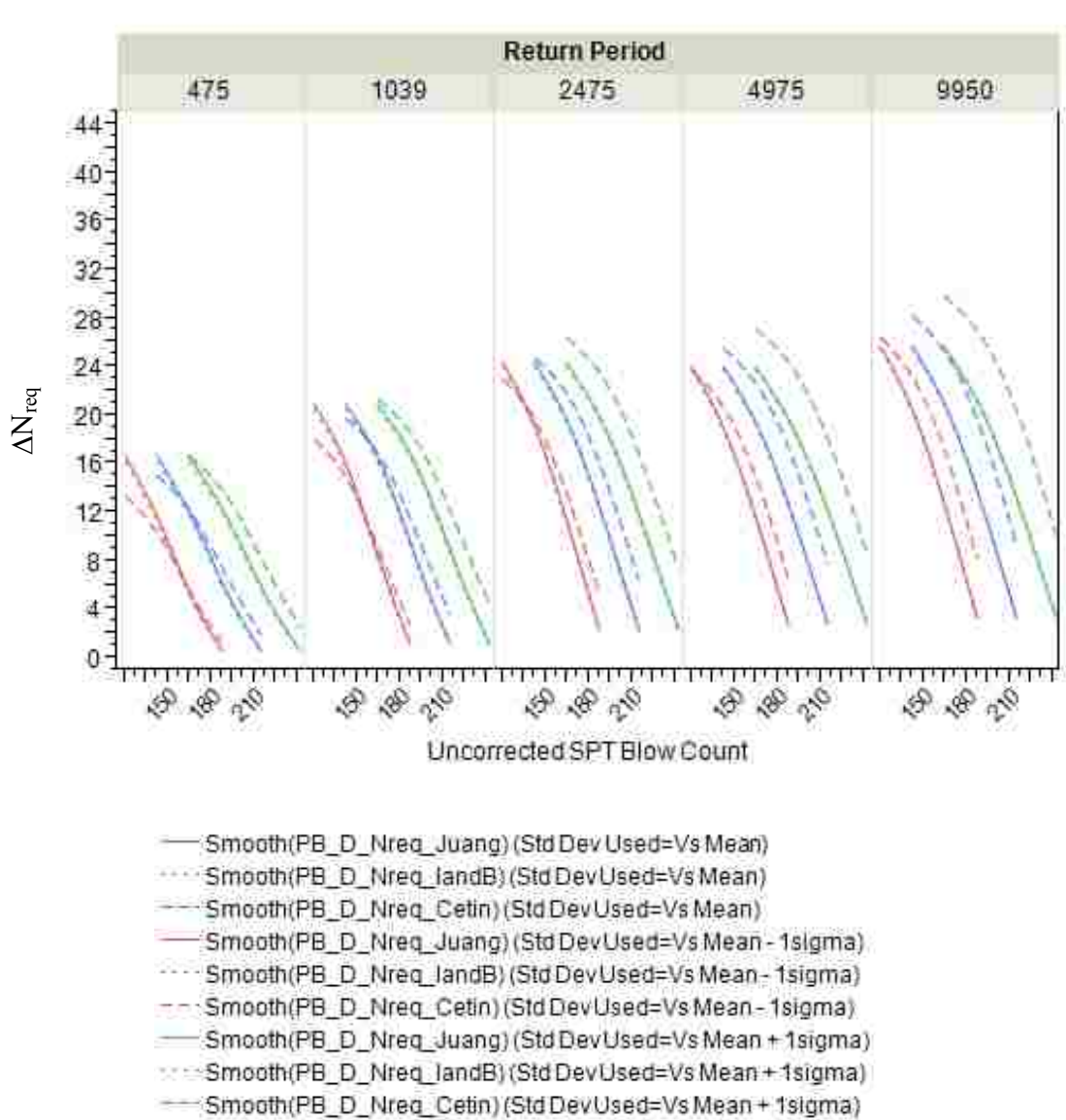


**Figure 7-12: Variations in  $\Delta N_{req}$  by return period.**



As the preceding images outline a trend in the Cetin et al. method which is counter to the current understanding of  $V_{s12}$  and liquefaction, an in depth look at the reasons for such a trend was conducted. An in depth look at the probability of liquefaction equation yields some interesting results that help us to understand why these trends are occurring. In examining the probability of liquefaction equation, an analysis should look at all of the different trends associated with the variables involved.

A sensitivity analysis was performed using the probability of liquefaction equation from the Cetin et al. method and incorporating all calculations starting with the depth reduction factor, working up through the  $CSR_{eq}$  equation, and finally calculating a probability of liquefaction from the values obtained. The analyses were run with 192,864 different combinations of acceleration, magnitude, N value, shear wave velocity, and depth. The ranges of values that were used in this study, and over which this study is valid, are shown below in Table 7-2. The ranges covered by this sensitivity analysis are similar in range and scope to those covered by the performance-based study that makes up the body of this thesis. This means that the trends seen in this study can be used to explain trends seen in the preceding performance-based study. These trends should not be considered valid for a wider range of values as this would constitute an extrapolation of the data.

**Table 7-2: Range of values in sensitivity analysis.**

	<b>Range</b>	<b>Increment</b>
<b><math>a_{max}</math> [g]</b>	0.1-1.1	0.2 g
<b><math>M_w</math></b>	5.0-9.0	0.1
<b><math>V_s</math> [m/s]</b>	120-240, 250	20 m/s
<b>Fines Content [%]</b>	0-40	10 %
<b>Depth [m]</b>	1-19	2 m
<b>SPT blow count</b>	5-35	5
<b><math>\gamma_{sat}</math> [KN/m<sup>3</sup>]</b>	held constant at 18	N/A

The results of this sensitivity study are interesting in that for the most part they follow trends that are reasonable compared to what is currently known about the mechanics of liquefaction. There are however a few inconsistencies in the results that should be noted and should be considered by engineers when analyzing data using the Cetin et al approach.

Looking at acceleration and its effect on the probability of liquefaction reveals a pattern in the data. As acceleration increases the probability of liquefaction increases (Figure 7-13). This is consistent with the current understanding of liquefaction, as higher accelerations would result in larger loads and should result in a greater liquefaction hazard. However, there are a few instances where this trend does not hold true. At low blow counts (in the range of 0-10 blows per foot) the region corresponding to accelerations from 0.350g to 0.475g results in a decrease in the probability of liquefaction as acceleration is increased. The significance of this decrease is small however, and is not considered to be very problematic in general, although it should be considered when analyzing soil profiles with small SPT blow counts.

A look at the effect of magnitude on the outcome of the equations is also useful. A plot of the average values by magnitude and blow count is shown (Figure 7-14). This plot shows a relationship that is consistent with the current theory of how liquefaction triggers. In this plot the relationship that the probability of liquefaction increases as magnitude increases can be seen. Figure 7-13 and Figure 7-14 are also useful in showing how the probability of liquefaction is affected by SPT blow count. As SPT blow count increases the probability of liquefaction decreases. This is consistent with the current understanding of liquefaction.

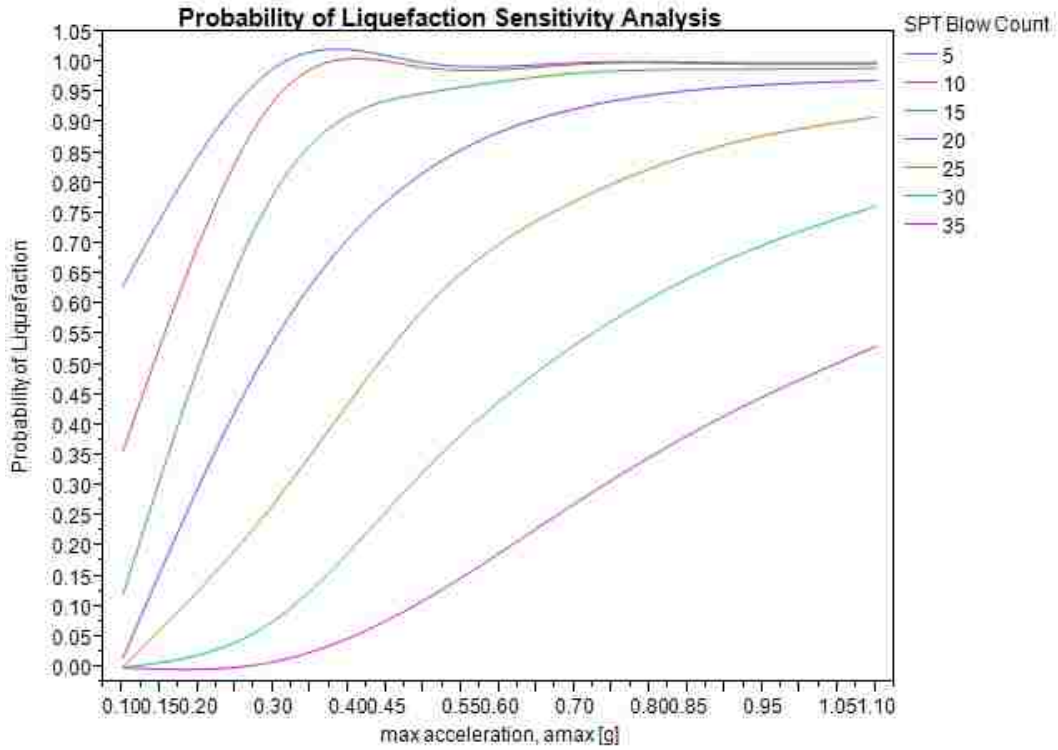


Figure 7-13: Plot of probability of liquefaction by acceleration.

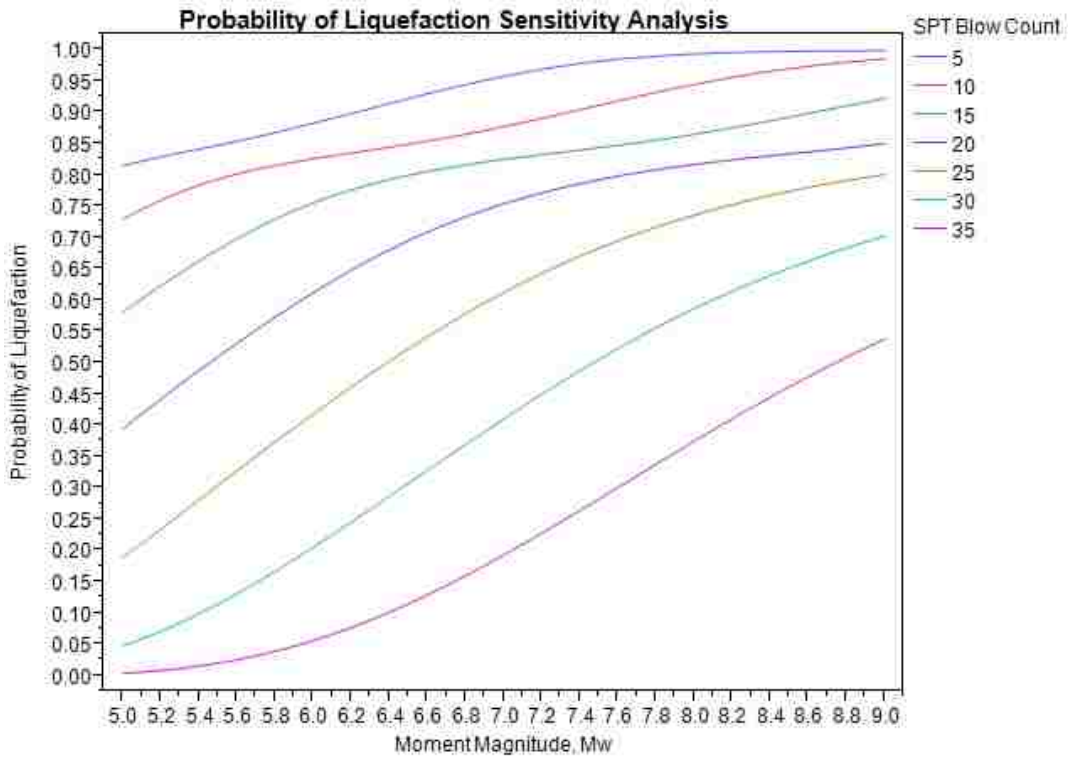


Figure 7-14: Plot of probability of liquefaction by magnitude and SPT blow count.

A look at the effect of depth on the probability of liquefaction reveals a trend of increased probability of liquefaction at intermediate depths, and decreased probability comparatively at shallow and deep depths (Figure 7-15). The large variation at high SPT blow count and shallow depths can also be seen, although this is not terribly concerning as most liquefaction analyses are not considered valid at shallow depths anyways.

A look at the effect of fines content on the probability of liquefaction shows almost no trend in the data, with fines content trending vary slightly downward at high SPT blow counts (Figure 7-16). This results in limiting the effect of fines content.

A look at the effect of  $V_{s12}$  on the overall probability of liquefaction reveals a pattern that is somewhat counterintuitive. If the statistical relationships matched with what is thought to occur base on engineering judgment, as shear wave velocity increases, the probability of liquefaction should decrease. This is not the case. A look at Figure 7-17 shows that as the shear wave velocity is increasing the average value of the probability of liquefaction is increasing. This trend possibly explains the observation why  $\Delta N_{req}$  increases in the Cetin et al. (2012) model with increasing  $V_{s12}$ .

The  $V_{s12}$  and SPT blow count have an interactive effect on each other. One of the questions of interest is whether the  $V_{s12}$  controls the relationship or whether the SPT blow count controls the relationship. A side by side comparison of the average effect of SPT blow count and the effect of  $V_{s12}$  show that the average effect of the SPT blow count is much larger than the effect of the shear wave velocity (Figure 7-18 and Figure 7-19). Thus it is postulated that the SPT blow count controls the outcome of this equation. This is further examined by looking at the effect of SPT blow count on the probability of liquefaction, broken out by  $V_{s12}$ . Again, we

see a much smaller effect from  $V_{s12}$  than from the STP blow count confirming our hypothesis that SPT blow count controls the relationship (compare Figure 7-17 and Figure 7-19).

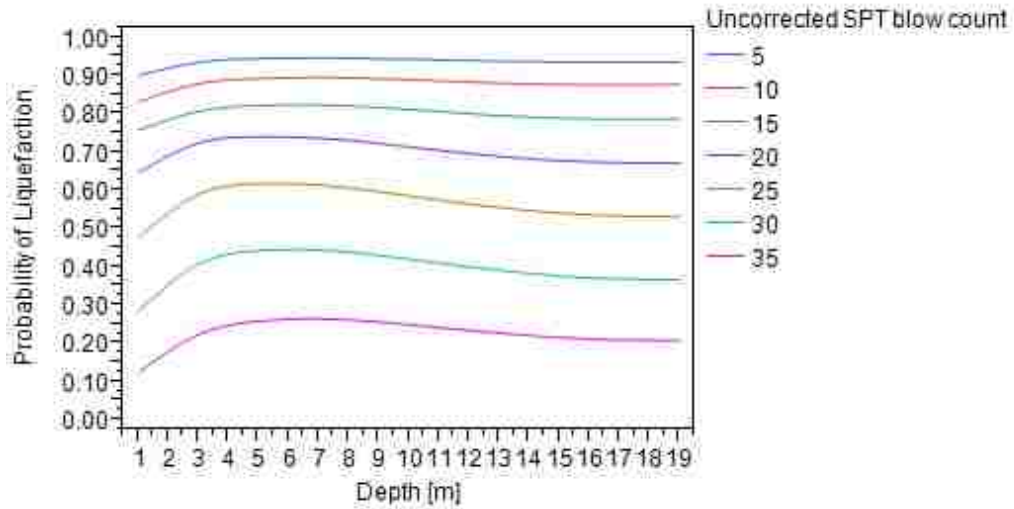


**Figure 7-15: Probability of liquefaction by depth.**

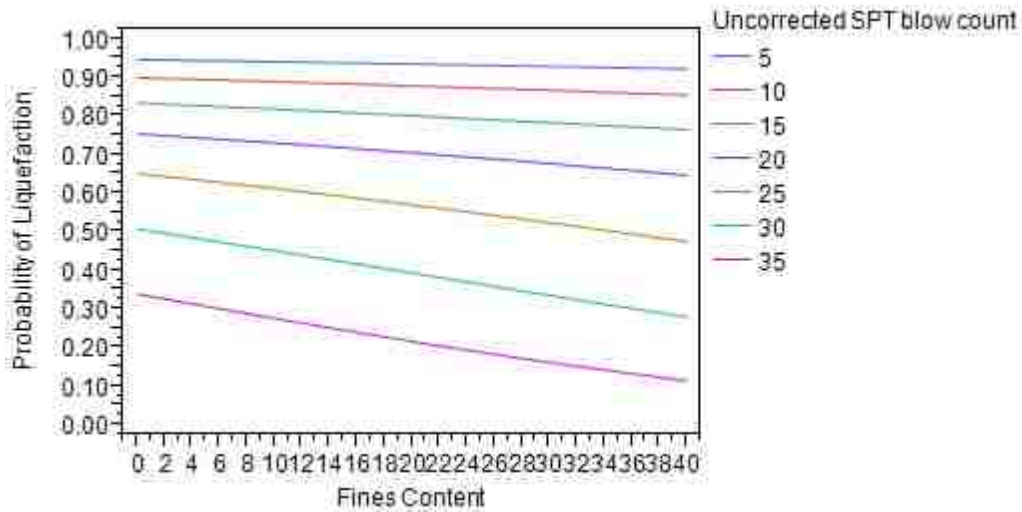


**Figure 7-16: Probability of liquefaction by fines content.**

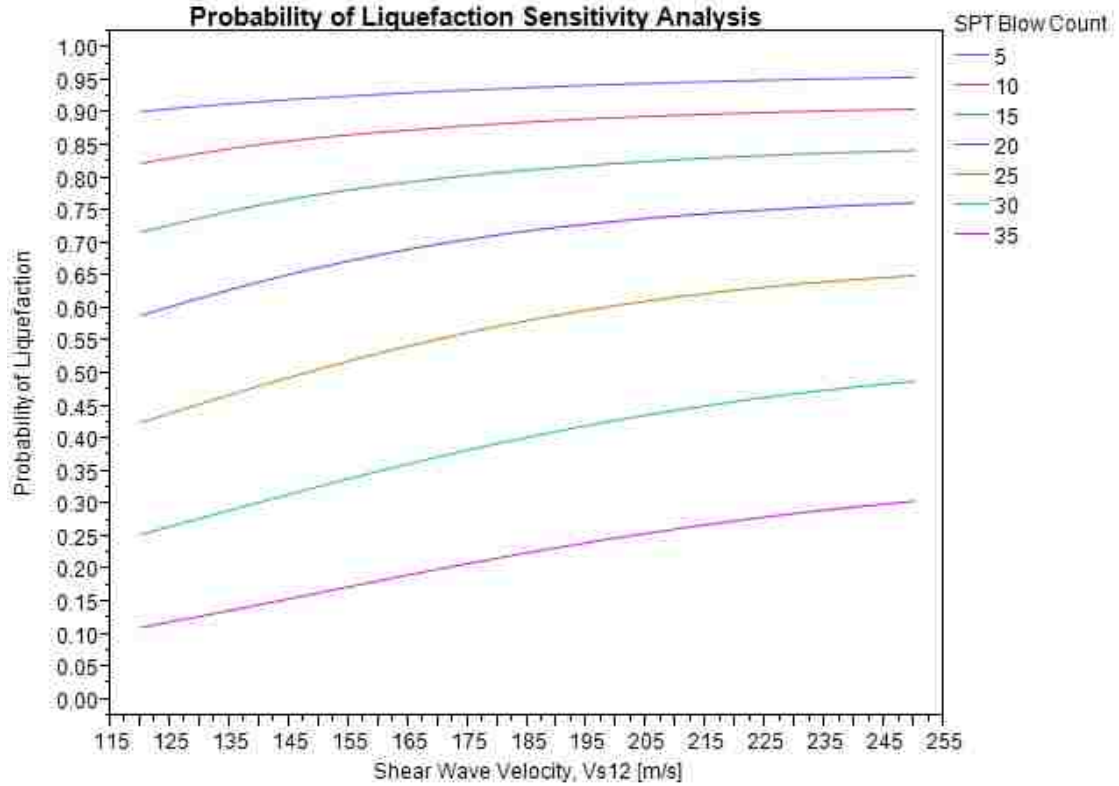


Figure 7-17: Probability of liquefaction by average shear wave velocity ( $V_{s12}$ ).

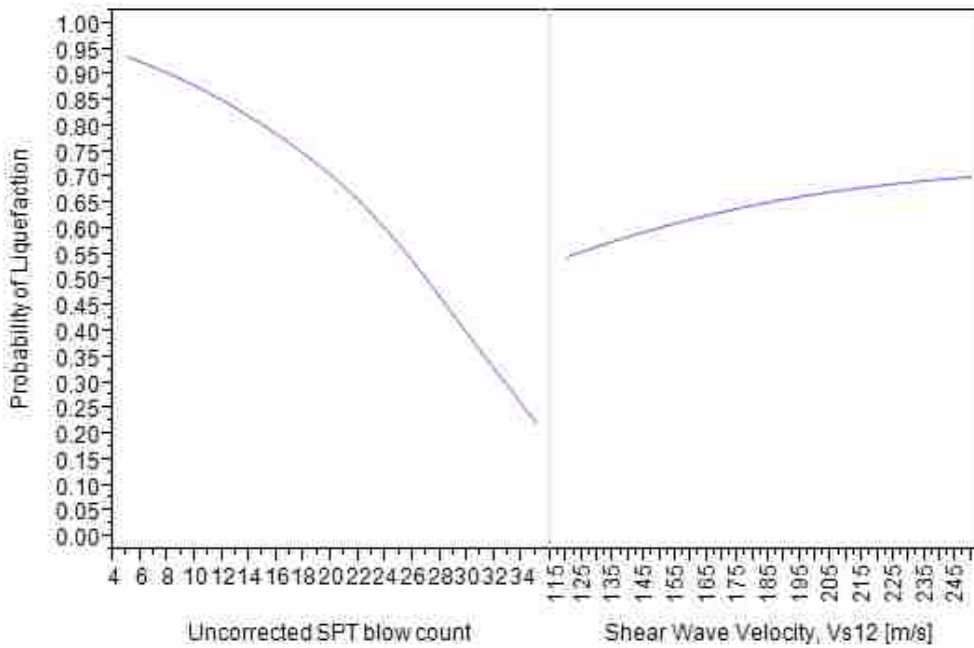
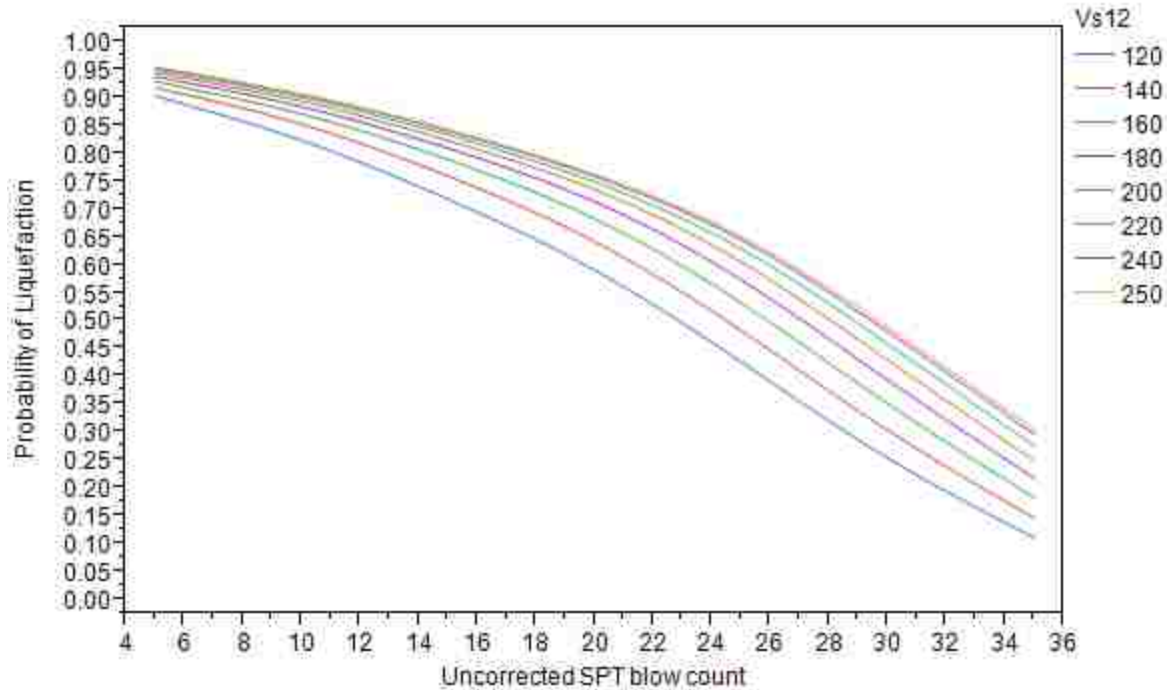


Figure 7-18: Comparison of effect of SPT resistance and  $V_{s12}$  on Probability of liquefaction.



**Figure 7-19: Comparison of effect of shear wave velocity and SPT blow count.**

#### 7.4 Fines Content Variation

Fines content variations affect the values associated with  $N_{site}$ , and thus can affect other aspects of the performance-based values. A look at fines content changes by  $\Delta N_{req}$  reveals how the different methods are affected and whether fines content can cause one method to be more or less conservative. For the 11 locations used in this study the change in fines content causes the  $\Delta N_{req}$  to change for the Boulanger and Idriss and Juang et al. methods (Figure 7-20). At higher fines contents (around 20 %), the Boulanger and Idriss and Juang et al equations become even less conservative on average than at lower fines contents. While difficult to determine the exact location where an increase occurs, it appears that around a fines content of 20% the difference between the average values for the three methods of  $\Delta N_{req}$  increases. It is hard to find an exact value where the relationship's difference increases, as the data was only collected for fines contents at certain intervals (i.e. incremented from 0 to 50 by 10's).

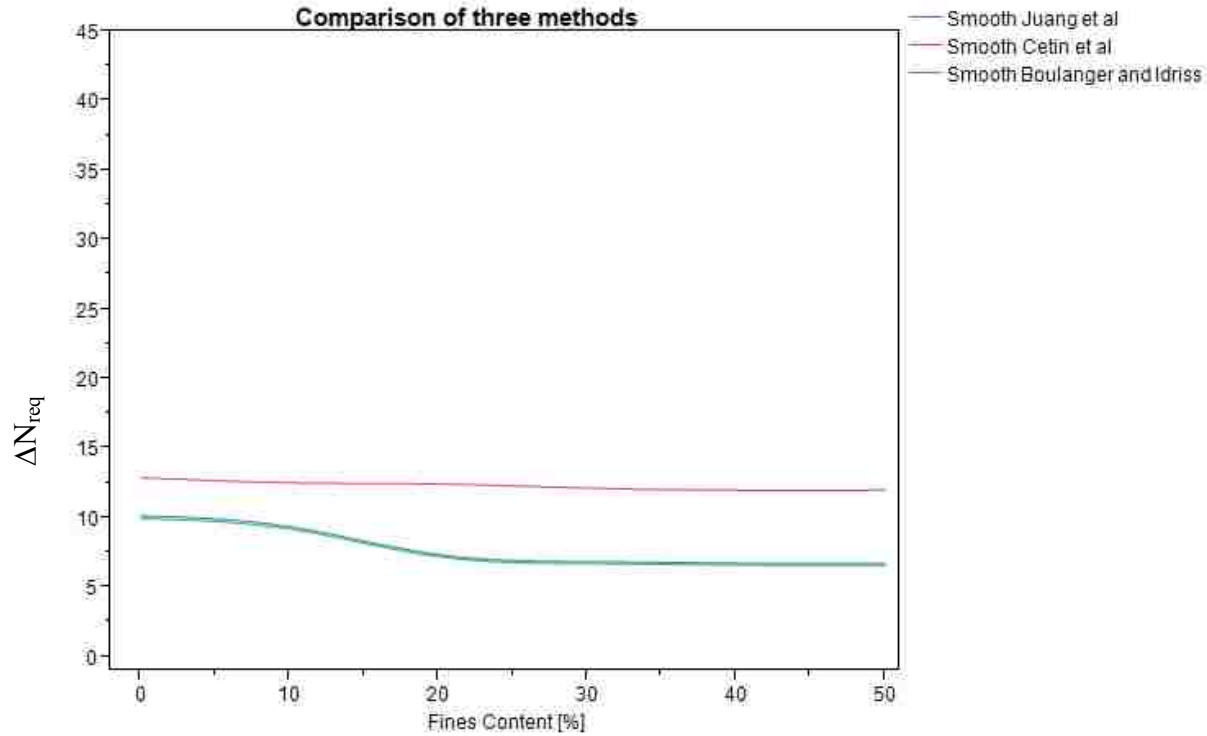


**Figure 7-20: Graph showing changes in fines content and the effects.**

Figure 7-21 is significant because it reveals that the average results of the Cetin et al. (2012) method do not predict a strong impact of fines content on the outcome of the analysis. The Boulanger and Idriss (2012) and Juang et al (2012) methods seem to be much more strongly influenced by the presence of fines, with larger fines contents needing less  $\Delta N_{req}$  than smaller fines contents.

A closer examination of fines content by location (Figure 7-21) shows a similar pattern to that shown with SPT blow count. In the low seismic group the difference between the average  $\Delta N_{req}$  values is relatively small, while in the high seismic group the changes are comparatively large. The pattern of larger differences in regions where higher accelerations exist seems to generally hold true with changes in fines content.



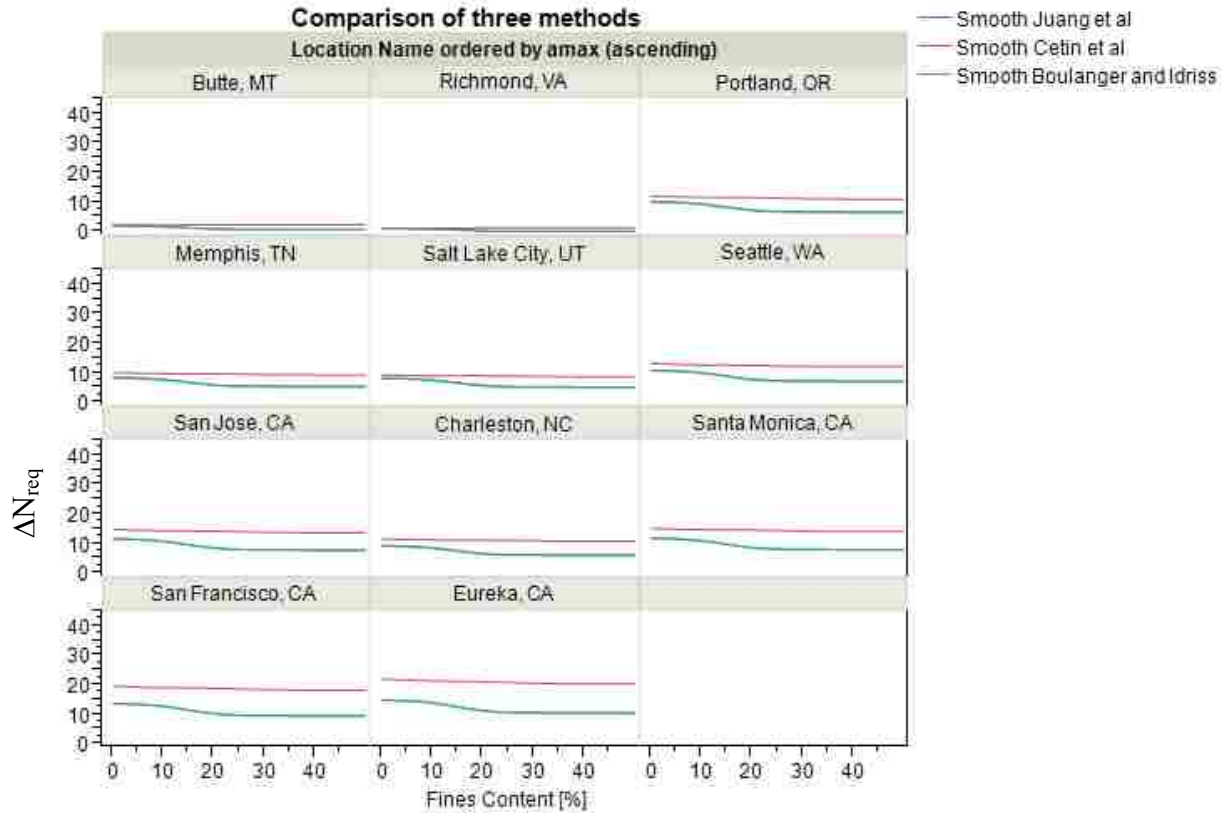


**Figure 7-21: Effects of fines content by location.**

Examination of Figure 7-22 reveals some insight into the differences between the methods. If a break up by uncorrected N value is also included, some instances where the Cetin et al equation is very slightly less conservative are revealed (Figure 7-22) such as in Salt Lake City at very low fines contents. For the most part the methods converge when fines and N values are small, especially in the low and medium seismicity groups. For the high seismicity group, the methods do not converge.

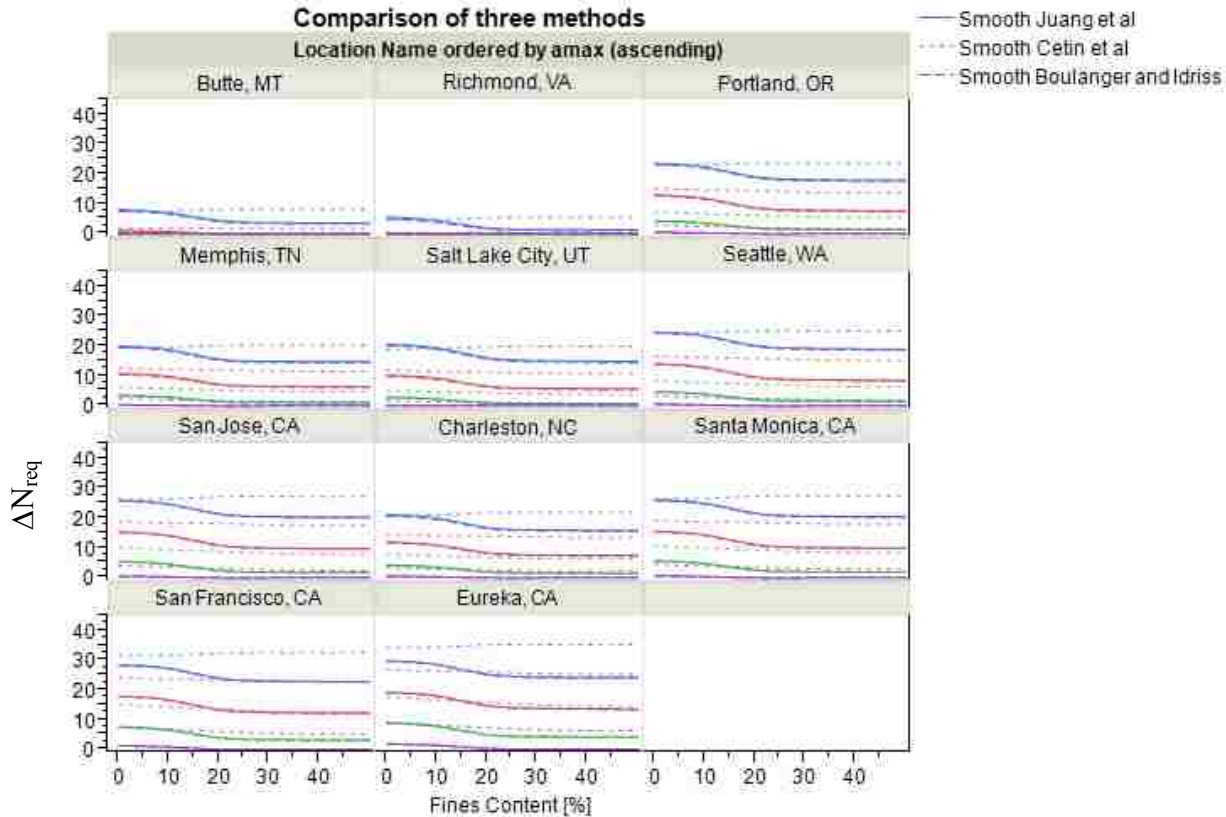


**Figure 7-22: Comparison of effects of fines content by location and uncorrected SPT blow count. (Blue N=5, Red N=15, Green N=25, Purple N=35).**

Another method of analysis used was to examine the data by return period and N value (Figure 7-23). This analysis produced some interesting results, where again, the Cetin et al approach becomes unconservative on average at lower return periods. In this case, the combination of low fines content and low return period, with low N value yielded average  $\Delta N_{req}$  values for the Cetin et al method, which were less conservative than the values obtained using either the Boulanger and Idriss (2012) or the Juang et al (2012) method (see  $T_R = 475$  and 1039 for  $N = 5$ ). For this data at return periods greater than or equal to 2475 years the two newer methods become less conservative than the Cetin et al (2012) method. There appears to be little or no effect of fines content by depth (Figure 7-24).

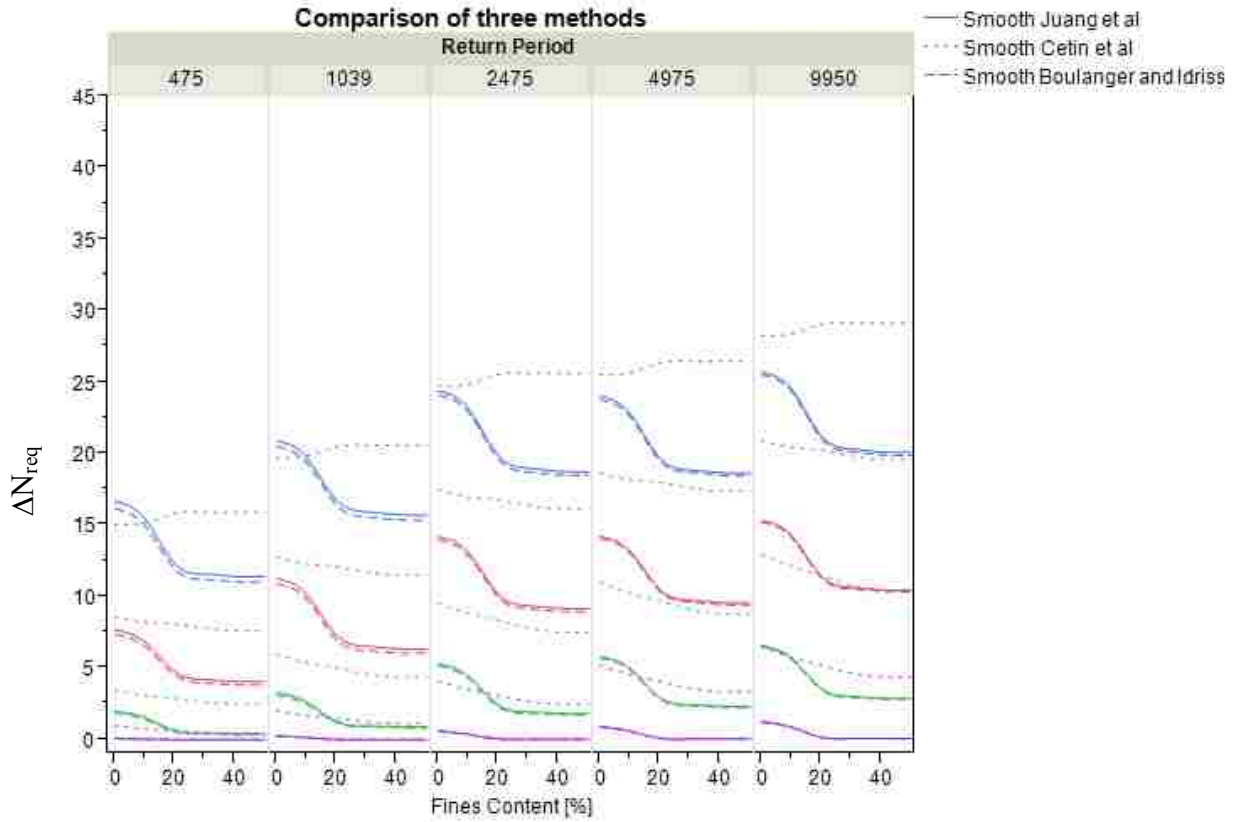


Figure 7-23: Differences in  $\Delta N_{req}$  with fines content, return period and N value. (Blue N=5, Red N=15, Green N=25, Purple N=35).

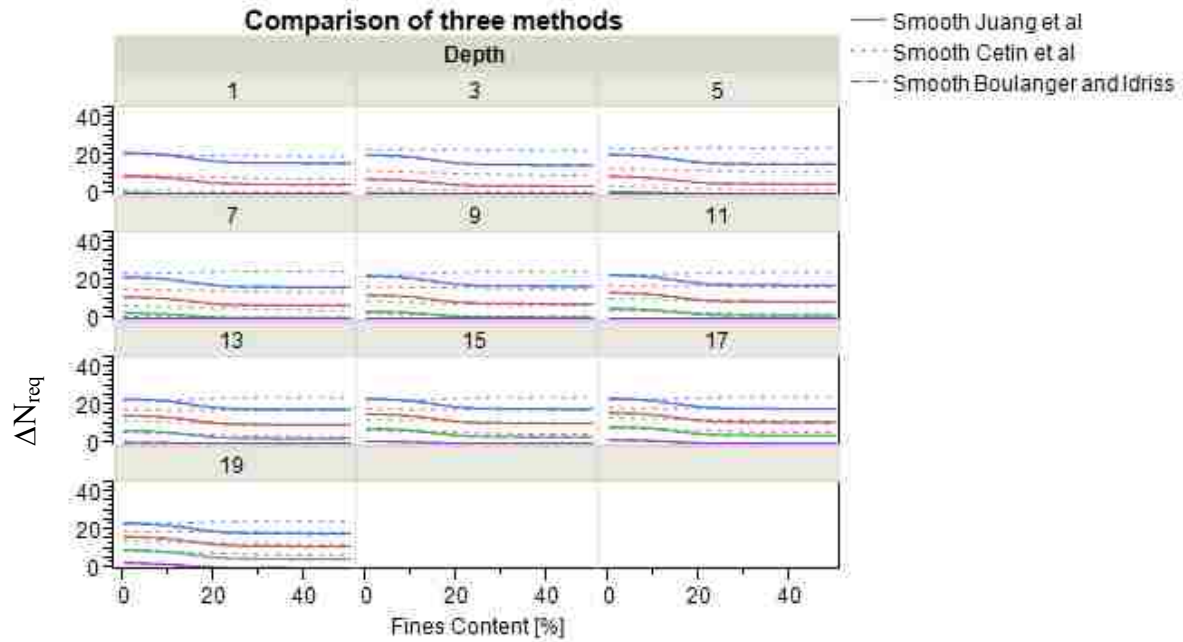
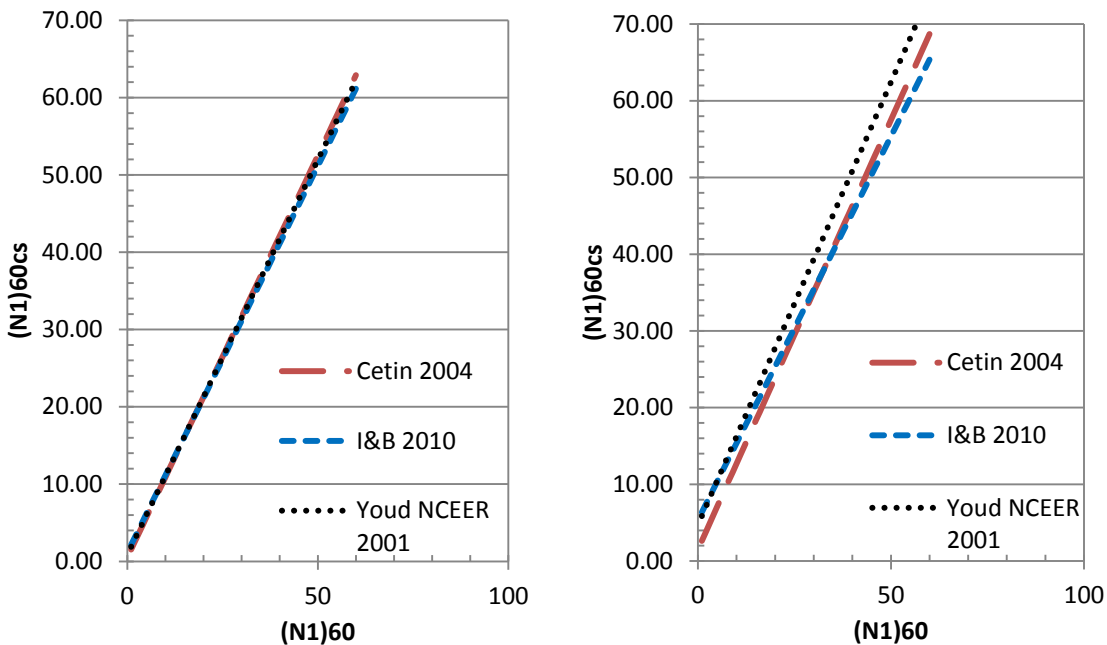


Figure 7-24: Fines content by depth and its effect on  $\Delta N_{req}$ .

Fines content affects all three methods differently as each method uses different correlations to correct to a clean sand blow count. Two graphs comparing the  $(N_1)_{60}$  to the  $(N_1)_{60cs}$  values for different fines contents are shown below (Figure 7-25). In both graphs the line representing the Boulanger and Idriss relationship crosses or approaches the line representing the Cetin et al relationship. This crossing causes the relationship between the Boulanger and Idriss and Juang et al performance-based approaches and the Cetin et al approach to change, in some cases causing them to approach each other, while in others affecting which method is more conservative. Other factors play a role in this as well, with the complex nature of the different interactions making exact predictions difficult.



**Figure 7-25: Comparison of fines content correction at FC = 10 (left) and FC = 30 (right).**

## 7.5 Depth Variation

A more detailed understanding of the differences between the three methods can be obtained by looking at the differences by depth. For this purpose a look at the effect on  $\Delta N_{req}$  as depth changes is beneficial.

A general overall look at how the average  $\Delta N_{req}$  values change with depth gives an understanding of some of the effects that depth has. The results of such an analysis reveal that at shallow depth the two methods produce values relatively closer together, while at larger depths these values tend to diverge (Figure 7-26).

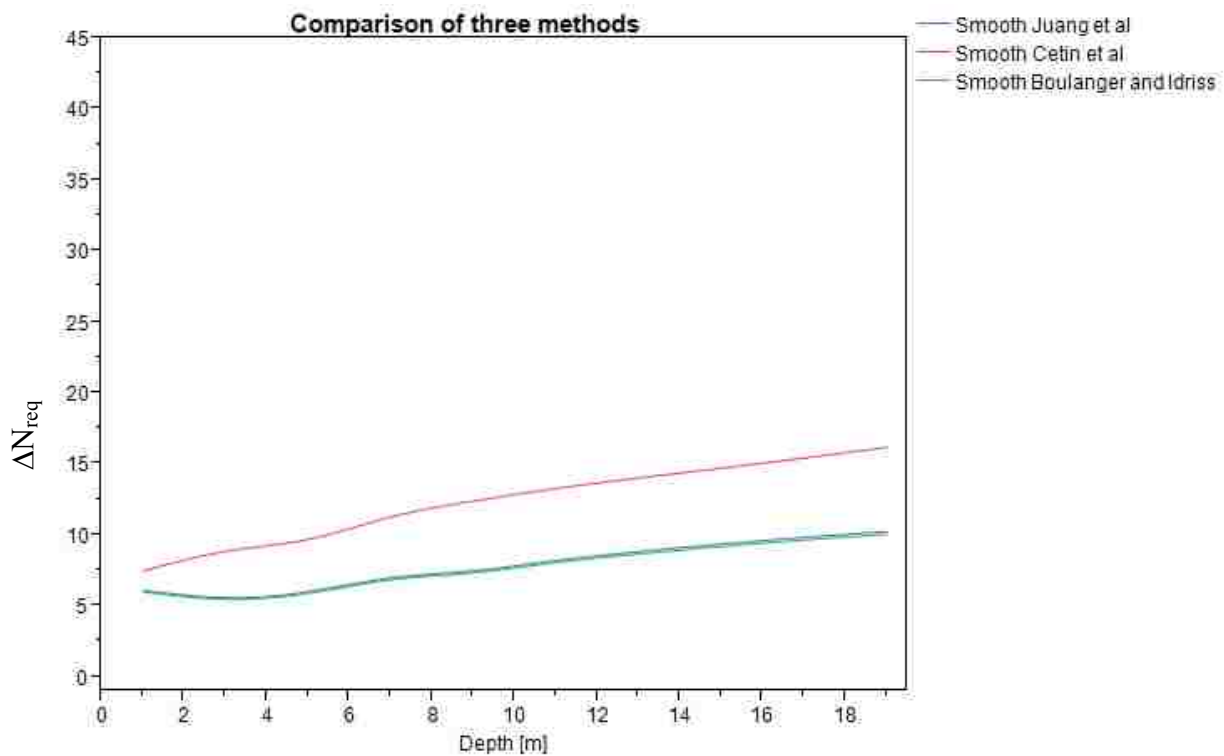


**Figure 7-26: Difference between new methods and Cetin et al method.**

Examination of  $\Delta N_{req}$  by depth and location shows some interesting results (Figure 7-27). Again, when depths are small, the methods are relatively close together while at larger depths the values tend to diverge. The previously observed effect of the low seismic group having the lowest difference and the high seismic group having the highest difference is also preserved here.

Examining these effects by uncorrected SPT blow count does not show the Cetin et al method, on average, ever becoming conservative when looking at the averages from the fully crossed set of variables used in this analysis. It does show that the pattern of smaller differences at shallower depths holds true in this case (Figure 7-28). A similar pattern holds true when examining differences with depth by return period, with differences increasing as depth increases (Figure 7-29). For return period, as return period increases the differences also increase.

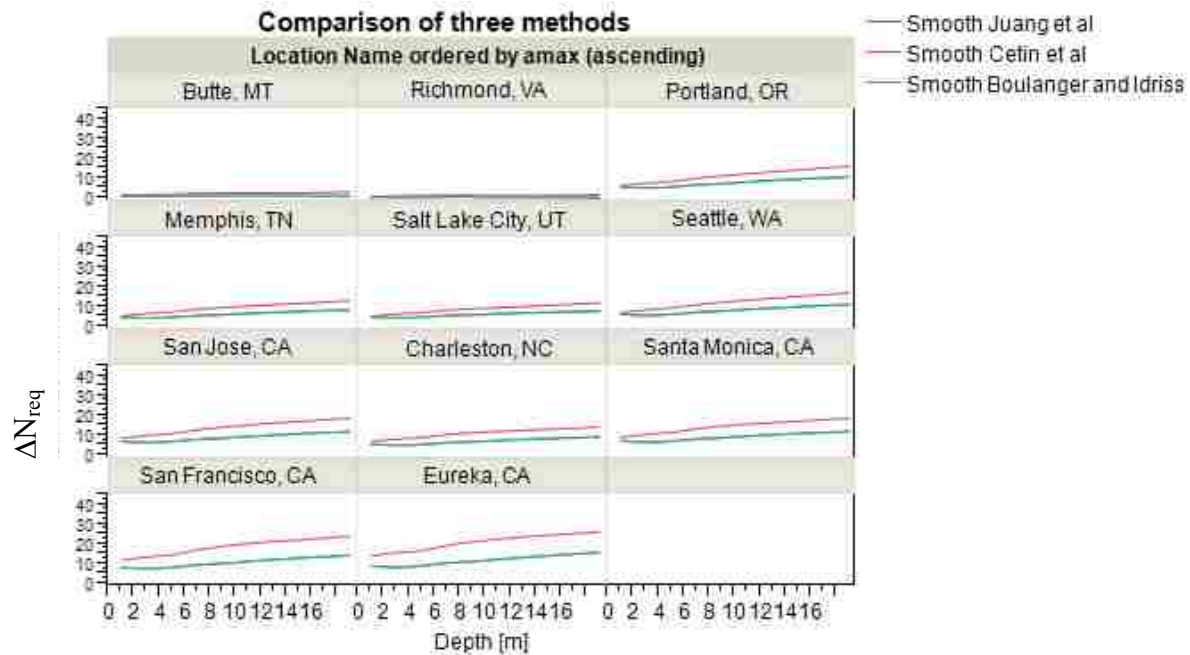
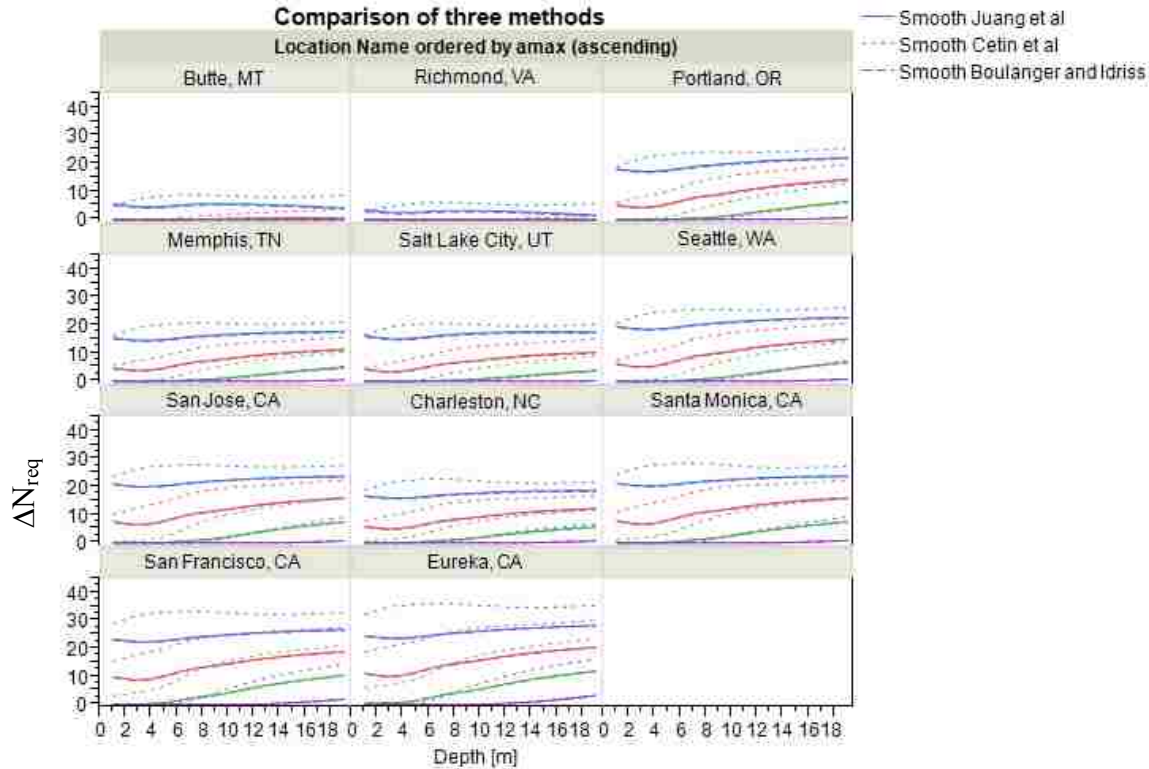
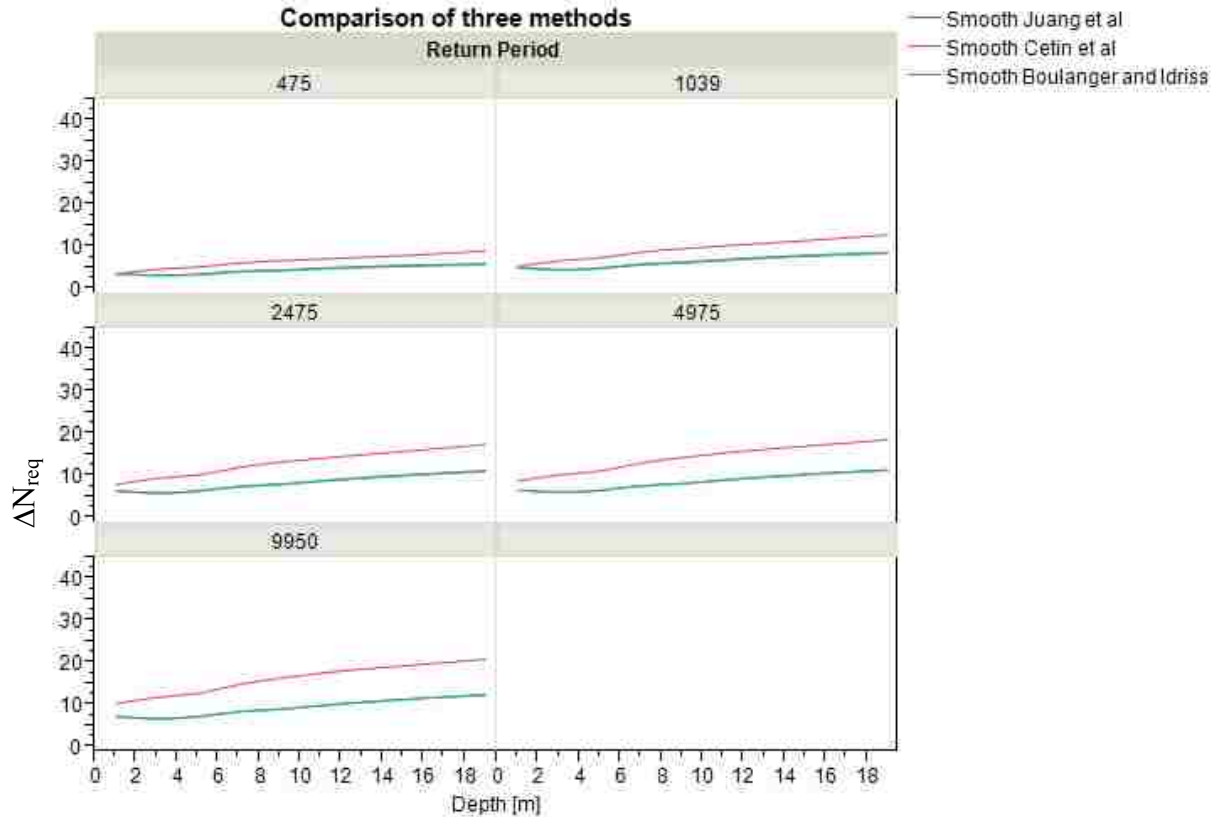


Figure 7-27:  $\Delta N_{req}$  vs. depth at  $N=25$  and  $RP = 2475$ .



**Figure 7-28: Comparison by depth and location (Blue N=5, Red N=15, Green N=25, Purple N=35).**

Overall, for these 11 sites, the change in depth can be seen to cause an increase in the  $\Delta N_{req}$  (Figure 7-29). The Cetin et al. method on average calls for larger  $\Delta N_{req}$  values, especially at greater depths which may be caused by differences in the depth reduction factor. Boulanger and Idriss and in turn Juang et al. both use the form of the equations set forth by Idriss and Boulanger (2010). This form is generally compatible and similar in shape to the recommendations given by the NCEER workshop and by Seed and Idriss (1971). The Cetin et al. depth reduction factor is a new version of the depth reduction factor found using modern statistical methods and was first introduced by Cetin and Seed (2004). A comparison of the Idriss and Boulanger (2010) and the Cetin and Seed (2004) depth reduction factors for a range of values is shown below in Figure 7-30.



**Figure 7-29: Changes in  $\Delta N_{req}$  by depth and  $T_R$ .**

A close examination and comparison of the depth reduction factor reveals a very similar pattern with depth to what was seen in the preceding analysis with increased differences at greater depths. At small depths the two methods predict relatively the same depth reduction factor (i.e. 1.0); at larger depths the differences between the methods become greater. In the same way the preceding analysis showed, the values are relatively close together at shallower depths and further apart at deeper depths.

For practical purposes when the magnitude of the earthquake being examined is about 7.5 with an acceleration of 1 and a shear wave velocity of 150 m/s, the two methods are relatively similar to depths of about 3 meters with the divergence between them being limited to about a 16% difference. At greater depths the divergence increases.



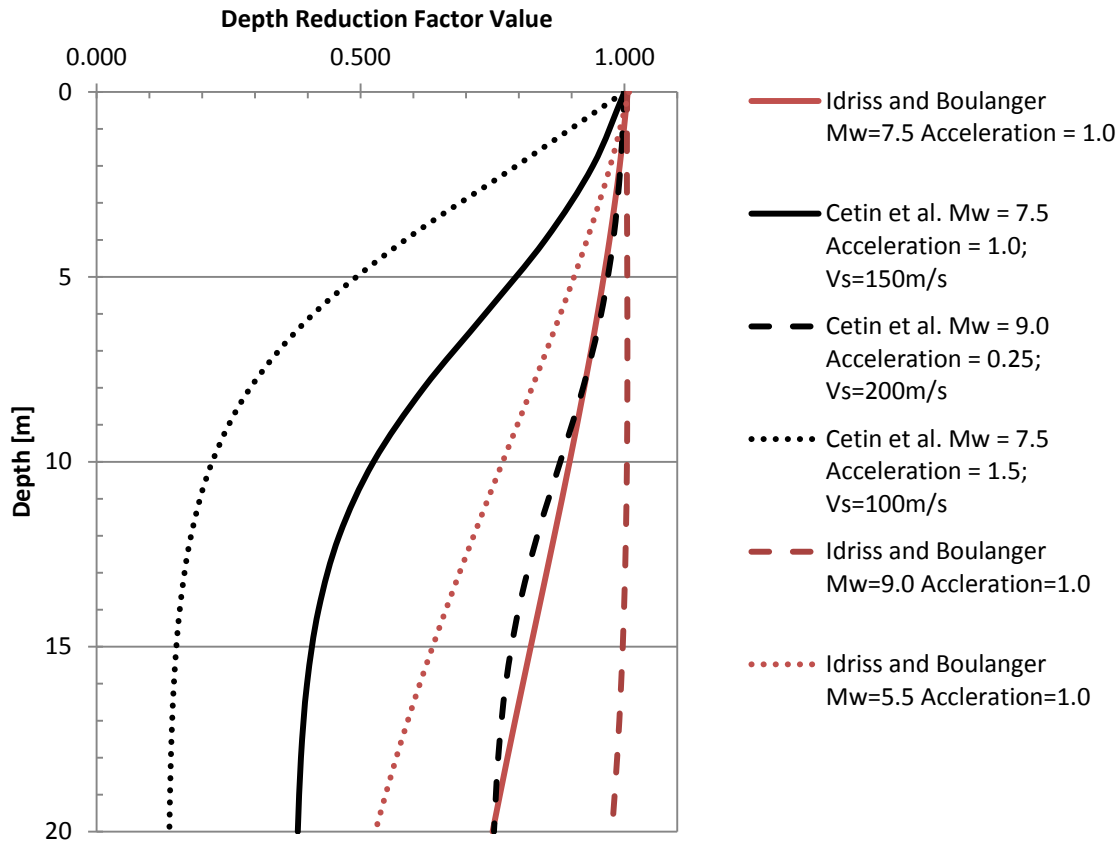


**Figure 7-30: Comparison of Cetin and Seed and Boulanger and Idriss depth reduction factors.**

Interestingly, the methods can be brought to match each other by leaving the magnitude and acceleration at those stated above for Boulanger and Idriss and for the Cetin et al depth reduction factor, increasing the magnitude to that of a 9.0, and decreasing the acceleration to 0.25 g. The difference between the average  $r_d$  values from the two methods is large; although, the ranges of possible values from the two different methods overlap each other. The Cetin et al method of calculating the depth reduction factor overall produces a wider range of possible

values however. The difference in the depth reduction factor at least partially explains the differences between the methods at greater depths.

### 7.5.1 K Sigma Limit

Boulanger and Idriss proposed a limit for  $K_\sigma$  of 1.1. However, they also stated that if the value was not limited the effect would be minimal (Idriss and Boulanger 2010). An understanding of how this limit affects the overall outcome of the analyses is useful in helping engineers determine whether the use of this limit is advisable or not.

If the  $K_\sigma$  limit as proposed by Boulanger and Idriss is not used and instead the value of  $K_\sigma$  used in their relationships is allowed to vary according to the equation, then the Boulanger and Idriss and the Juang et al. methods will tend to converge less sharply at shallow depths. The effect of the different  $K_\sigma$  limit is really only seen at these shallower depths (Figure 7-31).

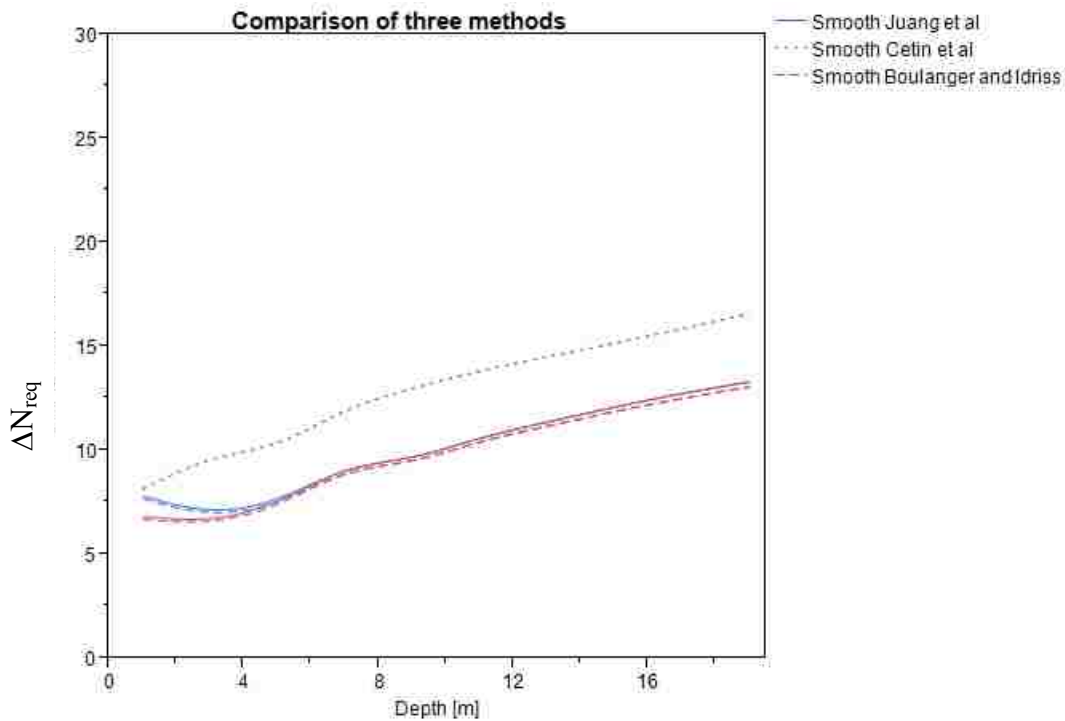
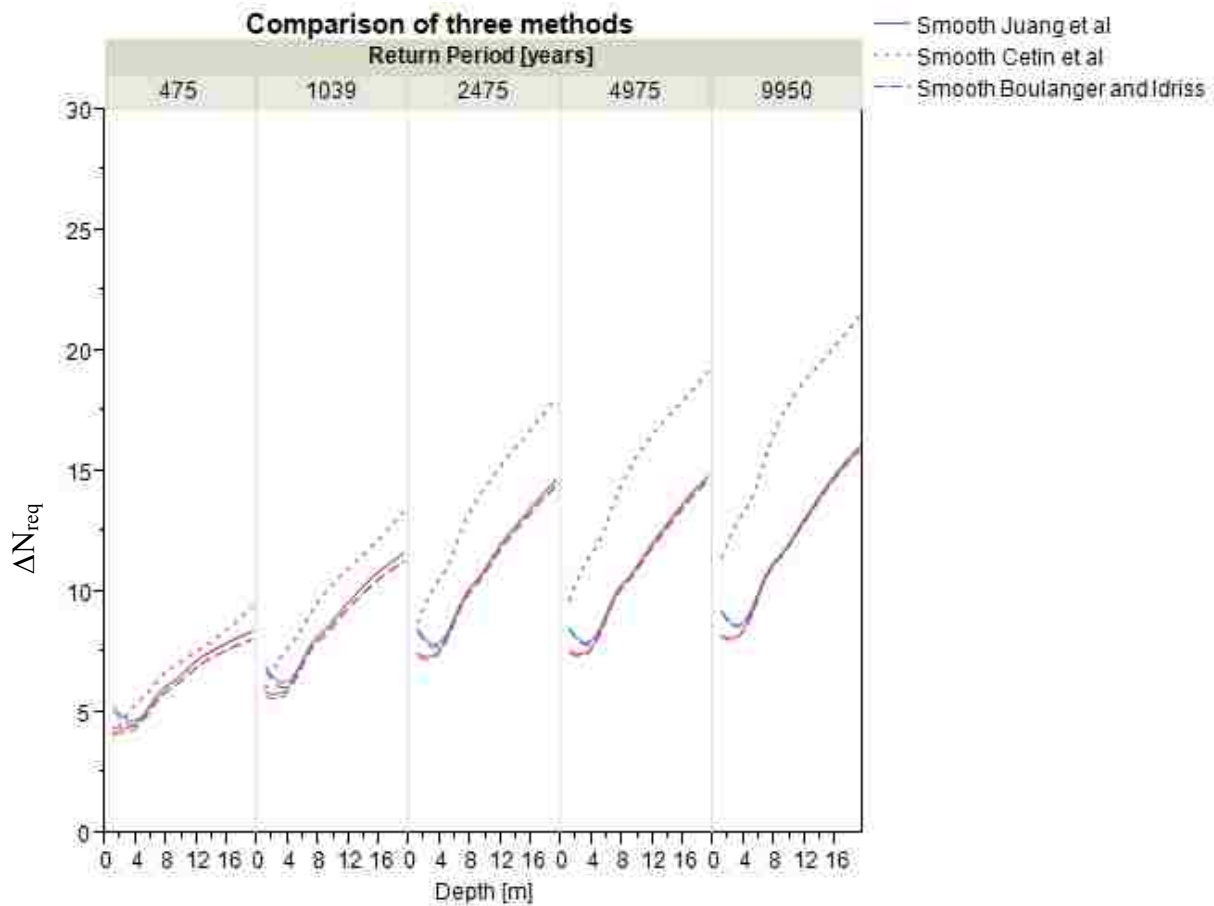


Figure 7-31:  $K_\sigma$  limit effect (red without limit, blue with limit).

A look at the effect of the  $K_\sigma$  limit by return period and SPT resistance value suggests, for small SPT resistances ( $N \leq 15$ ) and small return periods ( $\leq 1039$  years) the effect of the  $K_\sigma$  limit is more likely to affect which equations will be more conservative (Figure 7-32 and Figure 7-33). If the limit is used at small return periods and small N values then there are cases where the Cetin et al method becomes less conservative on average than the Boulanger and Idriss and the Juang et al methods (Figure 7-33). The effect of the  $K_s$  limit seems to only affect shallow depths to about 4 meters. The soil profiles used in this analyses were clean sands and so were closer together than they would be at higher fines contents. If fines were present the resulting relationships would be less likely to cross.



**Figure 7-32: Effect of  $K_\sigma$  limit with varying return periods. (Red without limit, Blue with limit).**

The effect of fines content has a large effect. For this analysis where fines content equaled 0 there are a large number of points where the three relationships will cross. A close examination of Figure 7-33 shows that with these lower fines contents (compared to the fines contents used in the study) the relationships will cross much more often, and in some cases the Boulanger and Idriss and Juang et al. methods are more conservative at almost every depth. This only holds true for this case where clean sands are used however, and as seen in the previous analyses of all 24 soil profiles, the average results of the three methods generally tend to leave the Cetin et al. method as the more conservative method overall.

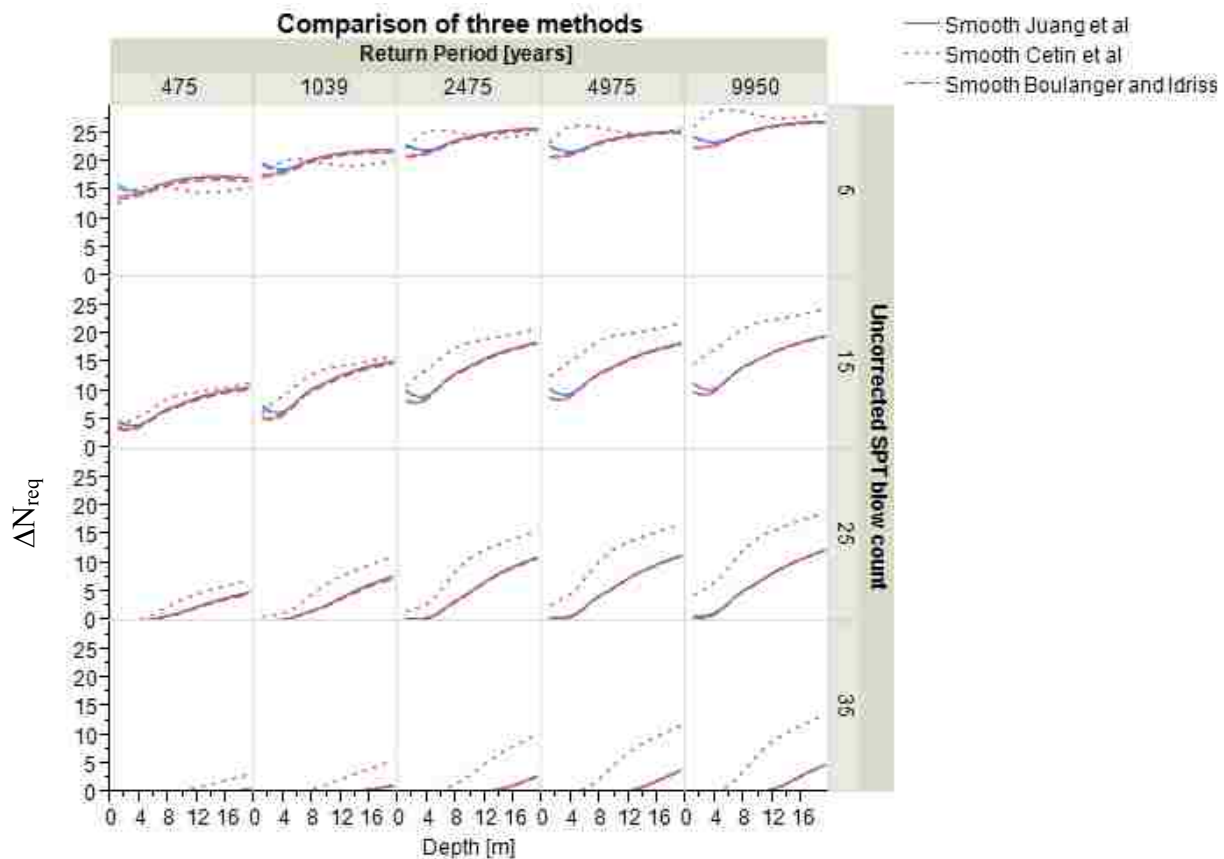


Figure 7-33: Effect of the  $K_{\sigma}$  limit by return period and uncorrected SPT blow count. (Red without limit, Blue with limit).

## 7.6 Return Period Variation

A direct examination of the return period shows the average trends in the data (Figure 7-34). For return period variation, the  $\Delta N_{req}$  value can be seen to increase. The divergence between the Cetin et al method and the two methods developed in this paper can be seen to become increasingly large at larger return periods. Overall, all of the methods are similar in that as return period increases, the  $\Delta N_{req}$  increases. For the Boulanger and Idriss and Juang et al methods the increase at return periods past about 1500 years seems to be almost negligible as the line begins to flatten out at larger return periods. An examination of the effect of return period by location shows similar results (Figure 7-35) and shows that the patterns seen previously are again preserved with regards to seismic groups.

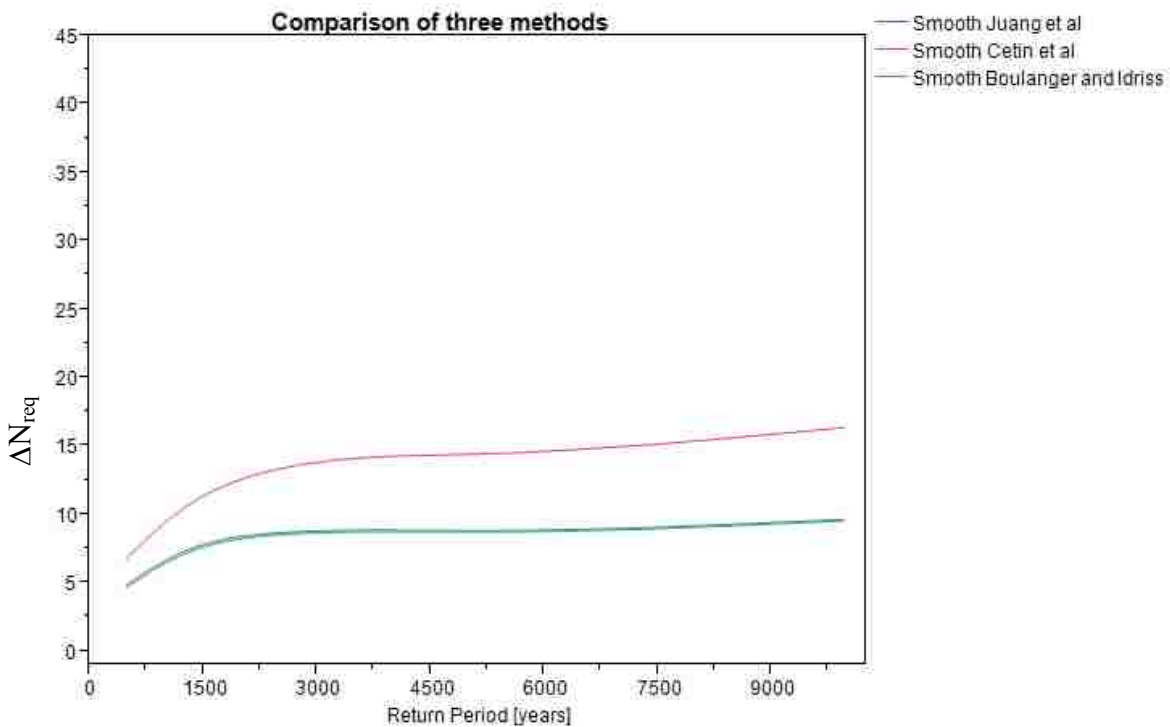
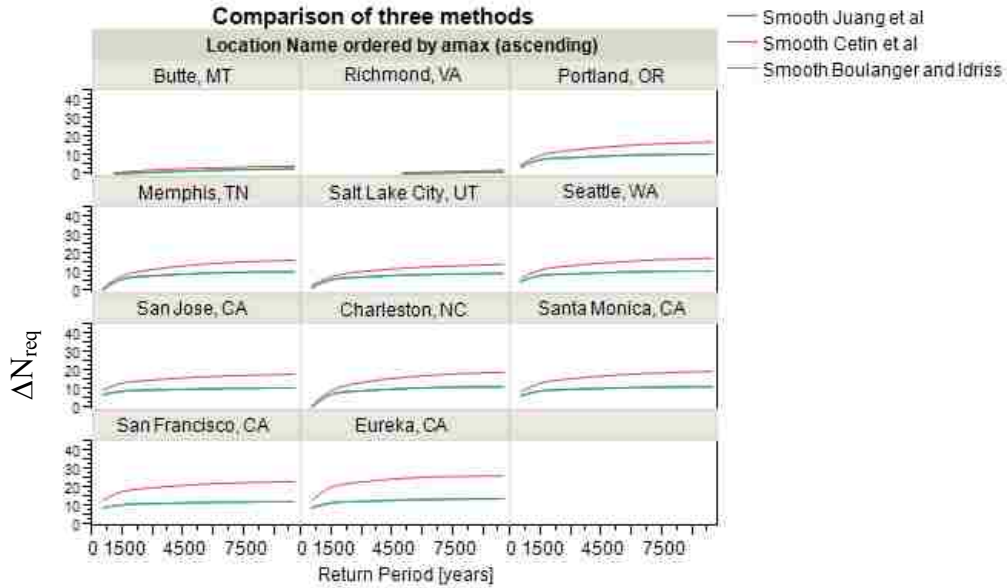


Figure 7-34: Return Period vs. Mean  $\Delta N_{req}$ .



**Figure 7-35: Return Period vs. Mean  $\Delta N_{req}$ .**

A closer look at the effect of return period by location with regards to SPT blow count reveals similar patterns as shown above (Figure 7-36), although for some locations at low return periods and low values of  $N$ , the three methods seem to converge. This occurs only in the low and medium seismicity groups. For high seismic groups and higher values of  $N$ , the Cetin et al. method is more conservative.

The effect of the return period on the differences in the equations can be either small or dramatic depending on the soil profile and the return period involved. However, as shown previously, as return period increases the differences between the respective methods increases as well. Some of this can be explained by the shape of the hazard curves associated with the each method. A typical hazard curve is shown in Figure 7-37, which shows that the hazard curves for the various models follow similar patterns. The difference between  $N_{req}$  increases with increasing return period (i.e. smaller mean annual rate of exceedance), similar to the pattern shown in Figure 7-34 through Figure 7-36.

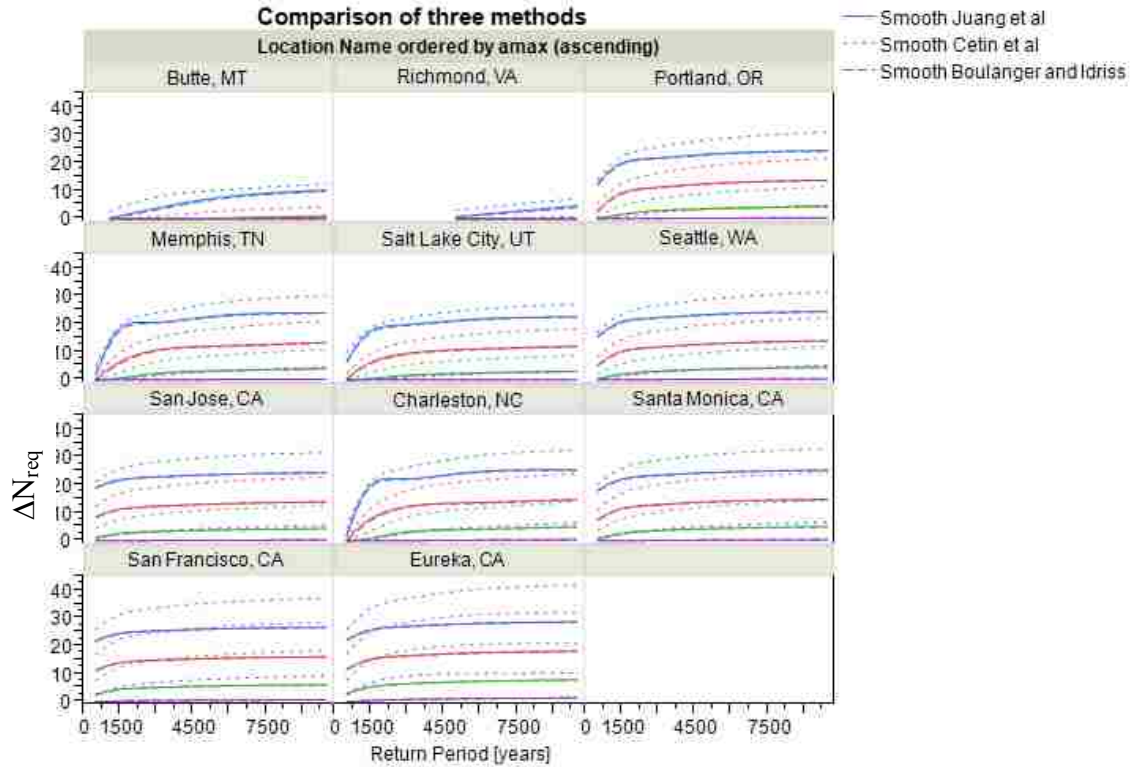


Figure 7-36: Effect of return period on  $\Delta N_{req}$  by location (Blue  $N=5$ , Red  $N=15$ , Green  $N=25$ , Purple  $N=35$ ).

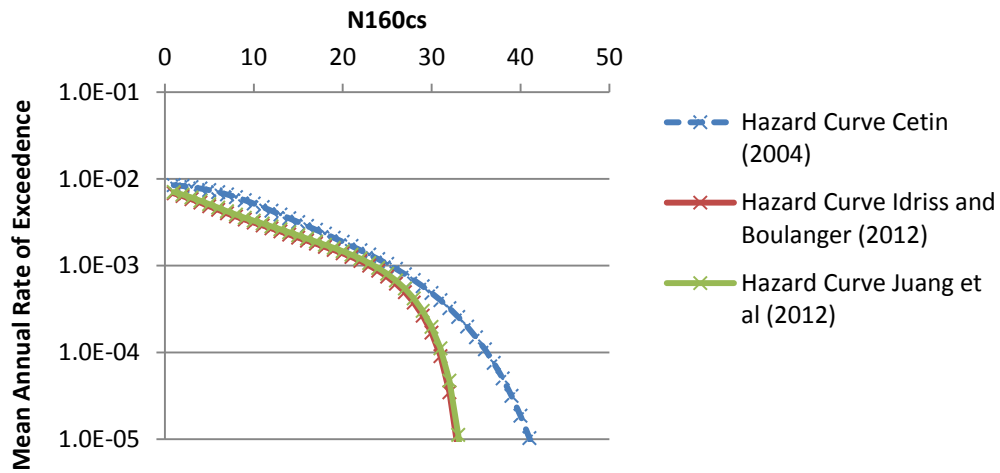


Figure 7-37: Hazard curve developed for  $N=15$  excluding parameter uncertainty for a soil layer at a depth of 8 meters located at latitude 40.671 North longitude 111.791 West.

## 7.7 Parameter Uncertainty Error Term

Looking at the parameter estimation error associated with the Boulanger and Idriss equations it is possible to see how the different ways of calculating the error change the way in which the analysis is run. To analyze the effect of parameter uncertainty and the different ways of handling the error involved, liquefaction analyses were run on soil profiles 1, 7, 13, and 19 (all the soil profiles with no fines). After running the analysis the methods of accounting for parameter uncertainty are compared to each other to see how the use of parameter uncertainty error affects the outcome of the results.

A brief overview of the analysis types helps to understand some of the trends that occur. First, the inclusion or exclusion of parameter uncertainty will increase or decrease the overall uncertainty. For practical purposes the practicing engineer should usually incorporate parameter uncertainty in the model as this will allow for variation due to inaccuracies in the measurements. There are several different ways that were proposed by the different authors in analyzing the uncertainties involved. These different ways include including or excluding parameter uncertainty, and using a constant or variable uncertainty term (Boulanger and Idriss (2012) method only). For the purposes of the analysis currently under consideration constant error is where a single overall uncertainty is used and variable error is where the COV is used in calculating error (applies only to Boulanger and Idriss method).

A direct comparison of the three different methods of accounting for error is shown in Figure 7-38. It should be noted that the slightly different shape of these graphs when compared to previous graphs occurs because these analyses were run only for a fines content of 0.



This fines content of 0 pulls the overall averages of the Cetin et al. method down at small SPT blow counts. This is consistent with the effect of fines content on the analysis (see fines content analysis on page 123).

When all three methods are compared directly the general trend when using constant parameter uncertainty is similar to that seen previously. The net effect of the increased uncertainty is to shift the curves upward. The use of variable uncertainty with the Boulanger and Idriss (2012) procedure, however, leads to a change in the overall relationship between the methods. When variable uncertainty is included in the Boulanger and Idriss method, the Boulanger and Idriss method becomes more conservative than the Juang et al method. It also becomes more conservative than the Cetin et al. method at low SPT resistance (N=5) and low return periods (Figure 7-39).

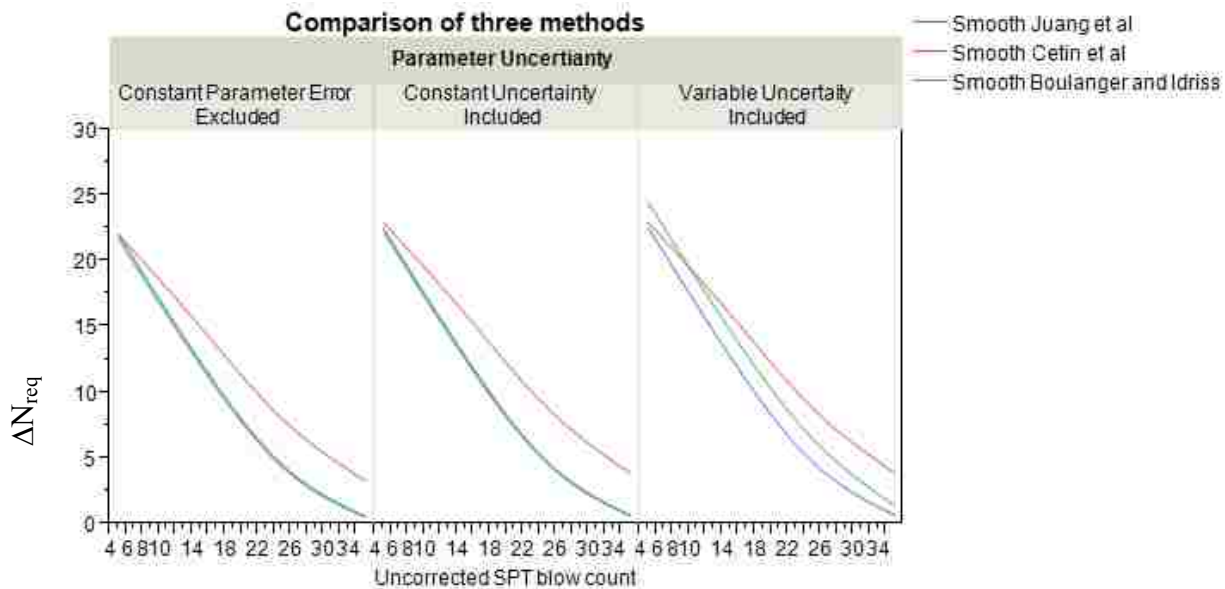


**Figure 7-38: Comparison of three methods for fines content of 0 and various ways of accounting for parameter error.**

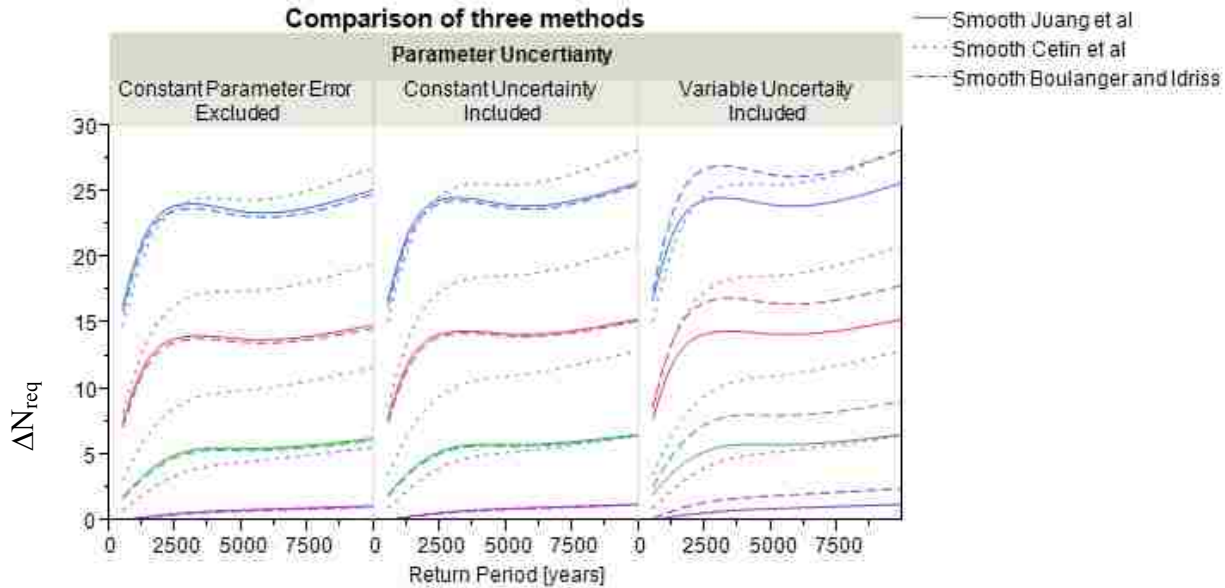


**Figure 7-39: Variation caused by uncertainty term in equations. (Blue N=5, Red N=15, Green N=25, Purple N=35).**

## 7.8 Applying Performance-Based Magnitude Scaling Factors

Due to the complexity of running the analysis with performance-based magnitude scaling factors ( $MSF_{PB}$ ) the analyses in this section are by necessity limited to two sites and a single soil profile. These limitations were considered necessary because the level of complexity increases exponentially due to the increase in the number of computations associated with the  $MSF_{PB}$  (See ). The sites were located in San Francisco, CA and Butte, MT. These sites were used with soil profile 7 for this analysis of  $MSF_{PB}$ . The analyses was run with liquefaction onset defined by  $r_u$  values of 0.90, 0.95, 0.99, and a standard definition typical of the respective relationships. The return periods analyzed were 475, 1039, 2475, 4975, 9950 years.

The results of the analysis show that for decreasing values of liquefaction onset, the results of the analysis will be less conservative. For example, shown below is a graph showing the  $MSF_{PB}$  by depth on soil profile 7 in San Francisco, CA. For this site if liquefaction is defined as  $r_u = 0.9$  then the results will be more conservative than at  $r_u = 0.95$  for all depths analyzed.

The difference between the 4 different definitions increases with depth, with the larger depths showing larger differences but retaining the same order (Figure 7-40). Similar results are obtained for the site in Butte, MT except that all of the trends are reversed (Figure 7-41). For the site in Butte and soil profile 7 the results become more conservative as  $r_u$  increases.

These results imply that when  $MSF_{PB}$  are used for low seismicity sites they result in a decreased  $\Delta N_{req}$  while at higher seismicity sites an increased  $\Delta N_{req}$  occurs. In Figure 7-42 it can be seen that the trend of  $MSF_{PB}$  reverse themselves at a magnitude 7.5. For the two sites used in this analysis of the effect of  $MSF_{PB}$  Butte is a low seismicity site with  $M_w < 7.5$ , and San Francisco was a high seismicity site with  $M_w > 7.5$ . Thus the reversal in the trends is due to the relationships proposed by Cetin and Bilge (2012) and their dependence on  $M_w = 7.5$ .

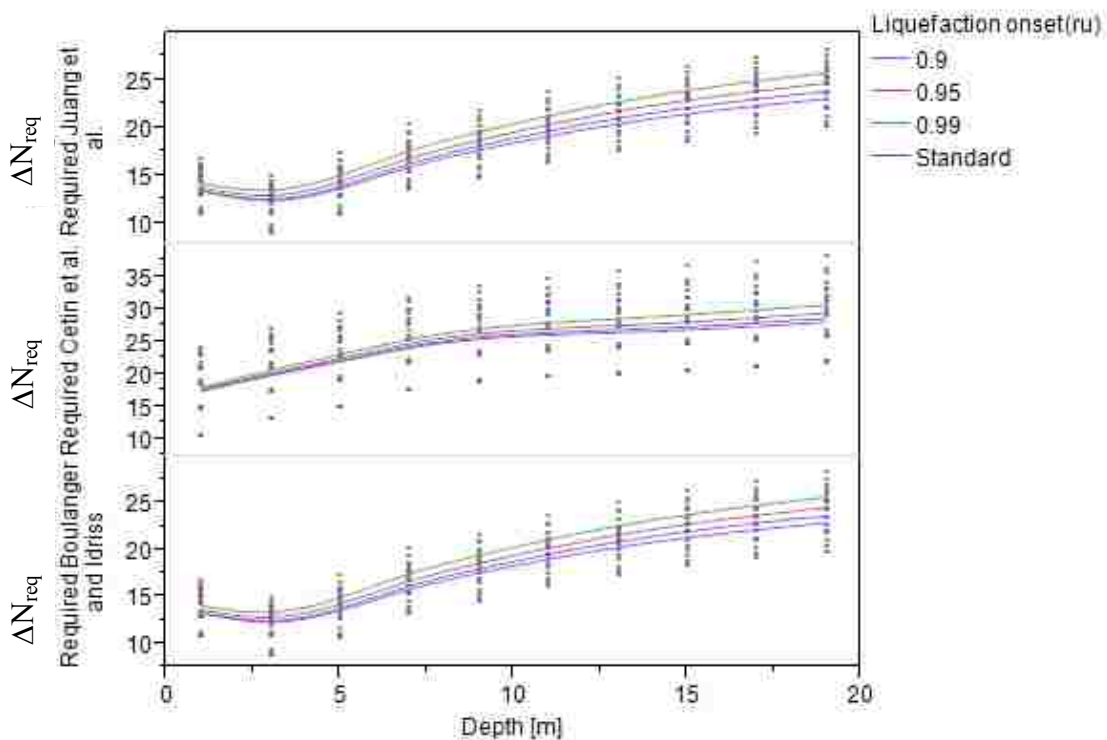


**Figure 7-40: Effect of performance-based magnitude scaling factors San Francisco.**

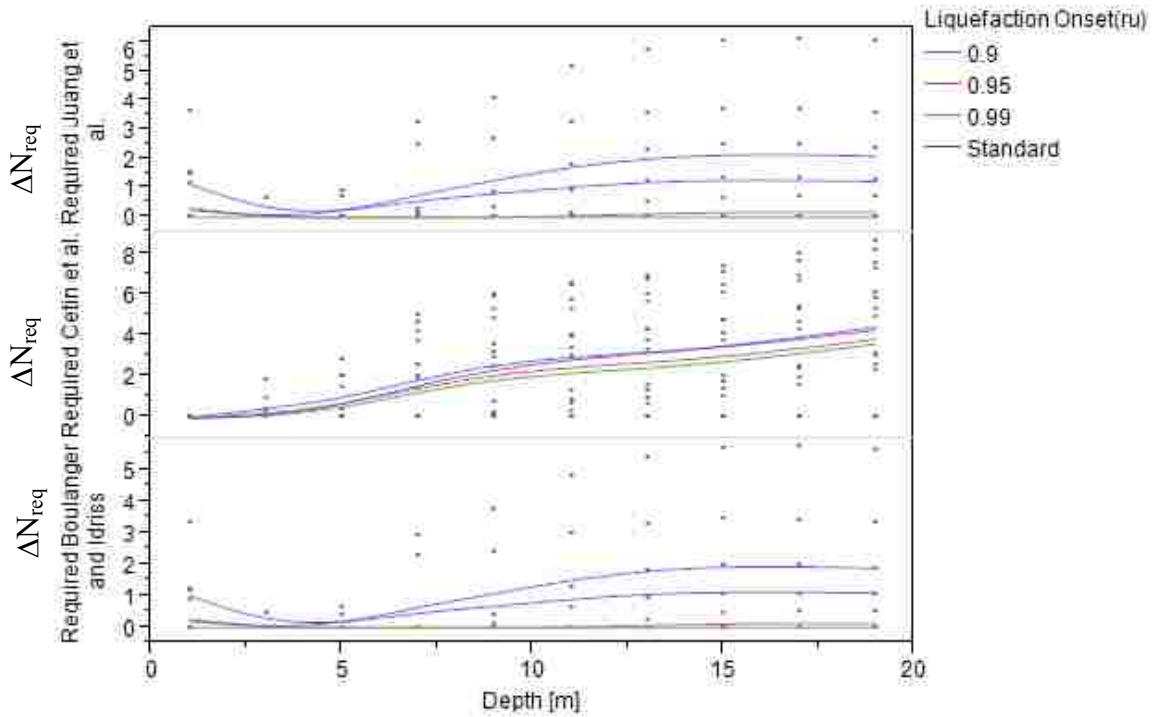


Figure 7-41: Effect of performance-based magnitude scaling factors Butte.

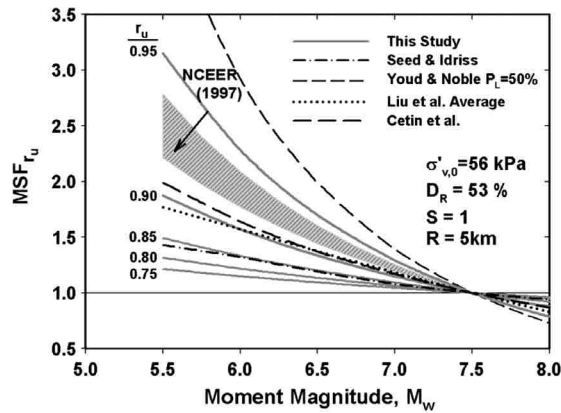


Figure 7-42:  $MSF_{PB}$  using  $r_u$  definition after Cetin and Bilge (2012).

### 7.9 Factor of Safety Prediction Differences

Having gained an understanding of where the differences between the equations lie, it is also important to look at how the two equations differ from each other in predicting liquefaction. Ultimately the use of the performance-based liquefaction initiation hazard curves will be used to

evaluate settlement, lateral spread, and other factors in a risk/hazard based analysis. In a completely performance-based approach to liquefaction hazard analysis the small differences in the factor of safety prediction outlined above can affect the outcome of the analysis. Currently, however, few tools exist for evaluation of liquefaction effects in a performance-based system. As such, the proceeding results and methods are likely to be used by some with deterministic relationships for the evaluation of lateral spread and settlement. For the deterministic case the question ultimately comes down to a binary (yes or no) response to the question of whether liquefaction will initiate. If it does not then there is no need to evaluate liquefaction effects, and if it does initiate the small differences in factor of safety may often be ignored.

A look at the differences in prediction of whether liquefaction will occur or not was conducted for soil profiles 1-24 at the 11 sites used in the study. For this set of data, the factor of safety was examined instead of the  $\Delta N_{req}$  as this is what is commonly used in liquefaction evaluation in a deterministic framework. For the purposes of this analysis a factor of safety against liquefaction of 1.00 was used in evaluating whether liquefaction would trigger. Using this factor of safety and the data set obtained using performance-based analysis the results seen in Table 7-3 were obtained.

**Table 7-3: Results of analysis of liquefaction triggering using a FS=1.2.**

Total Number of Measurements	12240
% of time Cetin et al. FS is greater than 1.0 and Boulanger and Idriss FS is less than 1.0	0.074% [total of 9]
% of time Boulanger and Idriss FS is greater than 1.0 and Cetin et al FS is less than 1.0	15.41% [total of 1886]
% of time different prediction occur	15.48%
Total number of times Boulanger and Idriss FS >1.0	5240
Total number times Cetin et al. FS >1.0	3363

The results are valid for soil profiles 1-24 analyzed at return periods of 475, 1033, 2475, 4975, and 9950 years, fines content 0-50% and soil depths ranging from 1 to 20 meters. For these conditions the results show that about 16% of the time the Cetin et al. method and Boulanger and Idriss method of performance-based liquefaction initiation evaluation will predict different results (i.e. liquefaction predicted to occur for one method, and not for the other). This is a small fraction, but can have significant impacts on project costs. A slight difference can result in the prediction of thicker liquefiable layers and as a result increase the overall cost of a project.

#### 7.10 Summary of Performance-Based Results

Overall, the Cetin et al. performance-based approach tends to be more conservative in general than the Boulanger and Idriss and Juang et al approaches. However, this is not always the case. At shallow depths (< 4 m with no  $K_\sigma$  limit), low return periods (<2475), and low fines contents (<10%) the Boulanger and Idriss and Juang et al methods can become more conservative than the Cetin et al method. In addition, when the parameter uncertainty error is accounted for as proposed by Boulanger and Idriss their form of the equation becomes more conservative than either of the others for low return periods (<4975 years) and low SPT resistance ( $N=5$ ). Areas of increased seismicity cause the Cetin and Seed et al. (2004) method to become increasingly conservative when compared to the other methods. A summary of the effect of each of the different variables on the value of  $\Delta N_{req}$  is shown below in Table 7-4.

**Table 7-4: Summary of effects of variables on value of  $\Delta N_{req}$ .**

<b>With increase in Parameter:</b>	<b>Boulanger and Idriss <math>\Delta N_{req}</math></b>	<b>Juang et al <math>\Delta N_{req}</math></b>	<b>Cetin et al <math>\Delta N_{req}</math></b>	<b>Difference between new and Cetin et al method</b>
------------------------------------	---	--	--	--

SPT Blow Count	Decreases	Decreases	Decreases	Generally Constant
Fines Content	Decreases	Decrease	Constant	Generally Increases for FC>10
Depth	Increases	Increases	Increases	Generally Increases
Return Period	Increases	Increases	Increases	Generally Increases to $T_R = 2475$
Shear Velocity	Decreases	Decreases	Decreases	Generally Constant
PB MSF	N/A	N/A	N/A	N/A
$K_\sigma$ Limit not used	Small depth decrease	Small Depth Decrease	N/A	Small Depth Increase
Parameter Uncertainty	Varies	Varies	Varies	Boulanger and Idriss more conservative than Cetin et al. approach for $N=5$ and $T_R < 4975$

## **8 COMPARISON OF CONVENTIONAL AND PERFORMANCE-BASED RESULTS**

A comparison of the conventional deterministic and performance-based methods is useful in understanding how the current state of the practice compares to the performance-based approaches. An in depth comparison between conventional procedures has been previously conducted by Seed (2010), Cox and Griffiths (2011), Idriss and Boulanger (2010), and Youd (2013) and their conclusions are considered adequate and well in advance of anything within the scope of this report. As such, a detailed analysis of the conventional deterministic differences will not be made. A brief overview of the differences between conventional procedures can be found in Appendix A.

A comparison of conventional and performance-based approaches has not previously been extensively examined and such a comparison is useful in understanding the results of these analyses and their usefulness to the engineering community. For the purposes of ease of computation and comparison the pseudo probabilistic approach was used with the mean values from a PSHA for the conventional case. A factor of safety of 1.2 was used with the conventional analyses and a factor of safety of 1.0 was used with the performance-based analyses. For these liquefaction analyses soil profiles 33-36 were analyzed at return periods of 475, 1033, 2475, 4975, 9950 years.



## 8.1 SPT Blow Count and Shear Wave Velocity

A plot showing comparisons of conventional and performance-based results by SPT blow count is shown below (Figure 8-1). This graph represents the averages over all 11 sites and 5 return periods analyzed.

One interesting fact that emerges from this graph is that the least conservative procedure when looking at required ground improvement to prevent liquefaction is the NCEER procedure. This is caused by the fact that the NCEER procedure considers any SPT resistance over 30 to be non-liquefiable while the other procedures do not. A direct comparison between procedures shows that for both the Cetin et al. and the Boulanger and Idriss approaches the performance-based approach is less conservative than the conventional approach, in some cases by as much as 20%. This large difference between conventional and performance-based methods can result in much different predictions of liquefaction initiation. At high SPT blow counts the conventional and performance-based methods have much smaller differences.

Similar trends are seen in the comparisons by  $V_{s12}$  with the conventional cases on average being more conservative than the performance-based approaches (Figure 8-2). Again the NCEER approach is the least conservative of the approaches.

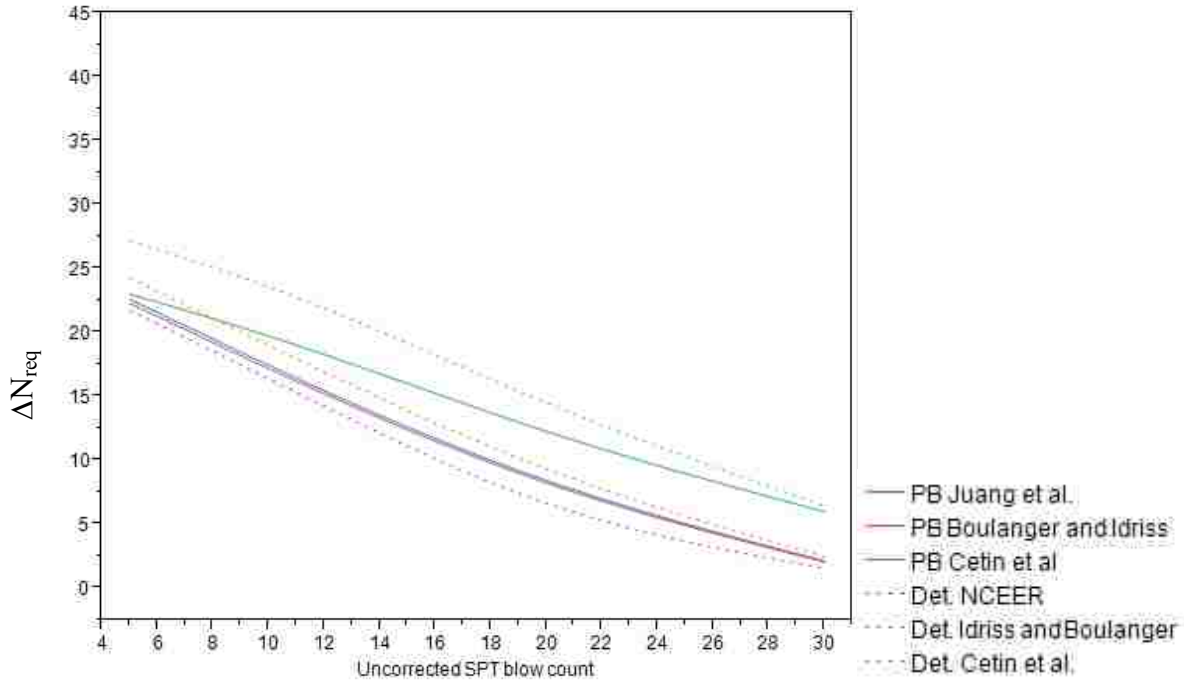


**Figure 8-1: Comparison of approaches by SPT blow count.**

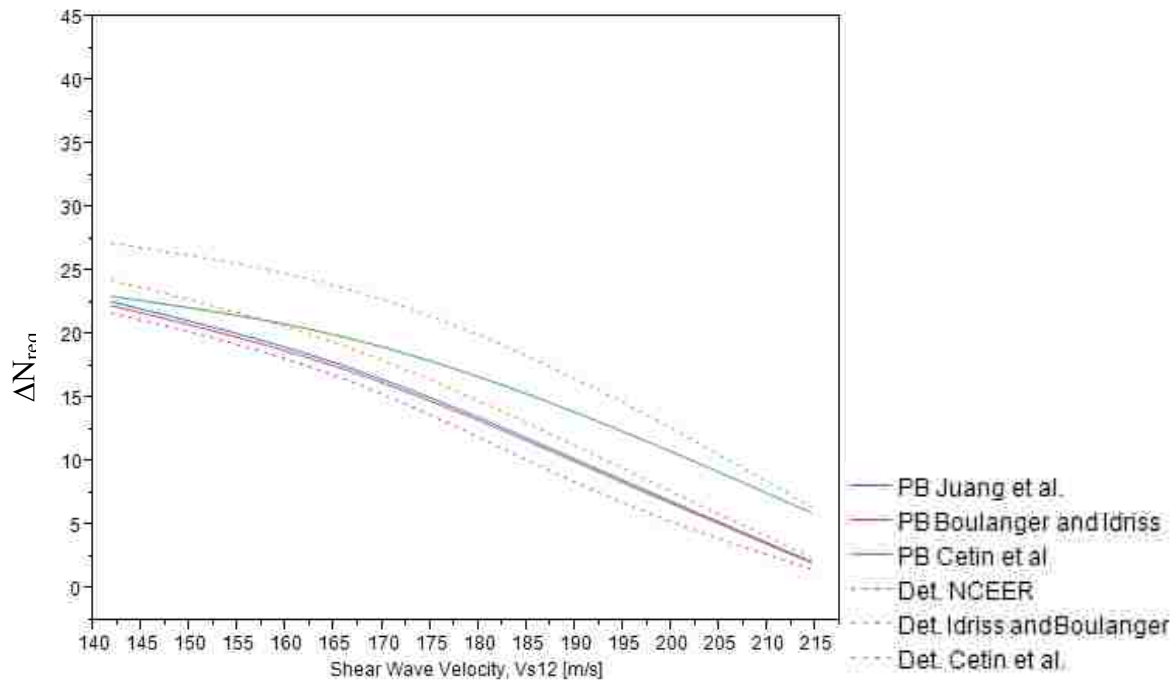


**Figure 8-2: Comparison of approaches by  $V_{s12}$ .**

## 8.2 Depth and Return Period.

Similar to the trends shown with SPT blow count and shear wave velocity, the conventional average value tends to be more conservative when looked at by depth and return period (Figure 8-3 and Figure 8-4). Two patterns of note develop in the graphs and deserve comment. One is the apparent discrepancy between the Cetin et al. conventional and performance-based approaches with depth. Further research is needed to determine the exact cause of this apparent discrepancy. The second is that the Boulanger and Idriss performance-based and conventional procedures have much less discrepancy between them than the Cetin et al. procedures tends to. Also, once again, the NCEER procedure is the least conservative method of the group.

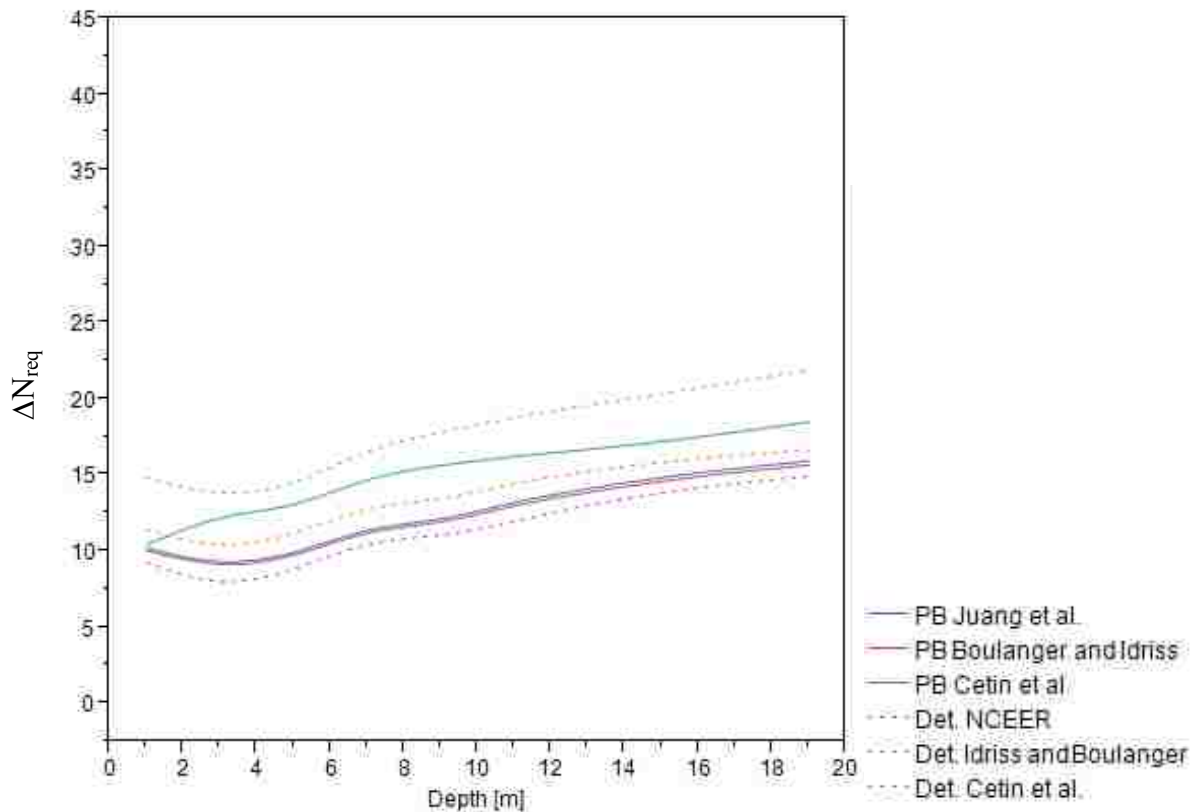
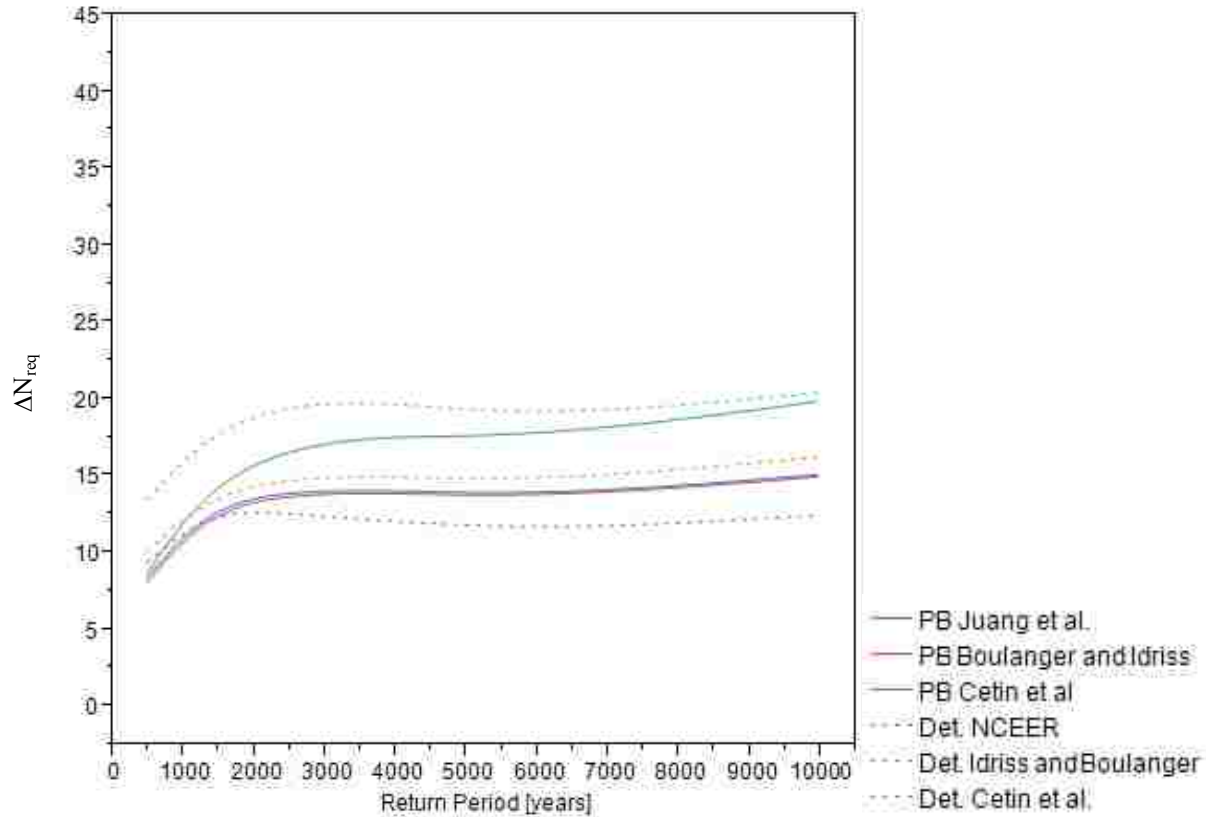


Figure 8-3: Comparison of conventional and performance-based procedures by depth.



**Figure 8-4: Comparison of procedures by return period.**

### 8.3 Direct Comparison of Methods

A direct comparison between the conventional and performance-based methods would be expected to yield a straight line if the two methods were equivalent (shown with a blue line). However, a previous comparison of the performance-based and conventional approach of Cetin et al has shown that these methods are not necessarily consistent with each other (Kramer and Mayfield 2007). A direct comparison of the Cetin et al. data from this study shows a similar trend (Figure 8-5) with the conventional approach yielding on average higher values than the performance-based approach.

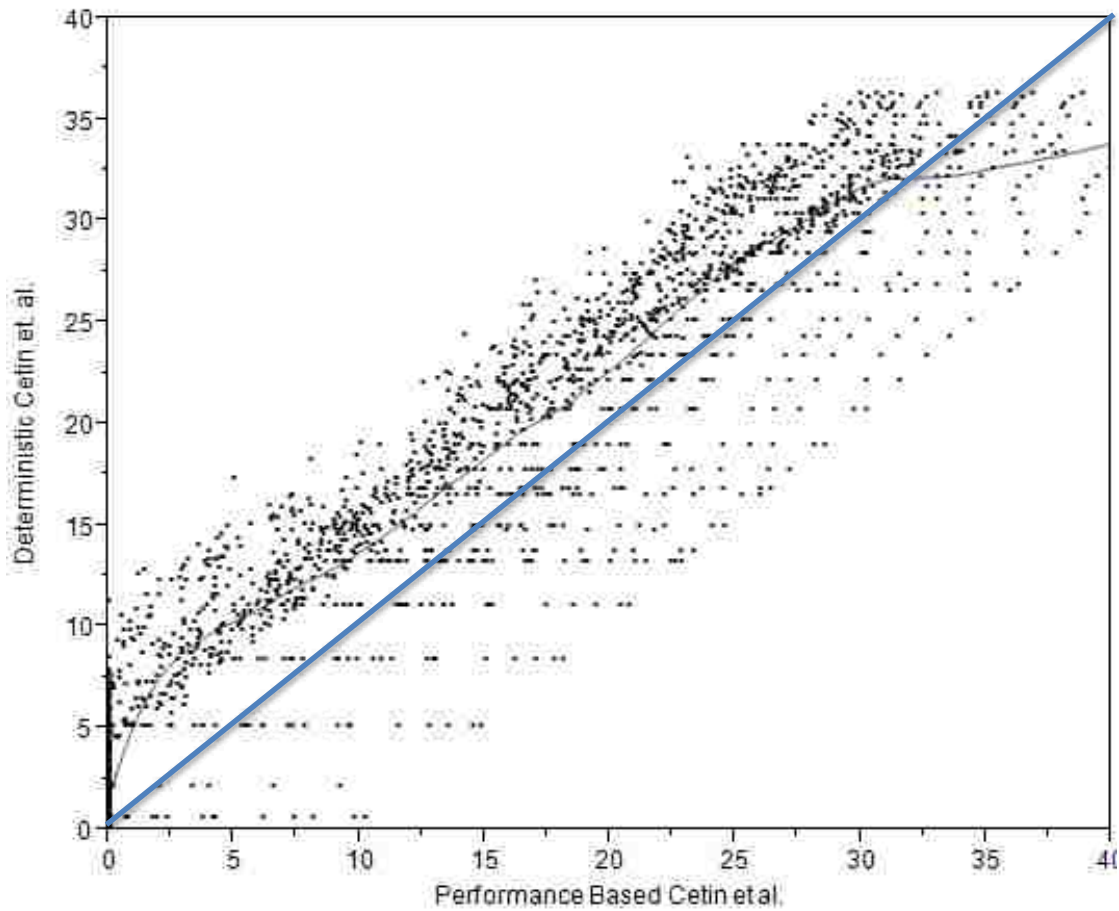


**Figure 8-5: Comparison of Cetin et al. conventional and performance-based approaches.**

A similar comparison of the Boulanger and Idriss performance-based approach and the Idriss and Boulanger conventional approach shows similar trends with the conventional approach tending to be more conservative. The comparison also shows that there is a much smaller amount of scatter between the conventional and performance-based approaches. This smaller amount of scatter shows that there is a much smaller amount of discrepancy between the conventional and performance-based approaches when using the Boulanger and Idriss conventional and performance-based approaches.

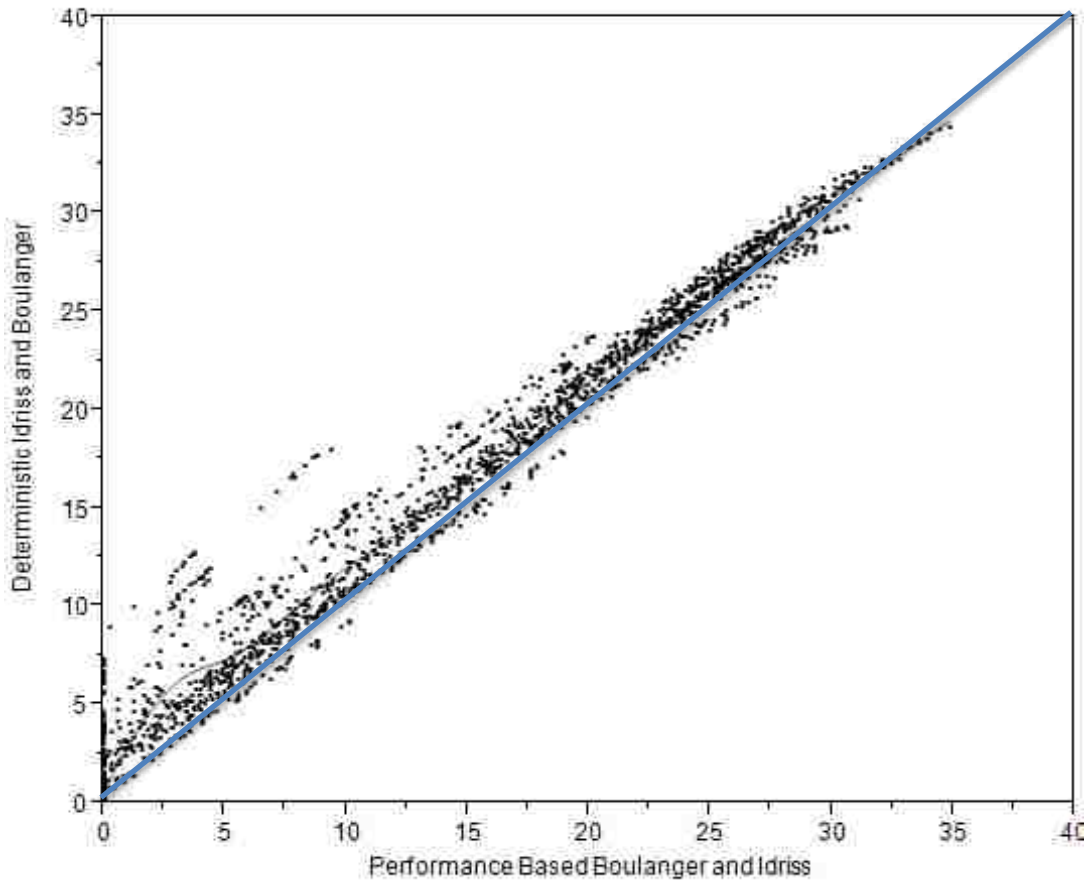


**Figure 8-6: Comparison of Boulanger and Idriss (performance-based) and Idriss and Boulanger (conventional).**

A look at a few specific cases reveals how this might work out in practice as well as some interesting trends. For these cases, the soil profile shown in Table 8-1 was used for both sites. An analysis of liquefaction initiation was then completed using the mean inputs into a conventional analysis. The sites used were Fresno, CA; and Memphis, TN.

For these sites, the conventional approaches perform similar to what would be expected, with the Cetin et al. approach consistently more conservative than the Idriss and Boulanger approach (Figure 8-7). For the performance-based approaches, there is considerable crossover between the two approaches.

**Table 8-1: Soil profile used in site specific liquefaction analyses.**

Sub Layer #	Thickness [m]	Sample Depth [m]	Soil Type	$V_s$ [m/s]	N	$D_R$	$\gamma$ [kN/m <sup>3</sup> ]
1	1	0.5	[SW]_Well-graded_sand	99.7	1	14.94	20
2	1	1.5	[SW]_Well-graded_sand	130.4	3	26.72	20
3	1	2.5	[SW]_Well-graded_sand	148.8	5	35.56	20
4	2	4	[SW]_Well-graded_sand	158.1	7	40.51	20
5	3	6	[SW]_Well-graded_sand	164	9	43.88	20
6	3	10	[SW]_Well-graded_sand	163.9	11	43.8	20
7	2	12	[SW]_Well-graded_sand	166.8	13	45.5	20
8	1	13.5	[SW]_Well-graded_sand	170.1	15	47.45	20
9	1	14.5	[SW]_Well-graded_sand	173.6	17	49.62	20
10	2	16.5	[SW]_Well-graded_sand	175.5	19	50.79	20
11	4	18	[SW]_Well-graded_sand	177.8	21	52.25	20
12	1	21.5	[SW]_Well-graded_sand	177.9	23	52.31	20
13	2	22.5	[SW]_Well-graded_sand	180.4	25	53.92	20
14	4	24.5	[SW]_Well-graded_sand	181.8	27	54.85	20
15	1	28.25	[SW]_Well-graded_sand	181.8	29	54.86	20

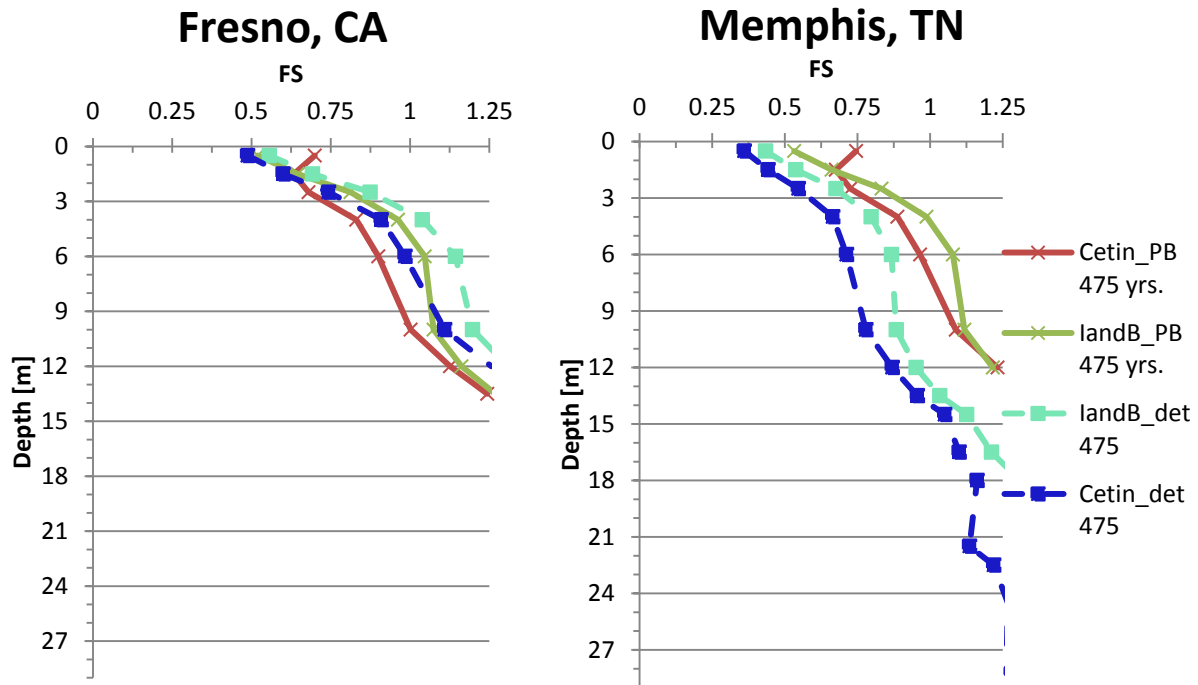


**Figure 8-7 Two site specific analyses for 475 year return period comparing conventional and performance-based analyses.**

There is also a much smaller amount of difference between the two methods after having accounted for the uncertainty associated with the methods using the performance-based approach (Figure 8-7). The California site has roughly equivalent values between the conventional and performance-based approaches although the performance-based approaches require an extra meter of ground improvement. The Memphis, TN site shows considerably more discrepancy between the methods. This results in depths up to 24 meters being predicted to liquefy using the conventional approach at the Memphis site as opposed to the performance-based approach which only predicts liquefaction down to 12 meters.

The large discrepancies at the Memphis, TN site may be the result of the use of incompatible pairs in the conventional approach coupled with the bi modal nature of the location. An incompatible pair occurs when an acceleration and magnitude do not occur naturally in the same seismic event. Thus the mean values used in these analyses were incompatible pairs as they do not represent any true seismic event. A bi modal site occurs when there are two locations that have large contributions to the seismic hazard. This is common in areas such as Cincinnati where there are two regions contributing to the seismic hazard. A detailed discussion of this concept is available in Appendix A.

#### **8.4 Statistical Comparison of Conventional and Performance-Based Procedures**

A statistical comparison between the conventional procedures and the newer performance-based procedures was made for the Idriss and Boulanger and Cetin and Seed et al procedures. This comparison was made to determine if the differences between the procedures were decreased by accounting for the uncertainty using a performance-based approach. The analyses were conducted for soil profiles 1-24 and return periods of 475, 1033, 2475, 4975, and 9950 years.



The statistical analysis was conducted using a paired t test to compare the conventional and performance-based approaches. The paired t test was used to analyze the ratio of  $N_{req}$  for Idriss and Boulanger to  $N_{req}$  for Cetin and Seed et al. for the performance-based and conventional procedures (Figure 8-8). The results of the paired t test showed a statistically significant difference between the means of .03886 with a 95% confidence interval from 0.0371 to 0.0406. The mean value of the conventional procedure is 0.8371, while the mean value of the performance-based procedure is 0.8759.

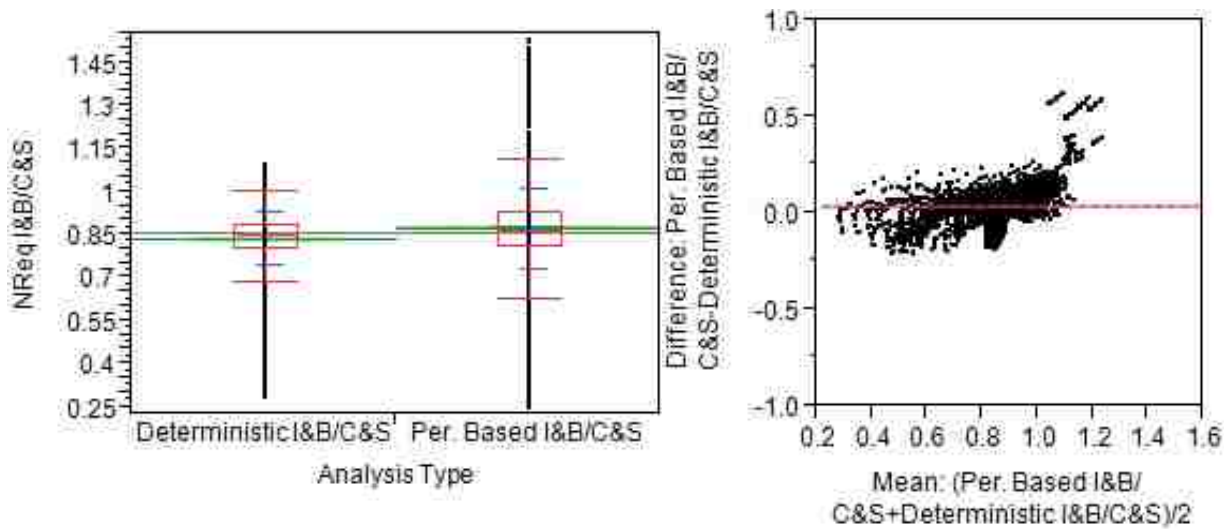


**Figure 8-8: Comparison of Conventional and Performance-Based Results.**

These results are significant because they show a smaller average difference using the performance-based methods than the deterministic methods. Thus, accounting for the uncertainty does decrease the differences on average between the two methods.

## 8.5 Summary of Comparison of Conventional and Performance-Based Procedures

In summary, the conventional procedures tend to generally be more conservative than the performance-based procedures. The differences between the Idriss and Boulanger and Cetin and Seed et al procedures are also larger when analyzed in the conventional way. Performances based procedures account more fully for the mean and the body of the data, and as such often are less conservative than the conventional analyses. Statistically the performance-based analyses on average agree more closely than the conventional procedures, thus accounting for the uncertainty brings the two methods more closely into agreement with each other.

## 9 CONCLUSIONS

This paper has proposed two new performance-based approaches using the Boulanger and Idriss and Juang et al. probabilistic equations. During the course of this study advances were made in the development of tools to help implement the proposed performance-based approaches. Further advances were made in the development of new procedures and approaches for the analysis of liquefaction initiation. Comparisons were made between the proposed performance-based procedures. Finally comparisons were made between the performance-based and conventional procedures.

Two new performance-based procedures were developed during the course of this work. The new performance-based procedures used the Juang and Ching et al. (2012) and Boulanger and Idriss (2012) methods of evaluating the probability of liquefaction. Further, the framework developed by Kramer and Mayfield (2007) was modified to allow the incorporation of performance-based magnitude scaling factors as proposed by Cetin and Bilge (2012). Finally, an equation was developed to determine a modified standard deviation for the Andrus and Stokoe equation which includes both parametric and model uncertainty. This equation was developed to better evaluate the uncertainties associated with shear wave velocity correlation when applied to performance-based methods.

PB LiquefY was developed during the course of this research to facilitate the implementation and study of the performance-based methods. Due to the complexity involved in

the full performance-based method a computer program is required. PB LiquefY was developed for use by both researchers and practicing engineers to make the implementation of the performance-based methods easier, and to assist in comparison of the newer performance-based methods to the conventional methods that are currently in use. PB LiquefY facilitates the analysis of liquefaction initiation and as such permits large comparative studies, mapping projects, and other research to be conducted. Other useful applications that PB LiquefY permits are the analysis of performance-based magnitude scaling factors, the analysis of the needed ground improvement to prevent liquefaction, and the incorporation of parameter uncertainty.

Using the analysis tool PB LiquefY which was developed during the course of this study, analyses were conducted comparing the Cetin and Seed et al. (2004), Juang and Ching et al. (2012), and Boulanger and Idriss (2012) methods of performance-based liquefaction initiation evaluation. These analyses resulted in the following conclusions:

- 1) The Cetin and Seed et al. (2012) method is not always more conservative than the Boulanger and Idriss (2012) or Juang and Ching et al. (2012) method. At shallow depths (<4m), low return periods (<2475 years), low blow counts (<10 blows/ft), and low fines contents ( $\leq 10\%$ ) cases exist where the Boulanger and Idriss (2012) and Juang and Ching et al. (2012) methods are more conservative on average.
- 2) Accounting for the variation in  $V_{s12}$  can cause the Cetin and Seed et al. (2004) method to become less conservative overall. This can cause the Cetin and Seed et al. (2004) method to become less conservative than the than the Boulanger and Idriss (2012) and Juang et al. (2012) methods at low blow counts ( $N=5$ ) and low fines contents ( $FC=0$ ).

- 3) The Cetin and Seed et al. (2004) method's use of  $V_{s12}$  is counter intuitive. If higher  $(1+\sigma)$  shear wave velocities are used from the Andrus and Stokoe correlation it results in higher probabilities of liquefaction and thus more conservative results.
- 4) The Cetin and Seed et al. (2004) method becomes increasingly more conservative in higher seismicity areas when compared by SPT blow count.
- 5) Areas with higher than average seismicity cause the Cetin and Seed et al. (2004) method to become increasingly conservative when compared to the Boulanger and Idriss (2012) and Juang and Ching et al. (2012) methods.
- 6) Accounting for parameter uncertainty as outlined by Boulanger and Idriss (2012) can cause the Boulanger and Idriss method to become more conservative than the Cetin and Seed et al. (2004) method at low return periods ( $<4975$ ) and low blow counts ( $N=5$ ). When accounting for uncertainty in this manner the  $\sigma_{tot}$  term must be capped at a blow count of 30 to prevent erroneous values. Without the cap the fragility curve will begin to increase at large SPT resistance.
- 7) It is recommended that the re regressed single constant error term for  $\sigma_{tot}$  be used with the Boulanger and Idriss (2012) method.
- 8) Performance-Based Magnitude Scaling Factors can increase or decrease the overall conservatism of all three of the relationships depending on whether the magnitude is greater than or less than  $M_w = 7.5$ .
- 9) When the performance-based liquefaction triggering results were evaluated in a binary sense (i.e. "yes" or "no"), Cetin and Seed et al. (2004) and Boulanger and Idriss (2012) differed in approximately 16% of the cases that were analyzed. This suggests that approximately 84% of the cases were in agreement, which supports the

earlier observations of Cox and Griffiths (2011) in their evaluation of deterministic liquefaction triggering.

Further comparisons were made between deterministic and performance-based analyses showing how the current conventional deterministic methods compare with the more recently developed performance-based methods. The comparison showed that:

- 1) The conventional methods of analysis are on average more conservative in their prediction of the amount of ground improvement required. The exception to this is the NCEER method which is on average less conservative in the prediction of ground improvement than any of the other methods of analyses.
- 2) The difference between the performance-based and conventional methods of analysis is largest for areas where a small amount of ground improvement is needed (i.e.  $\Delta N_{req}$  is small).
- 3) After accounting for uncertainty the performance-based methods of analyses have much smaller differences between them than the conventional methods of analysis.
- 4) The relative seismicity of a region and the types of seismicity in the region (i.e. bi modal vs. single mode) affect whether the deterministic methods will be more or less conservative. Generally areas with bi modal response should be analyzed with a performance-based method of analysis.

Overall the performance-based methods tend to be less conservative than the conventional methods. This can result in considerable cost savings to the engineer. Performance-based methods also lend themselves to communication of hazard and risk to all stakeholders.

In order to make the performance-based method useable in current practice several topics need further research. Research must be conducted into the performance-based analysis of effects. It would also be beneficial to develop a simplified method of performance-based analysis to help the average engineer to use and understand performance-based analysis and design.

## REFERENCES

- Anderson, J. G. and J. N. Brune (2000). Probabilistic seismic hazard analysis: Improving consistency with precarious rock observations by removing the ergodic assumption. 12th World Conference on Earthquake Engineering.
- Andrus, R. D. and K. H. I. Stokoe (2000). "Liquefaction Resistance of Soils from Shear-Wave Velocity." Journal of Geotechnical and Geoenvironmental Engineering **126**(11): 1015-1025.
- Atkinson, G. M. and D. M. Boore (2003). "Empirical ground motion relations for subduction zone earthquakes and their application to cascadia and other regions." Bulletin of the Seismological Society of America **93**(4): 1703-1729.
- Been, K. and M. G. Jeffries (1985). "A state parameter for sands." Geotechnique **35**(2): 99-112.
- Bhatia, S. K., J. Schwab, et al. (1985). Cyclic Simple Shear, Torsional Shear, and Triaxial - A comparative Study. Advances in the Art of Testing Soils Under Cyclic Conditions, Detroit, Michigan, American Society of Civil Engineers.
- Boulanger, R. W. (2003). "High Overburden Stress Effects in Liquefaction Analyses." Journal of Geotechnical and Geoenvironmental Engineering: 1071 - 1082.
- Boulanger, R. W. (2003). "Relating  $K_{\alpha}$  to relative state parameter index." Journal of Geotechnical and Geoenvironmental Engineering **129**: 770-773.
- Boulanger, R. W. (2013). Geotechnical Engineering and Lifelines. Learning from recent major earthquakes: Lessons for practice, Salt Lake City, UT, Earthquake Engineering Research Institute.
- Boulanger, R. W. and I. M. Idriss (2006). "Liquefaction Susceptibility Criteria for Silts and Clays." Journal of Geotechnical and Geoenvironmental Engineering: 1413 - 1426.
- Boulanger, R. W. and I. M. Idriss (2011). Cyclic Failure and Liquefaction: Current Issues. 5th International Conference on Earthquake Geotechnical Engineering. Santiago, Chile.
- Boulanger, R. W. and I. M. Idriss (2012). "Probabilistic SPT-Based Liquefaction Triggering Procedure." Journal of Geotechnical and Geoenvironmental Engineering.



- Bray, J. D. and R. B. Sancio (2006). "Assessment of the Liquefaction Susceptibility of Fine-Grained Soils." Journal of Geotechnical and Geoenvironmental Engineering **132**(9): 1165-1177.
- Casagrande, A. (1936). "Characteristics of cohesionless soils affecting the stability of slopes and earth fills." Journal of the Boston Society of Civil Engineers, reprinted in Contributions to Soil Mechanics: 257-276.
- Castro, G. (1969). Liquefaction of sands. Harvard Soil Mechanics Series 87. Cambridge, Massachusetts, Harvard University.
- Castro, G. (1975). "Liquefaction and cyclic mobility of sands." Journal of Geotechnical Engineering Division **101**(GT6): 551-569.
- Cetin, K. O. (2002). "Probabilistic Models for the Initiation of Seismic Soil Liquefaction." Structural Safety **24**: 67 - 82.
- Cetin, K. O. and H. T. Bilge (2012). "Cyclic Large Strain and Induced Pore Pressure Models for Saturated Clean Sands." Journal of Geotechnical and Geoenvironmental Engineering **138**(3): 309.
- Cetin, K. O. and H. T. Bilge (2012). "Performance-Based Assessment of Magnitude (Duration) Scaling Factors." Journal of Geotechnical and Geoenvironmental Engineering **138**(3): 324.
- Cetin, K. O., H. T. Bilge, et al. (2009). "Probabilistic model for the assessment of cyclically induced reconsolidation (volumetric) settlements." Journal of Geotechnical and Geoenvironmental Engineering **135**(3): 387 - 398.
- Cetin, K. O. and R. B. Seed (2004). "Nonlinear shear mass participation factor ( $r_d$ ) for cyclic shear stress ratio evaluation." Soil Dynamics and Earthquake Engineering **24**(2): 103-113.
- Cetin, K. O., R. B. Seed, et al. (2004). "Standard Penetration Test-Based Probabilistic and Deterministic Assessment of Seismic Soil Liquefaction Potential." Journal of Geotechnical and Geoenvironmental Engineering: 1314-1340.
- Cox, B. R. and S. C. Griffiths (2011). Practical Recommendations for Evaluation and Mitigation of Soil Liquefaction in Arkansas  
Department of Civil Engineering. Arkansas, University of Arkansas: 175.
- Day, R. W. (2002). Geotechnical Earthquake Engineering Handbook. San Francisco, CA USA.

- Faris, A. T. (2004). Probabilistic models for engineering assessment of liquefaction - induced lateral spreading displacements. Civil Engineerign, University of California Berkley. **Doctor of Philosophy**.
- Franke, K. (2011). A Performance-Based Model for the Computation of Kinematic Pile Response Due to Lateral Spread and its Application on Select Bridges Damaged During the M7.6 Earthquake in the Limon Province, Costa Rica. Department of Civil and Environmental Engineering. Provo, Utah, Brigham Young University. **Doctor of Philosophy**: 611.
- Gutenberg, B. and C. F. Richter (1944). "Frequency of earthquakes in California." Bulletin of the Seismological Society of America **34**(4): 185-188.
- Idriss, I. M. and R. W. Boulanger (2006). "Semi-empirical procedures for evaluating liquefaction potential during earthquakes." Soil Dynamics and Earthquake Engineering **26**(2-4): 115-130.
- Idriss, I. M. and R. W. Boulanger (2008). Soil Liquefaction During Earthquakes. Oakland, CA, Earthquake Engineering Research Institute.
- Idriss, I. M. and R. W. Boulanger (2010). SPT-Based Liquefaction Triggering Procedures. Davis, California, Center for Geotechnical Modeling: 259.
- IYISAN, R. (1996). "Correlations between shear wave velocity and in-situ penetration test results." Teknik Dergi **7**(2): 1187-1199.
- Juang, C. H., J. Ching, et al. (2012). "New models for probability of liquefaction using standard penetration tests based on an updated database of case histories." Engineering Geology **133-134**: 85-93.
- Kramer, S. L. (1996). Geotechnical Earthquake Engineering. Upper Saddle River, New Jersey, Prentice Hall.
- Kramer, S. L. (2008). Evaluation of Liquefaction Hazards in Washington State. Washington State, Washington State Department of Transportation.
- Kramer, S. L. and R. t. Mayfield (2007). "Return Period of Soil Liquefaction." Journal of Geotechnical and Geoenvironmental Engineering: 802 - 813.
- Liao, S. S. C., D. Veneziano, et al. (1988). "Regression Models for Evaluating Liquefaction Probability." Journal of Geotechnical Engineering **114**(4): 389 - 411.
- Liu, A. H., J. P. Stewart, et al. (2001). "Equivalent Number of Uniform Stress Cycles for Soil Liquefaction Analysis." Journal of Geotechnical and Geoenvironmental Engineering **127**(12): 1017-1026.

- Malvick, E. j., B. L. Kutter, et al. (2006). "Shear localization due to liquefaction-induced void redistribution in a layered infinite slope." Journal of Geotechnical and Geoenvironmental Engineering **132**(10): 1293-1303.
- Marcuson, W. F. I. and W. Bieganousky, A. (1977). "SPT and Relative Density in Coarse Sands." Journal of Geotechnical Engineering Division **103**(11): 1295-1309.
- Mayfield, R. T., S. L. Kramer, et al. (2010). "Simplified Approximation Procedure for Performance-Based Evaluation of Liquefaction Potential." Journal of Geotechnical and Geoenvironmental Engineering.
- Moss, R. E. S. (2008). "Quantifying Measurement Uncertainty of Thirty Meter Shear Wave Velocity." Bulletin of the Seismological Society of America **98**(3): 1399-1411.
- Oka, L. G., M. M. Dewoolkar, et al. (2012). "Liquefaction Assessment of cohesionless soils in the vicinity of large embankments." Soil Dynamics and Earthquake Engineering **43**: 33-44.
- Petersen, M. D., A. D. Frenkel, et al. (2008). Documentation for the 2008 update of the united states national seismic hazard maps. United States: 128.
- Power, M., B. Chiou, et al. (2008). "An overview of the NGA project." Earthquake Spectra **24**(1): 3-21.
- Pyke, R., H. B. Seed, et al. (1975). "Settlement of Sands under multi directional shaking." Journal of Geotechnical Engineering Division **101**(GT4).
- Seed, H. B. and I. M. Idriss (1971). "Simplified Procedure for Evaluating Soil Liquefaction." Soil Mechanics and Foundations Division, Proceedings of the American Society of Civil Engineers **97**(SM9): 1249-1273.
- Seed, H. B., K. Tokimatsu, et al. (1985). "Influence of SPT procedures in soil liquefaction resistance evaluations." Journal of Geotechnical Engineering **111**: 1425-1445.
- Seed, R. B. (2010). Technical Review and Comments: 2008 EERI Monograph Soil Liquefaction During Earthquakes. California, University of California Berkeley.
- Seed, R. B., K. O. Cetin, et al. (2003). Recent Advances in Soil Liquefaction Engineering: A Unified and Consistent Framework. Berkeley, CA, Earthquake Engineering Research Center: 72.
- Slemmons, D. (1982). Determination of design earthquake magnitudes for microzonation. Proceedings of the third international earthquake microzonation conference.

- Stewart, J. P., A. H. Liu, et al. (2003). "Amplification Factors for Spectral Acceleration in Tectonically Active Regions." Bulletin of the Seismological Society of America **93**(1): 332 - 352.
- Stewart, J. P. and D. H. Whang (2003). Simplified procedure to estimate ground settlement from seismic compression in compacted soils. Pacific Conference on Earthquake Engineering. Los Angeles, CA, USA: 8.
- Tokimatsu, K. and H. Seed (1987). "Evaluation of settlements in sands due to earthquake shaking." Journal of Geotechnical Engineering **113**(8).
- Toprak, S., T. L. Holzer, et al. (1999). CPT- and SPT- Based Probabilistic Assessment of Liquefaction Potential. Proceedings, 7th U.S.–Japan Workshop on Earthquake Resistant Design of Lifeline Facilities and Countermeasures Against Liquefaction, Seattle, U. S. Geological Survey.
- Toro, G. R., N. A. Abrahamson, et al. (1997). "Model of Strong Ground Motions from Earthquakes in Central and Eastern North America: Best Estimates and Uncertainties." Seismological Research Letters **68**(1).
- Unno, T., M. Kazama, et al. (2008). "Liquefaction of Unsaturated Sand Considering the Pore Air Pressure and Volume Compressibility of the Soil Particle Skeleton." Soils and Foundations Japanese Geotechnical Society **48**(1): 97-99.
- USGS, U. S. G. S. (2013). Quaternary Fault and Fold Database of the United States. USGS.gov, United States Geologic Survey.
- Vaid, Y. P. and J. C. Chern (1985). Cyclic and Monotonic Response of Undrained Sands. Advances in the Art of Testing Soils Under Cyclic Conditions, Detroit, Michigan, American Society of Civil Engineers.
- Vytiniotis, A. (2012). Contributions to the analysis and mitigation of liquefaction in loose sand slopes. Department of Civil and Environmental Engineering, Massachusetts Institute of Technology. **Doctor of Philosophy**: 419.
- Wells, D. and K. Coppersmith (1994). "New empirical relationships among magnitude, rupture length, rupture width, rupture area, and surface displacement." Bulletin of the Seismological Society of America **84**(4): 974-1002.
- Wong, I. (2012). "Seismic Hazard Analysis: Keeping up with the Science." Short Course,. Salt Lake City, Association of Environmental and Engineering Geologists.
- Yoshimi, Y., K. Tokimatsu, et al. (1994). "In situ liquefaction resistance of clean sands over a wide density range." Geotechnique **44**(3): 479-494.

- Youd, T. L. (2008). Liquefaction Hazard Assessment. Presentation Given to the Northern Kentucky Geotechnical Group.
- Youd, T. L. (2013). A look inside the debate over EERI monograph MNO 12. Salt Lake City, Utah, Utah Liquefaction Advisory Group.
- Youd, T. L. and S. F. Bartlett (1995). "Imperial prediction of liquefaction induced lateral spread." Journal of Geotechnical Engineering **121**(4): 316-331.
- Youd, T. L., C. M. Hansen, et al. (2002). "Revised multilinear regression equations for prediction of lateral spread displacement." Journal of Geotechnical and Geoenvironmental Engineering **128**(12): 1007-1017.
- Youd, T. L. and S. N. Hoose (1977). Liquefaction Susceptibility and Geologic Setting. Proceedings, 6th World Conference on Earthquake Engineering.
- Youd, T. L., I. M. Idriss, et al. (2001). "Liquefaction Resistance of Soils: Summary Report from the 1996 NCEER and 1998 NCEER/NSF Workshops on Evaluation of Liquefaction Resistance of Soils." Journal of Geotechnical and Geoenvironmental Engineering: 817-833.
- Youd, T. L. and S. K. Noble (1997). Liquefaction Criteria Based on Statistical and Probabilistic Analyses. T. L. Youd and I. M. Idriss, National Center for Earthquake Engineering Research.
- Youngs, R. R. and K. Coppersmith (1985). "Implications of fault slip rates and earthquake recurrence models to probabilistic seismic hazard estimates." Bulletin of the Seismological Society of America **75**(4): 939-964.
- Zhao, J. X., J. Zhang, et al. (2006). "Attenuation Relations of Strong Ground Motion in Japan Using Site Classification Based on Predominant Period." Bulletin of the Seismological Society of America **96**(3): 898-913.

## APPENDIX A.

This appendix contains detailed discussions of the development of several different terms used in this thesis as well as several detailed analyses that are useful in understanding liquefaction initiation.

### A.1 Detailed Discussion –Development of Constant Error Terms

The Boulanger and Idriss and Juang et al approaches do not incorporate the error associated with the models into a single term, rather, both models account for uncertainty in with multiple terms. In the case of the Boulanger and Idriss model, the final uncertainty can be accounted for in a single term that will vary as the blow count varies. In the case of the Juang et al. model, there are two statistically derived coefficients that are used.

In order to account for the uncertainty on a more constant basis to facilitate comparison to the Cetin et al. methodology it is desirable to re-regress the models and to find a single term for uncertainty. The models can then be compared on a more equal basis.

Boulanger and Idriss, in their model, used an equation to calculate the uncertainty in terms of CRR, CSR, and a COV for the SPT blow count. Their equation is given in the body of the report and repeated here for convenience.

$$\sigma_{tot}^2 = \left( \frac{1}{14.1} + \frac{2N}{126^2} - \frac{3N^2}{23.6^3} + \frac{4N^3}{25.4^4} \right)^2 (\sigma_{SPT})^2 + (\sigma_{\ln(CRR)})^2 + (\sigma_{\ln(CSR)})^2 \quad (65)$$

This error term is useful because it given engineers flexibility in the application of uncertainty. It does not, however, account directly for the uncertainty in the depth reduction factor, MSF, or some of the other areas where uncertainty can affect the outcome of the model. As a result it is advantageous to derive a single constant error term for the model. This was done using the database provided by Idriss and Boulanger and a set of terms derived; one term for parameter uncertainty included, one for parameter uncertainty excluded. These terms are given in the body of the report (Table 5-1).

A similar procedure was used for Juang et al. In the case of Juang et al, the database that was used was the same. However, it was found the Juang et al (2012) equation for  $P_L$  was different from the Boulanger and Idriss (2012) formulation due to the assumption that Jaung et al made that there was a 1:1 ratio between sites that liquefied and sites that didn't in the data base. When the Boulanger and Idriss (2012) equation which removed the parameter estimation error was adjusted to assume a 1:1 data distribution the equation almost perfectly lined up with the Juang et al model. Therefore to remove parameter estimation error form the Juang et al equation, a similar adjustment was made to the Boulanger and Idriss (2012) equation with parameter estimation error included and the Juang et al (2012) model parameters were modified such that they fit the Boulanger and Idriss equation. It was recognized that this is simply an approximation of the actual values back calculated from the dataset and equations, and that further statistical analysis is needed to find exact values. The values found in this analysis are shown in the body of the report for parameter error included and excluded (Table 5-2).

## A.2 Detailed Discussion – Standard Deviation for Andrus and Stokoe

The Andrus and Stokoe (2010) equation is an equation used to determine shear wave velocity from a corrected SPT blow count. Andrus and Stokoe developed a set of case histories for developing liquefaction initiation relationships. During the course of their study they also developed a shear wave correlation using SPT blow count. Andrus and Stokoe state that “the case history data in this study were used to investigate the  $V_{s1}$  and  $(N_1)_{60}$  relationship for well-documented sand layers with <10% fines.”(Andrus and Stokoe 2000) For their correlation they present a best fit relationship of the form,

$$V_{s1} = B_1[(N_1)_{60}]^{B_2} \quad (66)$$

where  $B_1$  and  $B_2$  are coefficients determined by the regression with values of 93.2 and 0.231 respectively, and  $(N_1)_{60}$  is the corrected SPT blow count. Andrus and Stokoe further reported the residual standard deviation ( $S_{res}$ ) as 12 m/s.

The data set used by Andrus and Stokoe to develop this relationship is to be commended for its quality. The high quality of the data set, however, poses a problem when examining the effect of the standard deviation, which was done in the body of this report. The quality of the measurements is such that to some extent the variability due to measurement error has been removed from the data set, and the reported standard deviation represents the equation or model variability only (epistemic uncertainty). More typical field practices for SPT measurements might result in a much larger standard deviation due to the less rigorous practices that are more often applied.

In order to account for this extra variability that is not accounted for in the original data set an additional amount uncertainty needs to be added to the model. This additional uncertainty



can be accounted for by adding some additional amount to the original standard deviation such that,

$$\sigma_{V_s}^2 = S_{\text{Parameter}}^2 + S_{\text{res}}^2 \quad (67)$$

where  $\sigma_{V_s}$  is the total standard deviation (includes model and parameter uncertainty),  $S_{\text{res}}$  is the residual standard deviation (model uncertainty) from the original Andrus and Stokoe equation, and  $S_{\text{parameter}}$  is the standard deviation associated with parameter uncertainty. In our case the parameter variability of interest is the SPT blow count.

On order to find the value of  $S_{\text{parameter}}$  for the Andrus and Stokoe equation a Monte Carlo simulation was run. The variability in the SPT blow count was accounted for using a coefficient of variation (COV) of 0.3. Using this coefficient of variation it was possible to develop a standard deviation for the SPT blow count ( $\sigma_{\text{SPT}}$ ) using,

$$\sigma_{\text{SPT}} = \text{COV} * (N_1)_{60\text{mean}} \quad (68)$$

where  $(N_1)_{60\text{mean}}$  is the mean value of the normally distributed SPT values. Using this standard deviation it is possible to develop a normal curve for the data using standard statistical relationships (Figure 0-1).

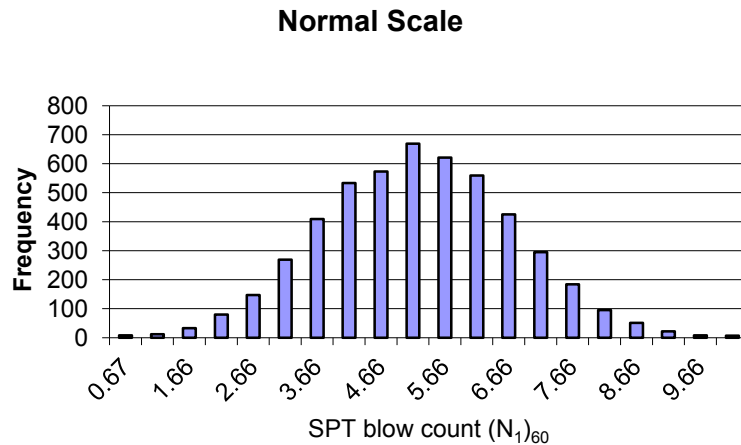


**Figure 0-1: Normal distribution for  $(N_1)_{60\text{mean}} = 5$  using 5,000 points.**

Once a normal curve for the SPT blow count is found, the Andrus and Stokoe equation can be used to find the mean value for shear wave velocity for each point. Model uncertainty will be accounted for separately so it is possible to neglect the model uncertainty at this stage. Using the values obtained for shear wave velocity for each point a distribution of values for shear wave velocity can be developed (Figure 0-2).

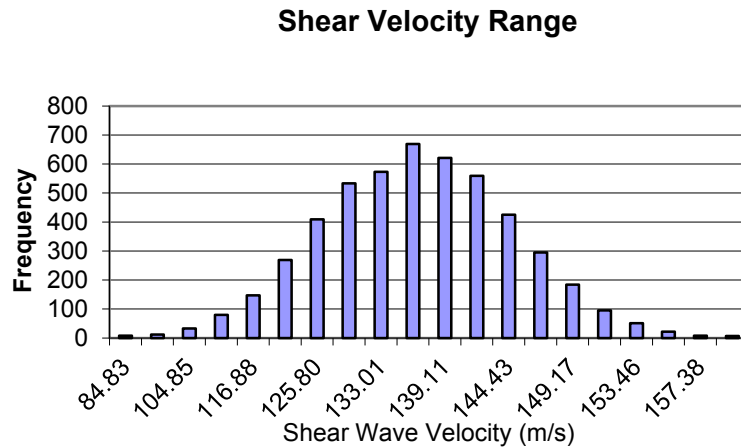


**Figure 0-2: Normal distribution of shear wave velocity using 5,000 data points.**

The distribution of shear wave velocity developed from variation in SPT blow count shown above only represents the shear wave velocity variation at a single point. To fully account for the variation in shear wave velocity caused by variation in the SPT blow count, normal distribution of shear wave velocity must be developed for a series of points.

In order to develop a relationship for the standard deviation caused by parameter uncertainty a Monte Carlo Simulation was performed. A program was provided by Dr. Norman Jones which was modified to develop normal distributions at series of points using the Andrus and Stokoe equation. Values for  $(N1)_{60mean}$  were allowed to range from 5-25 in 20 equal increments. A histogram for the corrected STP blow count was developed at each of the 20

increments. Each histogram consisted of 5,000 discrete values from which a histogram for the shear wave velocity was developed for a total of 100,000 points in the Monte Carlo analysis. The mean value of the histogram was checked against the mean value predicted by the Andrus and Stokoe equations using  $(N_1)_{60\text{mean}}$ . The difference between the predicted and actual mean of the histogram was not allowed to exceed 1 m/s. Using the data from the shear wave velocity histogram a standard deviation for the shear wave velocity was found.. A summary of the results is shown below in Figure 0-3 and Table 0-1. These results were then analyzed with a statistical program called JMP pro 10. Using this program an equation for the standard deviation was regressed.

$$S_{Parameter} = 4.686 \frac{m}{s} + 2.99 \frac{m}{s} * \ln(N_{160}) \quad (69)$$

$$Valid\ Range: 5 \leq (N_1)_{60} \leq 35$$

where  $(N_1)_{60cs}$  is the corrected SPT blow count. Although the valid range is from 5 to 35, reasonable values for the standard deviation can be found by extrapolation outside this range. Such extrapolation should be done with care. The resulting relationship has an  $R^2 = 0.978$ . A graph showing the results and the fitted line is shown below in Figure 0-4. The statistical output for the regression can be seen in Table 0-2. The final resulting equation for the standard deviation can now be rewritten to include both parameter uncertainty and model uncertainty.

The resulting equation given as:

$$\sigma_{v_s}^2 = \left(16.686 \frac{m}{s}\right)^2 + \left(2.99 \frac{m}{s} * \ln[(N_1)_{60}]\right)^2 \quad (70)$$

This is the final equation that was used to estimate the variation in shear wave velocity in this report. A final modification replacing  $(N_1)_{60}$  with  $(N_1)_{60cs}$  can be made to generalize this equation for use with soils containing fines.

**Table 0-1: Values found using Monte Carlo simulation.**

Mean of Class	Mean	StdDev	Mean + 1 Stdev	Mean - 1 Stdev
5.00	135.60	9.80	145.40	125.81
6.58	144.50	10.48	154.98	134.01
8.16	151.95	10.85	162.79	141.10
9.74	158.35	11.49	169.85	146.86
11.32	163.88	11.74	175.62	152.13
12.89	168.89	12.19	181.08	156.71
14.47	173.42	12.63	186.05	160.79
16.05	177.52	13.04	190.56	164.48
17.63	181.72	13.10	194.82	168.61
19.21	185.22	13.47	198.69	171.75
20.79	188.40	13.71	202.11	174.69
22.37	191.85	13.72	205.58	178.13
23.95	195.02	13.89	208.90	181.13
25.53	197.66	14.40	212.06	183.26
27.11	200.38	14.43	214.81	185.94
28.68	203.13	14.64	217.78	188.49
30.26	205.63	15.02	220.65	190.61
31.84	208.16	15.24	223.40	192.92
33.42	210.41	15.19	225.60	195.22
35.00	212.70	15.53	228.24	197.17

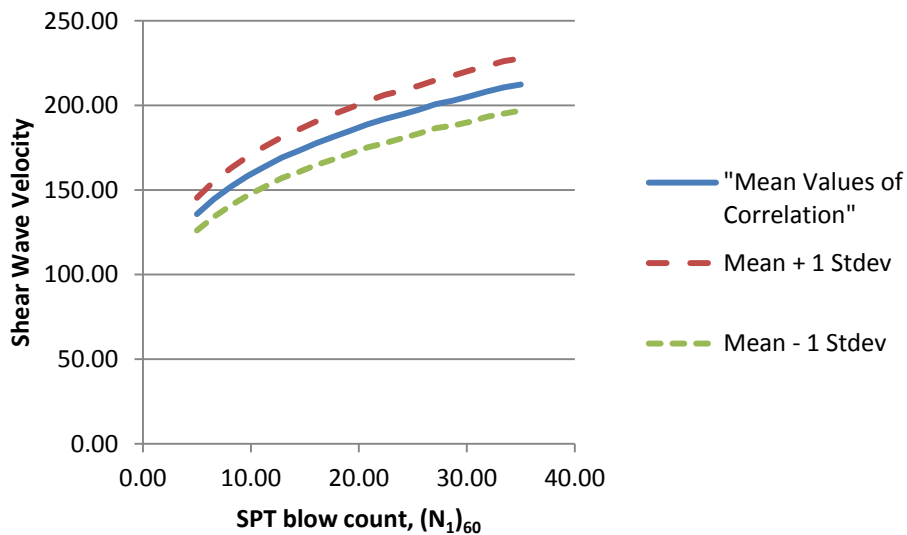


**Figure 0-3: Standard deviation in shear wave velocity due to parameter uncertainty.**

**Table 0-2: Statistical results of regression of standard deviation.**

RSquare	0.987438
RSquare Adj	0.98674
Root Mean Square Error	0.196581
Mean of Response	13.2514
Observations (or Sum Wgts)	20

Term	Estimate	Std Error	DFDen	t Ratio	Prob> t	Lower 95%	Upper 95%
Intercept	4.6863531	0.231908	18.00	20.21	<.0001*	4.1991333	5.1735729
Ln(N <sub>1</sub> ) <sub>60</sub>	2.9909244	0.079514	18.00	37.61	<.0001*	2.8238709	3.1579779

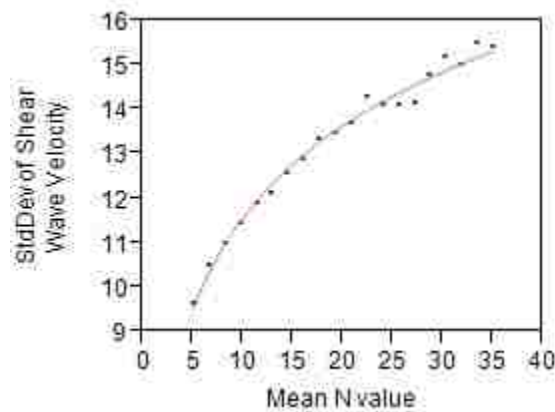


**Figure 0-4: Data and regression line for standard deviation of shear wave velocity.**

### **A.3 Detailed Discussion – Sensitivity Analysis of Cetin et al.**

A sensitivity analysis of the Cetin et al. method was conducted to understand how the various input parameters affected the probability of liquefaction. The details of the results of this analysis are discussed in the body of the report and will not be reiterated here although a

summary figure is provided (Figure 0-5). Rather the mechanics of the analysis, and the details of how parameters were selected, will be looked at instead.

For this analysis, different input parameters were examined. These input parameters included  $a_{max}$ ,  $M_w$ ,  $V_{s12}$ , depth, fines content, SPT blow count, and the unit weight. These parameters were varied over given ranges as shown in the body of the report and repeated in Table 0-3 for convenience.

**Table 0-3: Range of input parameters used sensitivity analysis.**

	<b>Range</b>	<b>Increment</b>
<b><math>a_{max}</math> [g]</b>	0.1-1.1	0.2 g
<b><math>M_w</math></b>	5.0-9.0	0.1
<b><math>V_s</math> [m/s]</b>	120-240, 250	20 m/s
<b>Fines Content [%]</b>	0-40	10 %
<b>Depth [m]</b>	1-19	2 m
<b>SPT blow count</b>	5-35	5
<b><math>\gamma_{sat}</math> [KN/m<sup>3</sup>]</b>	held constant at 18	N/A

The range of  $a_{max}$  was selected from 0.1-1.1 as this accounts for the range over which most seismic analyses will be run. Higher accelerations do occasionally occur but it was felt that this range was sufficient for the purposes of this study. Likewise the range of moment magnitude used, from 5.0 – 9.0, was selected based off of the general range of values common in liquefaction analyses. Shear wave velocities from 120 – 250 m/s were used in this analyses. This range corresponds to the limits laid out the Cetin and Seed et al. for applying the depth reduction factors. Depths were varied from 1-19 meters. This range corresponds to most of the valid range for the simplified procedure, and allows the first of the Cetin et al equations to be used (there is inadequate data at greater depths to justify use of the simplified procedure at these depths). Finally the SPT blow count was varied from 5-35. These values were used as they

correspond to the range of values used in this study, as well as the range of values for most liquefiable soils. Finally, unit weight was held constant at a value of 18 KN/m<sup>3</sup>.

Using the above values a sensitivity analysis was conducted. For the purposes of the sensitivity analysis a spreadsheet was created where values of initial vertical stress, initial vertical effective stress, CSR<sub>eq</sub>, r<sub>d</sub>, and probability of liquefaction were calculated based off of the input parameters. This allowed an in depth look at trends in the data.

For this analysis the equations used are shown here for validation and user convenience. The values for initial effective and total vertical stress were calculated based off of the typical approach,

$$\begin{aligned}\sigma_{vo} &= \gamma * h \\ \sigma'_{vo} &= (\gamma - u) * h\end{aligned}\quad (71)$$

where  $\gamma$  is the unit weight of the soil,  $u$  is the pore water pressure, and  $h$  is the depth. The depth reduction factor is calculated based of the equation given by Cetin et al as seen in the body of the report and repeated here for convenience,

$$r_d = \left( \frac{\left( 1 + \frac{(-23.013 - 2.949a_{max} + 0.999M_w + 0.0525V_{s12})}{(16.258 + 0.201\exp(0.341(-d + 0.0785V_{s12} + 7.586)))} \right)}{\left( 1 + \frac{(-23.013 - 2.949a_{max} + 0.999M_w + 0.0525V_{s12})}{(16.258 + 0.201\exp(0.341(0.0785V_{s12} + 7.586)))} \right)} \right) \pm \sigma_{\epsilon r_d}\quad (72)$$

For a detailed discussion of this equation see section 4.3.3.1 of the body of this report. The cyclic resistance factor CSR<sub>eq</sub> was found according to the equation given by Cetin et al. where:

$$CSR_{eq} = 0.65 * \frac{a_{max}}{g} * \frac{\sigma}{\sigma'} * r_d\quad (73)$$

This is the form of the CSR equation as given by Seed and Idriss and a detailed discussion of this equation is found in the body of the report in section 4.3.1. The probability of liquefaction was

found according to the equation provided by Cetin et al as shown in section 4.4.2 and repeated here for convenience.

$$P_L = \Phi \left( - \frac{N_{1,60}(1+\theta_1 FC) - \theta_2 \ln(CSR_{eq}) - \theta_3 \ln(M_w) - \theta_4 \ln\left(\frac{\sigma'_v}{P_d}\right) + \theta_5 FC + \theta_6}{\sigma_\epsilon} \right) \quad (74)$$

Using these equations and the input parameters listed above an analysis was completed with a total of 964,320 runs. A sample of the results is shown below in Table 0-4.

**Table 0-4: Sample of data used in sensitivity analysis of Cetin et al. (2004) method.**

V <sub>s</sub>	a <sub>max</sub>	M <sub>w</sub>	depth	r <sub>d</sub>	stress	effective stress	FC	N	CSR <sub>eq</sub>	P <sub>liq</sub>
120	0.1	5	1	0.948562	0.018	0.00819	0	5	0.135509	7.30781E-05
120	0.1	5.1	1	0.949062	0.018	0.00819	0	5	0.13558	0.000172898
120	0.1	5.2	1	0.94956	0.018	0.00819	0	5	0.135651	0.000384995
120	0.1	5.3	1	0.950057	0.018	0.00819	0	5	0.135722	0.00080953
120	0.1	5.4	1	0.950553	0.018	0.00819	0	5	0.135793	0.001612472
120	0.1	5.5	1	0.951047	0.018	0.00819	0	5	0.135864	0.003051538
120	0.1	5.6	1	0.95154	0.018	0.00819	0	5	0.135934	0.005502085
120	0.1	5.7	1	0.952031	0.018	0.00819	0	5	0.136004	0.009476911
120	0.1	5.8	1	0.952522	0.018	0.00819	0	5	0.136075	0.015632453
120	0.1	5.9	1	0.95301	0.018	0.00819	0	5	0.136144	0.024753939
120	0.1	6	1	0.953498	0.018	0.00819	0	5	0.136214	0.037714314
120	0.1	6.1	1	0.953984	0.018	0.00819	0	5	0.136283	0.055406049
120	0.1	6.2	1	0.954468	0.018	0.00819	0	5	0.136353	0.078650723
120	0.1	6.3	1	0.954952	0.018	0.00819	0	5	0.136422	0.108096992
120	0.1	6.4	1	0.955434	0.018	0.00819	0	5	0.136491	0.144121831
120	0.1	6.5	1	0.955914	0.018	0.00819	0	5	0.136559	0.186751359
120	0.1	6.6	1	0.956394	0.018	0.00819	0	5	0.136628	0.235615539
120	0.1	6.7	1	0.956872	0.018	0.00819	0	5	0.136696	0.289945941
120	0.1	6.8	1	0.957348	0.018	0.00819	0	5	0.136764	0.348618631
120	0.1	6.9	1	0.957824	0.018	0.00819	0	5	0.136832	0.410236754
120	0.1	7	1	0.958298	0.018	0.00819	0	5	0.1369	0.473241157



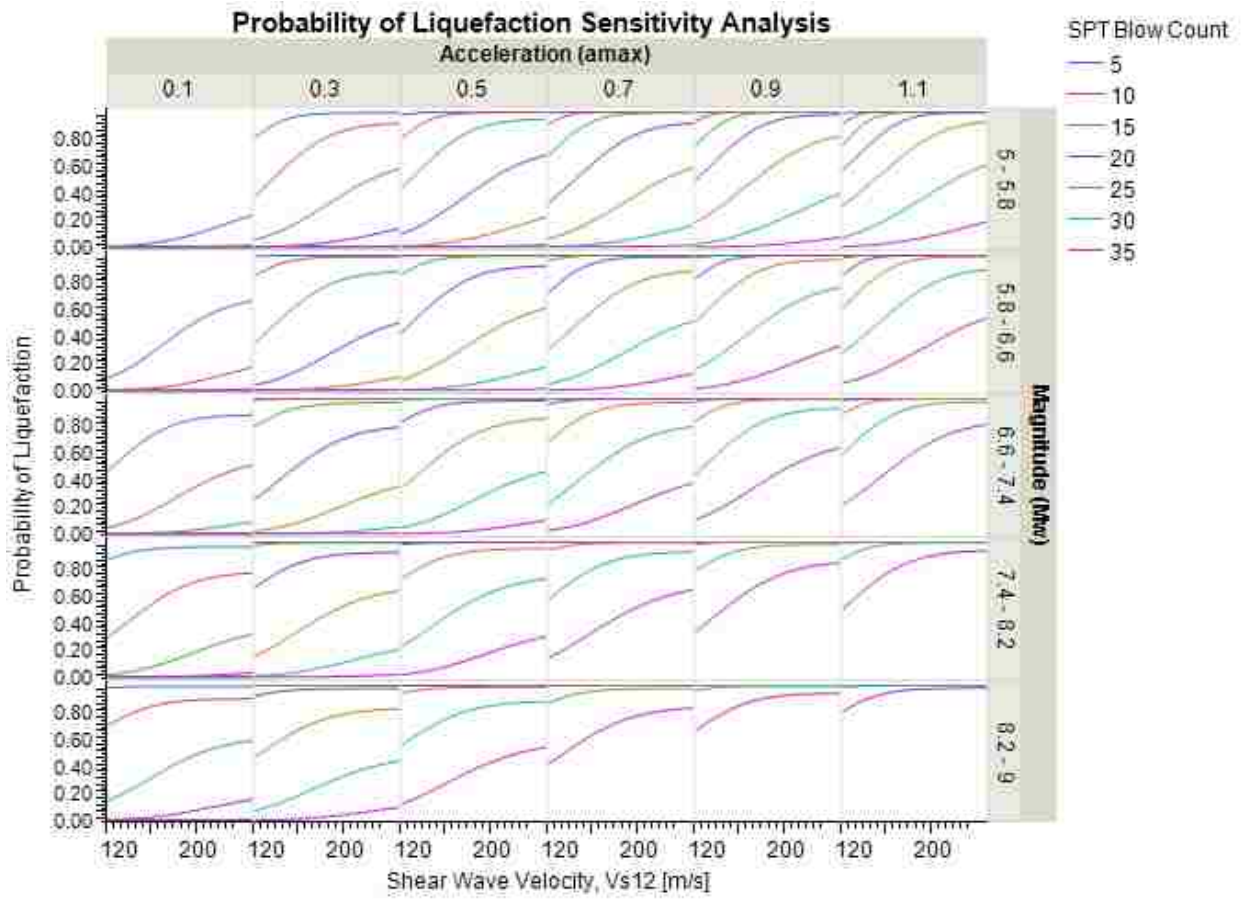


**Figure 0-5: Summary of sensitivity analysis results.**

#### A.4 Detailed Discussion – Performance-Based Magnitude Scaling Factors

Performance-based magnitude scaling factors ( $MSF_{PB}$ ) were proposed by Cetin and Bilge (2012). These factors allow the MSF in the simplified method to be scaled according to the definition of liquefaction onset. Most relationships use a fixed definition of liquefaction onset and cannot deal with differences such as these. The implementation of these factors is discussed in the body of the report and further details will be offered here.

As with any performance-based calculation, it is desirable to account for both the mean values as well as the less likely higher and lower values. In the case of performance-based magnitude scaling factors this scatter is best represented by the variable  $c$ . The equation for  $c$  is given in the body of the report and is repeated here for convenience.

$$\ln(c) = \ln((-6.0591 + 0.3120 * S) * (-m)^{1.4391}) \pm 0.056 \quad (75)$$

where the standard deviation of 0.056 is the standard deviation of the data in a normal distribution. Thus, for performance-based magnitude scaling factors, the spread in the data can be accounted for using a normal distribution of the parameter  $c$  with the high and low values contributing 16% to the calculation and the median value contributing 68%. This accounts for the uncertainty associated with the  $MSF_{PB}$ .

One difficulty that arises in using this approach is that the Cetin and Bilge (2012) equations valid range contains regions where the relationships between  $m$  and  $c$  are mathematically undefined. In these regions the coefficient of  $m$  was capped at a value of 0 to prevent the equations from becoming undefined. This is consistent with graphs of  $m$  provided by Cetin and Bilge (2012) which have values ranging from -1.0 to 0.0 (Figure 0-6).

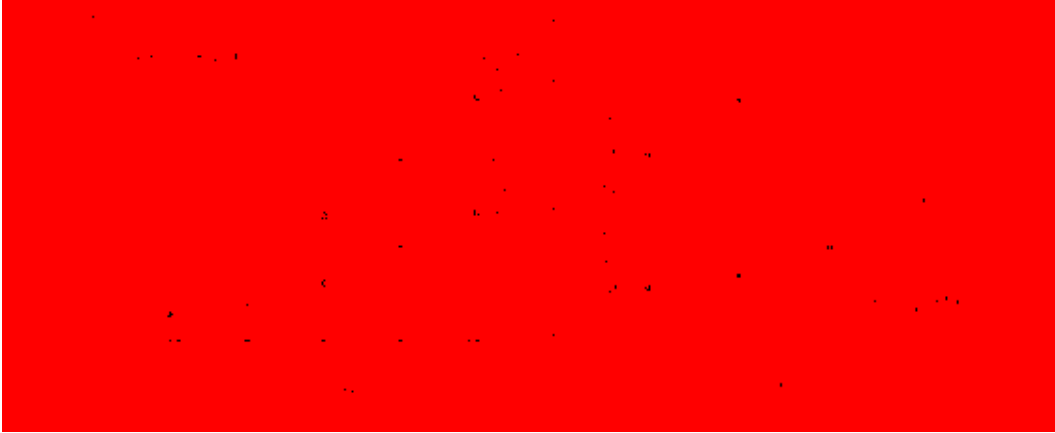


**Figure 0-6:  $m$  values plot after Cetin and Bilge (2012).**

Using this value for  $m$  gives a  $c$  of 0 and results in a MSF of 1.0. The invalid ranges where this applies usually occur at shallow depths and low relative densities where the simplified method is not well defined. Further problems occur where the input data is outside the range considered valid for the Cetin and Bilge (2012) equations. For these cases, limiting values are applied to prevent the parameters from going outside the valid range.

#### **A.5 Detailed Discussion – Liquefaction Initiation Current State of the Practice and State of the Art**

Currently in practice there exist three different methods for analyzing liquefaction initiation: deterministic scenario based, deterministic pseudo probabilistic, and fully performance-based. These three methods were developed over time as the concepts evolved and to address different issues.

The fully deterministic based approach was the approach originally used by various authors to develop the simplified method. At the time the prevailing system of seismic hazard analysis was the DSHA. In this type of analysis values are obtained for the controlling or critical

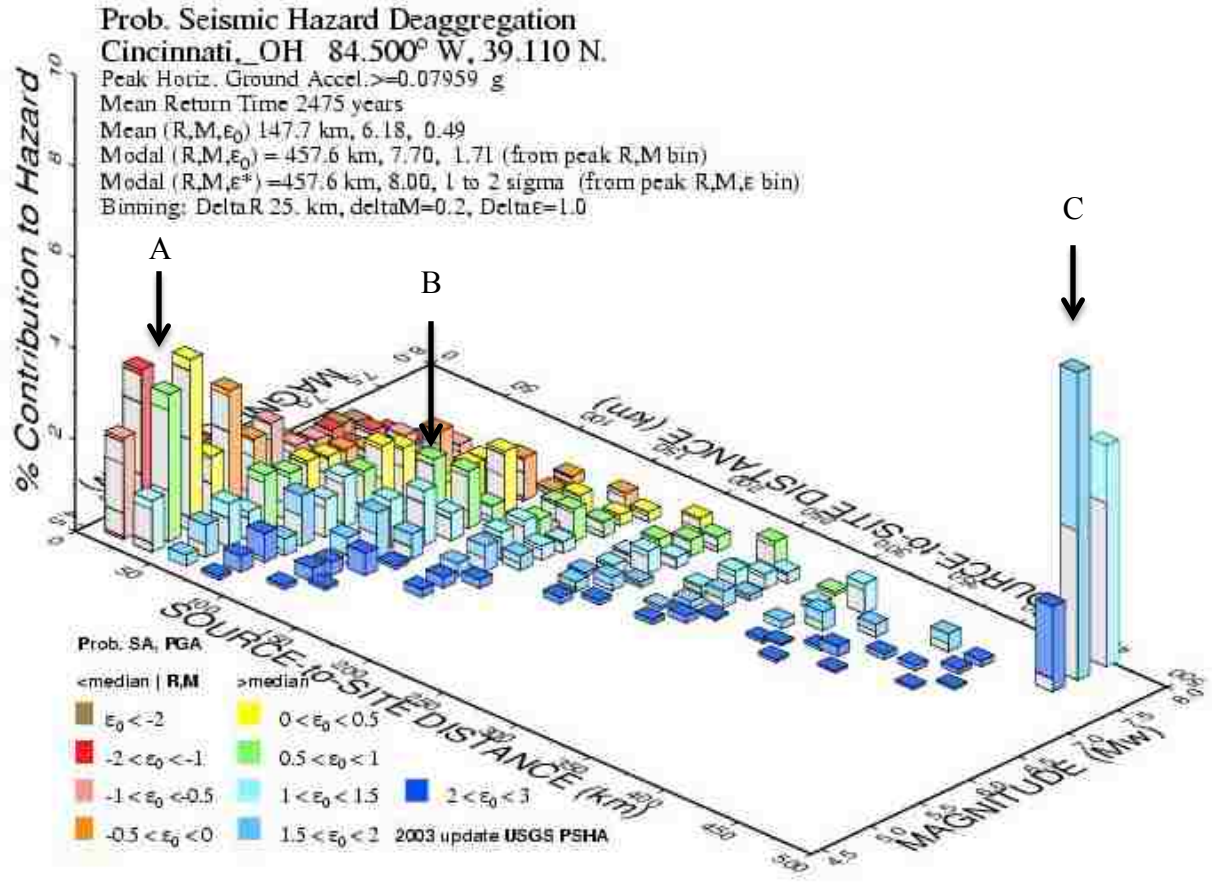
seismic event. A fully deterministic or scenario based approach to liquefaction initiation analysis uses the output from this analysis to determine whether a site will liquefy. The main problem with this type of analysis is that it does not account for the variation of the data. The analysis only considers the single event, or in some cases a few scenario events.

To overcome this problem, geophysicists developed the PSHA. Using a PSHA the variability and uncertainty in the seismic hazard analysis can be more fully accounted for. In order to account for this uncertainty in an analysis of liquefaction engineers typically will use the mean or modal values from the output of a PSHA. This method in this paper will be referred to as the pseudo probabilistic approach. The pseudo probabilistic approach is currently widely used in practice, and has been widely used in an attempt by engineers to merge the PSHA with the deterministic analysis of liquefaction. However the merging of a fully probabilistic analysis of the hazard from a PSHA into a scenario based deterministic analysis can result in inconsistencies in the analysis. In particular it can result in the use of incompatible pairs. A compatible pair is a pair of acceleration and magnitude values from a seismic event. An incompatible pair occurs when an acceleration is paired with a magnitude other than the one that produced it. This will generally occur most often in areas that have more than one major area contributing to the response, resulting in bi or tri modal deaggregations. To account for this type of response a performance-based approach or a simplified equivalent should be used. The performance-based approach should be used for a situation like this as it incorporates the uncertainties and accounts for all of the possible scenarios at this site. This will result in a much more realistic analysis of the liquefaction hazard associated with this site. A good example of such a Scenario is shown for a site located in Cincinnati which has a bi modal PSHA (Figure 0-7).

The bi modal nature of this site is easily identified by looking at the two locations of greatest contribution, locations A and C. Only one of the modes is accounted for by using the modal values provided by the PSHA. The other alternative, of using the mean output from the PSHA, results in an incompatible pair, with the resulting values not corresponding to any major contributing scenario (point C). A comparison of these techniques for a site in Cincinnati is shown (Figure 0-8 and Table 0-6 - Table 0-9) using a uniform soil profile (Table 0-5). An  $FS_{liq}$  of 1.2 was used in the deterministic analyses and 1.0 for the performance-based analyses.

The scenario based input parameter values used in these analyses were developed by Youd (2008) using the attenuation relationship of Toro, Abrahamson et al. (1997). For the mean and modal input values from the USGS deaggregation website were used.

For these analyses it can be seen that the modal inputs do not agree well with the scenario based, mean pseudo probabilistic, or performance-based analyses. For a return period of 2475 years the modal input predicts liquefaction for the bottom two layers, while the mean, performance-based, and scenario based analyses have at least two out of three relationships predicting no liquefaction. It is recommended that the pseudo probabilistic mean and modal approaches currently used in practice should be used with care to evaluate liquefaction initiation, especially in areas where bi modal responses occur. The use of a performance-based method of analysis is preferred.



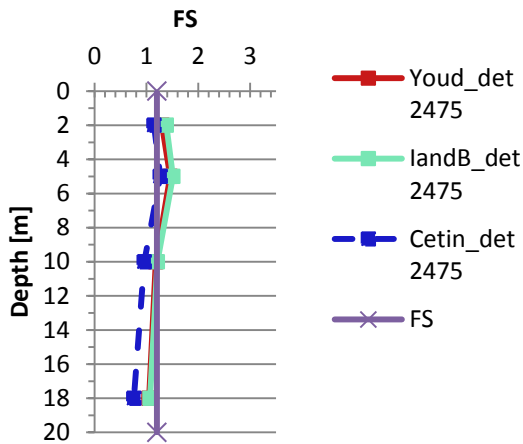
GMT 2008 Jul 20 16:21:20 Distance (R), magnitude (M), epsilon (ε<sub>0</sub>) deaggregation for a site on ROCK ε<sub>0</sub> V<sub>s</sub>=780 m/s top 30 m USGS COHT PSHA2003v3 LUPDATE bins with H 0.05% contrib. omitted

**Figure 0-7: Bi modal event for site located in Cincinnati.**

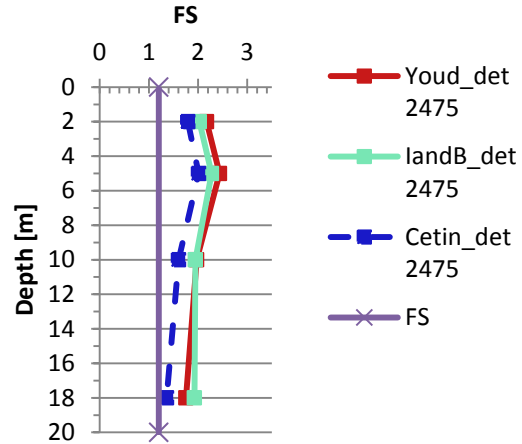
**Table 0-5: Soil properties used in comparative analyses (input from PB LiquefY).**

Sub Layer #	Bottom Depth [m]	Thickness [m]	Sample Depth [m]	C1	Soil Type	V <sub>s</sub> [m/s]	N	D <sub>R</sub>	Susceptible?	γ [kN/m <sup>3</sup> ]
1	4	4	2	1	Sand	170.3	11	47.61	Default	18
2	8	4	5	1	Sand	174	11	49.89	Default	18
3	12	4	10	1	Sand	162.6	11	43.04	Default	18
4	20	8	18	1	Sand	151.9	11	37.16	Default	18

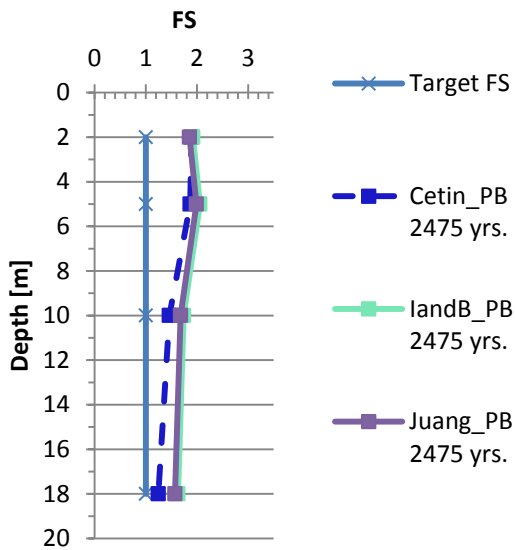
### FS<sub>liq</sub> vs. Depth Pseudo Probabilistic Modal Based



### FS<sub>liq</sub> vs. Depth Pseudo Probabilistic Mean Based



### FS<sub>liq</sub> vs. Depth Performance-based



### FS<sub>liq</sub> vs. Depth Scenario Based

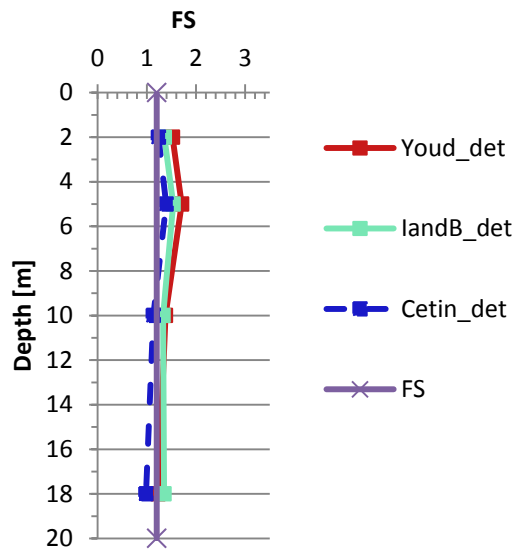


Figure 0-8: Comparison of pseudo probabilistic, scenario based, and performance-based analyses for Cincinnati site with  $T_R = 2475$  years and uniform SPT of 10 blows/ft.

**Table 0-6: Performance-based.**

Sub - Layer #	Sample Depth [m]	Cetin et al. FS <sub>liq</sub>	Idriss and Boulanger FS <sub>liq</sub>	Youd et al. FS <sub>liq</sub>
1	2.00	No_Liq	No_Liq	No_Liq
2	5.00	No_Liq	No_Liq	No_Liq
3	10.00	No_Liq	No_Liq	No_Liq
4	18.00	No_Liq	No_Liq	No_Liq

**Table 0-7: Scenario based.**

Sub - Layer #	Sample Depth [m]	Cetin et al. FS <sub>liq</sub>	Idriss and Boulanger FS <sub>liq</sub>	Youd et al. FS <sub>liq</sub>
1	2.00	No_Liq	No_Liq	No_Liq
2	5.00	No_Liq	No_Liq	No_Liq
3	10.00	1.13	No_Liq	No_Liq
4	18.00	0.98	No_Liq	No_Liq

**Table 0-8: Mean pseudo probabilistic.**

Sub - Layer #	Sample Depth [m]	Cetin et al. FS <sub>liq</sub>	Idriss and Boulanger FS <sub>liq</sub>	Youd et al. FS <sub>liq</sub>
1	2.00	No_Liq	No_Liq	No_Liq
2	5.00	No_Liq	No_Liq	No_Liq
3	10.00	No_Liq	No_Liq	No_Liq
4	18.00	No_Liq	No_Liq	No_Liq

**Table 0-9: Modal pseudo probabilistic.**

Sub - Layer #	Sample Depth [m]	Cetin et al. FS <sub>liq</sub>	Idriss and Boulanger FS <sub>liq</sub>	Youd et al. FS <sub>liq</sub>
1	2.00	1.14	No_Liq	No_Liq
2	5.00	No_Liq	No_Liq	No_Liq
3	10.00	0.96	No_Liq	1.18
4	18.00	0.76	1.07	1.05



## **A.6 Detailed Discussion – Comparison between Deterministic Methods, Past Research**

A detailed discussion of the differences between the deterministic methods of analyzing liquefaction has been made by several different authors (Idriss and Boulanger 2010; Seed 2010; Boulanger and Idriss 2011; Cox and Griffiths 2011; Youd 2013). An overview of the main points will be discussed here. The interested reader is referred to the existing paper for an extensive discussion.

Idriss and Boulanger (2010) and Boulanger and Idriss (2011) discuss the differences between their method and the method of Cetin and Seed et al. They site 11 specific case histories which they feel were interpreted in error due to either misinterpreting of data or miscalculation of values. They postulate that were these case histories to be corrected the results of the analysis performed by Cetin and Seed et al. would yield very similar results to those produced by their relationship.

Seed (2010) also looked at the differences between his model and the model of Idriss and Boulanger. Seed's conclusions in part agreed with those of Boulanger and Idriss in that he also felt that there were some errors in the database that led to differences between the two models. In his case he felt that the data base of Boulanger and Idriss was in error and that a misrepresentation of some of the case histories had been made. He further outlined several other differences that he felt were critical. These differences included:

1. That the curve of the Idriss and Boulanger is centered incorrectly about 1.0 atmosphere of overburden pressure.
2. That the values of  $K_{\sigma}$  values found using their approach were too low.
3. That the values of  $r_d$  were incorrect and that no documentation of how they were developed had been released.

Boulanger and Idriss subsequently modified their  $K_{\sigma}$  value limit to allow values greater than 1.1 and released documentation on how their  $r_d$  values were developed. Cetin and Seed et al. have not yet responded to the concerns raised by Boulanger and Idriss.

A third comparison of the models was made by Cox and Griffiths (2012). They concluded that there were differences between the three most commonly used methods (NCEER, Idriss and Boulanger, and Cetin and Seed et al.) but that these differences were small and could generally be best accounted for by using any two of the three methods which agreed. For example in the case where two methods predicted liquefaction occurring, and one method did not then liquefaction would be said to be occurring. They further concluded that much of the difference between the Cetin and Seed and Idriss and Boulanger approaches occurred due to the  $C_N$  correction term. Youd (2013) concurred with some of the findings of Cox and Griffiths in that the differences between the deterministic methods were small and not of great concern when analyzing liquefaction effects deterministically.

## APPENDIX B.

The following tables contain sample output from PB Liquefy.

### B.1 Analysis Details - Soil Profiles

This section includes details of the soil profiles used in the analysis. These are listed in abbreviated form in the body of the report (Table 6-4). Soil profiles will be shown in the order they are listed in the abbreviated table. A table of abbreviations used in the soils tables is provided below (Table 0-1).

**Table 0-1: List of abbreviations.**

L	Layer Number
D	Depth of Bottom of Layer
T	Thickness of Layer
Sa	Sample Depth
S	Sampler Type
So	Soil Type
V	Shear Wave Velocity
N	SPT Blow Count
FC	Fines Content
Dr	Relative Density
Su	Susceptability
UW	unit weight

**Table 0-2: Soil profiles 1 and 2.**

Profile #	L	D	T	Sa	S	So	V	N	FC	D	Su	UW
1	1	2	2	1	1	[SW]_Well-graded_sand	144.59243 25	5	0	33.40097 304	Default	20. 314
1	2	4	2	3	1	[SW]_Well-graded_sand	148.83401 04	5	0	35.55805 113	Default	20. 314
1	3	6	2	5	1	[SW]_Well-graded_sand	145.72762 82	5	0	33.97116 87	Default	20. 314
1	4	8	2	7	1	[SW]_Well-graded_sand	140.17291 62	5	0	31.23046 705	Default	20. 314
1	5	1 0	2	9	1	[SW]_Well-graded_sand	137.78558 02	5	0	30.09058 001	Default	20. 314
1	6	1 2	2	11	1	[SW]_Well-graded_sand	134.62878 43	5	0	28.61824 617	Default	20. 314
1	7	1 4	2	13	1	[SW]_Well-graded_sand	132.05605 59	5	0	27.44766 145	Default	20. 314
1	8	1 6	2	15	1	[SW]_Well-graded_sand	129.89135 25	5	0	26.48307 264	Default	20. 314
1	9	1 8	2	17	1	[SW]_Well-graded_sand	128.02710 61	5	0	25.66722 727	Default	20. 314
1	1 0	2 0	2	19	1	[SW]_Well-graded_sand	126.39291 74	5	0	24.96334 542	Default	20. 314
Profile #	L	D	T	Sa	S	So	V	N	L	D	Su	UW
2	1	2	2	1	1	[SW]_Well-graded_sand	149.38171 4	5	10	35.84188 819	Default	20. 314
2	2	4	2	3	1	[SW]_Well-graded_sand	153.29004 36	5	10	37.90260 331	Default	20. 314
2	3	6	2	5	1	[SW]_Well-graded_sand	150.42374 8	5	10	36.38525 66	Default	20. 314
2	4	8	2	7	1	[SW]_Well-graded_sand	145.35513 59	5	10	33.78349 767	Default	20. 314
2	5	1 0	2	9	1	[SW]_Well-graded_sand	143.20179 52	5	10	32.70954 351	Default	20. 314
2	6	1 2	2	11	1	[SW]_Well-graded_sand	140.38036 43	5	10	31.33059 518	Default	20. 314
2	7	1 4	2	13	1	[SW]_Well-graded_sand	138.10473 31	5	10	30.24164 676	Default	20. 314
2	8	1 6	2	15	1	[SW]_Well-graded_sand	136.20796 38	5	10	29.34981 052	Default	20. 314
2	9	1 8	2	17	1	[SW]_Well-graded_sand	134.58854 46	5	10	28.59973 465	Default	20. 314
2	1 0	2 0	2	19	1	[SW]_Well-graded_sand	133.18033 55	5	10	27.95597 056	Default	20. 314

**Table 0-3: Soil profiles 3 and 4.**

Profile #	L	D	T	Sa	S	So	V	N	L	D	Su	UW
3	1	2	2	1	1	[SW]_Well-graded_sand	161.62532 58	5	2	42.505269 59	Default	20. 314
3	2	4	2	3	1	[SW]_Well-graded_sand	164.83566 16	5	2	44.353861 7	Default	20. 314
3	3	6	2	5	1	[SW]_Well-graded_sand	162.47478 31	5	2	42.990290 32	Default	20. 314
3	4	8	2	7	1	[SW]_Well-graded_sand	158.38993 77	5	2	40.685016 38	Default	20. 314
3	5	1 0	2	9	1	[SW]_Well-graded_sand	156.69210 49	5	2	39.746930 94	Default	20. 314
3	6	1 2	2	11	1	[SW]_Well-graded_sand	154.50402 41	5	2	38.555318 43	Default	20. 314
3	7	1 4	2	13	1	[SW]_Well-graded_sand	152.77102 75	5	2	37.625375 31	Default	20. 314
3	8	1 6	2	15	1	[SW]_Well-graded_sand	151.34935 36	5	2	36.871604 2	Default	20. 314
3	9	1 8	2	17	1	[SW]_Well-graded_sand	150.15263 77	5	2	36.243462 85	Default	20. 314
3	1 0	2 0	2	19	1	[SW]_Well-graded_sand	149.12522 26	5	2	35.708815 21	Default	20. 314
Profile #	L	D	T	Sa	S	So	V	N	L	D	Su	UW
4	1	2	2	1	1	[SW]_Well-graded_sand	166.82553 15	5	3	45.520958 51	Default	20. 314
4	2	4	2	3	1	[SW]_Well-graded_sand	169.92175 04	5	3	47.369423 5	Default	20. 314
4	3	6	2	5	1	[SW]_Well-graded_sand	167.64350 18	5	3	46.005446 33	Default	20. 314
4	4	8	2	7	1	[SW]_Well-graded_sand	163.71914 47	5	3	43.706140 62	Default	20. 314
4	5	1 0	2	9	1	[SW]_Well-graded_sand	162.09510 14	5	3	42.773134 83	Default	20. 314
4	6	1 2	2	11	1	[SW]_Well-graded_sand	160.00876 07	5	3	41.590420 61	Default	20. 314
4	7	1 4	2	13	1	[SW]_Well-graded_sand	158.36196 44	5	3	40.669465 18	Default	20. 314
4	8	1 6	2	15	1	[SW]_Well-graded_sand	157.01492 19	5	3	39.924387 35	Default	20. 314
4	9	1 8	2	17	1	[SW]_Well-graded_sand	155.88388 88	5	3	39.304509 59	Default	20. 314
4	1 0	2 0	2	19	1	[SW]_Well-graded_sand	154.91503	5	3	38.777661 11	Default	20. 314

**Table 0-4: Soil profiles 5 and 6.**

Profile #	L	D	T	Sa	S	So	V	N	L	D	Su	UW
5	1	2	2	1	1	[SW]_Well-graded_sand	168.650378	5	4	46.60561483	Default	20.314
5	2	4	2	3	1	[SW]_Well-graded_sand	171.7554106	5	4	48.48281482	Default	20.314
5	3	6	2	5	1	[SW]_Well-graded_sand	169.4705291	5	4	47.09757633	Default	20.314
5	4	8	2	7	1	[SW]_Well-graded_sand	165.5367401	5	4	44.76319716	Default	20.314
5	5	10	2	9	1	[SW]_Well-graded_sand	163.9095952	5	4	43.81626342	Default	20.314
5	6	12	2	11	1	[SW]_Well-graded_sand	161.8200171	5	4	42.6161724	Default	20.314
5	7	14	2	13	1	[SW]_Well-graded_sand	160.1712945	5	4	41.68191786	Default	20.314
5	8	16	2	15	1	[SW]_Well-graded_sand	158.8231126	5	4	40.92623971	Default	20.314
5	9	18	2	17	1	[SW]_Well-graded_sand	157.6914401	5	4	40.2976575	Default	20.314
5	10	20	2	19	1	[SW]_Well-graded_sand	156.722273	5	4	39.76349672	Default	20.314
Profile #	L	D	T	Sa	S	So	V	N	L	D	Su	UW
6	1	2	2	1	1	[SW]_Well-graded_sand	168.650378	5	5	46.60561483	Default	20.314
6	2	4	2	3	1	[SW]_Well-graded_sand	171.7554106	5	5	48.48281482	Default	20.314
6	3	6	2	5	1	[SW]_Well-graded_sand	169.4705291	5	5	47.09757633	Default	20.314
6	4	8	2	7	1	[SW]_Well-graded_sand	165.5367401	5	5	44.76319716	Default	20.314
6	5	10	2	9	1	[SW]_Well-graded_sand	163.9095952	5	5	43.81626342	Default	20.314
6	6	12	2	11	1	[SW]_Well-graded_sand	161.8200171	5	5	42.6161724	Default	20.314
6	7	14	2	13	1	[SW]_Well-graded_sand	160.1712945	5	5	41.68191786	Default	20.314
6	8	16	2	15	1	[SW]_Well-graded_sand	158.8231126	5	5	40.92623971	Default	20.314
6	9	18	2	17	1	[SW]_Well-graded_sand	157.6914401	5	5	40.2976575	Default	20.314
6	10	20	2	19	1	[SW]_Well-graded_sand	156.722273	5	5	39.76349672	Default	20.314

**Table 0-5: Soil profiles 7 and 8.**

Profile #	L	D	T	Sa	S	So	V	N	L	D	Su	UW
7	1	2	2	1	1	[SW]_Well-graded_sand	186.363378 1	1 5	0	57.8521823 3	Default	20.31 4
7	2	4	2	3	1	[SW]_Well-graded_sand	191.830294 7	1 5	0	61.5883511 7	Default	20.31 4
7	3	6	2	5	1	[SW]_Well-graded_sand	187.826517 6	1 5	0	58.8397901 8	Default	20.31 4
7	4	8	2	7	1	[SW]_Well-graded_sand	180.667118 7	1 5	0	54.0927556 7	Default	20.31 4
7	5	1 0	2	9	1	[SW]_Well-graded_sand	177.590111 3	1 5	0	52.1184134 1	Default	20.31 4
7	6	1 2	2	1	1	[SW]_Well-graded_sand	173.521356 5	1 5	0	49.5682564	Default	20.31 4
7	7	1 4	2	3	1	[SW]_Well-graded_sand	170.205399	1 5	0	47.5407441 8	Default	20.31 4
7	8	1 6	2	5	1	[SW]_Well-graded_sand	167.415339 8	1 5	0	45.8700273 5	Default	20.31 4
7	9	1 8	2	7	1	[SW]_Well-graded_sand	165.012536	1 5	0	44.4569417 2	Default	20.31 4
7	1 0	2 0	2	9	1	[SW]_Well-graded_sand	162.906250 6	1 5	0	43.2377826	Default	20.31 4
Profile #	L	D	T	Sa	S	So	V	N	L	D	Su	UW
8	1	2	2	1	1	[SW]_Well-graded_sand	189.090760 5	1 5	1 0	59.7003917	Default	20.31 4
8	2	4	2	3	1	[SW]_Well-graded_sand	194.422250 6	1 5	1 0	63.4037533 1	Default	20.31 4
8	3	6	2	5	1	[SW]_Well-graded_sand	190.515708	1 5	1 0	60.6784526 4	Default	20.31 4
8	4	8	2	7	1	[SW]_Well-graded_sand	183.558178 1	1 5	1 0	55.9838196 8	Default	20.31 4
8	5	1 0	2	9	1	[SW]_Well-graded_sand	180.580478 7	1 5	1 0	54.0366230 5	Default	20.31 4
8	6	1 2	2	1	1	[SW]_Well-graded_sand	176.656240 9	1 5	1 0	51.5270075 2	Default	20.31 4
8	7	1 4	2	3	1	[SW]_Well-graded_sand	173.470325 7	1 5	1 0	49.5367087 9	Default	20.31 4
8	8	1 6	2	5	1	[SW]_Well-graded_sand	170.799078 1	1 5	1 0	47.9003972 3	Default	20.31 4
8	9	1 8	2	7	1	[SW]_Well-graded_sand	168.506058 7	1 5	1 0	46.5193334 8	Default	20.31 4
8	1 0	2 0	2	9	1	[SW]_Well-graded_sand	166.502106 2	1 5	1 0	45.3301532 2	Default	20.31 4

**Table 0-6: Soil profiles 9 and 10.**

Profile #	L	D	T	Sa	S	So	V	N	L	D	Su	UW
9	1	2	2	1	1	[SW]_Well-graded_sand	196.56308 49	1 5	2 0	64.924606 35	Default	20. 314
9	2	4	2	3	1	[SW]_Well-graded_sand	201.53820 63	1 5	2 0	68.533975 69	Default	20. 314
9	3	6	2	5	1	[SW]_Well-graded_sand	197.88818 61	1 5	2 0	65.875684 94	Default	20. 314
9	4	8	2	7	1	[SW]_Well-graded_sand	191.45285 63	1 5	2 0	61.326359 37	Default	20. 314
9	5	1 0	2	9	1	[SW]_Well-graded_sand	188.72719 97	1 5	2 0	59.452218 12	Default	20. 314
9	6	1 2	2	11	1	[SW]_Well-graded_sand	185.16431 55	1 5	2 0	57.049526 02	Default	20. 314
9	7	1 4	2	13	1	[SW]_Well-graded_sand	182.29824 87	1 5	2 0	55.155392 15	Default	20. 314
9	8	1 6	2	15	1	[SW]_Well-graded_sand	179.91496 74	1 5	2 0	53.606494 65	Default	20. 314
9	9	1 8	2	17	1	[SW]_Well-graded_sand	177.88451 31	1 5	2 0	52.305606 58	Default	20. 314
9	1 0	2 0	2	19	1	[SW]_Well-graded_sand	176.12232 55	1 5	2 0	51.190517 98	Default	20. 314
Profile #	L	D	T	Sa	S	So	V	N	L	D	Su	UW
10	1	2	2	1	1	[SW]_Well-graded_sand	201.04877 49	1 5	3 0	68.174239 64	Default	20. 314
10	2	4	2	3	1	[SW]_Well-graded_sand	205.99000 53	1 5	3 0	71.852910 92	Default	20. 314
10	3	6	2	5	1	[SW]_Well-graded_sand	202.36368 85	1 5	3 0	69.143020 15	Default	20. 314
10	4	8	2	7	1	[SW]_Well-graded_sand	195.98644 86	1 5	3 0	64.513054 05	Default	20. 314
10	5	1 0	2	9	1	[SW]_Well-graded_sand	193.29240 45	1 5	3 0	62.608922 28	Default	20. 314
10	6	1 2	2	11	1	[SW]_Well-graded_sand	189.77787 71	1 5	3 0	60.170949 95	Default	20. 314
10	7	1 4	2	13	1	[SW]_Well-graded_sand	186.95699 12	1 5	3 0	58.251782 41	Default	20. 314
10	8	1 6	2	15	1	[SW]_Well-graded_sand	184.61590 04	1 5	3 0	56.684425 33	Default	20. 314
10	9	1 8	2	17	1	[SW]_Well-graded_sand	182.62492 92	1 5	3 0	55.369552 84	Default	20. 314
10	1 0	2 0	2	19	1	[SW]_Well-graded_sand	180.89980 26	1 5	3 0	54.243662 88	Default	20. 314



**Table 0-7: Soil profiles 11 and 12.**

Profile #	L	D	T	Sa	S	So	V	N	L	D	Su	UW
11	1	2	2	1	1	[SW]_Well-graded_sand	203.032972 9	1 5	4 0	69.6389498 3	Default	20.31 4
11	2	4	2	3	1	[SW]_Well-graded_sand	208.005252 7	1 5	4 0	73.3831270 3	Default	20.31 4
11	3	6	2	5	1	[SW]_Well-graded_sand	204.35601	1 5	4 0	70.6249136 1	Default	20.31 4
11	4	8	2	7	1	[SW]_Well-graded_sand	197.940399 1	1 5	4 0	65.9133127 1	Default	20.31 4
11	5	1 0	2	9	1	[SW]_Well-graded_sand	195.230979 5	1 5	4 0	63.9759966 9	Default	20.31 4
11	6	1 2	2	1	1	[SW]_Well-graded_sand	191.697228	1 5	4 0	61.4959168 1	Default	20.31 4
11	7	1 4	2	3	1	[SW]_Well-graded_sand	188.861654 5	1 5	4 0	59.5439347 2	Default	20.31 4
11	8	1 6	2	5	1	[SW]_Well-graded_sand	186.508918 6	1 5	4 0	57.9500183 2	Default	20.31 4
11	9	1 8	2	7	1	[SW]_Well-graded_sand	184.508459 6	1 5	4 0	56.6130456 2	Default	20.31 4
11	1 0	2 0	2	9	1	[SW]_Well-graded_sand	182.775439 5	1 5	4 0	55.4683724 9	Default	20.31 4
Profile #	L	D	T	Sa	S	So	V	N	L	D	Su	UW
12	1	2	2	1	1	[SW]_Well-graded_sand	203.032972 9	1 5	5 0	69.6389498 3	Default	20.31 4
12	2	4	2	3	1	[SW]_Well-graded_sand	208.005252 7	1 5	5 0	73.3831270 3	Default	20.31 4
12	3	6	2	5	1	[SW]_Well-graded_sand	204.35601	1 5	5 0	70.6249136 1	Default	20.31 4
12	4	8	2	7	1	[SW]_Well-graded_sand	197.940399 1	1 5	5 0	65.9133127 1	Default	20.31 4
12	5	1 0	2	9	1	[SW]_Well-graded_sand	195.230979 5	1 5	5 0	63.9759966 9	Default	20.31 4
12	6	1 2	2	1	1	[SW]_Well-graded_sand	191.697228	1 5	5 0	61.4959168 1	Default	20.31 4
12	7	1 4	2	3	1	[SW]_Well-graded_sand	188.861654 5	1 5	5 0	59.5439347 2	Default	20.31 4
12	8	1 6	2	5	1	[SW]_Well-graded_sand	186.508918 6	1 5	5 0	57.9500183 2	Default	20.31 4
12	9	1 8	2	7	1	[SW]_Well-graded_sand	184.508459 6	1 5	5 0	56.6130456 2	Default	20.31 4
12	1 0	2 0	2	9	1	[SW]_Well-graded_sand	182.775439 5	1 5	5 0	55.4683724 9	Default	20.31 4

**Table 0-8: Soil profiles 13 and 14.**

Profile #	L	D	T	Sa	S	So	V	N	L	D	Su	UW
13	1	2	2	1	1	[SW]_Well-graded_sand	209.70444 45	2 5	0	74.686846 23	Default	20. 314
13	2	4	2	3	1	[SW]_Well-graded_sand	215.85606 47	2 5	0	79.510219 47	Default	20. 314
13	3	6	2	5	1	[SW]_Well-graded_sand	211.35083 48	2 5	0	75.961842 48	Default	20. 314
13	4	8	2	7	1	[SW]_Well-graded_sand	203.29475 76	2 5	0	69.833447 29	Default	20. 314
13	5	1 0	2	9	1	[SW]_Well-graded_sand	199.83237 06	2 5	0	67.284582 39	Default	20. 314
13	6	1 2	2	11	1	[SW]_Well-graded_sand	195.25402 5	2 5	0	63.992343 84	Default	20. 314
13	7	1 4	2	13	1	[SW]_Well-graded_sand	191.52276 07	2 5	0	61.374836 83	Default	20. 314
13	8	1 6	2	15	1	[SW]_Well-graded_sand	188.38326 08	2 5	0	59.217950 67	Default	20. 314
13	9	1 8	2	17	1	[SW]_Well-graded_sand	185.67951 79	2 5	0	57.393664 97	Default	20. 314
13	1 0	2 0	2	19	1	[SW]_Well-graded_sand	183.30943 1	2 5	0	55.819737 31	Default	20. 314
Profile #	L	D	T	Sa	S	So	V	N	L	D	Su	UW
14	1	2	2	1	1	[SW]_Well-graded_sand	211.96912 24	2 5	1 0	76.443656 31	Default	20. 314
14	2	4	2	3	1	[SW]_Well-graded_sand	218.03998 75	2 5	1 0	81.261703 96	Default	20. 314
14	3	6	2	5	1	[SW]_Well-graded_sand	213.59254 84	2 5	1 0	77.716551 2	Default	20. 314
14	4	8	2	7	1	[SW]_Well-graded_sand	205.65926 7	2 5	1 0	71.603431 61	Default	20. 314
14	5	1 0	2	9	1	[SW]_Well-graded_sand	202.25840 41	2 5	1 0	69.065179 55	Default	20. 314
14	6	1 2	2	11	1	[SW]_Well-graded_sand	197.77065 01	2 5	1 0	65.791023 81	Default	20. 314
14	7	1 4	2	13	1	[SW]_Well-graded_sand	194.12182 44	2 5	1 0	63.191881 1	Default	20. 314
14	8	1 6	2	15	1	[SW]_Well-graded_sand	191.05830 38	2 5	1 0	61.053130 4	Default	20. 314
14	9	1 8	2	17	1	[SW]_Well-graded_sand	188.42526 65	2 5	1 0	59.246535 37	Default	20. 314
14	1 0	2 0	2	19	1	[SW]_Well-graded_sand	186.12147 78	2 5	1 0	57.689767 65	Default	20. 314

**Table 0-9: Soil profiles 15 and 16.**

Profile #	L	D	T	Sa	S	So	V	N	L	D	Su	UW
15	1	2	2	1	1	[SW]_Well-graded_sand	218.19423 42	2 5	2 0	81.386184 8	Default	20. 314
15	2	4	2	3	1	[SW]_Well-graded_sand	224.03745 34	2 5	2 0	86.177413 51	Default	20. 314
15	3	6	2	5	1	[SW]_Well-graded_sand	219.75330 05	2 5	2 0	82.650146 23	Default	20. 314
15	4	8	2	7	1	[SW]_Well-graded_sand	212.16106 44	2 5	2 0	76.593564 68	Default	20. 314
15	5	1 0	2	9	1	[SW]_Well-graded_sand	208.92842 27	2 5	2 0	74.089904 57	Default	20. 314
15	6	1 2	2	11	1	[SW]_Well-graded_sand	204.68548 03	2 5	2 0	70.871604 04	Default	20. 314
15	7	1 4	2	13	1	[SW]_Well-graded_sand	201.25664 74	2 5	2 0	68.326903 18	Default	20. 314
15	8	1 6	2	15	1	[SW]_Well-graded_sand	198.39366 79	2 5	2 0	66.240450 95	Default	20. 314
15	9	1 8	2	17	1	[SW]_Well-graded_sand	195.94542 72	2 5	2 0	64.483830 22	Default	20. 314
15	1 0	2 0	2	19	1	[SW]_Well-graded_sand	193.81337 44	2 5	2 0	62.974747 16	Default	20. 314
Profile #	L	D	T	Sa	S	So	V	N	L	D	Su	UW
16	1	2	2	1	1	[SW]_Well-graded_sand	222.60593 27	2 5	3 0	84.989977 28	Default	20. 314
16	2	4	2	3	1	[SW]_Well-graded_sand	228.45647	2 5	3 0	89.898939 56	Default	20. 314
16	3	6	2	5	1	[SW]_Well-graded_sand	224.16601 82	2 5	3 0	86.284490 95	Default	20. 314
16	4	8	2	7	1	[SW]_Well-graded_sand	216.57585 29	2 5	3 0	80.085214 35	Default	20. 314
16	5	1 0	2	9	1	[SW]_Well-graded_sand	213.34988 52	2 5	3 0	77.525565 05	Default	20. 314
16	6	1 2	2	11	1	[SW]_Well-graded_sand	209.12163 33	2 5	3 0	74.238287 63	Default	20. 314
16	7	1 4	2	13	1	[SW]_Well-graded_sand	205.71005 62	2 5	3 0	71.641712 08	Default	20. 314
16	8	1 6	2	15	1	[SW]_Well-graded_sand	202.86551 22	2 5	3 0	69.514685 1	Default	20. 314
16	9	1 8	2	17	1	[SW]_Well-graded_sand	200.43616 8	2 5	3 0	67.725403 57	Default	20. 314
16	1 0	2 0	2	19	1	[SW]_Well-graded_sand	198.32307 87	2 5	3 0	66.189447 23	Default	20. 314

**Table 0-10: Soil profiles 17 and 18.**

Profile #	L	D	T	Sa	S	So	V	N	L	D	Su	UW
17	1	2	2	1	1	[SW]_Well-graded_sand	224.73443 61	2 5	4 0	86.758765 17	Default	20. 314
17	2	4	2	3	1	[SW]_Well-graded_sand	230.62744 08	2 5	4 0	91.758287 55	Default	20. 314
17	3	6	2	5	1	[SW]_Well-graded_sand	226.30573 25	2 5	4 0	88.077097 76	Default	20. 314
17	4	8	2	7	1	[SW]_Well-graded_sand	218.66187 42	2 5	4 0	81.764208 34	Default	20. 314
17	5	1 0	2	9	1	[SW]_Well-graded_sand	215.41378 57	2 5	4 0	79.158015 17	Default	20. 314
17	6	1 2	2	11	1	[SW]_Well-graded_sand	211.15725 46	2 5	4 0	75.811327 77	Default	20. 314
17	7	1 4	2	13	1	[SW]_Well-graded_sand	207.72350 75	2 5	4 0	73.168149 14	Default	20. 314
17	8	1 6	2	15	1	[SW]_Well-graded_sand	204.86096 13	2 5	4 0	71.003184 09	Default	20. 314
17	9	1 8	2	17	1	[SW]_Well-graded_sand	202.41661 73	2 5	4 0	69.182170 16	Default	20. 314
17	1 0	2 0	2	19	1	[SW]_Well-graded_sand	200.29078 05	2 5	4 0	67.619117 28	Default	20. 314
Profile #	L	D	T	Sa	S	So	V	N	L	D	Su	UW
18	1	2	2	1	1	[SW]_Well-graded_sand	224.73443 61	2 5	5 0	86.758765 17	Default	20. 314
18	2	4	2	3	1	[SW]_Well-graded_sand	230.62744 08	2 5	5 0	91.758287 55	Default	20. 314
18	3	6	2	5	1	[SW]_Well-graded_sand	226.30573 25	2 5	5 0	88.077097 76	Default	20. 314
18	4	8	2	7	1	[SW]_Well-graded_sand	218.66187 42	2 5	5 0	81.764208 34	Default	20. 314
18	5	1 0	2	9	1	[SW]_Well-graded_sand	215.41378 57	2 5	5 0	79.158015 17	Default	20. 314
18	6	1 2	2	11	1	[SW]_Well-graded_sand	211.15725 46	2 5	5 0	75.811327 77	Default	20. 314
18	7	1 4	2	13	1	[SW]_Well-graded_sand	207.72350 75	2 5	5 0	73.168149 14	Default	20. 314
18	8	1 6	2	15	1	[SW]_Well-graded_sand	204.86096 13	2 5	5 0	71.003184 09	Default	20. 314
18	9	1 8	2	17	1	[SW]_Well-graded_sand	202.41661 73	2 5	5 0	69.182170 16	Default	20. 314
18	1 0	2 0	2	19	1	[SW]_Well-graded_sand	200.29078 05	2 5	5 0	67.619117 28	Default	20. 314

**Table 0-11: Soil profiles 19 and 20.**

Profile #	L	D	T	Sa	S	So	V	N	L	D	Su	UW
19	1	2	2	1	1	[SW]_Well-graded_sand	226.65390 79	3 5	0	88.370668 21	Default	20. 314
19	2	4	2	3	1	[SW]_Well-graded_sand	233.30273 57	3 5	0	94.077760 39	Default	20. 314
19	3	6	2	5	1	[SW]_Well-graded_sand	228.43336 85	3 5	0	89.879264 12	Default	20. 314
19	4	8	2	7	1	[SW]_Well-graded_sand	219.72615 49	3 5	0	82.628049 13	Default	20. 314
19	5	1 0	2	9	1	[SW]_Well-graded_sand	215.98391 88	3 5	0	79.612191 52	Default	20. 314
19	6	1 2	2	11	1	[SW]_Well-graded_sand	211.03552 61	3 5	0	75.716762 33	Default	20. 314
19	7	1 4	2	13	1	[SW]_Well-graded_sand	207.00268 06	3 5	0	72.619686 27	Default	20. 314
19	8	1 6	2	15	1	[SW]_Well-graded_sand	203.60942 91	3 5	0	70.067624 15	Default	20. 314
19	9	1 8	2	17	1	[SW]_Well-graded_sand	200.68715 49	3 5	0	67.909100 2	Default	20. 314
19	10	2 0	2	19	1	[SW]_Well-graded_sand	198.12550 46	3 5	0	66.046803 88	Default	20. 314
Profile #	L	D	T	Sa	S	So	V	N	L	D	Su	UW
20	1	2	2	1	1	[SW]_Well-graded_sand	228.72568 55	3 5	1 0	90.128399 58	Default	20. 314
20	2	4	2	3	1	[SW]_Well-graded_sand	235.32106 9	3 5	1 0	95.848281 81	Default	20. 314
20	3	6	2	5	1	[SW]_Well-graded_sand	230.48978 66	3 5	1 0	91.639784 2	Default	20. 314
20	4	8	2	7	1	[SW]_Well-graded_sand	221.86588 52	3 5	1 0	84.379587 4	Default	20. 314
20	5	1 0	2	9	1	[SW]_Well-graded_sand	218.16630 41	3 5	1 0	81.363636 97	Default	20. 314
20	6	1 2	2	11	1	[SW]_Well-graded_sand	213.28155 82	3 5	1 0	77.471834 39	Default	20. 314
20	7	1 4	2	13	1	[SW]_Well-graded_sand	209.30734 28	3 5	1 0	74.381060 46	Default	20. 314
20	8	1 6	2	15	1	[SW]_Well-graded_sand	205.96862 47	3 5	1 0	71.836769 19	Default	20. 314
20	9	1 8	2	17	1	[SW]_Well-graded_sand	203.09746 59	3 5	1 0	69.686838 92	Default	20. 314
20	10	2 0	2	19	1	[SW]_Well-graded_sand	200.58402 73	3 5	1 0	67.833588 97	Default	20. 314

**Table 0-12: Soil profiles 21 and 22.**

Profile #	L	D	T	Sa	S	So	V	N	L	D	Su	UW
21	1	2	2	1	1	[SW]_Well-graded_sand	234.39986 45	3 5	2 0	95.037980 01	Default	20. 314
21	2	4	2	3	1	[SW]_Well-graded_sand	240.83724 14	3 5	2 0	100	Default	20. 314
21	3	6	2	5	1	[SW]_Well-graded_sand	236.11887 15	3 5	2 0	96.553029 34	Default	20. 314
21	4	8	2	7	1	[SW]_Well-graded_sand	227.73707 51	3 5	2 0	89.287322 43	Default	20. 314
21	5	1 0	2	9	1	[SW]_Well-graded_sand	224.15939 85	3 5	2 0	86.278975 88	Default	20. 314
21	6	1 2	2	11	1	[SW]_Well-graded_sand	219.45443 53	3 5	2 0	82.407039 13	Default	20. 314
21	7	1 4	2	13	1	[SW]_Well-graded_sand	215.64385 69	3 5	2 0	79.341124 98	Default	20. 314
21	8	1 6	2	15	1	[SW]_Well-graded_sand	212.45581 42	3 5	2 0	76.824074 45	Default	20. 314
21	9	1 8	2	17	1	[SW]_Well-graded_sand	209.72465 16	3 5	2 0	74.702424 59	Default	20. 314
21	1 0	2 0	2	19	1	[SW]_Well-graded_sand	207.34222 67	3 5	2 0	72.877763 6	Default	20. 314
Profile #	L	D	T	Sa	S	So	V	N	L	D	Su	UW
22	1	2	2	1	1	[SW]_Well-graded_sand	238.85286 8	3 5	3 0	98.989219 23	Default	20. 314
22	2	4	2	3	1	[SW]_Well-graded_sand	245.32275 76	3 5	3 0	100	Default	20. 314
22	3	6	2	5	1	[SW]_Well-graded_sand	240.57977 77	3 5	3 0	100	Default	20. 314
22	4	8	2	7	1	[SW]_Well-graded_sand	232.16536 46	3 5	3 0	93.087856 2	Default	20. 314
22	5	1 0	2	9	1	[SW]_Well-graded_sand	228.57866 6	3 5	3 0	90.003051 73	Default	20. 314
22	6	1 2	2	11	1	[SW]_Well-graded_sand	223.86690 31	3 5	3 0	86.035478 04	Default	20. 314
22	7	1 4	2	13	1	[SW]_Well-graded_sand	220.05545 27	3 5	3 0	82.896318 77	Default	20. 314
22	8	1 6	2	15	1	[SW]_Well-graded_sand	216.87017 65	3 5	3 0	80.320973 69	Default	20. 314
22	9	1 8	2	17	1	[SW]_Well-graded_sand	214.14412 25	3 5	3 0	78.151603 93	Default	20. 314
22	1 0	2 0	2	19	1	[SW]_Well-graded_sand	211.76836 18	3 5	3 0	76.287029 61	Default	20. 314

**Table 0-13: Soil profiles 23 and 24.**

Profile #	L	D	T	Sa	S	So	V	N	L	D	Su	UW
23	1	2	2	1	1	[SW]_Well-graded_sand	241.10185 96	3 5	4 0	100	Default	20.3 14
23	2	4	2	3	1	[SW]_Well-graded_sand	247.62169 35	3 5	4 0	100	Default	20.3 14
23	3	6	2	5	1	[SW]_Well-graded_sand	242.84200 51	3 5	4 0	100	Default	20.3 14
23	4	8	2	7	1	[SW]_Well-graded_sand	234.36382 1	3 5	4 0	95.006351 04	Default	20.3 14
23	5	1 0	2	9	1	[SW]_Well-graded_sand	230.75053 57	3 5	4 0	91.864327 02	Default	20.3 14
23	6	1 2	2	11	1	[SW]_Well-graded_sand	226.00446 13	3 5	4 0	87.823499 43	Default	20.3 14
23	7	1 4	2	13	1	[SW]_Well-graded_sand	222.16581 74	3 5	4 0	84.626685 71	Default	20.3 14
23	8	1 6	2	15	1	[SW]_Well-graded_sand	218.95823 8	3 5	4 0	82.004266 22	Default	20.3 14
23	9	1 8	2	17	1	[SW]_Well-graded_sand	216.21342 72	3 5	4 0	79.795415 92	Default	20.3 14
23	1 0	2 0	2	19	1	[SW]_Well-graded_sand	213.82158 61	3 5	4 0	77.897045 5	Default	20.3 14
Profile #	L	D	T	Sa	S	So	V	N	L	D	Su	UW
24	1	2	2	1	1	[SW]_Well-graded_sand	241.10185 96	3 5	5 0	100	Default	20.3 14
24	2	4	2	3	1	[SW]_Well-graded_sand	247.62169 35	3 5	5 0	100	Default	20.3 14
24	3	6	2	5	1	[SW]_Well-graded_sand	242.84200 51	3 5	5 0	100	Default	20.3 14
24	4	8	2	7	1	[SW]_Well-graded_sand	234.36382 1	3 5	5 0	95.006351 04	Default	20.3 14
24	5	1 0	2	9	1	[SW]_Well-graded_sand	230.75053 57	3 5	5 0	91.864327 02	Default	20.3 14
24	6	1 2	2	11	1	[SW]_Well-graded_sand	226.00446 13	3 5	5 0	87.823499 43	Default	20.3 14
24	7	1 4	2	13	1	[SW]_Well-graded_sand	222.16581 74	3 5	5 0	84.626685 71	Default	20.3 14
24	8	1 6	2	15	1	[SW]_Well-graded_sand	218.95823 8	3 5	5 0	82.004266 22	Default	20.3 14
24	9	1 8	2	17	1	[SW]_Well-graded_sand	216.21342 72	3 5	5 0	79.795415 92	Default	20.3 14
24	1 0	2 0	2	19	1	[SW]_Well-graded_sand	213.82158 61	3 5	5 0	77.897045 5	Default	20.3 14

**Table 0-14: Soil profiles 25 and 26.**

Profile #	L	D	T	Sa	S	So	V	N	L	D	Su	UW
25	1	2	2	1	1	[SW]_Well-graded_sand	122.22192 15	5	0	33.400973 04	Default	20. 314
25	2	4	2	3	1	[SW]_Well-graded_sand	126.08926 16	5	0	35.558051 13	Default	20. 314
25	3	6	2	5	1	[SW]_Well-graded_sand	123.25589 28	5	0	33.971168 7	Default	20. 314
25	4	8	2	7	1	[SW]_Well-graded_sand	118.20420 68	5	0	31.230467 05	Default	20. 314
25	5	1 0	2	9	1	[SW]_Well-graded_sand	116.03921 9	5	0	30.090580 01	Default	20. 314
25	6	1 2	2	11	1	[SW]_Well-graded_sand	113.18242 57	5	0	28.618246 17	Default	20. 314
25	7	1 4	2	13	1	[SW]_Well-graded_sand	110.85944 32	5	0	27.447661 45	Default	20. 314
25	8	1 6	2	15	1	[SW]_Well-graded_sand	108.90867 55	5	0	26.483072 64	Default	20. 314
25	9	1 8	2	17	1	[SW]_Well-graded_sand	107.23154 8	5	0	25.667227 27	Default	20. 314
25	1 0	2 0	2	19	1	[SW]_Well-graded_sand	105.76364 17	5	0	24.963345 42	Default	20. 314
Profile #	L	D	T	Sa	S	So	V	N	L	D	Su	UW
26	1	2	2	1	1	[SW]_Well-graded_sand	166.96294 36	5	0	33.400973 04	Default	20. 314
26	2	4	2	3	1	[SW]_Well-graded_sand	171.57875 92	5	0	35.558051 13	Default	20. 314
26	3	6	2	5	1	[SW]_Well-graded_sand	168.19936 36	5	0	33.971168 7	Default	20. 314
26	4	8	2	7	1	[SW]_Well-graded_sand	162.14162 56	5	0	31.230467 05	Default	20. 314
26	5	1 0	2	9	1	[SW]_Well-graded_sand	159.53194 15	5	0	30.090580 01	Default	20. 314
26	6	1 2	2	11	1	[SW]_Well-graded_sand	156.07514 29	5	0	28.618246 17	Default	20. 314
26	7	1 4	2	13	1	[SW]_Well-graded_sand	153.25266 86	5	0	27.447661 45	Default	20. 314
26	8	1 6	2	15	1	[SW]_Well-graded_sand	150.87402 95	5	0	26.483072 64	Default	20. 314
26	9	1 8	2	17	1	[SW]_Well-graded_sand	148.82266 42	5	0	25.667227 27	Default	20. 314
26	1 0	2 0	2	19	1	[SW]_Well-graded_sand	147.02219 32	5	0	24.963345 42	Default	20. 314



**Table 0-15: Soil profiles 27 and 28.**

Profile #	L	D	T	Sa	S	So	V	N	L	D	Su	UW
27	1	2	2	1	1	[SW]_Well-graded_sand	144.59243 25	5	0	33.400973 04	Default	20. 314
27	2	4	2	3	1	[SW]_Well-graded_sand	148.83401 04	5	0	35.558051 13	Default	20. 314
27	3	6	2	5	1	[SW]_Well-graded_sand	145.72762 82	5	0	33.971168 7	Default	20. 314
27	4	8	2	7	1	[SW]_Well-graded_sand	140.17291 62	5	0	31.230467 05	Default	20. 314
27	5	1 0	2	9	1	[SW]_Well-graded_sand	137.78558 02	5	0	30.090580 01	Default	20. 314
27	6	1 2	2	11	1	[SW]_Well-graded_sand	134.62878 43	5	0	28.618246 17	Default	20. 314
27	7	1 4	2	13	1	[SW]_Well-graded_sand	132.05605 59	5	0	27.447661 45	Default	20. 314
27	8	1 6	2	15	1	[SW]_Well-graded_sand	129.89135 25	5	0	26.483072 64	Default	20. 314
27	9	1 8	2	17	1	[SW]_Well-graded_sand	128.02710 61	5	0	25.667227 27	Default	20. 314
27	1 0	2 0	2	19	1	[SW]_Well-graded_sand	126.39291 74	5	0	24.963345 42	Default	20. 314
Profile #	L	D	T	Sa	S	So	V	N	L	D	Su	UW
28	1	2	2	1	1	[SW]_Well-graded_sand	145.25762 4	1 0	0	47.236109 07	Default	20. 314
28	2	4	2	3	1	[SW]_Well-graded_sand	149.86150 63	1 0	0	50.286678 16	Default	20. 314
28	3	6	2	5	1	[SW]_Well-graded_sand	146.48871 99	1 0	0	48.042487 5	Default	20. 314
28	4	8	2	7	1	[SW]_Well-graded_sand	140.47246 82	1 0	0	44.166550 06	Default	20. 314
28	5	1 0	2	9	1	[SW]_Well-graded_sand	137.89292 39	1 0	0	42.554506 35	Default	20. 314
28	6	1 2	2	11	1	[SW]_Well-graded_sand	134.48795 88	1 0	0	40.472311 87	Default	20. 314
28	7	1 4	2	13	1	[SW]_Well-graded_sand	131.71822 66	1 0	0	38.816855 08	Default	20. 314
28	8	1 6	2	15	1	[SW]_Well-graded_sand	129.39156 22	1 0	0	37.452720 49	Default	20. 314
28	9	1 8	2	17	1	[SW]_Well-graded_sand	127.39071 17	1 0	0	36.298940 92	Default	20. 314
28	1 0	2 0	2	19	1	[SW]_Well-graded_sand	125.63903 15	1 0	0	35.303501 66	Default	20. 314

**Table 0-16: Soil profiles 29 and 30.**

Profile #	L	D	T	Sa	S	So	V	N	L	D	Su	UW
29	1	2	2	1	1	[SW]_Well-graded_sand	194.14366 61	1 0	0	47.236109 07	Default	20.3 14
29	2	4	2	3	1	[SW]_Well-graded_sand	199.49602 4	1 0	0	50.286678 16	Default	20.3 14
29	3	6	2	5	1	[SW]_Well-graded_sand	195.57721 09	1 0	0	48.042487 5	Default	20.3 14
29	4	8	2	7	1	[SW]_Well-graded_sand	188.55490 72	1 0	0	44.166550 06	Default	20.3 14
29	5	1 0	2	9	1	[SW]_Well-graded_sand	185.53066 66	1 0	0	42.554506 35	Default	20.3 14
29	6	1 2	2	11	1	[SW]_Well-graded_sand	181.52569 61	1 0	0	40.472311 87	Default	20.3 14
29	7	1 4	2	13	1	[SW]_Well-graded_sand	178.25647 23	1 0	0	38.816855 08	Default	20.3 14
29	8	1 6	2	15	1	[SW]_Well-graded_sand	175.50193 63	1 0	0	37.452720 49	Default	20.3 14
29	9	1 8	2	17	1	[SW]_Well-graded_sand	173.12684 8	1 0	0	36.298940 92	Default	20.3 14
29	1 0	2 0	2	19	1	[SW]_Well-graded_sand	171.04260 31	1 0	0	35.303501 66	Default	20.3 14
Profile #	L	D	T	Sa	S	So	V	N	L	D	Su	UW
30	1	2	2	1	1	[SW]_Well-graded_sand	169.70064 51	1 0	0	47.236109 07	Default	20.3 14
30	2	4	2	3	1	[SW]_Well-graded_sand	174.67876 51	1 0	0	50.286678 16	Default	20.3 14
30	3	6	2	5	1	[SW]_Well-graded_sand	171.03296 54	1 0	0	48.042487 5	Default	20.3 14
30	4	8	2	7	1	[SW]_Well-graded_sand	164.51368 77	1 0	0	44.166550 06	Default	20.3 14
30	5	1 0	2	9	1	[SW]_Well-graded_sand	161.71179 53	1 0	0	42.554506 35	Default	20.3 14
30	6	1 2	2	11	1	[SW]_Well-graded_sand	158.00682 75	1 0	0	40.472311 87	Default	20.3 14
30	7	1 4	2	13	1	[SW]_Well-graded_sand	154.98734 94	1 0	0	38.816855 08	Default	20.3 14
30	8	1 6	2	15	1	[SW]_Well-graded_sand	152.44674 92	1 0	0	37.452720 49	Default	20.3 14
30	9	1 8	2	17	1	[SW]_Well-graded_sand	150.25877 99	1 0	0	36.298940 92	Default	20.3 14
30	1 0	2 0	2	19	1	[SW]_Well-graded_sand	148.34081 73	1 0	0	35.303501 66	Default	20.3 14

**Table 0-17: Soil profiles 31 and 32.**

Profile #	L	D	T	Sa	S	So	V	N	L	D	Su	UW
31	1	2	2	1	1	[SW]_Well-graded_sand	172.65332 18	2 0	0	66.801946 08	Default	20. 314
31	2	4	2	3	1	[SW]_Well-graded_sand	178.12164 55	2 0	0	71.116102 26	Default	20. 314
31	3	6	2	5	1	[SW]_Well-graded_sand	174.11577 27	2 0	0	67.942337 4	Default	20. 314
31	4	8	2	7	1	[SW]_Well-graded_sand	166.96746 03	2 0	0	62.460934 09	Default	20. 314
31	5	1 0	2	9	1	[SW]_Well-graded_sand	163.90137 25	2 0	0	60.181160 02	Default	20. 314
31	6	1 2	2	11	1	[SW]_Well-graded_sand	159.85304 65	2 0	0	57.236492 35	Default	20. 314
31	7	1 4	2	13	1	[SW]_Well-graded_sand	156.55898 75	2 0	0	54.895322 91	Default	20. 314
31	8	1 6	2	15	1	[SW]_Well-graded_sand	153.79115 24	2 0	0	52.966145 27	Default	20. 314
31	9	1 8	2	17	1	[SW]_Well-graded_sand	151.41036 5	2 0	0	51.334454 54	Default	20. 314
31	1 0	2 0	2	19	1	[SW]_Well-graded_sand	149.32563 41	2 0	0	49.926690 85	Default	20. 314
Profile #	L	D	T	Sa	S	So	V	N	L	D	Su	UW
32	1	2	2	1	1	[SW]_Well-graded_sand	225.68438 41	2 0	0	66.801946 08	Default	20. 314
32	2	4	2	3	1	[SW]_Well-graded_sand	231.90118 35	2 0	0	71.116102 26	Default	20. 314
32	3	6	2	5	1	[SW]_Well-graded_sand	227.34928 38	2 0	0	67.942337 4	Default	20. 314
32	4	8	2	7	1	[SW]_Well-graded_sand	219.19491 94	2 0	0	62.460934 09	Default	20. 314
32	5	1 0	2	9	1	[SW]_Well-graded_sand	215.68413 53	2 0	0	60.181160 02	Default	20. 314
32	6	1 2	2	11	1	[SW]_Well-graded_sand	211.03580 39	2 0	0	57.236492 35	Default	20. 314
32	7	1 4	2	13	1	[SW]_Well-graded_sand	207.24225 32	2 0	0	54.895322 91	Default	20. 314
32	8	1 6	2	15	1	[SW]_Well-graded_sand	204.04654 66	2 0	0	52.966145 27	Default	20. 314
32	9	1 8	2	17	1	[SW]_Well-graded_sand	201.29152 15	2 0	0	51.334454 54	Default	20. 314
32	1 0	2 0	2	19	1	[SW]_Well-graded_sand	198.87422 59	2 0	0	49.926690 85	Default	20. 314

**Table 0-18: Soil profiles 33 and 34.**

Profile #	L	D	T	Sa	S	So	V	N	L	D	Su	UW
33	1	2	2	1	1	[SW]_Well-graded_sand	199.16885 29	2 0	0	66.801946 08	Default	20.3 14
33	2	4	2	3	1	[SW]_Well-graded_sand	205.01141 45	2 0	0	71.116102 26	Default	20.3 14
33	3	6	2	5	1	[SW]_Well-graded_sand	200.73252 83	2 0	0	67.942337 4	Default	20.3 14
33	4	8	2	7	1	[SW]_Well-graded_sand	193.08118 99	2 0	0	62.460934 09	Default	20.3 14
33	5	1 0	2	9	1	[SW]_Well-graded_sand	189.79275 39	2 0	0	60.181160 02	Default	20.3 14
33	6	1 2	2	11	1	[SW]_Well-graded_sand	185.44442 52	2 0	0	57.236492 35	Default	20.3 14
33	7	1 4	2	13	1	[SW]_Well-graded_sand	181.90062 03	2 0	0	54.895322 91	Default	20.3 14
33	8	1 6	2	15	1	[SW]_Well-graded_sand	178.91884 95	2 0	0	52.966145 27	Default	20.3 14
33	9	1 8	2	17	1	[SW]_Well-graded_sand	176.35094 32	2 0	0	51.334454 54	Default	20.3 14
33	1 0	2 0	2	19	1	[SW]_Well-graded_sand	174.09993	2 0	0	49.926690 85	Default	20.3 14
Profile #	L	D	T	Sa	S	So	V	N	L	D	Su	UW
34	1	2	2	1	1	[SW]_Well-graded_sand	190.99716 73	3 0	0	81.815340 86	Default	20.3 14
34	2	4	2	3	1	[SW]_Well-graded_sand	197.03916 63	3 0	0	87.099081 51	Default	20.3 14
34	3	6	2	5	1	[SW]_Well-graded_sand	192.61315 4	3 0	0	83.212029 28	Default	20.3 14
34	4	8	2	7	1	[SW]_Well-graded_sand	184.71356 45	3 0	0	76.498708 69	Default	20.3 14
34	5	1 0	2	9	1	[SW]_Well-graded_sand	181.32458 85	3 0	0	73.706567 09	Default	20.3 14
34	6	1 2	2	11	1	[SW]_Well-graded_sand	176.84930 45	3 0	0	70.100100 46	Default	20.3 14
34	7	1 4	2	13	1	[SW]_Well-graded_sand	173.20728 29	3 0	0	67.232765 19	Default	20.3 14
34	8	1 6	2	15	1	[SW]_Well-graded_sand	170.14667 08	3 0	0	64.870014 78	Default	20.3 14
34	9	1 8	2	17	1	[SW]_Well-graded_sand	167.51374 34	3 0	0	62.871609 93	Default	20.3 14
34	1 0	2 0	2	19	1	[SW]_Well-graded_sand	165.20798 77	3 0	0	61.147458 56	Default	20.3 14

**Table 0-19: Soil profiles 35 and 36.**

Profile #	L	D	T	Sa	S	So	V	N	L	D	Su	UW
35	1	2	2	1	1	[SW]_Well-graded_sand	246.45291 1	3 0	0	81.815340 86	Default	20. 314
35	2	4	2	3	1	[SW]_Well-graded_sand	253.24338 55	3 0	0	87.099081 51	Default	20. 314
35	3	6	2	5	1	[SW]_Well-graded_sand	248.27134 64	3 0	0	83.212029 28	Default	20. 314
35	4	8	2	7	1	[SW]_Well-graded_sand	239.36570 49	3 0	0	76.498708 69	Default	20. 314
35	5	1 0	2	9	1	[SW]_Well-graded_sand	235.53203 27	3 0	0	73.706567 09	Default	20. 314
35	6	1 2	2	11	1	[SW]_Well-graded_sand	230.45674 33	3 0	0	70.100100 46	Default	20. 314
35	7	1 4	2	13	1	[SW]_Well-graded_sand	226.31523	3 0	0	67.232765 19	Default	20. 314
35	8	1 6	2	15	1	[SW]_Well-graded_sand	222.82674 64	3 0	0	64.870014 78	Default	20. 314
35	9	1 8	2	17	1	[SW]_Well-graded_sand	219.81958 11	3 0	0	62.871609 93	Default	20. 314
35	1 0	2 0	2	19	1	[SW]_Well-graded_sand	217.18126 08	3 0	0	61.147458 56	Default	20. 314
Profile #	L	D	T	Sa	S	So	V	N	L	D	Su	UW
36	1	2	2	1	1	[SW]_Well-graded_sand	218.72503 92	3 0	0	81.815340 86	Default	20. 314
36	2	4	2	3	1	[SW]_Well-graded_sand	225.14127 59	3 0	0	87.099081 51	Default	20. 314
36	3	6	2	5	1	[SW]_Well-graded_sand	220.44225 02	3 0	0	83.212029 28	Default	20. 314
36	4	8	2	7	1	[SW]_Well-graded_sand	212.03963 47	3 0	0	76.498708 69	Default	20. 314
36	5	1 0	2	9	1	[SW]_Well-graded_sand	208.42831 06	3 0	0	73.706567 09	Default	20. 314
36	6	1 2	2	11	1	[SW]_Well-graded_sand	203.65302 39	3 0	0	70.100100 46	Default	20. 314
36	7	1 4	2	13	1	[SW]_Well-graded_sand	199.76125 65	3 0	0	67.232765 19	Default	20. 314
36	8	1 6	2	15	1	[SW]_Well-graded_sand	196.48670 86	3 0	0	64.870014 78	Default	20. 314
36	9	1 8	2	17	1	[SW]_Well-graded_sand	193.66666 22	3 0	0	62.871609 93	Default	20. 314
36	1 0	2 0	2	19	1	[SW]_Well-graded_sand	191.19462 43	3 0	0	61.147458 56	Default	20. 314

## B.1 Analysis Details – Sample Output

This section contains sample output from a liquefaction initiation analysis using PB LiquefY.

Latitude	Longitude	DET_amax	DET_Mw	DET_FSliq_Cetin	DET_FSliq_landB	NCEER (FSliq)
45.983	-112.527	0.1002815 79	6.03	1.110144818	1.224971837	1.19117891
45.983	-112.527	0.1002815 79	6.03	1.237611851	1.340679041	1.313226397
45.983	-112.527	0.1002815 79	6.03	1.196511641	1.318790511	1.255907864
45.983	-112.527	0.1002815 79	6.03	1.147590632	1.244414023	1.151392445
45.983	-112.527	0.1002815 79	6.03	1.161211207	1.244367186	1.122243785
45.983	-112.527	0.1002815 79	6.03	1.176749035	1.249229812	1.067712737
45.983	-112.527	0.1002815 79	6.03	1.169989647	1.273935226	1.020428371
45.983	-112.527	0.1002815 79	6.03	1.140496183	1.312378652	0.996838982
45.983	-112.527	0.1002815 79	6.03	1.098056608	1.360289236	0.99126694
45.983	-112.527	0.1002815 79	6.03	1.051457985	1.41410345	1.001054797
45.983	-112.527	0.1384679 04	6.03	0.804265232	0.887152237	0.862678636
45.983	-112.527	0.1384679 04	6.03	0.897557342	0.970950003	0.95106818
45.983	-112.527	0.1384679 04	6.03	0.869255175	0.955097837	0.909556805
45.983	-112.527	0.1384679 04	6.03	0.835791814	0.901232706	0.833864381
45.983	-112.527	0.1384679 04	6.03	0.848219459	0.901198785	0.812754264
45.983	-112.527	0.1384679 04	6.03	0.86200255	0.904720409	0.773261649
45.983	-112.527	0.1384679 04	6.03	0.858925998	0.922612627	0.739017244
45.983	-112.527	0.1384679 04	6.03	0.838471637	0.950454224	0.721933277
45.983	-112.527	0.1384679 04	6.03	0.807945806	0.985152149	0.717897878
45.983	-112.527	0.1384679 04	6.03	0.774012264	1.024125617	0.724986465

DET_Nsite_ Cetin	DET_Nsite_I andB	DET_Nsite_N CEER	DET_Nreq_ Cetin	DET_Nreq_I andB	DET_Nreq_N CEER	DET_D_Nreq _Cetin
6.3	6.69375	6.69375	6.5	3.7	3.5	0.2
6.699	7.58625	7.58625	5.4	3.2	3.4	0
6.57137030 5	7.28191753 8	6.924242	5.7	3.2	3.2	0
5.80379856 3	6.03321620 1	5.852052	5.6	2.9	3	0
5.26152930 5	5.47157459 2	5.432658	4.9	2.3	2.8	0
4.81820061 5	4.83981467 3	4.914024	4.2	1.7	2.8	0
4.45809135	4.35592158 1	4.520245	3.9	0.9	2.9	0
4.16340755 5	3.97124161 8	4.208119	4	0.1	2.7	0
3.92072251 5	3.65683160 9	3.952839	4.3	0	2.5	0.379277
3.71723194 5	3.39425862 5	3.739012	4.7	0	2.1	0.982768
6.3	6.69375	6.69375	11	8.6	7.2	4.7
6.699	7.58625	7.58625	9.8	8.1	7	3.101
6.57137030 5	7.28191753 8	6.924242	10.2	8.1	6.8	3.62863
5.80379856 3	6.03321620 1	5.852052	9.9	7.7	6.6	4.096201
5.26152930 5	5.47157459 2	5.432658	9.2	7.1	6.4	3.938471
4.81820061 5	4.83981467 3	4.914024	8.5	6.4	6.4	3.681799
4.45809135	4.35592158 1	4.520245	8.2	5.6	6.4	3.741909
4.16340755 5	3.97124161 8	4.208119	8.2	4.8	6.3	4.036592
3.92072251 5	3.65683160 9	3.952839	8.5	3.9	6.1	4.579277
3.71723194 5	3.39425862 5	3.739012	8.9	3.1	5.7	5.182768

DET_D_Nreq_lan dB	DET_D_Nreq_NC EER	DET_ana_Type	DET_Return_P.	DET_Depth	DET_Layer_Num	DET_FC
0	0	Mean	475	1	1	0
0	0	Mean	475	3	2	0
0	0	Mean	475	5	3	0
0	0	Mean	475	7	4	0
0	0	Mean	475	9	5	0
0	0	Mean	475	11	6	0
0	0	Mean	475	13	7	0
0	0	Mean	475	15	8	0
0	0	Mean	475	17	9	0
0	0	Mean	475	19	10	0
1.90625	0.50625	Mean	1039	1	1	0
0.51375	0	Mean	1039	3	2	0
0.818082	0	Mean	1039	5	3	0
1.666784	0.747948	Mean	1039	7	4	0
1.628425	0.967342	Mean	1039	9	5	0
1.560185	1.485976	Mean	1039	11	6	0
1.244078	1.879755	Mean	1039	13	7	0
0.828758	2.091881	Mean	1039	15	8	0
0.243168	2.147161	Mean	1039	17	9	0
0	1.960988	Mean	1039	19	10	0



DET_Vs	DET_Pi	DET_LL	DET_Dr	DET_Wc	DET_Eff_Stress	DET_Tot_Stress
144.5924	0	0	33.40097	0	10.514	20.314
148.834	0	0	35.55805	0	31.542	60.942
145.7276	0	0	33.97117	0	52.57	101.57
140.1729	0	0	31.23047	0	73.598	142.198
137.7856	0	0	30.09058	0	94.626	182.826
134.6288	0	0	28.61825	0	115.654	223.454
132.0561	0	0	27.44766	0	136.682	264.082
129.8914	0	0	26.48307	0	157.71	304.71
128.0271	0	0	25.66723	0	178.738	345.338
126.3929	0	0	24.96335	0	199.766	385.966
144.5924	0	0	33.40097	0	10.514	20.314
148.834	0	0	35.55805	0	31.542	60.942
145.7276	0	0	33.97117	0	52.57	101.57
140.1729	0	0	31.23047	0	73.598	142.198
137.7856	0	0	30.09058	0	94.626	182.826
134.6288	0	0	28.61825	0	115.654	223.454
132.0561	0	0	27.44766	0	136.682	264.082
129.8914	0	0	26.48307	0	157.71	304.71
128.0271	0	0	25.66723	0	178.738	345.338
126.3929	0	0	24.96335	0	199.766	385.966

DET_rd_Cetin	DET_rd_landB	DET_rd_NCEER	DET_Uncorrected_N_Value
0.973227	0.994073	0.99235	5
0.898619	0.95988	0.97705	5
0.798222	0.919166	0.96175	5
0.688064	0.873784	0.94645	5
0.591247	0.82562	0.93115	5
0.521404	0.77646	0.8803	5
0.477875	0.727895	0.8269	5
0.453172	0.681263	0.7735	5
0.439892	0.637622	0.7201	5
0.432961	0.597755	0.6667	5
0.972897	0.994073	0.99235	5
0.897366	0.95988	0.97705	5
0.795729	0.919166	0.96175	5
0.684211	0.873784	0.94645	5
0.586197	0.82562	0.93115	5
0.515492	0.77646	0.8803	5
0.471425	0.727895	0.8269	5
0.446417	0.681263	0.7735	5
0.432973	0.637622	0.7201	5
0.425956	0.597755	0.6667	5

***Performance_Base d***	PB_am ax	PB_M w	PB_FSliq_Ce tin	PB_FSliq_lan dB	PB_FSliq_Jua ng	PB_Nsite_Ce tin
***	N/A	N/A	1.431	1.275	1.21	6.3
***	N/A	N/A	1.174	1.369	1.302	6.699
***	N/A	N/A	1.133	1.353	1.286	6.57137
***	N/A	N/A	1.127	1.28	1.215	5.803799
***	N/A	N/A	1.17	1.279	1.212	5.261529
***	N/A	N/A	1.208	1.282	1.215	4.818201
***	N/A	N/A	1.221	1.263	1.235	4.458091
***	N/A	N/A	1.208	1.231	1.231	4.163408
***	N/A	N/A	1.179	1.204	1.204	3.920723
***	N/A	N/A	1.144	1.183	1.183	3.717232
***	N/A	N/A	1.033	0.92	0.882	6.3
***	N/A	N/A	0.848	1.005	0.964	6.699
***	N/A	N/A	0.818	0.986	0.946	6.57137
***	N/A	N/A	0.815	0.928	0.889	5.803799
***	N/A	N/A	0.846	0.924	0.884	5.261529
***	N/A	N/A	0.875	0.924	0.881	4.818201
***	N/A	N/A	0.885	0.938	0.893	4.458091
***	N/A	N/A	0.876	0.962	0.914	4.163408
***	N/A	N/A	0.855	0.993	0.942	3.920723
***	N/A	N/A	0.829	1.029	0.975	3.717232

PB_Nsite_la ndB	PB_Nsite_Ju ang	PB_Nreq_C etin	PB_Nreq_la ndB	PB_Nreq_Ju ang	PB_D_Nreq_ Cetin	PB_D_Nreq_I andB
6.69375	6.69375	1.371	3.077	3.837	0	0
7.58625	7.58625	4.497	2.87	3.598	0	0
7.281918	7.281918	4.852	2.769	3.509	0	0
6.033216	6.033216	4.156	2.417	3.156	0	0
5.471575	5.471575	3.101	1.888	2.657	0	0
4.839815	4.839815	2.214	1.263	2.022	0	0
4.355922	4.355922	1.71	1	1.335	0	0
3.971242	3.971242	1.565	1	1	0	0
3.656832	3.656832	1.655	1	1	0	0
3.394259	3.394259	1.866	1	1	0	0
6.69375	6.69375	5.863	8.004	8.705	0	1.31625
7.58625	7.58625	8.974	7.519	8.172	2.281	0
7.281918	7.281918	9.344	7.513	8.175	2.77863	0.238082
6.033216	6.033216	8.636	7.19	7.874	2.836201	1.156784
5.471575	5.471575	7.573	6.686	7.392	2.318471	1.218425
4.839815	4.839815	6.671	6.031	6.765	1.861799	1.200185
4.355922	4.355922	6.152	5.325	6.046	1.701909	0.974078
3.971242	3.971242	5.992	4.559	5.305	1.836592	0.588758
3.656832	3.656832	6.086	3.769	4.537	2.169277	0.113168
3.394259	3.394259	6.314	2.981	3.769	2.602768	0

PB_D_Nreq_Juan g	PB_ana_Typ e	PB_Return_P .	PB_Dept h	PB_Layer_Nu m	PB_F C	PB_Vs
0	N/A	475	1	1	0	144.592432 5
0	N/A	475	3	2	0	148.834010 4
0	N/A	475	5	3	0	145.727628 2
0	N/A	475	7	4	0	140.172916 2
0	N/A	475	9	5	0	137.785580 2
0	N/A	475	11	6	0	134.628784 3
0	N/A	475	13	7	0	132.056055 9
0	N/A	475	15	8	0	129.891352 5
0	N/A	475	17	9	0	128.027106 1
0	N/A	475	19	10	0	126.392917 4
2.01625	N/A	1039	1	1	0	144.592432 5
0.59375	N/A	1039	3	2	0	148.834010 4
0.898082	N/A	1039	5	3	0	145.727628 2
1.846784	N/A	1039	7	4	0	140.172916 2
1.928425	N/A	1039	9	5	0	137.785580 2
1.930185	N/A	1039	11	6	0	134.628784 3
1.694078	N/A	1039	13	7	0	132.056055 9
1.338758	N/A	1039	15	8	0	129.891352 5
0.883168	N/A	1039	17	9	0	128.027106 1
0.375741	N/A	1039	19	10	0	126.392917 4

PB_P I	PB_L L	PB_Dr	PB_W c	PB_Eff_Stre ss	PB_Tot_Stre ss	PB_CSR %	PB_Uncorrected_N_Val ue
0	0	33.4009730 4	0	10.514	20.314	8.602	5
0	0	35.5580511 3	0	31.542	60.942	8.479	5
0	0	33.9711687	0	52.57	101.57	8.42	5
0	0	31.2304670 5	0	73.598	142.198	8.215	5
0	0	30.0905800 1	0	94.626	182.826	7.915	5
0	0	28.6182461 7	0	115.654	223.454	7.574	5
0	0	27.4476614 5	0	136.682	264.082	7.434	5
0	0	26.4830726 4	0	157.71	304.71	7.434	5
0	0	25.6672272 7	0	178.738	345.338	7.434	5
0	0	24.9633454 2	0	199.766	385.966	7.434	5
0	0	33.4009730 4	0	10.514	20.314	11.914	5
0	0	35.5580511 3	0	31.542	60.942	11.557	5
0	0	33.9711687	0	52.57	101.57	11.553	5
0	0	31.2304670 5	0	73.598	142.198	11.319	5
0	0	30.0905800 1	0	94.626	182.826	10.96	5
0	0	28.6182461 7	0	115.654	223.454	10.503	5
0	0	27.4476614 5	0	136.682	264.082	10.025	5
0	0	26.4830726 4	0	157.71	304.71	9.522	5
0	0	25.6672272 7	0	178.738	345.338	9.023	5
0	0	24.9633454 2	0	199.766	385.966	8.545	5

## **APPENDIX C**

PB LiquefY was developed for use by researchers and engineers in the evaluation of liquefaction initiation. As such PB LiquefY gives a wide range of tools to use when analyzing the input hazard curves. It allows the creation of hazard curves, magnitude hazard contribution charts, deaggregation charts for both the seismic and liquefaction hazards, and other charts and graphs for easy comparison of the different methods. These different tools and charts and their use are discussed in detail in this appendix.

### **C.1 PBliquefY – Overview**

PBliquefY is a computer program written to help the researcher and practicing engineer to use and develop performance-based analyses of liquefaction initiation. As such, it has been designed to be versatile and useful over a wide range of applications. This section will help the reader to more fully grasp the potential of PBliquefY, and allow a better understanding of how it performs, and some of the uses and limitations of the program.

The versatility of the program allows both simple and complex applications and analysis. In order to assist the user in the application of this program a number of tutorials have been provided to help understand both how to apply the program, as well as some of the limitations of the program. These tutorials are provided for example purposes only to assist in the implementation of the program.

### **C.1.1 Basic Analysis**

For most engineering applications the simplified method is used to determine if further analysis is warranted or to determine if ground improvement will be needed. As this program is based off of the simplified method the basic analysis tools available will often be adequate for most engineering purposes. More detailed analyses can, however, be conducted and details of some of the more sophisticated tools available will be shown later. To assist the first time user of this program in the basic analysis of liquefaction initiation, a tutorial is provided showing the use of the program for a basic analysis.

#### **C.1.1.1 Opening the Program**

When the program is first opened, several things may occur. If the program has never been opened before then the content of the program must be enabled using the EXCEL© security options. To do this click on the enable content button which should have shown up at the top of the EXCEL© screen. If the button does not show up, then the security options must be modified in the trust center. This is done in EXCEL© by going to options section under the files tab and selecting the trust center. You should enable EXCEL© to allow a warning to pop up when a macro attempts to run (this will allow the program to run after you confirm that you have started the macro). The user must also ensure that iterative calculation is turned on. To enable iterative calculations the user should select the file tab at the top of the screen and then select the EXCEL© options. In the options window click on the formula section and enable iterative calculations and set the maximum number of iterations to a value of 500, and the minimum difference between iterations to a value of 0.001. Alternatively the program can enable iterative calculations for the user if the user selects the yes option when the pop up box asks if the user wishes to enable iterative calculations.



Once the content of the program has been enabled, the program will run. The first page to appear will be the title page. From this page, most other pages within the program can be accessed. This can be done by using the program flow chart available on the bottom right of the screen (Figure 0-1).

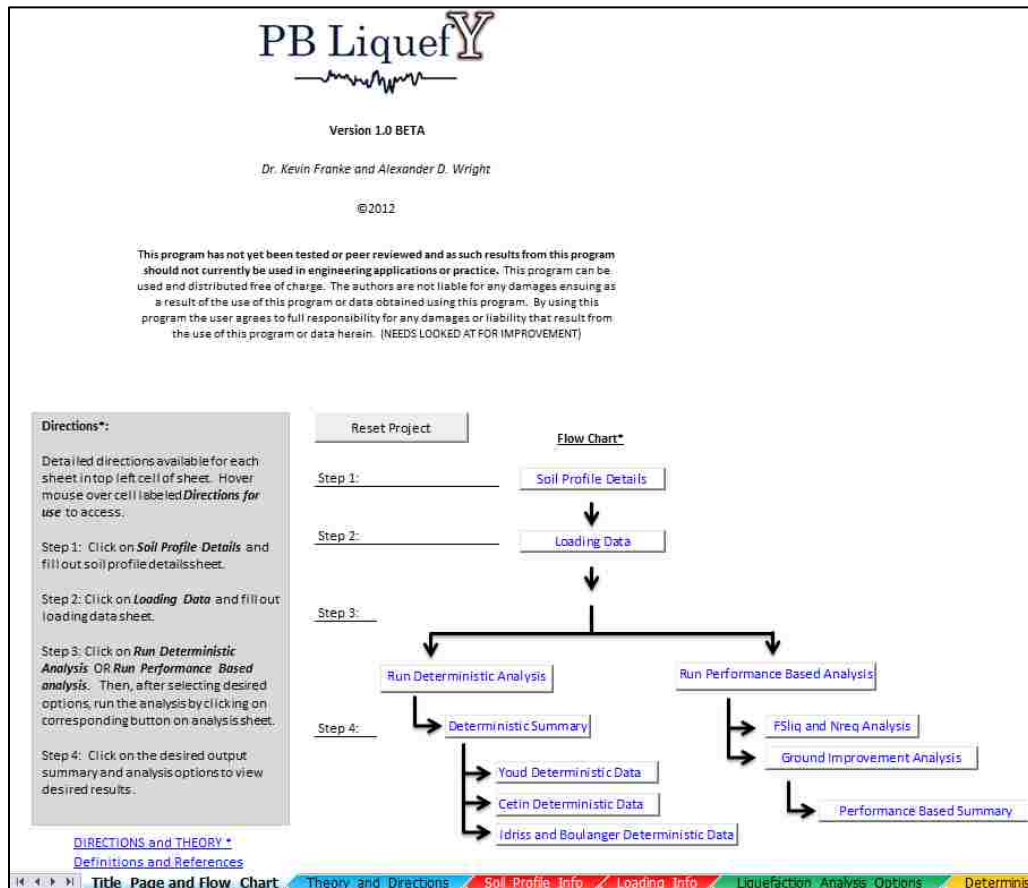


**Figure 0-1: Title page and flow chart.**

This program flow chart enables the user to access the pages within the program in the correct order so that all of the required information is entered prior to running the analysis. Data must be entered in the order shown on the flow chart for the program to run correctly.

The first step on this page is to click on RESET PROJECT (Step 0). This will clear any previous data entered and reset the program for a new project. On this page you will also see a definitions and references hyperlink that can be accessed for further sources of information about the program.

### C.1.1.2 Step 1: Soil Profile Details Page

Next we need to enter the site's soil profile details. Click on the SOIL PROFILE DETAILS hyperlink shown in blue next to step 1 in the flow chart. This will take you to the soil profile details page (Figure 0-2).

**Directions For Use**  
(RED VALUES ARE VALUES INPUT BY USER)

**Site Details (Optional)**

Date of Analysis	Month/Day/Year	Latitude	Longitude
Location	Address	-	-117.1564
Description	Site Description	Northing	Easting
Analysis Performed By	Name of Engineer	-	-
Analysis Checked By	Name of Engineer	on Date	Check Date
Site Details	Site Details/Boring ID		

**SPT Information**

Hammer Used: Safety Hammer (60%)

Efficiency of Hammer: 60%

Borehole Diameter: 115 [mm]

Rod Stickup Length: 1.5 [m]

Units: Metric

**Soil Profile Information**

Depth to Water Table: 2 [m]

# of Sub-layers in Profile: 12

Generate Sub Layers

**Applied Loads and Fills**

Applied Loading

- Apply Embankment Load
- Apply Uniform Load
- User Defined
- No Additional Load

Figure 0-2: Soil profile details page.

**Table 0-1: Site soil profile details for a single soil column.**

Sub Layer #	Bottom Depth [m]	Sample Depth [m]	Soil Type
1	1	0.5	[SP-SM] Poorly graded sand with silt
2	2	1.5	[SP-SM] Poorly graded sand with silt
3	4	3	[SW] Well-graded sand
4	8	5	[SW] Well-graded sand
5	9	8.5	msc. 1
6	12	11	[SW] Well-graded sand
7	17	15	msc. 1
8	19	18.5	[MH] Elastic Silt
9	20	19.5	[MH] Elastic Silt
10	21	20.5	[MH] Elastic Silt
11	22	21.5	[MH] Elastic Silt
12	23	22.25	[GC] Clayey gravel with sand

Sub Layer #	N	PI	LL	WC	FC	$\gamma$ [kN/m <sup>3</sup> ]
1	2	0	0	4	4	15
2	5	0	0	4	7	14
3	12	0	0	25	1	18
4	15	0	0	22	1	18
5	20	0	0	26	0	19
6	18	0	0	24	1	17
7	22	0	0	25	0	18
8	17	15	60	18	95	16
9	16	14	60	12	95	15
10	17	17	55	12	95	15
11	15	18	52	13	95	15
12	28	1	3	27	12	20

For a given site, after the on site investigation has been conducted, lets assume that the following criteria were found to exist (Table 0-1). These criteria are found based on the findings of the soil investigation using a standard penetration test (SPT) and laboratory test data. It should be noted that the more accurate the input data the more accurate the results of the program will be.

The soil profile page should now be up and available (Figure 0-2). Detailed instructions for this page can be found in the top left corner of the page under the *Directions for Use* heading (Shown in orange), and can be accessed by hovering over the cell. Input values on this page are shown in red. Black values should not be changed by the user.

Site details can be provided by the user at the top of the page, but are not required. The kind of SPT used and the efficiency of the hammer as well as the borehole size and rod stickup length should all be provided by the user. For this example lets specify a safety hammer which has a 60% efficiency. We will also use a borehole diameter of 115 mm and a rod stickup length of 1.5 meters. Under SPT information the user should also specify the type of units that will be used in entering the data. We will be using metric units, so make sure that the units box says 'Metric'. The upper portion of the page should now look like the upper portion of Figure 0-3.

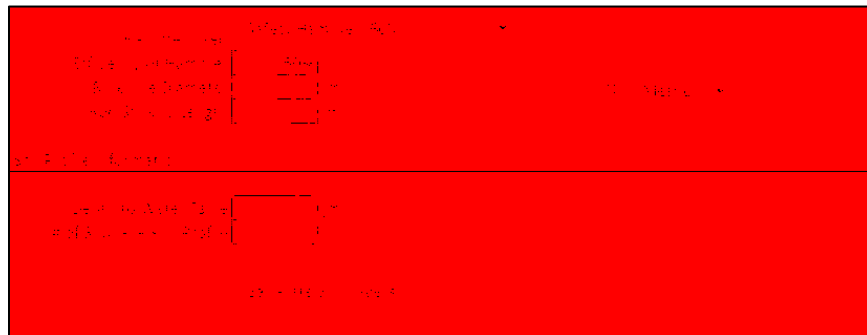


**Figure 0-3: Soil profile information entered on Soil Info Page.**

Next the user should specify the depth to the water table and the number of sub layers that will be used in the analysis. In our case we have 7 distinct soil layers, which have been sub divided into 12 sub layers. This is done to allow for a more detailed analysis and to account for multiple samples in the same layer. As a general rule of thumb sub layers should not be thicker than about 5 meters.

For Depth to Water Table enter a value of 2 meters into the box. For the # of Sub-layers in Profile enter a value of 12 corresponding to the 12 sub layers we will be using. Finally click on the GENERATE SUB LAYERS button. The program will now generate a table for data entry. Your program should now appear as it does in Figure 0-5.

In the next section titled “Applied loads and fills” you see options for applying loads and auto calculation options. We will not be applying a load in this tutorial, we will however be using the options for auto calculation. Ensure that both the  $V_S$  and  $D_R$  auto calculation are turned on by checking both of the auto calculation options (Figure 0-4). For this analysis the box titled Cd should read 60 and the shear wave velocity should be calculated using the mean value from the Andrus and Stokoe equation (see below).

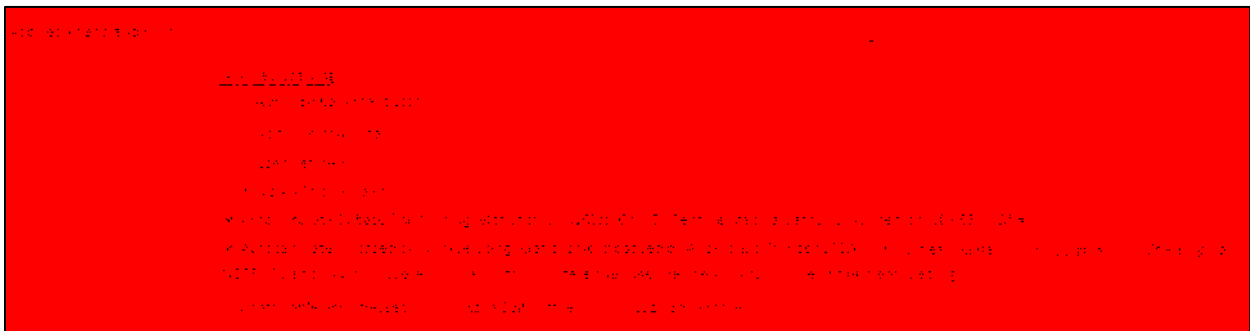


**Figure 0-4: Applied loading section.**

We are now ready to fill in the soil profile details for each of the sub layers in our analysis. There should be a blank table at the bottom of the screen. The user needs to enter values into the table corresponding to the soil profile. Enter data into the soil profile table such that it looks like Figure 0-5. The soil profile picture should automatically generate as the data is entered into the table. The black values in the table are entered by the program, and values for

shear wave velocity ( $V_s$ ) and relative density ( $D_R$ ) do not need entered as they will be auto calculated.

A final major set of assumptions made within this part of the program is the selection of susceptibility. The user can specify whether the layer is susceptible or not by selecting yes or no. However the default is to use the relationships associated with a given analysis type. For example if default is selected, the code will use the Bray and Sancio (2006) form of susceptibility analysis to determine which of the layers are susceptible. Layers above the water table are assumed to be not susceptible under any criteria, and layers that are sand specified as sand or of 'msc' soil type are considered susceptible always. The user is encouraged to select susceptibility by hand for any layers they feel will be incorrectly identified using the default setting. For this tutorial leave susceptibility as default.

Once all of the data that is known is entered push on the UPDATE TABLE AND STRESSES button to generate the shear wave velocity and relative density that we specified as being auto calculated. The user will also note that a set of values for the soil stresses now also shows up on the right hand side of the soil profile image (Figure 0-6). This page is now complete.

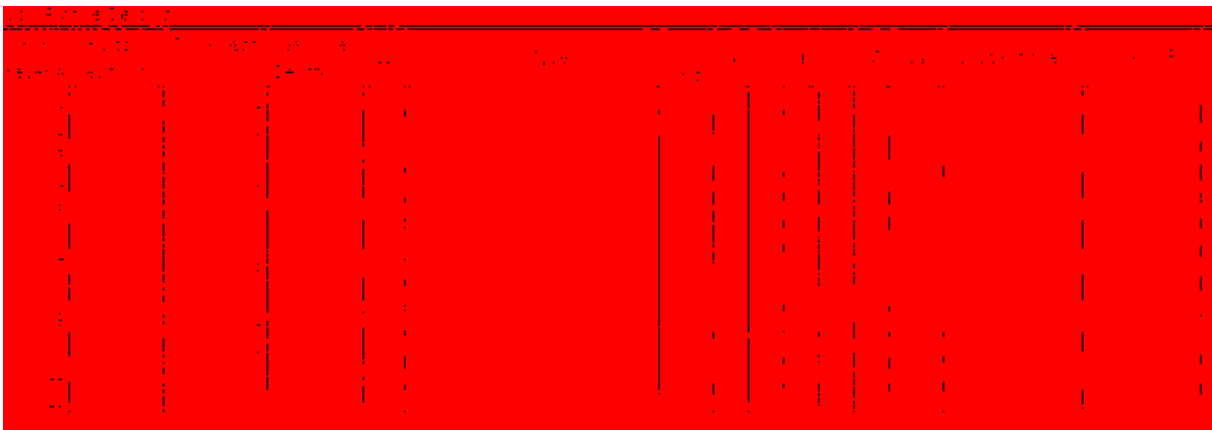


**Figure 0-5: Soil profile details table and figure.**

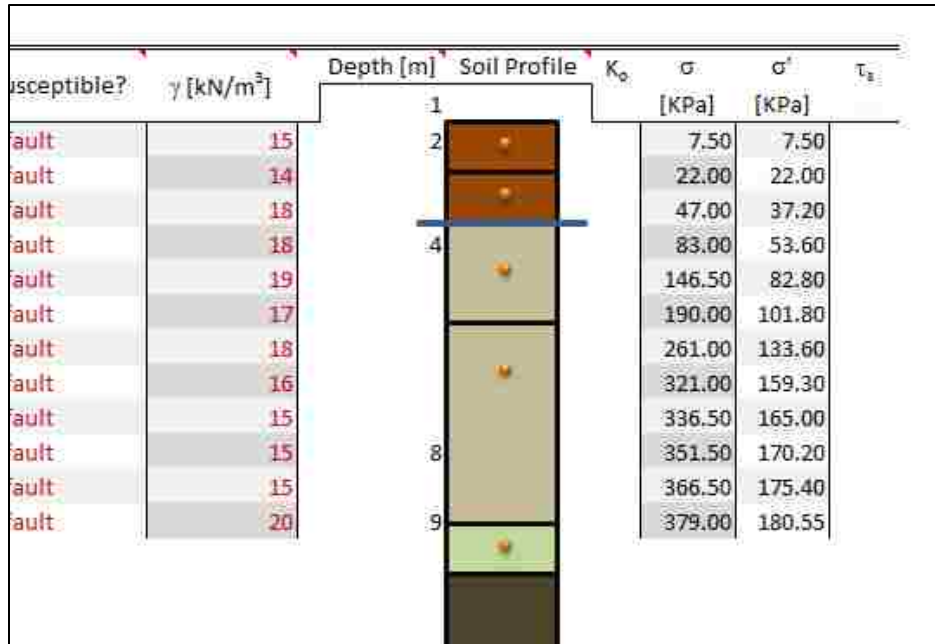


**Figure 0-6: Stresses calculated using PB Liquefy.**

In review, on this page the following steps were performed:

- 1) Fill in information for the type of SPT used (SPT information section).
- 2) Fill in information about the ground water table and number of sub layers (Soil Profile Information).
- 3) Fill in information for the soil profile, with data filled out for each of the soil sub layers (Soil Profile Details).
- 4) Review information to ensure program calculated values correctly and information entered correctly. The program will attempt to catch any major errors made by the user and prompt the user to correct these values.

Once all of these steps are completed return to the flow chart by clicking on the RETURN TO FLOW CHART hyperlink at the top of the page (shown in blue).

### **C.1.1.3 Step 2: Loading Data Input Page**

The user now needs to enter values for the loading data. This can be done on the loading data page. To get to the loading data page click on the **LOADING DATA** hyperlink button in the flow chart under step 2. The page should be blank and should look like Figure 0-7. The user will notice several sections on this page, the soil amplification factor section, the deaggregation data section, and the graph section which will appear below the **GENERAE PLOTS AND DATA** button after data is entered. As on every page, detailed directions are available in the top left hand corner in the orange box labeled *Directions for Use*.

The first step on this page is to enter the soil amplification factor. For this tutorial we will use the default amplification factor. To do this click on the drop box next to ‘Type:’ in the amplification factor section and select “Use Default - Stewart et al (2003) Quaternary values”. This will automatically enter values corresponding to a quaternary age alluvium.



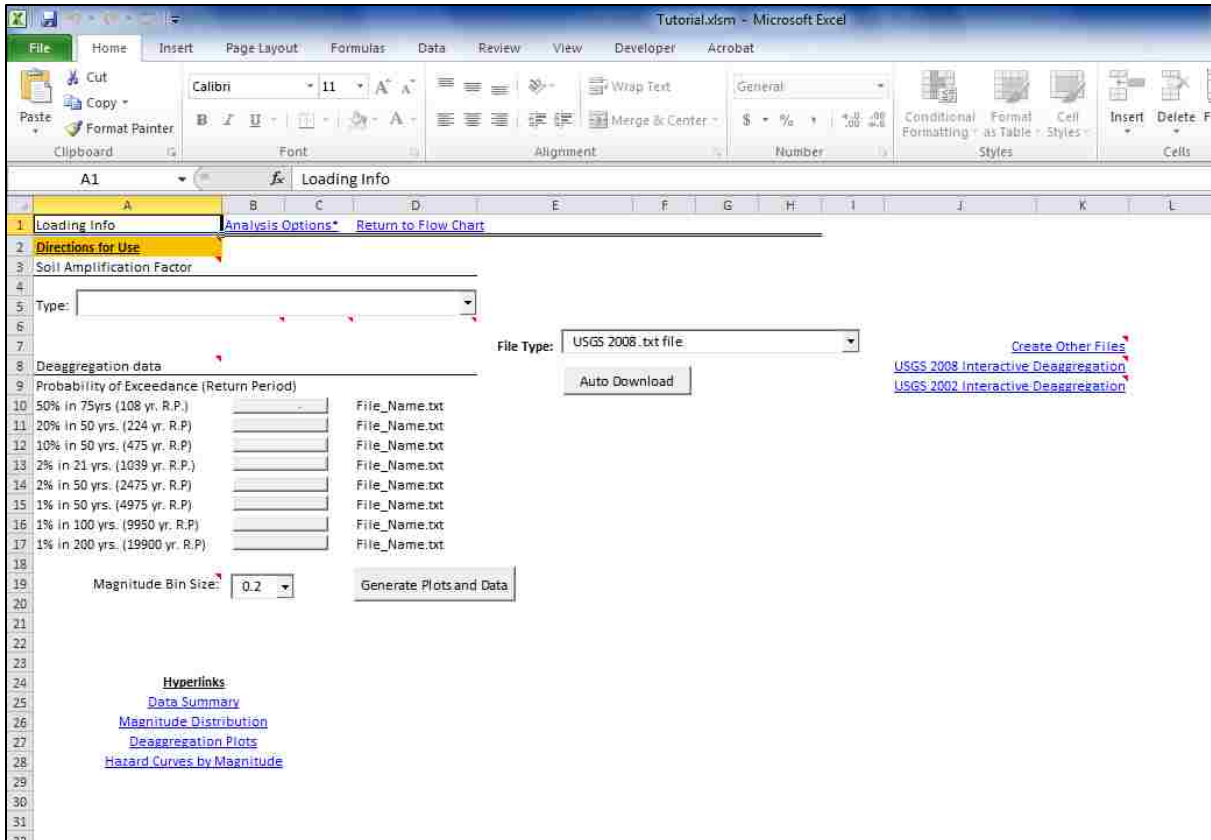


**Figure 0-7: Loading data page.**

Next we need to download seismic hazard data for our site. This can be done with the auto download button or manually. We will outline the manual download procedure. We are going to use the USGS 2008 deaggregations which can be generated using the USGS website. First ensure that the drop box next to ‘File Type:’ in the deaggregation data section is set to “USGS 2008 .txt file”. This tells the program what file type we are using. Click on the USGS 2008 interactive deaggregation hyperlink which will take us to the USGS website. The site may take a few seconds to open. When it opens it should look like Figure 0-8.

We will be creating data for our fictional site. We will assume our site is in Salt Lake City, Utah. In order to create files we need to input some information on the website. First lets

input a value for the location. For location the user can specify an area code, a city name, or a latitude and longitude. We will enter a city name. Type into the address box “Salt Lake City, Utah”. Then under Exceedance options change the values so they say 50% in 75 years, which corresponds to the 108 yr return period. Push the compute button located at the bottom of the screen. It will generate a file. Click on the txt link which will appear just above the compute button. A new page will appear with a text file containing the values we need.



**Figure 0-8: USGS interactive deaggregations website.**

The new text file will need to be copied into notepad for use in the program. Open notepad on the computer by typing notepad into the search bar under the windows menu. Then copy in the text as shown in Figure 0-9.

Save the file as something you will remember and repeat the steps for each of the eight exceedance values specified in the program (Table 0-2). You are now ready to upload the files.

To upload the files click on the button to the right of the corresponding probability of exceedance. For example the first grey button under the deaggregation section is for the file generated using an exceedance of 50% in 75 years. Click on this button and a menu will pop up. Select your file and push the open command (Figure 0-10).

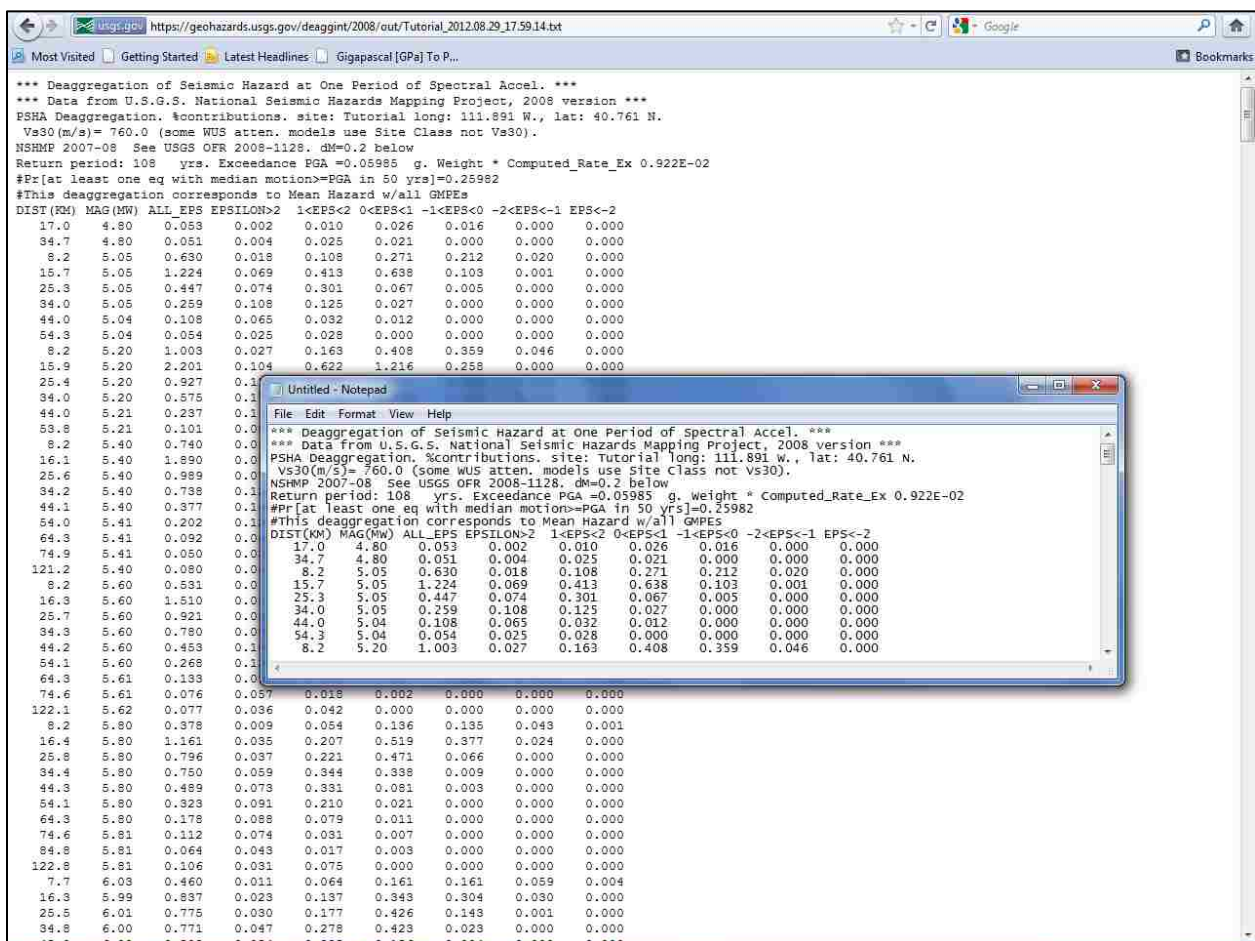
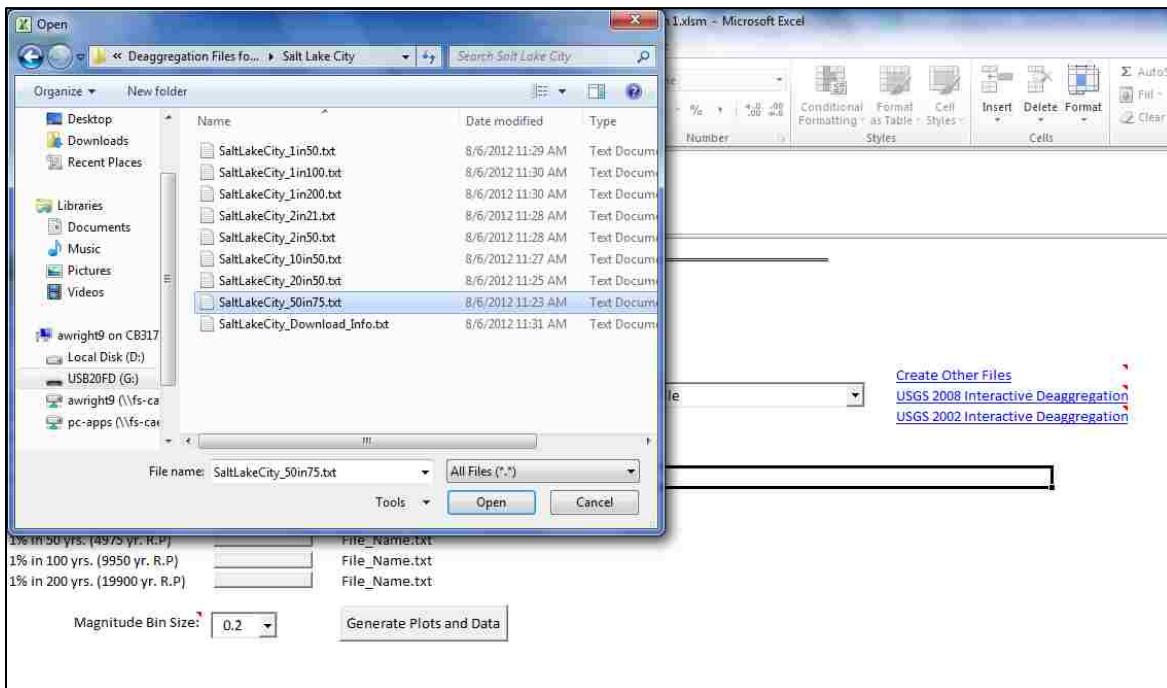


Figure 0-9: Deaggregation produced using the USGS 2008 interactive deaggregation website.

**Table 0-2: Probability of exceedance for 8 deaggregation files to be uploaded.**

50% in 75yrs (108 yr. R.P.)
20% in 50 yrs. (224 yr. R.P)
10% in 50 yrs. (475 yr. R.P)
2% in 21 yrs. (1039 yr. R.P.)
2% in 50 yrs. (2475 yr. R.P)
1% in 50 yrs. (4975 yr. R.P)
1% in 100 yrs. (9950 yr. R.P)
1% in 200 yrs. (19900 yr. R.P)

If the file uploads correctly you will see a file extension. The first file you open will be at a new location for this run, and the program will ask you if it is ok that the file does not match a previously uploaded location. Select yes. If after this you see a warning about location then one of your files has been made using a different location and you will need to inspect the files. Upload all 8 files for the eight corresponding return periods.



**Figure 0-10: Uploading file for 50% in 75 years.**

The user can now select the magnitude bin size. We will be using a magnitude bin size of 0.5, as this will allow the analysis to run more quickly and will be adequate for this analysis. Click on the drop box next to ‘Magnitude Bin Size:’ and select 0.5 (located to the left of the GENERATE PLOTS AND DATA button). Next, click on the GENERATE PLOTS AND DATA button. This will generate magnitude bin size plots, hazard curves, and deaggregations corresponding to the data you uploaded. The screen should now look like Figure 0-11. To access the other graphs generated you can either scroll down the page or click on the hyperlink available next to the hazard curve graph. It is recommended that you always view the graphs to ensure the accuracy of the data. For example, one of the files uploaded may have been from the wrong location. This can result in data that is inconsistent with the desired site location.

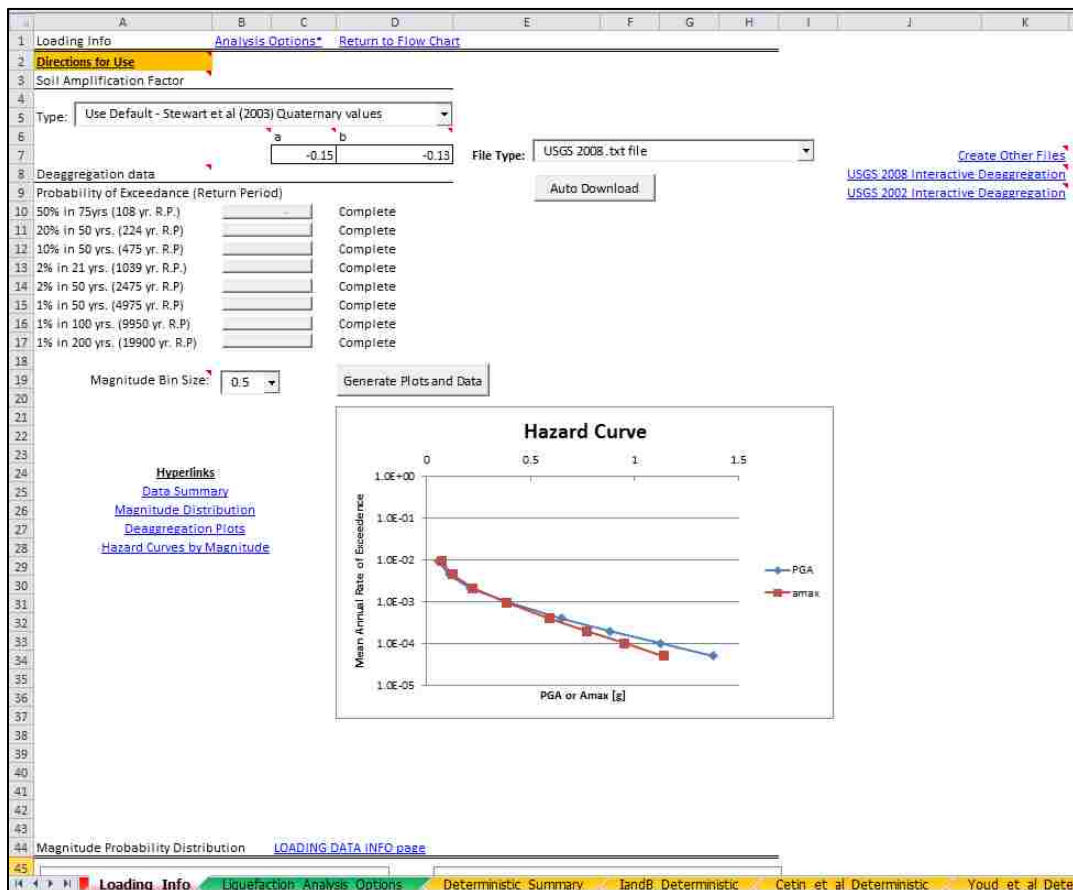


**Figure 0-11: Loading data page after data and graphs are generated.**

To review, the following steps need to be completed on the loading data page:

- 1) Choose a site amplification factor.
- 2) Upload data to the program for the seismic loading from the USGS or another source.
- 3) Select a magnitude bin size.
- 4) Generate the plots and graphs.
- 5) Review the graphs and data uploaded to ensure accuracy of the upload, and to ensure that the program is working correctly.

The loading data sheet is now complete. Return to the flow chart by clicking on the hyperlink at the top of the page.

#### **C.1.1.4 Step 3a: Analysis Options Page; Deterministic**

The program is now ready to run an analysis. At this point there are two different directions the analysis can go: deterministic and performance-based analyses. This section will discuss the deterministic analysis. Click on the RUN DETERMINISTIC ANALYSIS under step 3 on the flow chart. This will take us to the analysis options page (Figure 0-12).

On this page we can run both the deterministic and performance-based analysis. Both have detailed directions available for them in the orange *Direction for Use* boxes. To run the deterministic analysis we must first pick the type of deterministic analysis to run. Click on the drop box next to 'Analysis Type' under the Deterministic section. We will use the option "Mean magnitude – specify return period". This will open a user form where the user can specify which return period they would like to use (Figure 0-13). For our purposes we want a return period of 475 years.

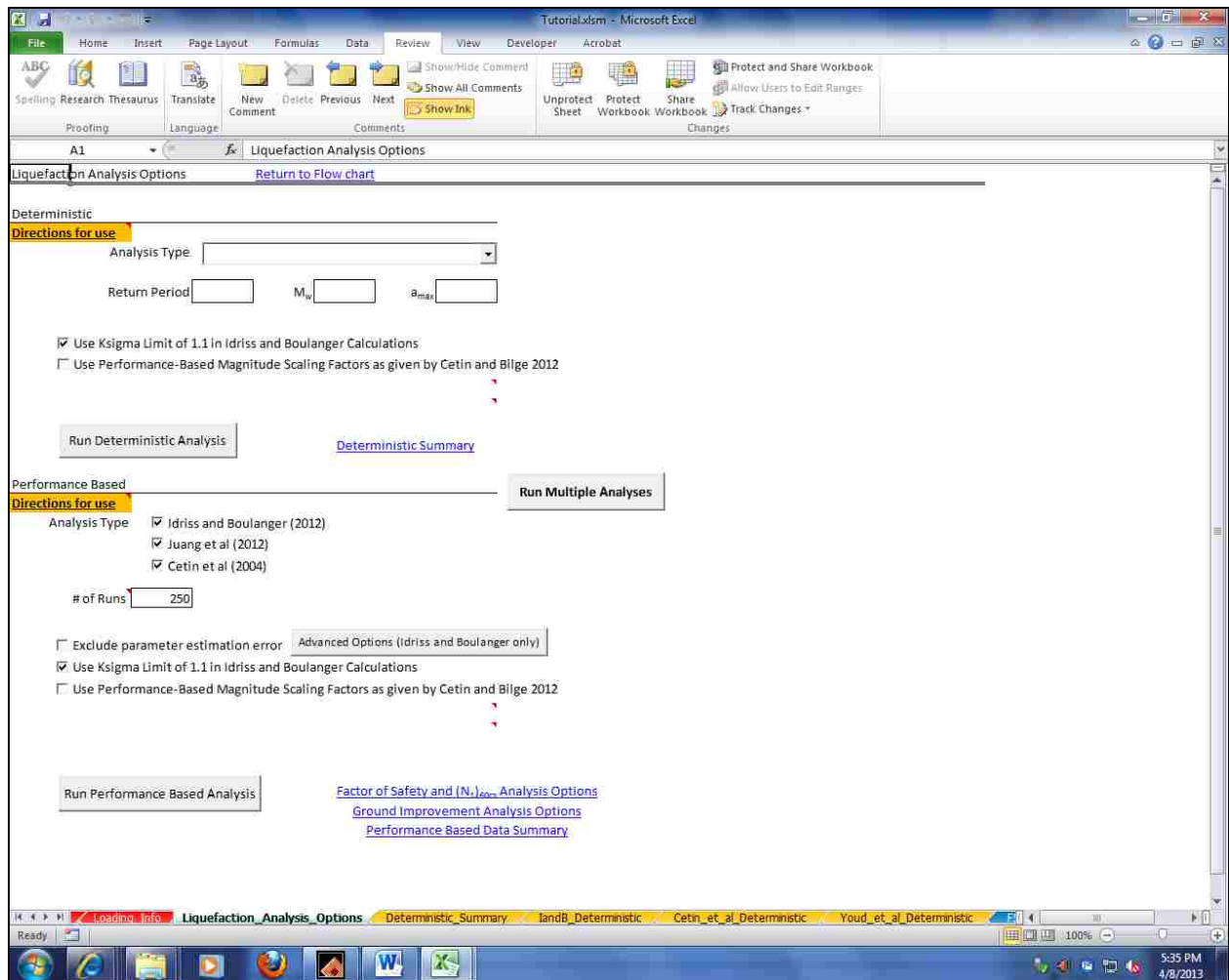


**Figure 0-12: Liquefaction analysis options page.**

When we select this return period and hit ok the program will automatically pull the mean magnitude and return period from our uploaded files. They will appear below the analysis type after we select them (Figure 0-14).

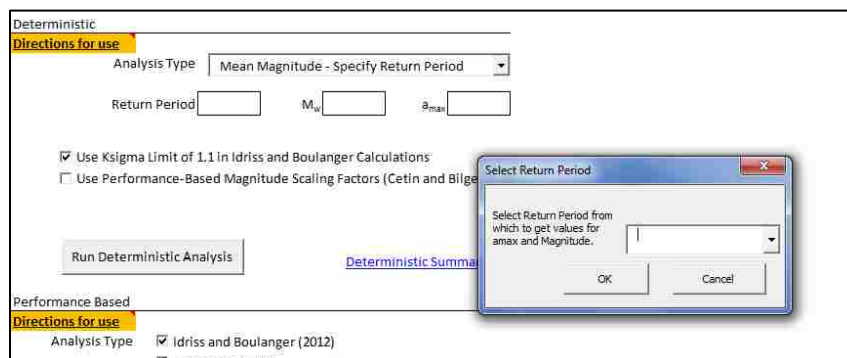


**Figure 0-13: Specify return period user form.**

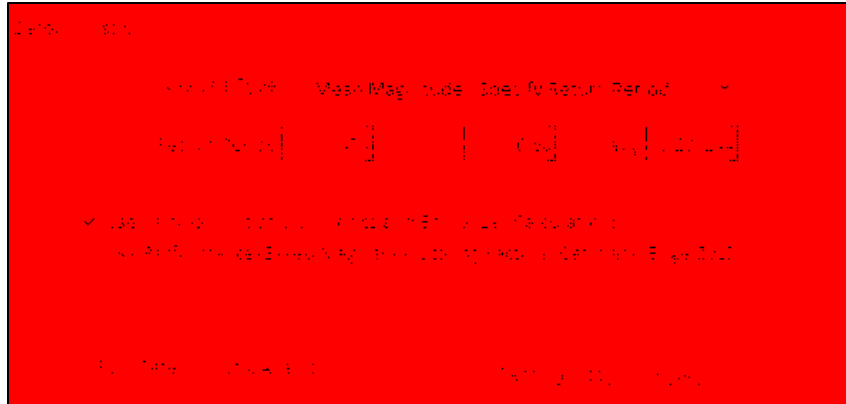


**Figure 0-14: Deterministic  $M_w$  and  $a_{max}$ .**

In this tutorial we also want to use the  $K_\sigma$  limit of 1.1. Check the box next to this option. We can now run the analysis. Click on run deterministic analysis. A progress bar will appear showing the progress of the current analysis along with the options checked. When it is done a message box will appear telling the user that the analysis is complete. At this point we can view the results. Return to the Flow Chart page by clicking on the Return to Flow Chart hyperlink at the top of the page.

#### **C.1.1.5 Step 4a: Viewing Deterministic Results**

To view the overview of the results click on the Deterministic Summary hyperlink under step 4 in the flow chart. This will take us to the deterministic summary page (Figure 0-15). On this page we can view and graph results of our analysis with depth. The numerical version of the results appears on the left. Layers that were not susceptible to liquefaction appear as a “Not\_Susc.”. Any factor of safety values that were calculated to be greater than the specified factor of safety (in this case 1.5) are shown as “No\_Liq”. Any other values will appear as a numerical value shown in red where the value is the factor of safety against liquefaction



occurring ( $FS_{liq}$ ). To graph these results by depth select the types of analysis to graph, then select the GENERAE GRAPH  $FS_{liq}$  button. This will graph the output from the selected analyses types by depth. The last option to show sub layer thicknesses allows the user to specify whether to graph the data by layer, or by sample depth.

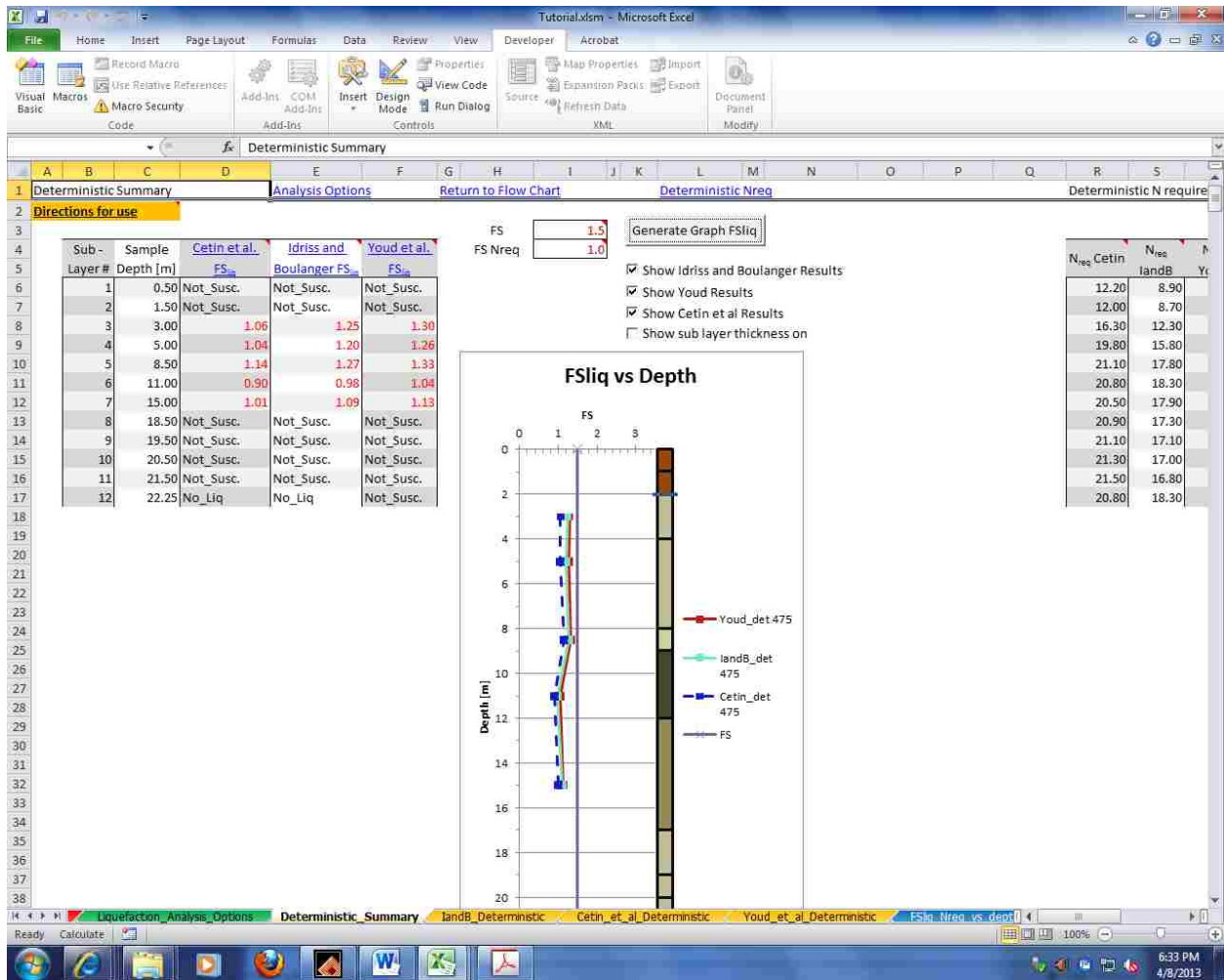
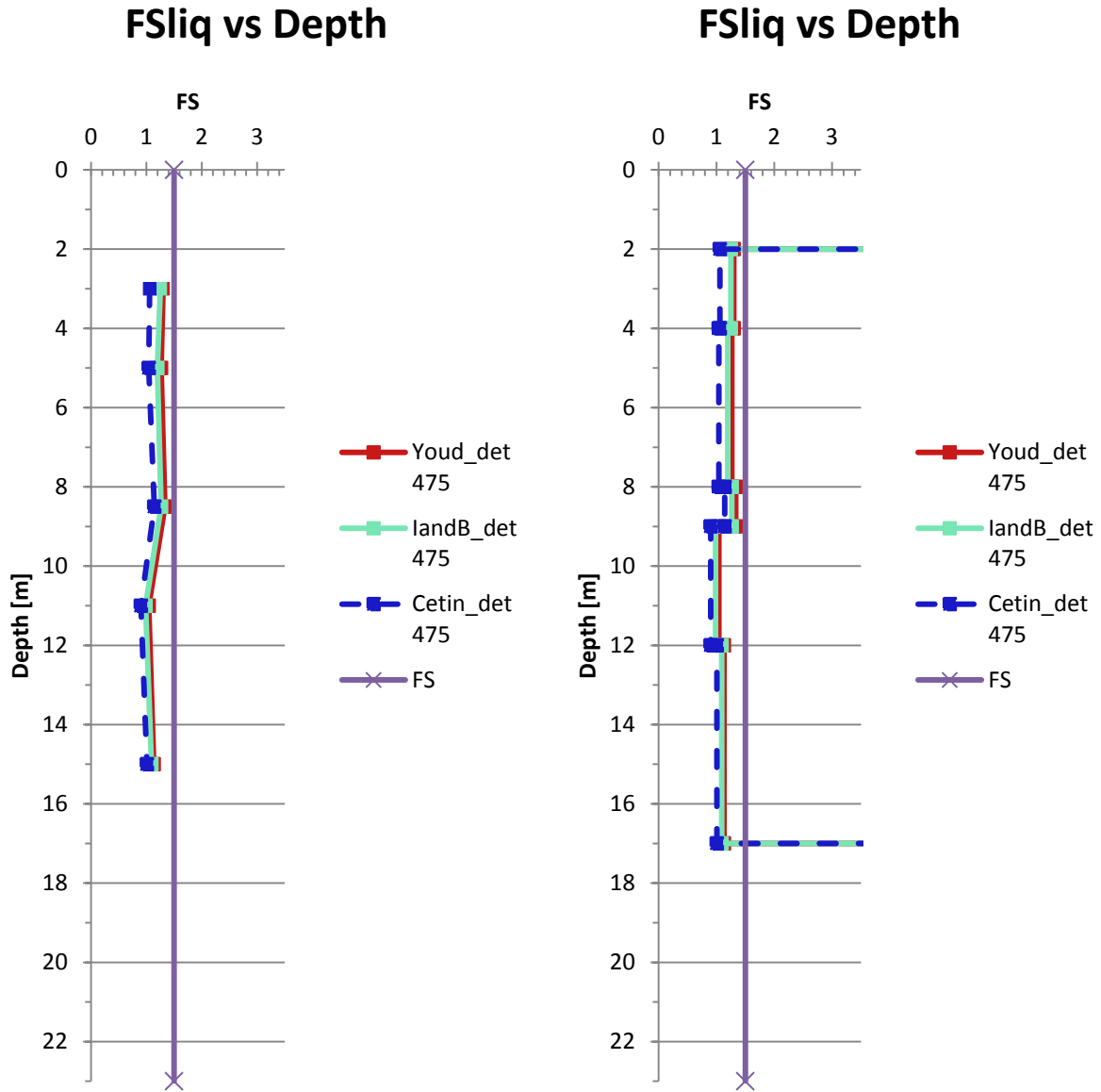


Figure 0-15: Deterministic Summary Page.

After selecting the GENERATE GRAPH  $FS_{liq}$  button a graph of the data will appear. This graph can be modified by change the options in the program and regenerating the graph, or we can modify the graph appearance using the built in tools available in EXCEL©. The graph

will appear as seen in Figure 0-16. To run a performance-based analyses the user must return to the flow chart page. To return to the flow chart, click on the hyperlink at the top of the page.



**Figure 0-16: Deterministic graphs a) by sample depth b) by layer depth.**

### C.1.1.6 Step 3b: Analysis Options Page; Performance-Based

A performance-based analysis is a more sophisticated version of liquefaction analysis which accounts for more of the uncertainty involved. This analysis is run from the performance-based analysis page. To access this page, click on the Run Performance-Based Analysis hyperlink. This will take us back to the analysis options page. We want to run a performance-based analysis using all three methods presently incorporated in the program. For the tutorial we want to run all three possible analysis types, so make sure that there is a check box next to each analysis (Figure 0-17). We want a sufficient number of runs to ensure that there will be sufficient analysis of each part of the hazard curves. A value of 250 is recommended as a minimum for our tutorial. Enter 250 into the box labeled “# of Runs”. At this point we need to select the options for our analysis. We want to exclude parameter estimation error, and include a  $K_{\sigma}$  limit of 1.1 where applicable. To do this, select the options as shown in Figure 0-17. We can now run the analysis. This will take a few minutes with the overall speed dependent on the speed of the computer used. Push the button RUN PERFORMANCE BASED ANALYSIS. A progress bar will pop up showing the progress of the analysis. When it is finished a message box will appear telling the user that the performance-based analysis is complete.

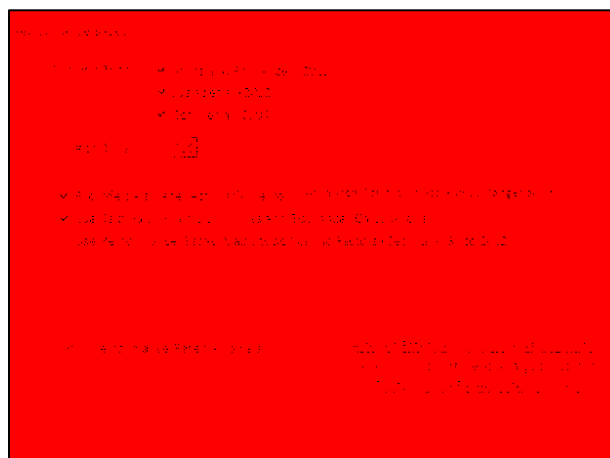


**Figure 0-17: Performance-Based Analysis Options.**

### C.1.1.7 Step 4b: Viewing Performance-Based Analysis

There are several options available to view the results of the analysis. These include analysis by layer, analysis by depth, and analyzing the soil for ground improvement. We will look at each of these pages individually.

To access the analysis by layer and by depth return to the flow chart page and click on the hyperlink on the flow chart labeled  $FS_{liq}$  and  $N_{req}$  analysis. This will take you to the analysis options page (Figure 0-18).



**Figure 0-18:  $FS_{liq}$  and  $N_{req}$  Analysis Options Page.**

This page gives you options for developing graphs based on different return periods. To create graphs for  $FS_{liq}$  and  $(N_1)_{60cs req}$  vs. depth, select a return period. Select the return period corresponding to 2475 years. Further select the options to graph the results of all three analyses,

and to graph the  $(N_1)_{60cs_{site}}$  as calculated by the different methods. This will allow the generation of two graphs, one for the factor of safety and one for the  $(N_1)_{60cs_{req}}$  to prevent liquefaction ( $N_{req}$ ) (Figure 0-19). The factor of safety graph will only show factors of safety for layers that are considered susceptible, while the graph of  $N_{req}$  will show the  $N_{req}$  for all layers.

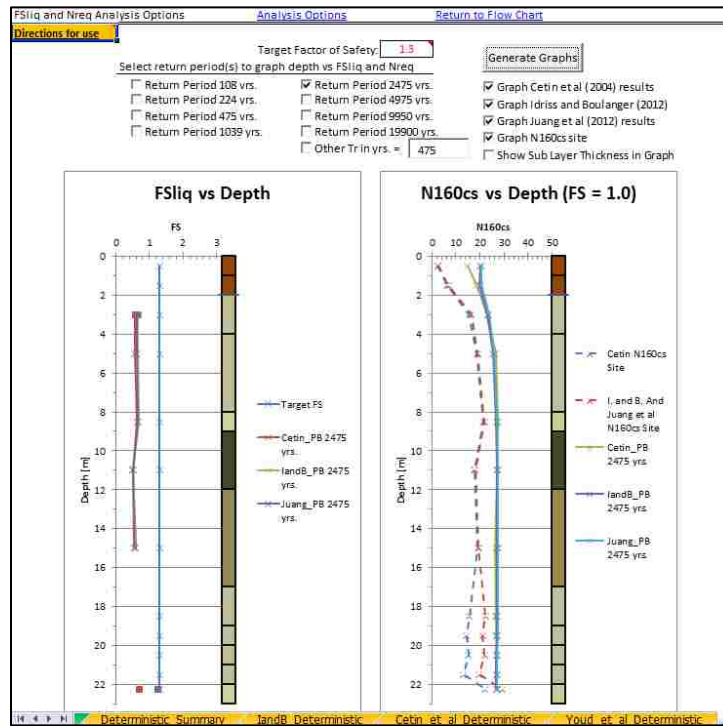


**Figure 0-19:  $FS_{liq}$  and  $N_{req}$  graphs developed from performance-based analysis.**

These graphs are useful for seeing where liquefaction will trigger, and how much we need to increase the  $(N_1)_{60cs}$  value by at our site in order to prevent liquefaction from occurring. Each of the graphs has a small version of the soil graphic included with it to help in determining which layers are going to liquefy. The sub layer thicknesses can be shown on this graph and work in a similar fashion to the deterministic graphs.

Further down the page, analysis by soil layer is available. For this section a single soil layer is analyzed and hazard curves and deaggregations of the liquefaction hazard are created.

For this analysis a sub layer of interest must be selected. Under the sub layer specific analysis section in the drop box next to ‘Sub layers of interest’ select sub layer 3. In order to see all of the possible output, place a check in each of the option boxes available under sub layer of interest. Then type a return period of 2475 years into the box labeled  $T_R$ . This box specifies what return period we want specific values for. Now click on the GENERATE GRAPHS button. This will generate two hazard curves (Figure 0-20) and three deaggregations graphs (one for each analyses type run) (Figure 0-21).

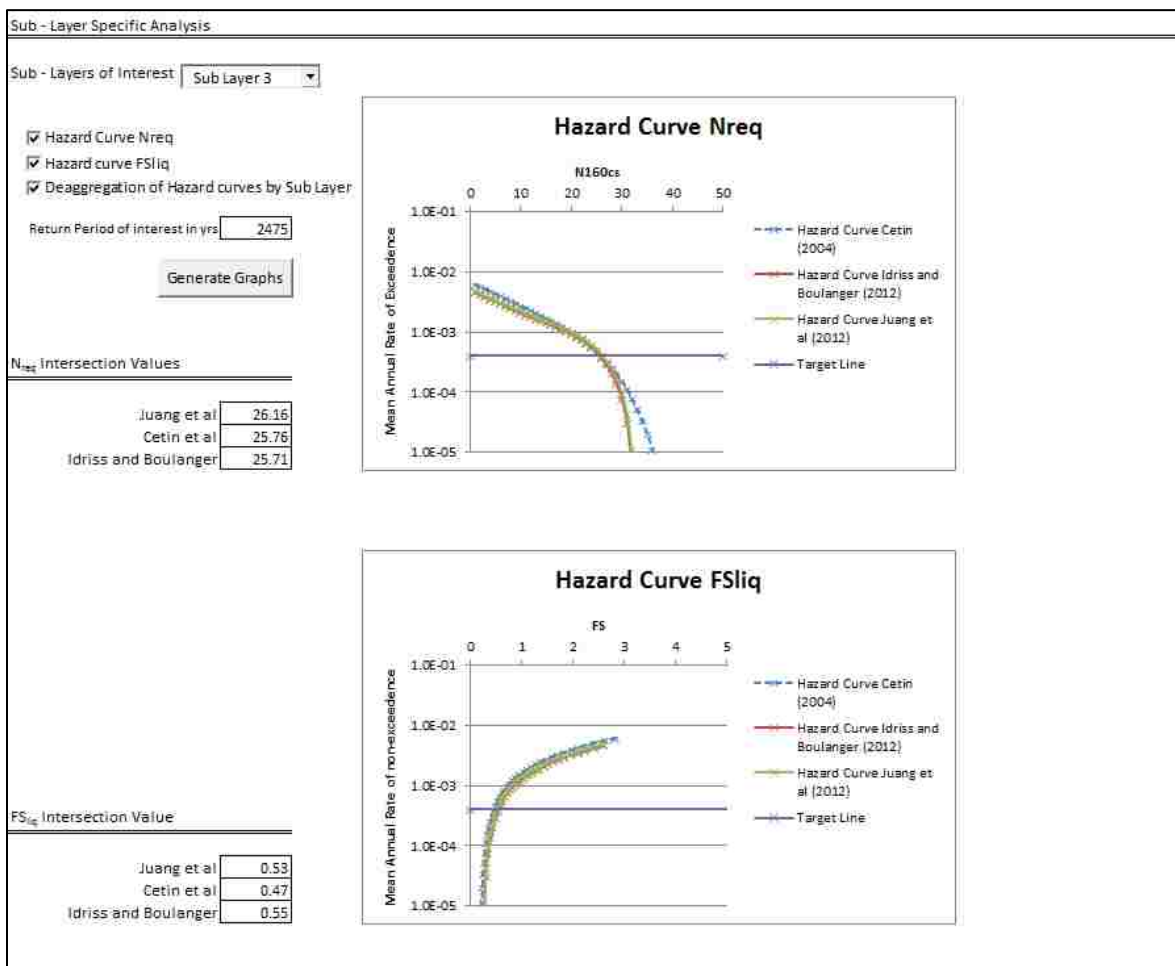


**Figure 0-20: Hazard curves developed using PB LiquefY.**

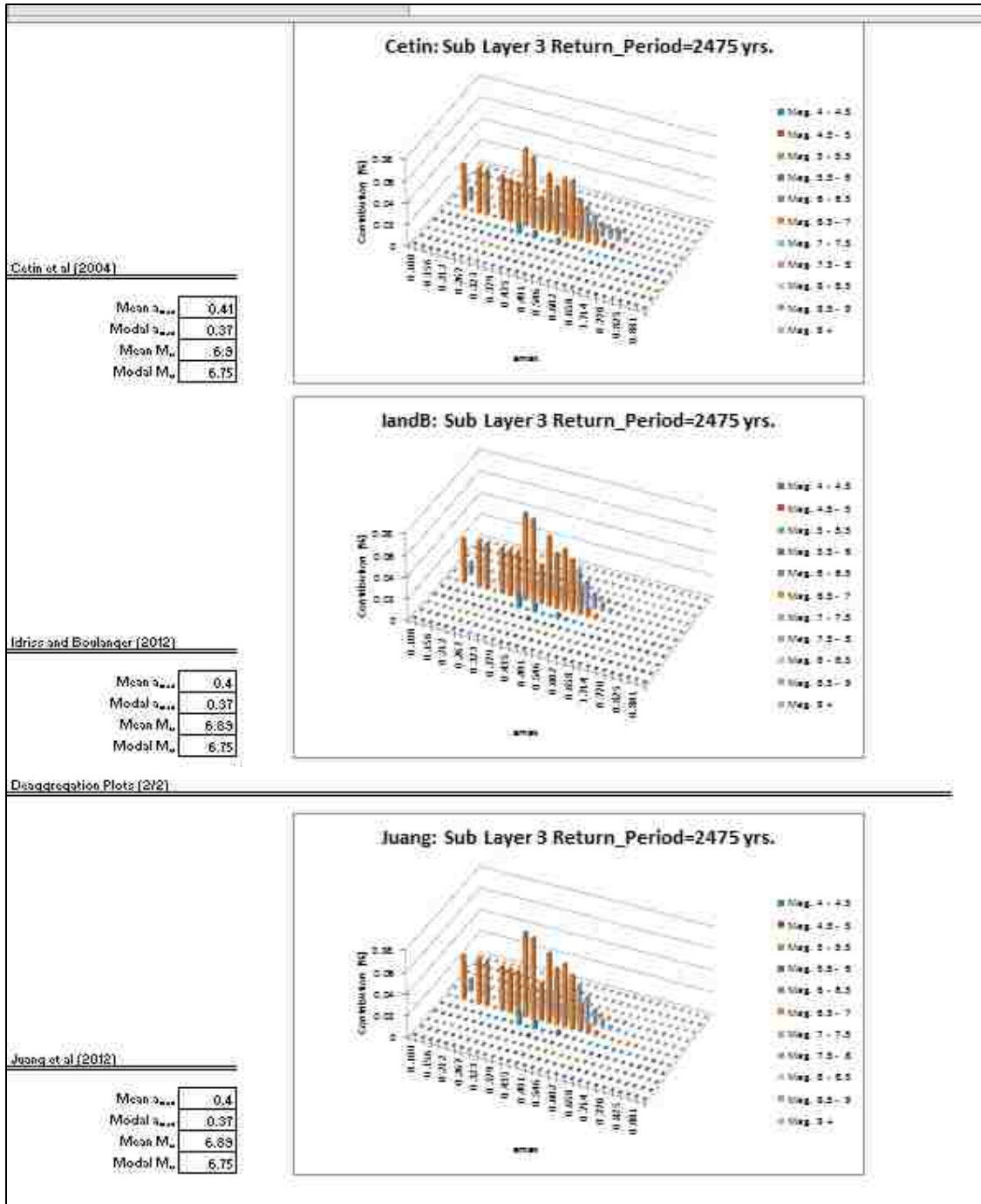


**Figure 0-21: Deaggregation charts developed using PB LiquefY.**

These can be used in the liquefaction analysis to determine where liquefaction will trigger, what sorts of improvement can be achieved, and what seismic events are contributing to the liquefaction hazard the most.

We will now look at the ground improvement page. This can be accessed from the flow chart by clicking on the ‘Ground Improvement Analysis’ hyperlink. This will take the you to the ground improvement analysis options page (Figure 0-22).

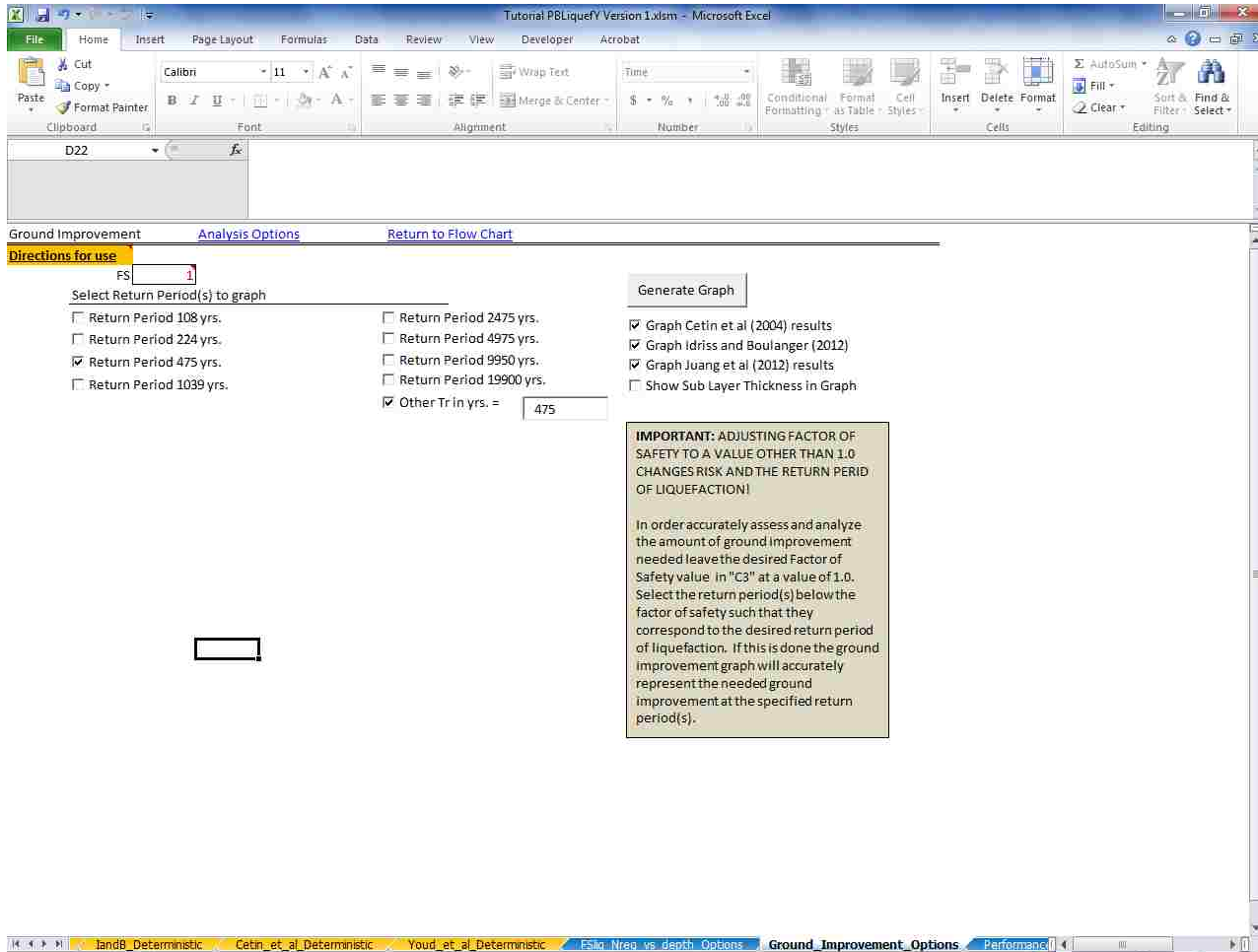


**Figure 0-22: Ground improvement analysis options page.**

This page can be used to create and analyze the amount of ground improvement (in the form of  $(N_1)_{60cs}$ ) that will be needed at the site to prevent liquefaction from triggering. We will use a return period of 2475 years and graph all of the analysis types. This will create a graph of the needed ground improvement (Figure 0-23).



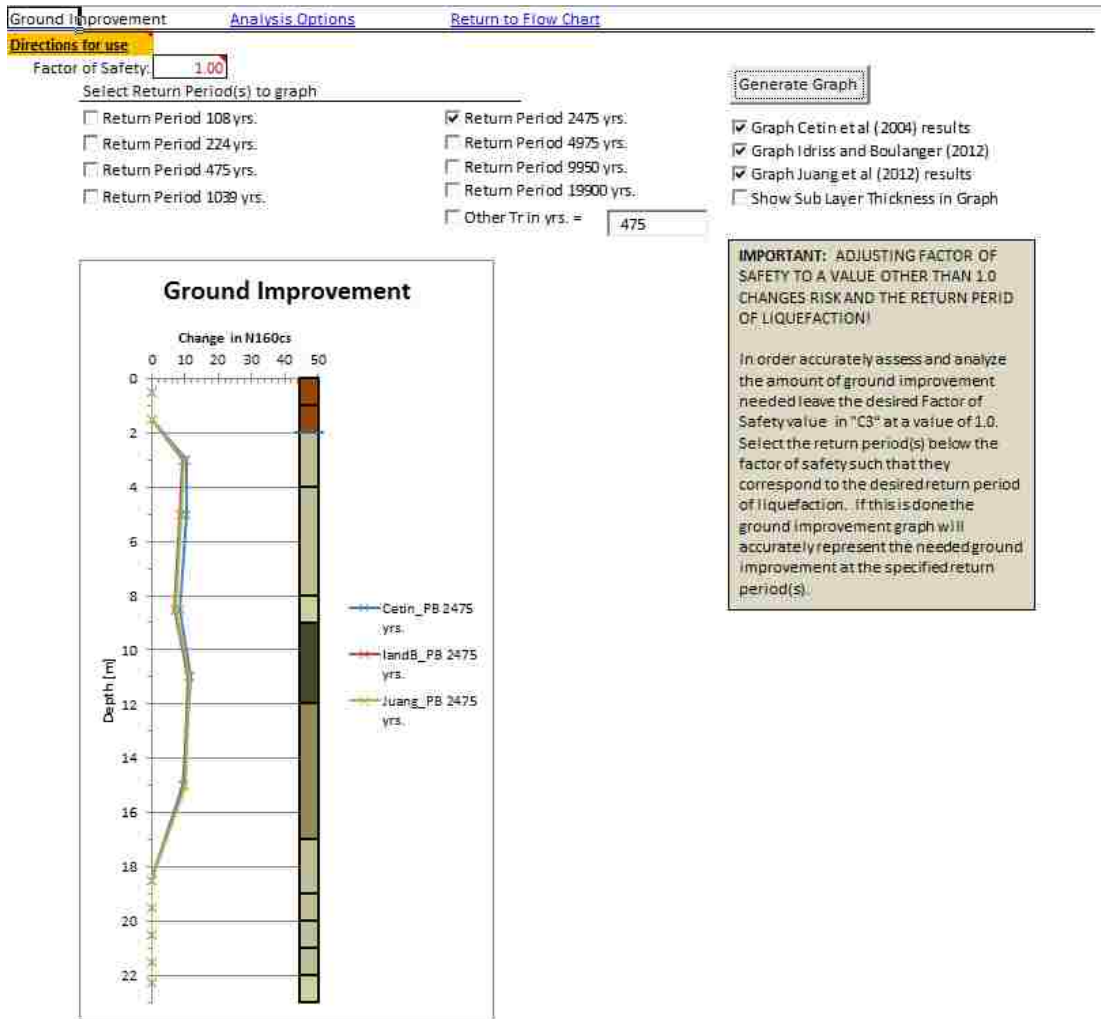


**Figure 0-23: Ground improvement for tutorial.**

This graph shows that ground improvement will be needed across most of the soil profile (from 2 to 17 meters) to prevent liquefaction from triggering based on our desired return period of liquefaction of 2475 years.

The next step is the summary page. Click on the ‘Performance-Based Summary’ hyperlink in the flow chart. This page shows all of the analysis conducted up to this point and gives specific numerical values for the analysis. It also contains numerical values for the

magnitude bins, mean and modal accelerations, graphs of  $FS_{liq}$  vs. depth for both deterministic and performance-based analysis, and a graph of the hazard curve broken up by magnitude (Figure 0-24). Further information about the use of this page is given later.

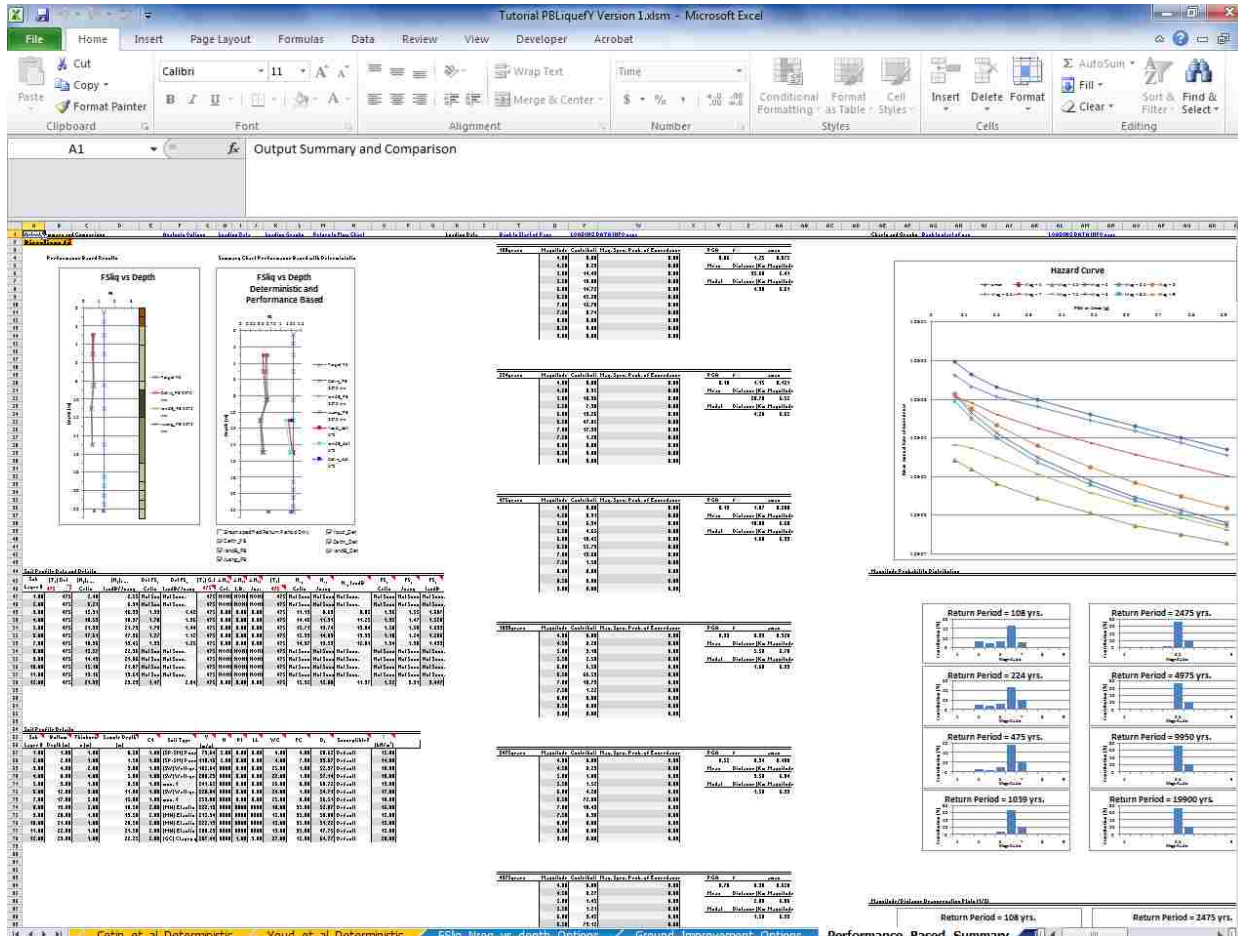


Figure 0-24: Performance-based summary page.

This concludes the basic tutorial. For further information, or to learn about more options available within the analysis, view the other tutorials and read through the theory sections of this document.

**C.1.2 Using Applied Loadings and  $K_\alpha$**

Using applied loadings can be essential in a liquefaction analysis. Recently Oka, Dewoolkar et al. (2012) showed that the influence of large embankment loads can lead to changes in the stresses that widely effect the liquefaction initiation analysis. To account for the effects due to applied loads the program has several options available to the user.

Go to the soil profile details page, either by clicking on the tab, or by navigating using the hyperlinks. Input all information as if you are running a regular analysis (see Basic Analysis). Once this has been done, it is time to apply a loading. Look under the applied Loads and Fills section of the page. You will see a section labeled ‘Applied Loads’ (Figure 0-25). Currently the selection should say ‘No Additional Load’. There are additional options available. We will go through each option individually.

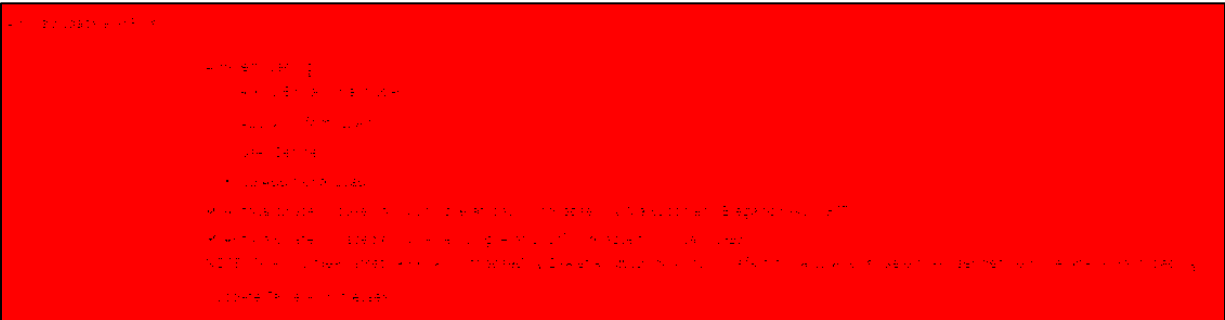


**Figure 0-25: Applied loads and fills section.**

**C.1.2.1 User Defined Load Case**

We will start with the user defined load case. This case is normally selected when the user want to apply a load case that is not available. This option allows the user to specify the stresses, and values for  $K_0$  and  $K_\alpha$  where applicable. Click on the ‘User Defined’ control. This

will open a pop up window where the user specifies what sorts of loading they will be entering (Figure 0-26). There are several options available on this page. We will go through each.

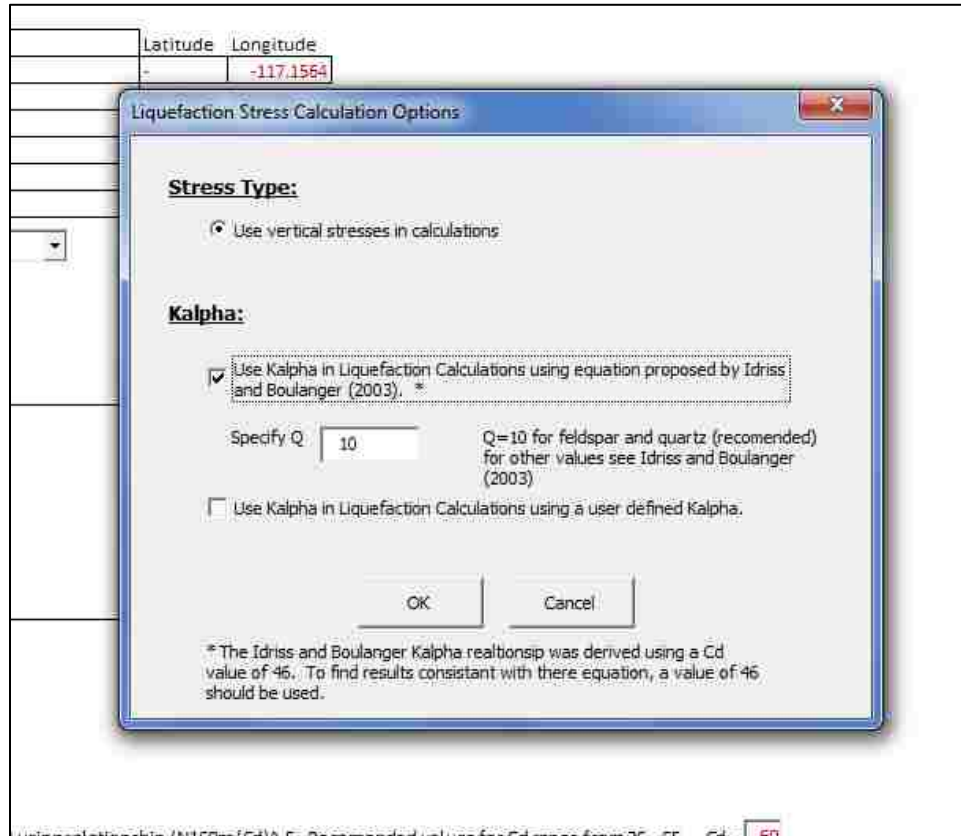


**Figure 0-26: User defined controls.**

The first set of options in this box allows the user to select the type of stresses to use in the analysis. The current program allows only the use of vertical stresses.

The second section in the options box allows the user to use  $K_{\alpha}$  in the liquefaction analysis. If neither box is checked, then the analysis will set the  $K_{\alpha}$  value to 1.0 which corresponds to a free field case. There are two options available for the use for  $K_{\alpha}$ . The first option is to use the correlation created by Boulanger (2003).

This relationship was republished by Idriss and Boulanger (2008) and uses the following equations.

$$\xi = \frac{1}{Q - \ln\left(\frac{100(1+2K_o)\sigma'_t}{3P_a}\right)} - D_R \quad (76)$$

$$a = 1267 + 636\alpha^2 - 634 \exp(\alpha) - 632 \exp(-\alpha) \quad (77)$$

$$b = \exp[-1.11 + 12.3\alpha^2 + 1.31 \ln(\alpha + 0.0001)] \quad (78)$$

$$c = 0.128 + 0.126\alpha + 2.52\alpha^3 \quad (79)$$

$$K_\alpha = a + b * \exp\left(-\frac{\xi_R}{c}\right) \quad (80)$$

$$\alpha = \frac{\tau}{\sigma'_t} \quad (81)$$

limits:  $\alpha \leq 0.35$  ;  $-0.6 \leq \xi_R \leq 0.1$

Where alpha is initial shear stress over the initial effective consolidation stress,  $\xi$  is the state parameter, Q is a number related to the material type, and a, b, and c are coefficients developed by the equations. When this box is clicked a new set of options appears where you can change the value of Q (Figure 0-27).

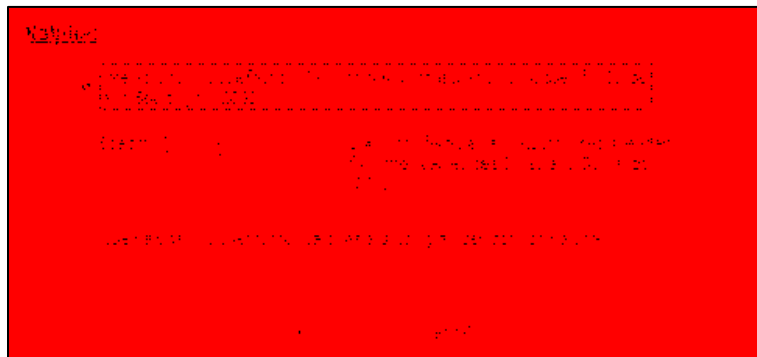


**Figure 0-27:  $K_\alpha$  options.**

Q should be selected according to the values specified in Table 0-3. For most engineering applications a value of 10 (the default) should be used.

**Table 0-3: Approximate values for  $Q$ .**

$Q$	Material Type
10	Quartz and Feldspar
8	limestone
7	anthracite
5.5	chalk

The second option available for  $K_\alpha$  is to use a user defined  $K_\alpha$ . This option allows the user to input any value of  $K_\alpha$  that is desired on a sub layer by sub layer basis. These values are input in the same part of the table as the stresses in the column that will be labeled  $K_\alpha$ .

Since the user specified the use of  $K_\alpha$ , a value for  $K_0$  is also required for calculations within the spreadsheet. This value can be entered by hand, or a default value can be used (0.5).

We will use the default value so select *Use default*.

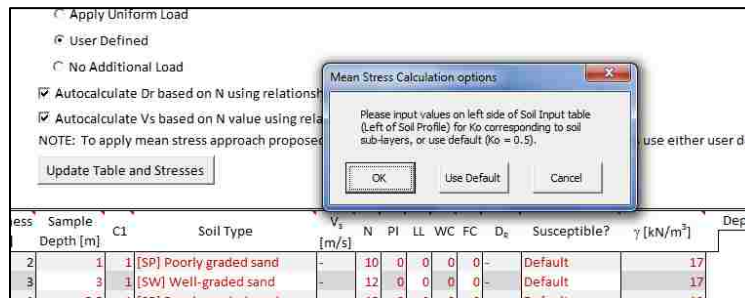


**Figure 0-28:  $K_0$  options box.**

At this point the user will notice a new portion of the soil profile details table has appeared. It is located on the far right side of the table to the right of the soil profile graphic (Figure 0-29). This table must be filled out in its entirety for the program to run correctly. Depending on the options selected this portion of the table will change to reflect the required values. Select the button UPDATE TABLE AND STRESSES once required values are entered.

This completes the application of a user defined load. Proceed as outlined previously from this point.

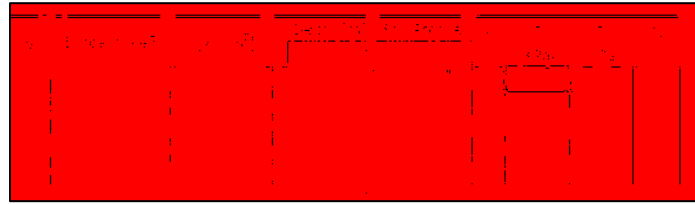


**Figure 0-29: User input portion of table.**

### C.1.2.2 Uniform Load Case

The next option that we will discuss is the option to apply uniform loading. Again the soils table should be filled out as completely as possible. To use a uniform surface load as our applied loading select the ‘Apply Uniform Load’ option button. This will open up the options window for the uniform loading options (Figure 0-30).

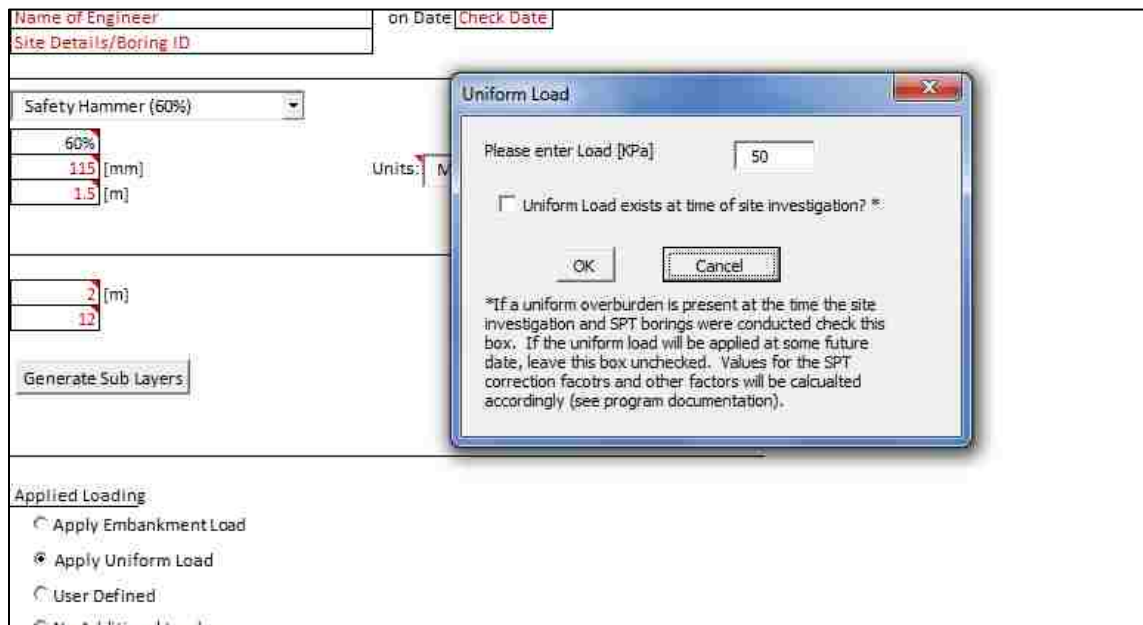


**Figure 0-30: Uniform load controls.**

In this form an applied load is entered that will be applied uniformly across the surface of the soil profile. Enter a load of 20 KPa. Next, the program must be told if the load exists at the time of the boring or if it will be applied at some future date. If the load exists at the site at the time of the boring ensure that the option for this is checked (for detailed discussions see C.1.2.4 Detailed Discussion – Applied Loadings and  $K_o$ ). For this tutorial we will not be selecting this box as it is assumed that the uniform load has not yet been applied. Press OK then press the UPDATE TABLE AND STRESSES button. This will generate the stresses based on the applied load and soil profile (Figure 0-31).

$D_b$	Susceptible?	$\gamma$ [kN/m <sup>3</sup> ]	Depth [m]	Soil Profile	$K_o$	$\sigma$ [KPa]	$\sigma'$ [KPa]	$\tau_h$
			0					
46.1	Default	17		Soil Profile		37.00	27.20	
51.51	Default	17			71.00	41.60		
55.42	Default	19			114.50	60.60		
47.93	Default	18			133.00	69.30		
58.86	Default	20			182.00	93.80		
			2					

Figure 0-31: Loading after application of uniform load.

### C.1.2.3 Embankment Load Case

One of the most versatile auto calculated loading cases is the embankment loading case. This case allows for the application of an embankment load of varying shape and size. Again, remember that the soils table should be filled out prior to selecting this option. Select the ‘Apply Embankment Load’ option button. This will open the embankment loading options form (Figure 0-32).



This form shows all of the options for manipulating the embankment loading case. Note that there are four options for defining the weight and size of the embankment, and one option (X) for defining the location of the soil profile with respect to the embankment center. This is useful because it allows the examination of liquefaction under different points of the embankment loading to see whether liquefaction will trigger, and allow the engineer a more full understanding of the effect of the embankment. The embankment loading can also be used to represent square and triangular loading by specifying a 0 length or slope, which will eliminate either the center or edge of the embankment.

For this tutorial enter values into the table corresponding to the values in Figure 0-32. You will note that the distance  $x$  is located at the toe of the slope. This value can be extended past the toe of the slope or can be 0 for cases where an evaluation of liquefaction potential under the center of the slope is desired. Finally choose whether the embankment is present at the time of the SPT testing as discussed previously.

Once all of the values have been entered select 'OK'. This will open up the form we saw earlier (see User Defined load case). Follow the directions for this form as before. Vertical stresses will be calculated internally by the program using the embankment load relationships. To see the stresses generated press the UPDATE TABLE AND STRESSES BUTTON and look to the right of the soils profile graphic. Ensure that values are correct before proceeding.

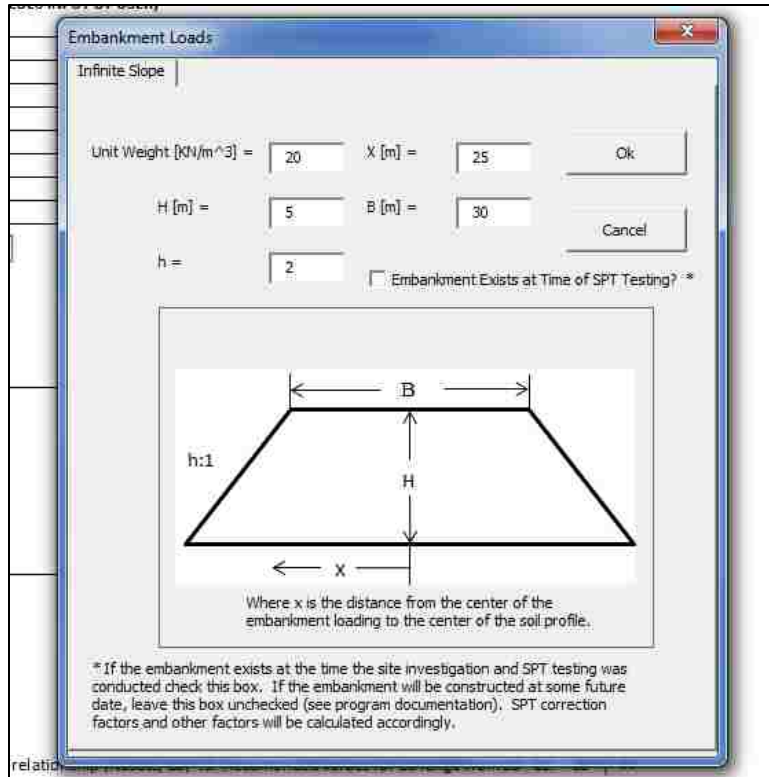


**Figure 0-32: Embankment loading options.**

#### **C.1.2.4 Detailed Discussion – Applied Loadings and $K_{\alpha}$**

For most liquefaction analyses the free field case is used. This means that there are assumed to be no shear stresses in the soil as would occur if there were an embankment nearby or a slope. Recent earthquakes, such as the Tohoku earthquake in Japan, have shown that one of the major problems liquefaction can cause is the failure of dams and levees. For this case the free field assumption does not apply, and current published methods for dealing with this case using the simplified method leave much to be desired. A first approximation of liquefaction initiation can be made using  $K_{\alpha}$ . This can be done using the methodology laid out here which was developed in cooperation with Dr. Kevin Franke, James Gingree, and others. This methodology should be used only as a simple first approximation and should not be used in engineering design.

The first factor that needs to be evaluated to determine how the term  $K_{\alpha}$  should be used is the embankment. If the embankment exists at the time that the SPT borings were carried out, then the correction terms and the  $K_s$  should be evaluated based off of free field conditions. If the embankment already existed at the time of the SPT boring, the induced stresses that exist at that time should be used in these evaluations.

The CSR and  $K_{\alpha}$  factors should be evaluated based off of the existing conditions at the time of the earthquake. Other factors should be calculated as is normal. A flow chart illustrating the analysis using the embankment loads is shown below (Figure 0-33).

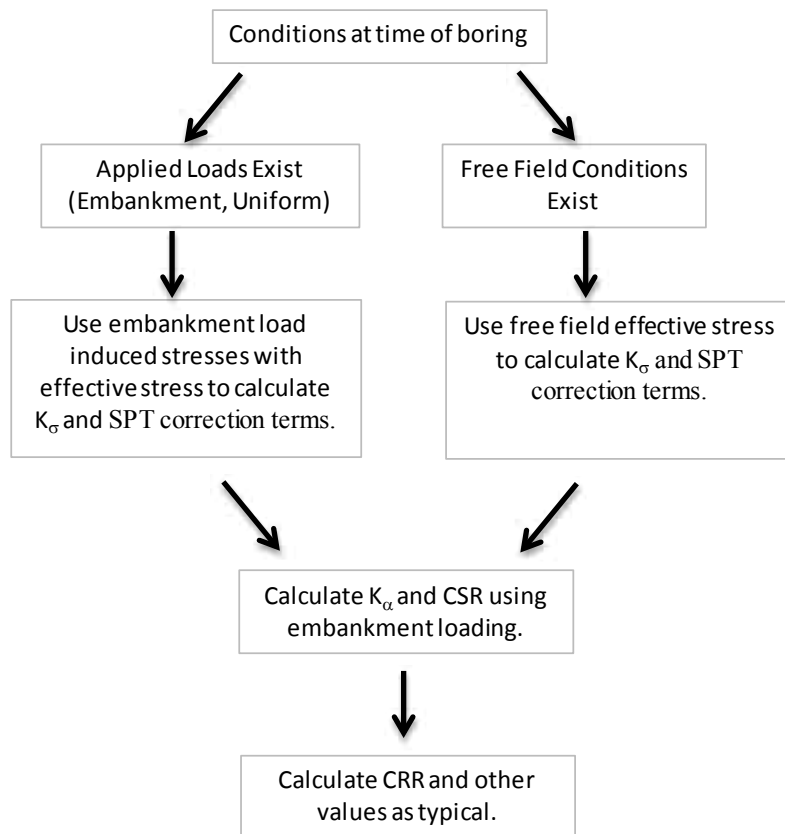


**Figure 0-33: Flow chart for calculations in the presence of an embankment.**

### C.1.2.5 Detailed Discussion – Multiple Analysis Run

PB LiquefY was built for use by the researcher and engineer. One of the useful aspects of the program is the multiple analysis run tool (Figure 0-35). This tool enables the engineer or researcher to create liquefaction parameter maps, perform sensitivity studies, analyze multiple soil profiles at the same time, and return large amounts of data in a form usable by both ARC\_GIS and JMP Pro 10.

In order to use this tool it is necessary to save the required information in a location and form that can be used by the program. Currently the multiple analysis tool is only available with multi download compatible seismic loading (USGS 2008 or 2002). The program allows the creation of lists of soil profile files, lists of latitudes and longitudes, and the evaluation of multiple return periods automatically based off of user input. The lists for soil profile and latitude longitude can be created on the Create\_Other\_Text\_File tab. Detailed instructions for their creation are available on this sheet. In general to create the needed input text files, input data into the appropriate columns and click save text file. For the latitude and longitude list values must be in the United States. For longitude, west is represented by a negative value. Once all desired locations have been input, create the input text file by selecting the SAVE LAT LONG LIST button.

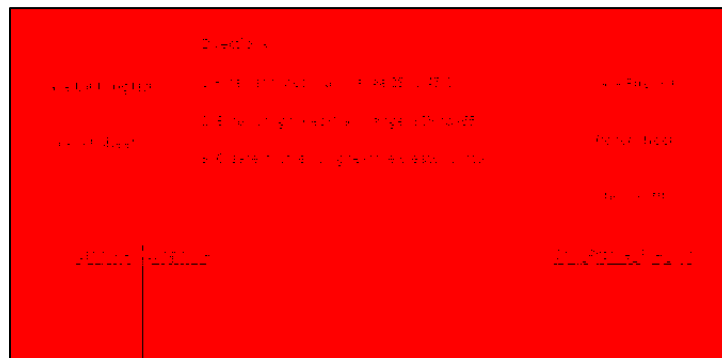


**Figure 0-34: Input text file creator page.**

Soil profiles must be saved prior to creating a list of soil profiles to run using the SAVE SOIL PROFILE button on sheet 2. Once soil profiles have been saved to the hard drive the soil profile list can be created using the CHOOSE\_FILE button. Files will be added in the order they are selected. When finished Save the soil profile list to a text file using the SAVE FILE LIST button. These files will be used in the multiple analysis run input page.

**Multiple Run Options**

**Location:**

Upload List of Lat/Long

NOTE: Use text creator to make a list of latitudes and longitudes that can be read by program.

**Run Options:**

Deterministic Options

Performance Based Options

Upload Soil Profile List (Optional)

Run program for multiple soil profiles (requires list made by program).

**Output:**

PB Liquefy Standard (Generates multiple PB Liquefy Files)

Generate Text File

Generate Excel File

Choose File Location

Return Values for:

Single Return Period  RP of Interest:

Multiple Return Periods

Choose From List

Minimum RP:  Max RP:  by:

Created By: Cody Hatch

**Figure 0-35: Multiple run options for use in multi analysis.**

Once the files have been created the multiple analyses can be run from the Liquefaction Analysis Options page. On this page is a button labeled RUN MULTIPLE ANALYSES. When this button is clicked an option box appears allowing the user to select a single run, multiple run, or auto download (Figure 0-36).

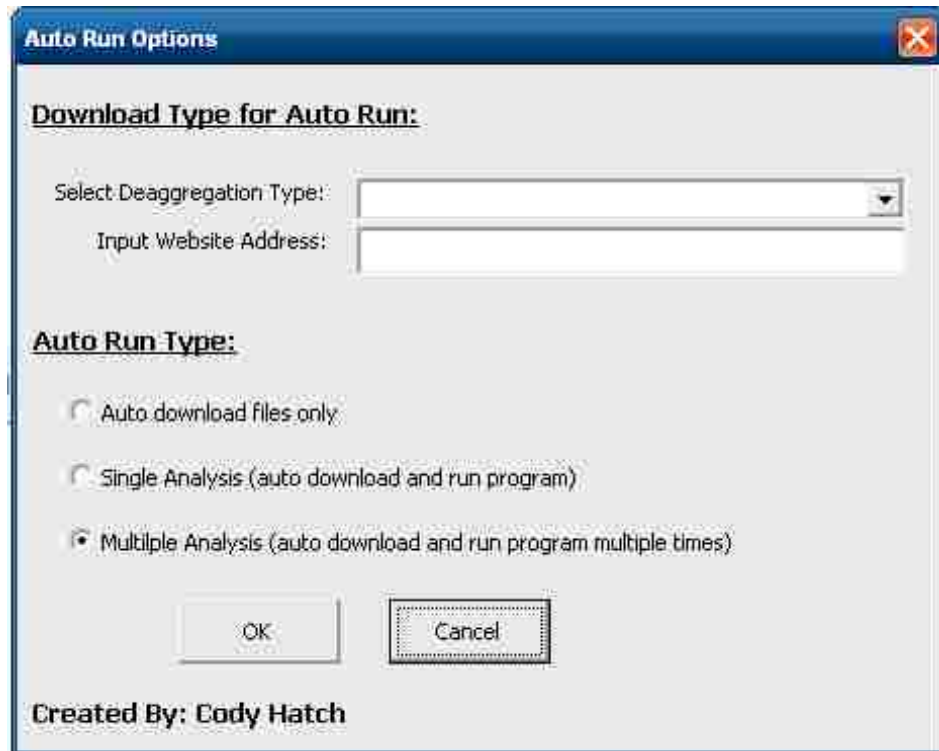


**Figure 0-36: Selection of auto run analysis type.**

The auto download option can be used to auto download seismic loading data from the USGS website. The user will still be required to run the analysis manually. The single run options allows the user to run the analysis automatically and creates a text output file of the desired output for a single location only (selected using the output options button on the form). The multi analysis run will allow the user to run multiple analyses. All of the input must be filled out prior to running the analyses. The program will prompt the user for any input that is missing.

A step by step process to run a multi analysis is shown below:

- 1) Create and save all desired soil profiles using the SAVE SOIL PROFILE button on sheet 2.
- 2) Create and save a text file list of the soil profiles to use in the multi analysis run using the Create\_Other\_Text\_Files page.
- 3) Create and save a list of latitudes and longitudes on the Create\_Other\_Text\_Files page.
- 4) Open the multi analysis run options on the Liquefaction analysis page.
- 5) Select the type of seismic loading files to use in the analysis (USGS 2002 or 2008).
- 6) Select the type of run (multi, single, or auto download).
- 7) Upload the location list file by clicking on the UPLOAD LIST OF LAT/LONG button in the Multiple Run Options dialogue box.
- 8) Upload the soil profile list file by clicking on the UPLOAD SOIL PROFILE LIST button in the Multiple Run Options dialogue box.
- 9) Choose the desired type of output – text files are recommended.
- 10) Choose the output desired by clicking on the OUTPUT OPTIONS button.
- 11) Choose a file location to save the output to.
- 12) Choose the desired return period(s) to return output for.
- 13) Run the analysis.

When the analysis completes two files will be generated, an error file and a text file containing the results. It is recommended that the values in the output file be checked for errors and that the error output file be examined.

### C.1.3 Using Amplification Factors

Using amplification factors in the calculations can be critical to arriving at useful and accurate results. Amplification factors can be calculated by several different means. The program allows the user several options in entering amplification factors. Depending on the project, the type of deaggregation files used and other factors the user may wish to use different amplifications of the amplification factors.

To access the menu for amplification factor go the loading data page (Figure 0-37). On this page you will see a drop box next to ‘Type:’ in the Soil amplification factor section of the page. Click on the drop box arrow on the right side of the drop box.

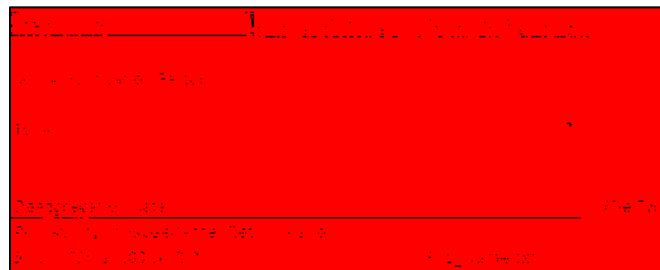


**Figure 0-37: Loading data page, soil amplification factor section.**

At this point you will see a menu drop down with three options available (Figure 0-38). We will go through these options in the order they are shown.

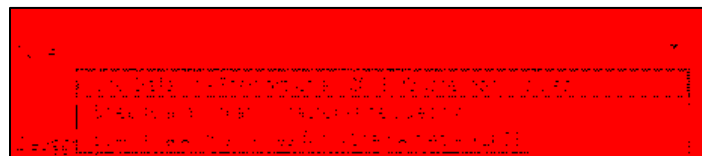


**Figure 0-38: Amplification factor menu.**

The first option the user will see is “Use Default – Stewart et al (2003) Quaternary values”. This option will use a correlation proposed by Stewart, Liu et al. (2003). This relationship is of the form,



$$F_a = \frac{a_{max}}{PGA} = \exp[a + b * \ln(PGA)] \quad (82)$$

where  $F$  is the amplification factor,  $a_{max}$  is the acceleration at the surface,  $a$  and  $b$  are factors derived from the statistical analysis performed by Stewart et al (2003), and  $PGA$  is the peak ground acceleration of bedrock. The values of  $a$  and  $b$  used with the default setting are -0.15 and -0.13 respectively. These values correspond to values correlated with quaternary age alluvium.

If desired the user can enter values for  $a$  and  $b$  by hand. This would normally be done when the age of the alluvium is known to be other than that listed above. To do so, obtain values for  $a$  and  $b$  corresponding to the soil site characteristics from Table 0-4. These values are then input by selecting “Specify  $a$  and  $b$  values from Stewart et al (2003)” and typing the correct values into the corresponding boxes for  $a$  and  $b$ .

**Table 0-4: Values for  $a$  and  $b$  table after Stewart, Liu et al. (2003).**

Geology	Period	$a$	$b$	$r$	Rejection Confidence for $b = 0$ Model (%)
Holocene (H)	PHA	$-0.24 \pm 0.14$	$-0.17 \pm 0.05$	0.54	100
	0.3 s	$-0.18 \pm 0.13$	$-0.15 \pm 0.05$	0.53	100
	1.0 s	$0.24 \pm 0.15$	$-0.05 \pm 0.06$	0.57	91
	3.0 s	$0.36 \pm 0.19$	$-0.05 \pm 0.08$	0.64	82
Pleistocene (P)	PHA	$0.14 \pm 0.27$	$0.02 \pm 0.10$	0.47	29
	0.3 s	$0.22 \pm 0.27$	$0.07 \pm 0.10$	0.48	80
	1.0 s	$0.21 \pm 0.32$	$-0.02 \pm 0.12$	0.52	23
	3.0 s	$-0.03 \pm 0.37$	$-0.19 \pm 0.14$	0.51	99
Tertiary (T)	PHA	$0.23 \pm 0.35$	$-0.02 \pm 0.14$	0.62	21
	0.3 s	$0.09 \pm 0.37$	$-0.05 \pm 0.14$	0.65	49
	1.0 s	$0.09 \pm 0.34$	$-0.05 \pm 0.14$	0.58	55
	3.0 s	$0.10 \pm 0.45$	$-0.06 \pm 0.18$	0.69	48
Mesozoic +	PHA	$-0.13 \pm 0.30$	$-0.08 \pm 0.12$	0.52	78
	0.3 s	$-0.46 \pm 0.33$	$-0.14 \pm 0.13$	0.57	96
	1.0 s	$-0.45 \pm 0.46$	$-0.12 \pm 0.19$	0.75	78
	3.0 s	$-0.74 \pm 0.63$	$-0.22 \pm 0.27$	0.79	89

There are times when using a correlation, however, is not the best options. For sites where a soil amplification factor is found by some alternative means this value can be input by the user. This value is input by selecting “Specify amplification factor (site specific)”. The F value (amplification factor) can now be input into the program.

#### C.1.4 Using Other Loading File Types

In the basic analysis USGS 2008 deaggregation files were used in the analysis. There are several other options available for use in uploading deaggregation data. The file types supported by the program are the USGS 2002 and 2008 deaggregation text files and the EZFRISK text files. Other file types must be modified using the ‘Create Other Files’ hyperlink (Figure 0-39).

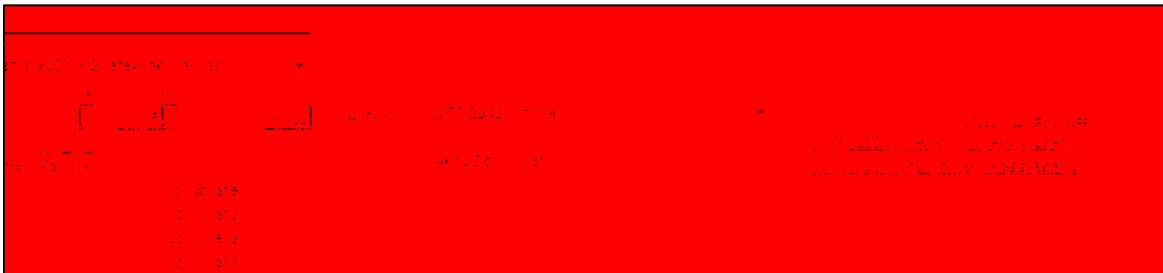


**Figure 0-39: Deaggregation data file uploading section a) buttons for uploading data (left of image) and b) file type selector drop box (right of image).**

An important factor to consider when uploading files is that the files should be of the original form and contain all of the data that is to be analyzed. It is also important for the user to ensure that the files are uploaded correctly and that they are uploaded for the correct site. To help the user ensure they upload correctly and to allow the user more ability to analyze the files, graphs are provided at the bottom of this page which will appear after all of the files have been uploaded and the GENERATE PLOTS AND DATA button pushed.

Occasionally it is desirable to use other return periods other than those specified by PB LiquefY. These return period can be used, but the program will note the discrepancy between the return period specified and the return period used. It is important that if a different return period set is used that the user ensures that the files are still uploaded in order of their return period (smallest to largest). To check that the files uploaded correctly and in the correct order, a good check is to ensure that the hazard curve graph shown below the GENERATE PLOTS AND DATA button is of the correct shape and the points are in the correct locations.

We will now look at uploading files of a type other than the types supported by PB LiquefY. Click on the hyperlink to the right of the file selection drop box which says ‘Create Other Files’. This will take you to the file creator page (Figure 0-40).

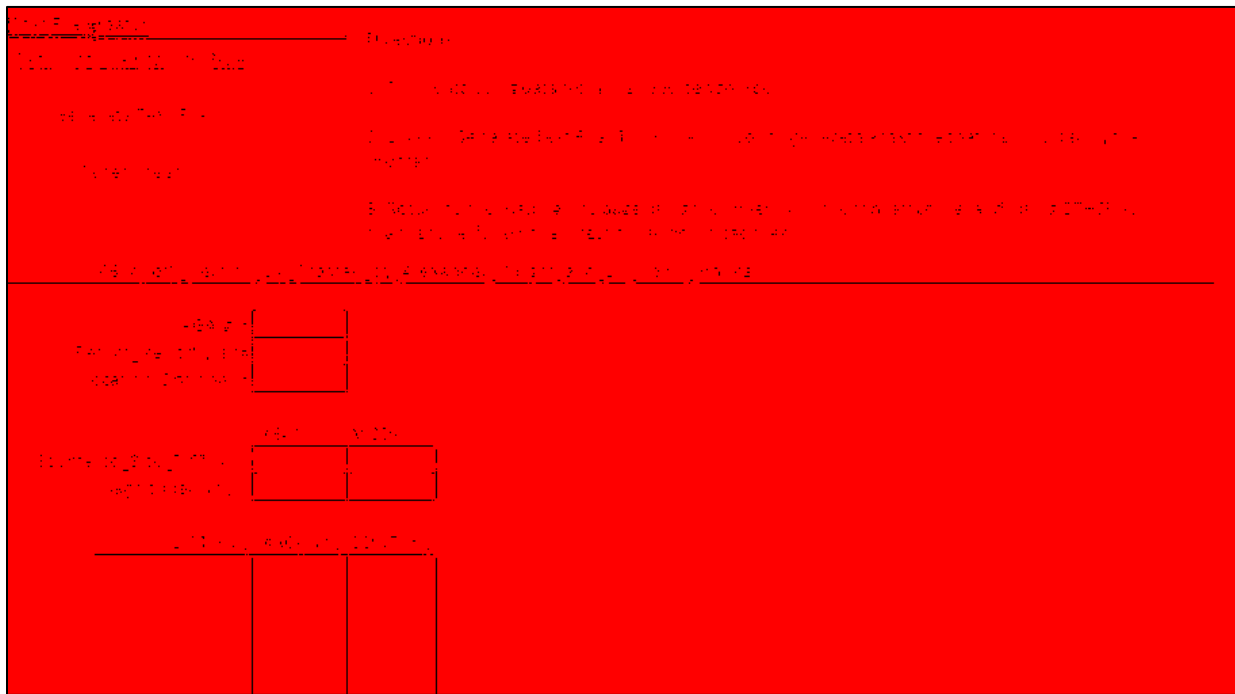


**Figure 0-40: File creator page.**

This page allows users to create text files which can be read by the program. Using the unsupported file type input data for PGA, Return Period, Location (optional), Source to site distance, magnitude, and the numbers corresponding to the deaggregation for distance (DIST), magnitude(MAG), and contribution (CONT.(%)). Contribution should be the numerical value corresponding to the percent contribution to the hazard, sometimes listed as epsilon. The values for contribution should add to be 100%. If unsure of correct values for input on this sheet, consult an expert in the field.

Once all of the values have been entered a file can be created by clicking GENERATE TEXT FILE. This will allow the user to save the file wherever they wish. Make sure to name the file something that will be easy to remember later such as MEXICO\_SITE\_1\_ReturnPeriod\_225. Repeat this process for all eight required return periods and return to the loading info page by clicking on the hyperlink at the top of the page titled 'Return to Loading Info Page'. Upload the newly created files as before, remembering to make sure that the 'File type:' says "Other". This will allow the program to correctly read and upload the files. Remember that the user should check that the files uploaded correctly by viewing the graphs and available data.

### **C.1.5 Using Performance-Based and Deterministic Advanced Options**

The performance-based and deterministic analysis described in the basic analysis section uses mostly default settings and does not give the user a good understanding of the capabilities of the program, or the ability to implement these capabilities. In order to better understand what these capabilities are, as well as to gain a fuller understanding of the limitations within which these capabilities operate, this portion of the tutorials will go through each of the options

available starting with the deterministic options, and then going through the performance-based options.

There are several options available for use within the deterministic settings of the program. These options can be accessed by opening the deterministic analysis page (Figure 0-41). Under the deterministic section of the page the user will see several options available. Click on the drop box next to “Analysis Type”. Under this drop box you will see three options. These options are: “Mean Magnitude – Specify Return Period”, “Modal Magnitude – Specify Return Period”, and “User Defined – Specify  $a_{max}$  and  $M_w$ ”. These three options were included to allow the engineer the flexibility to use either mean, modal pseudo probabilistic approaches; or a scenario based approach to liquefaction initiation analysis.

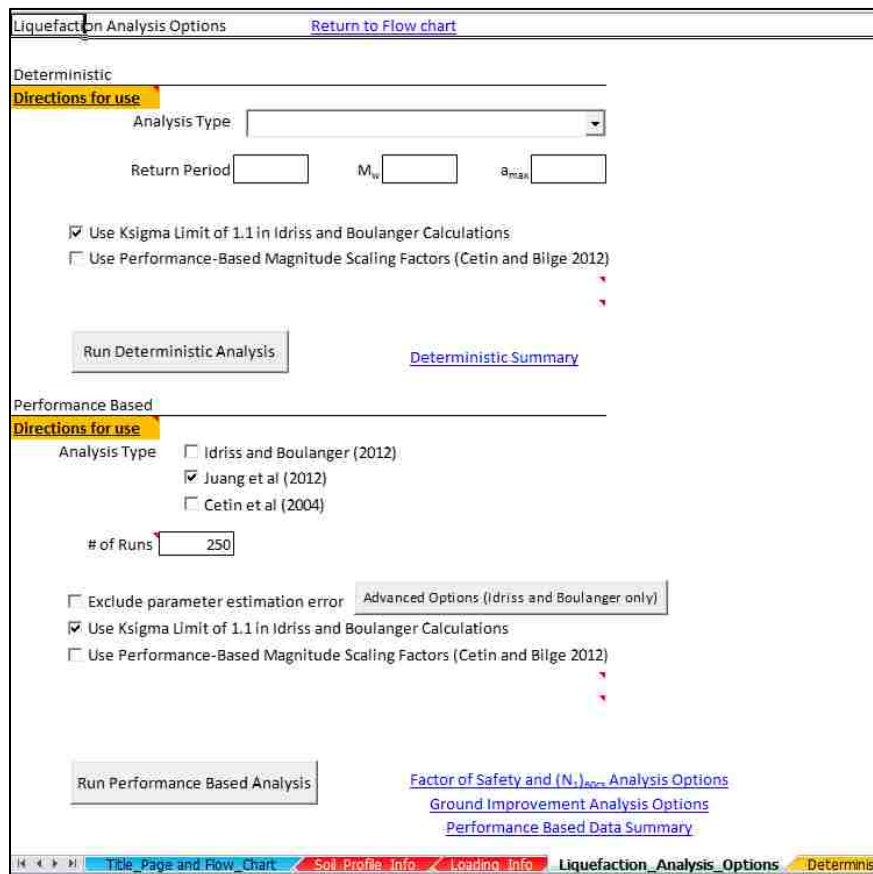


Figure 0-41: Deterministic and performance-based analysis options page.

Other options are also available for use with the deterministic approach. The first option shows that use of a limiting value of 1.1 for  $k_{\sigma}$ . This limiting value applies only to the Boulanger and Idriss approach. In Idriss and Boulanger (2010) the authors show that this limiting value can be excluded. Thus the user is given the option to include or exclude this value.

The second option available for deterministic analysis is to use performance-based magnitude scaling factors. These performance-based magnitude scaling factors were proposed by Cetin and Bilge (2012). These allow the engineer to specify the strain or pore water pressure ratio at which the site will liquefy. Common to most other analysis, which do not use a performance-based magnitude scaling factor, is the assumption that liquefaction will trigger at about 5% strain. The use of the performance-based magnitude scaling factors allows an engineer to change the definition used in the analysis to better meet the needs of the project and site. For further details about how to run a deterministic analysis please see the basic analysis tutorial.

The performance-based approach to liquefaction triggering is a relatively recent advance in the field of engineering. Kramer and Mayfield (2007) proposed a method whereby this type of analysis could be completed using the Cetin (2004) probabilistic approach in their analysis. They compared the Cetin (2004) approach to the NCEER approach and were able to show that for disparate sites, the use of the traditional deterministic method was not consistent from seismic region to seismic region in providing results of liquefaction triggering.

This program takes this one step further, and provides the user the ability to use both the Cetin et al (2004) model proposed by Kramer and Mayfield (2007), as well as allowing the use of the more recently proposed Juang et al (2012) and Boulanger and Idriss (2012) models within

a performance-based framework. Several options are also available for use in these analyses. These will be examined in the order they appear in the program.

The first option that is available to the user is the # of runs that the user wishes to use (Figure 0-42).

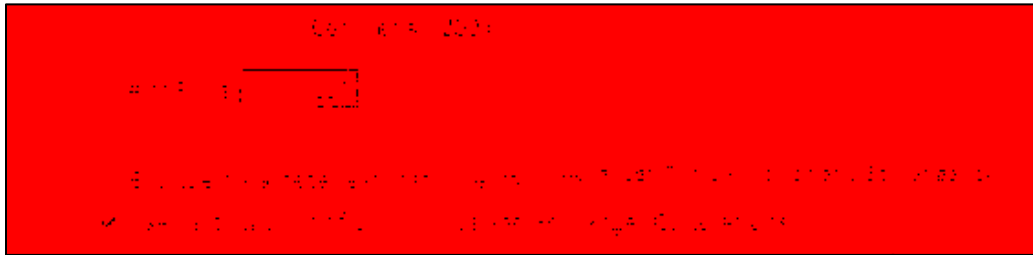


**Figure 0-42: Number of runs box.**

The number of runs specified by the user is essential. To determine the number of runs that need to be used on any given analysis the following equation is useful.

$$\Delta\lambda = \frac{(\lambda_{max} - \lambda_{min})}{n} \tag{83}$$

where  $\Delta\lambda$  is the increment of the probability of exceedance,  $\lambda_{max}$  is the largest mean annual rate of exceedance for the total hazard curve,  $\lambda_{min}$  is the minimum value of the mean annual rate of exceedance for the hazard curve, and  $n$  is the number of runs (Figure 0-43).

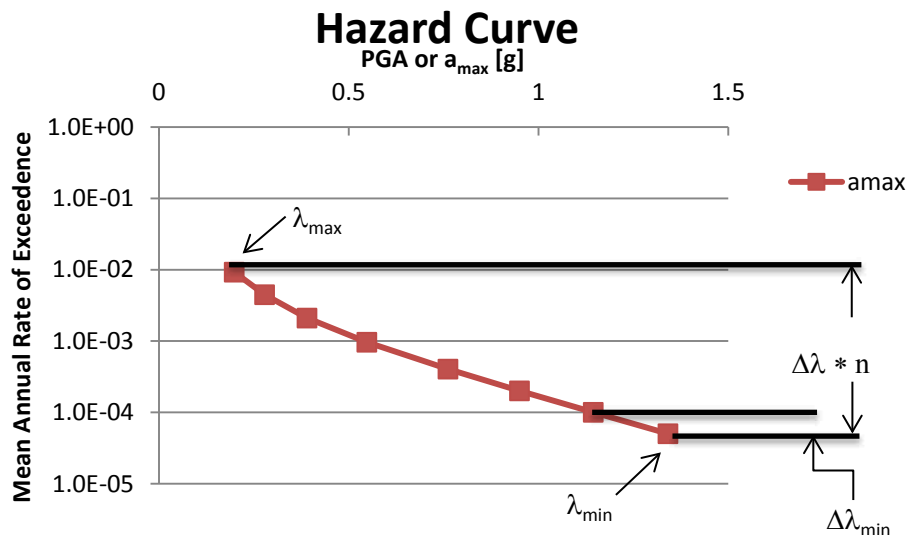


**Figure 0-43: Example hazard curve with variables for calculating n.**

If the value of  $\Delta\lambda$  is greater than the value of the difference between the smallest two probabilities of exceedance ( $\Delta\lambda_{min}$ ; see equation 84) then the results will be somewhat inaccurate unless the value of  $n$  is increased.

$$\text{if } \Delta\lambda \geq \Delta\lambda_{min} \text{ then the value of } n \text{ should be increased} \quad (84)$$

$$\Delta\lambda_{min} = \lambda_{min+1} - \lambda_{min} \quad (85)$$

However, it should be noted that an analysis run with a lower value of  $n$  will also run more quickly. The program imposes an absolute minimum of 30 for all cases, independent of any other variables. The program imposes no limit on the upper bound for  $n$ . In general a value of around 250 runs for most cases is sufficient to meet these requirements, and the default of the program is to use a value of 250 runs.

The next option available is to include or exclude parameter estimation error. If the user checks the box to exclude parameter estimation error, the program will run the selected probability models without including error due to measurements. However if this box is left unchecked the values will be run with the estimated  $\sigma_{tot}$  for parameter estimation error included (see Appendix A.).

In addition to the ability to include or exclude parameter estimation error, the program also includes the feature for advanced error estimation. Currently this feature is only available for the Boulanger and Idriss (2012) model. To enter the required values for advanced estimation error click on the button titled ADVANCED OPTIONS. An input box titled “Advanced Options” will appear (Figure 0-44).



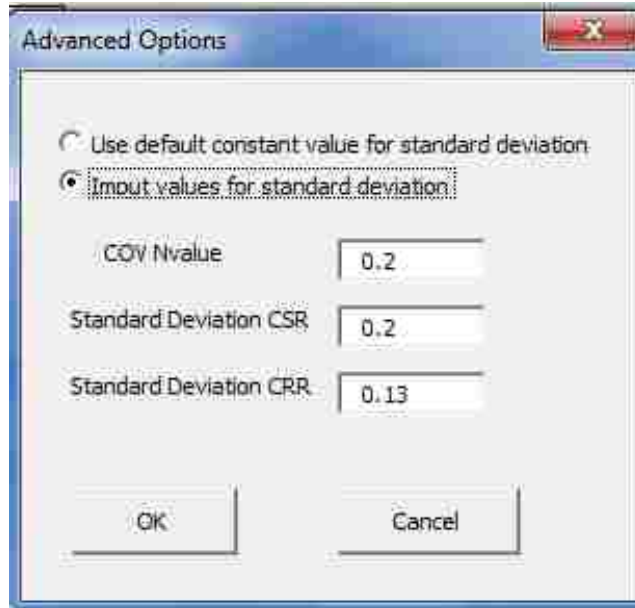


**Figure 0-44: Advanced Boulanger and Idriss (2012) error options input box.**

In this box you will see two options. The first option is “Use Default Constant value for Standard Deviation”. If this option is selected, the program will use default values for COV, CSR, and CRR (Table 0-5). However, if the user wishes to input values of COV, CSR, and CRR themselves this can be done by selecting “Input values for standard deviation”. A set of input boxes will appear and values can be input by hand.

**Table 0-5: Default values for Boulanger and Idriss (2012)  $\sigma_{tot}$  equation.**

	Default
COV	0.2
$\sigma_{CSR}$	0.2
$\sigma_{CRR}$	0.13

The next option available under the performance-based analysis concerns the use of the  $K_{\sigma}$  limit for the Boulanger and Idriss calculations. This option is similar to above, except that it will apply or remove the limit from both the Boulanger and Idriss (2012) calculations as well as the Juang et al (2012) calculations. This is done because the Juang et al (2012) calculations used the Boulanger and Idriss formulations for  $K_{\sigma}$  and other values in their analysis.

The last option available allows the user to apply performance-based magnitude scaling factors. This option is similar to what was discussed above, except that it will apply the performance-based magnitude scaling factors with a range of contributions. This will apply the mean and mean plus or minus one standard deviation in the analysis with the mean contributing 68% to the hazard, and the mean plus and minus one standard deviation contributing 16% each. This was done to represent the normal curve for the sample means such that the normal curve is divided into three parts with the central mean point collecting 68% of the contribution and the mean plus and mean minus one collecting the 16% contribution from each tail (Figure 0-45).

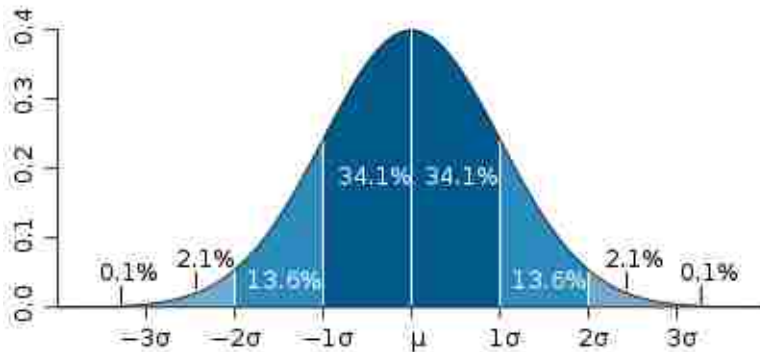


**Figure 0-45: Normal curve from Wikipedia.**

It should be noted that several assumptions are made for the different types of analysis. For a complete discussion of the different assumptions made with regards to the Juang, Boulanger and Idriss, and Cetin analysis, or with the performance-based analysis, please see the published version of the code.

### **C.1.6 Using Graphs**

The updating and use of graphs within PB LiquefY is relatively simple and strait forward. Graphs can be modified in one of two ways. They can be modified in the standard way that all

EXCEL© graphs are modified and changed, and they can be modified using the controls built into the program.

Most of the controls built into the program are self-explanatory and the use of the controls can be found through experimentation and use of the controls. Controls associated with graphs are usually found under the button associated with the creation of those graphs. For example the deterministic factor of safety vs. depth graph can be modified by using the controls under the GENERATE GRAPH AND FSliq button (Figure 0-46). By changing the options selected under the control, the graph will change. For example if we unselect Boulanger and Idriss Results and Youd results, the graph generated will only show the Cetin et al results.

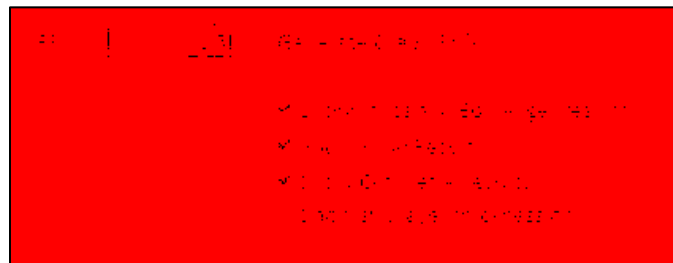


**Figure 0-46: Deterministic graph controls.**

The output line can also be changed by selecting ‘Show sub layer thickness on’. This will create a graph where points are created corresponding to the top and bottom of each layer, rather than the sample depth only. Other graphs throughout the program use a similar set of controls and can be modified in a similar way. The user is encouraged to experiment with the graph controls to become proficient in their use.

### C.1.7 Analysis Options for Factor of Safety and $(N_1)_{60cs}$ Required

There are two main analysis tools built into PB LiquefY. These tools allow the user to analyze soil profiles for liquefaction initiation by depth and by sub layer. Both options can be accessed through the flow chart link titled ‘FS<sub>liq</sub> and N<sub>req</sub> Analysis’.

#### C.1.7.1 Analysis by Return Period

The first set of options available at the top of the page allows the user control over the output analysis by return period (Figure 0-47). At the very top of the page the user will note that the ‘Target Factor of Safety:’ box is set in red to a value of 1.3. This value can be changed by the user and after the graphs are regenerated a new FS<sub>liq</sub> line will be drawn. It should be noted here that this target factor of safety does not directly affect the output data but will affect the appearance of the graph.

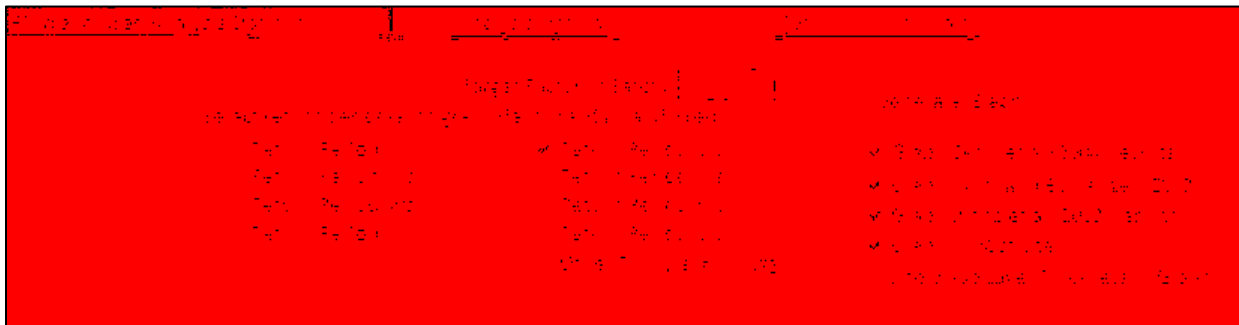


**Figure 0-47: Graphing and analysis options by return period.**

Below this in the section titled “Select return period(s)...” the user is given the option to select which return periods they wish to graph. This allows quick easy comparison of factors of safety and Nreq values. The last return period is titled ‘Other Tr in yrs. =’ and this option allows the user to input any return period for which they wish a value returned.

When analyzing the resulting graphs it is helpful to see an example. A graph of  $FS_{liq}$  vs. depth is shown in Figure 0-48. To prevent clutter only the Boulanger and Idriss (2012) and Juang et al (2012) lines are shown, however the Cetin et al (2012) analysis is also available to the user. In this graph it can be seen that for the layers with sample depths ranging from 8-18 m with a reference factor of safety of 1.3 that there is some hazard of liquefaction initiating.

Further understanding can be achieved through an examination of the  $(N_1)_{60cs}$  vs. depth graph (Figure 0-48). This graph shows the  $(N_1)_{60cs}$  values required to resist liquefaction, as well as the  $(N_1)_{60cs}$  values currently in-situ. This graph does not exclude non susceptible layers, unlike the  $FS_{liq}$  graph, and gives an engineer a better understanding of the existing conditions and the required conditions to resist liquefaction.

It should be noted here that different curves show up with different combinations. If graphing the  $(N_1)_{60cs}$  site and only graphing the Cetin et al (2004) results, only the corresponding  $(N_1)_{60cs}$  site curve for Cetin et al (2004) will show, and similar for Boulanger and Idriss and Juang analysis without Cetin. If no analysis are selected and the graph is created then the graph will only show the  $(N_1)_{60cs}$  site values for both types of analysis.

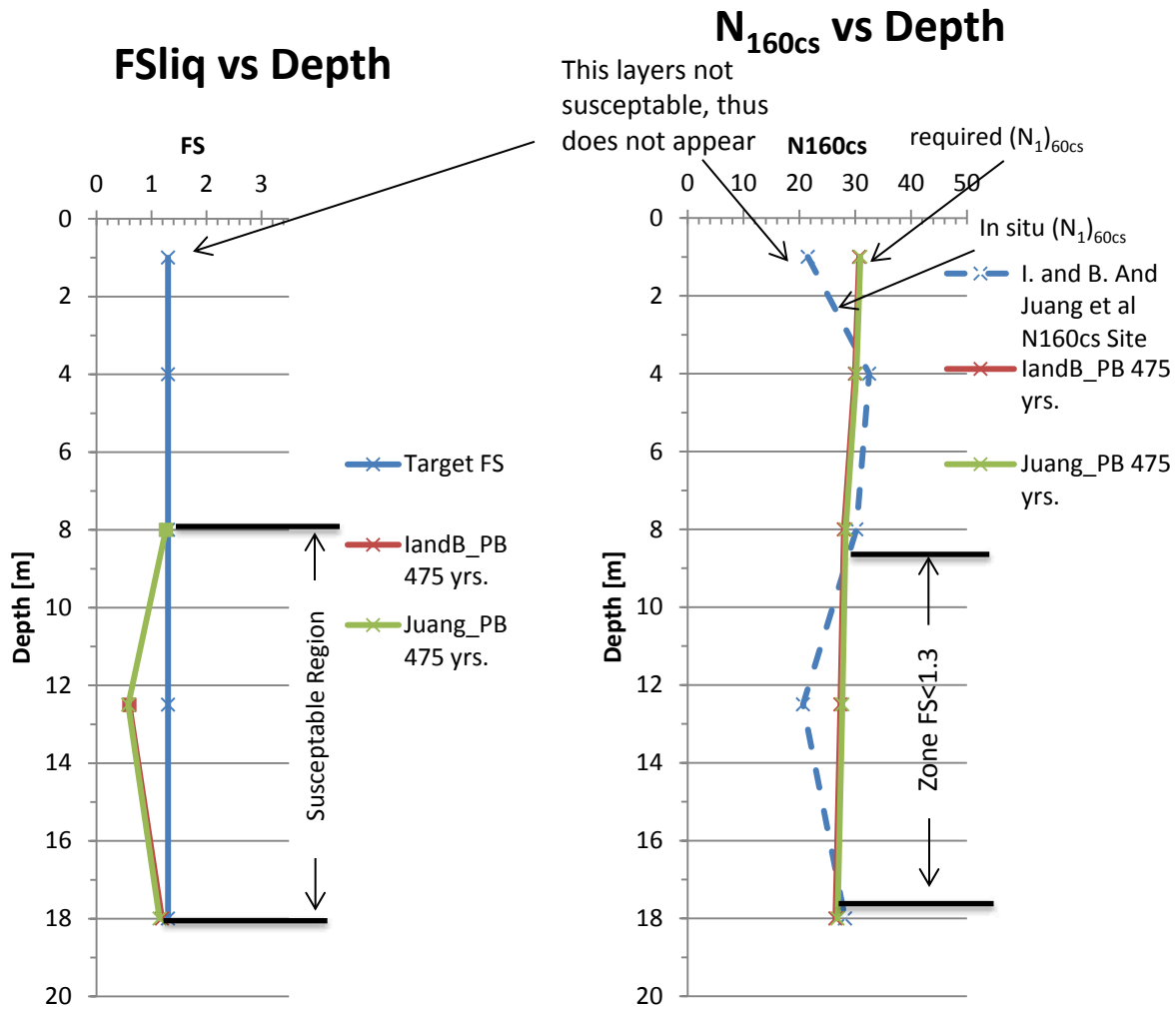


**Figure 0-48: FS<sub>liq</sub> vs. depth at a return period of 475 years (left); N<sub>req</sub> vs. Depth graph (right).**

### C.1.7.2 Analysis by Sub Layer

The analysis by sub layer can be accessed using the flow chart by clicking on the link titled “FSliq and Nreq Analysis”. This will take you to the same page as the analysis by return period. To access the analysis by layer, scroll down the page until you arrive at the ‘Sub – Layer Specific Analysis’ section (Figure 0-49).

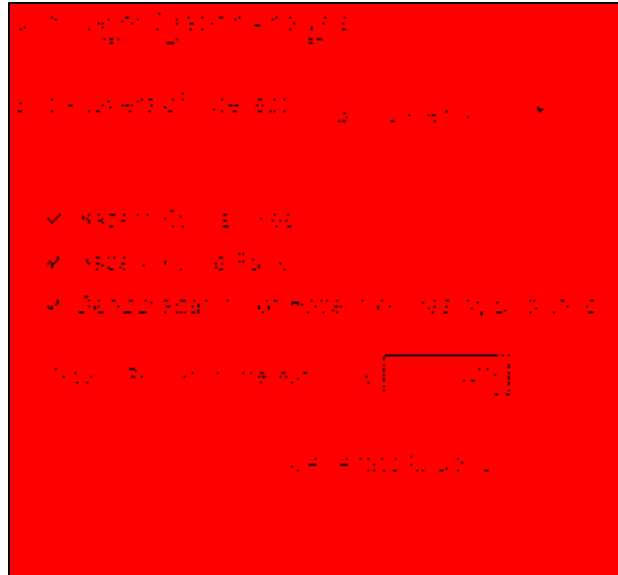


**Figure 0-49: Analysis by sub layer.**

This section provides the user with several different useful graphs including hazard curves for  $N_{req}$  and  $FS_{liq}$ , as well as deaggregations for each of the analyses run.

The first step in generating these graphs is to determine a sub layer that is of interest. For example, in the previous section we saw that sub layer four had the greatest need for improvement to prevent liquefaction. We may want to look at sub layer four in more detail. This sort of analysis is useful in that it allows the user to see how sensitive liquefaction initiation is to  $(N_1)_{60cs}$  of the site. First we will generate graphs for sub layer four, and then we will look at some of what those graphs can tell us. To generate graphs for sub layer four, select the sub layer from the drop box under the “Sub – Layer Specific Analysis” section. We also want all three types of graphs to be generated so ensure that all three option boxes are checked for “Hazard Curve Nreq”, “Hazard Curve FSliq”, and “Deaggregation of Hazard Curves by Sub Layer”. We must also enter a return period into the “Return Period of interest in yrs.” box in order to generate target lines and deaggregations. To generate the graphs select GENERATE GRAPHS.

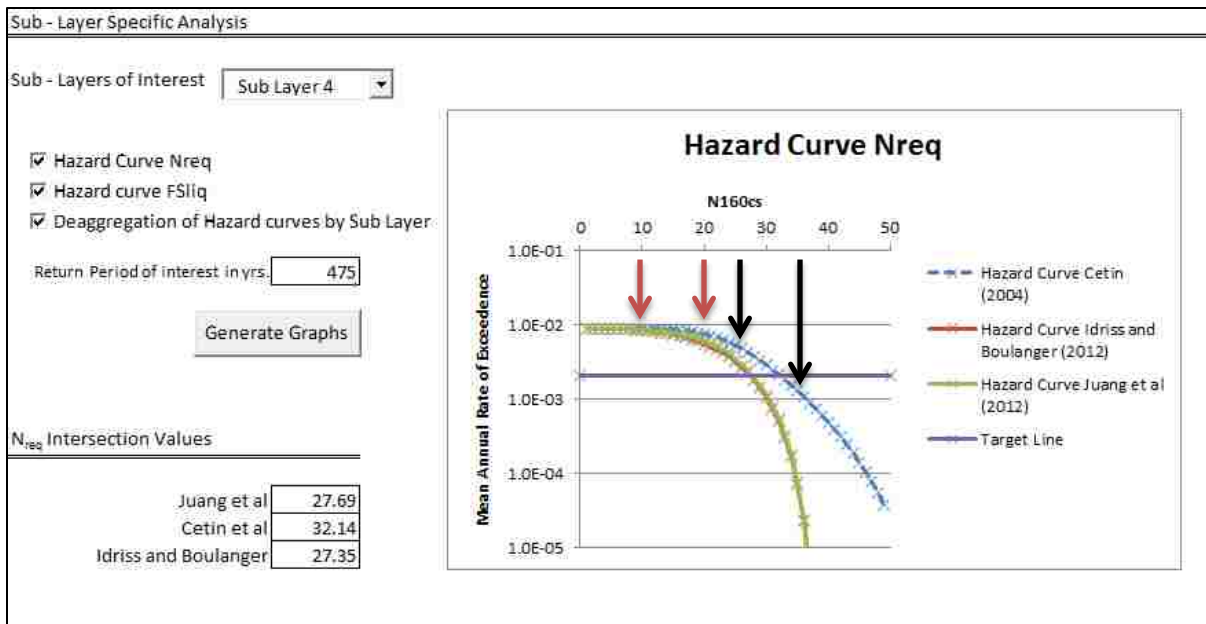


**Figure 0-50: Hazard curve for  $(N_1)_{60cs}$  required.**

The top graph which will appear is the  $N_{req}$  hazard curve (Figure 0-50). The purple line shows the target return period input by the user, in our case 475 years. To the left of the graph near the bottom left corner the user will see a set of values corresponding to the intersection of the target line and the hazard curves. In this case we see that the target line intersected the graph at an  $(N_1)_{60cs}$  value for Juang et al (2012) of about 28, for Cetin et al (2004) of about 32, and for Boulanger and Idriss (2012) of about 27.

This curve can be highly useful when deciding whether ground improvement will be used. If you look at the graph you will notice that if our ground is at a  $(N_1)_{60cs}$  value of about 10, and our improvement technique can increase it to about 20, then the mean annual rate of exceedance would not have changed almost at all. However, if we are at about 25 and can improve it to 35 a much larger difference in our mean annual rate of exceedance will occur. This can help the user in making decisions about what to do about liquefaction potential at a site.



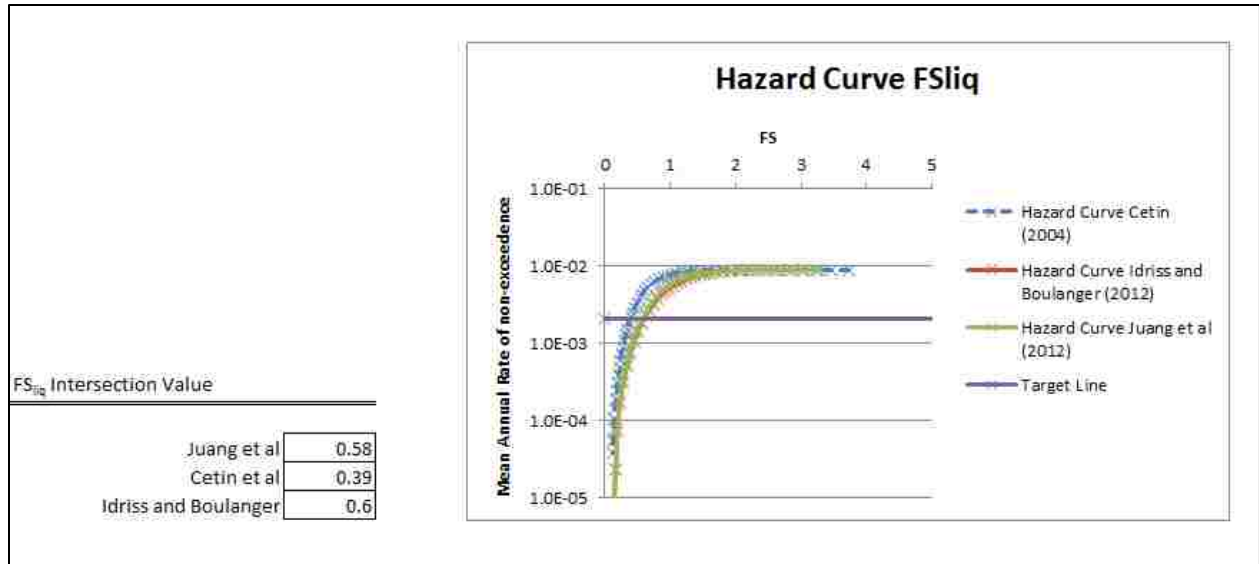


**Figure 0-51: Hazard curve for factor of safety.**

The next graph the user will see further down the screen is a graph of the factor of safety hazard curve (Figure 0-51). This graph can be used similar to the graph above, and will help the user determine what sorts of changes will occur and how much improvement can be achieved. Again, values for the intersection of the target line and the individual curves are shown in the bottom left hand corner with Juang et al (2012) having a value of about 0.6, Cetin et al (2004) having a value of about 0.4, and Boulanger and Idriss (2012) having a value of about 0.6.

The final graphs that can be seen in this part of the program are the deaggregation plots. These plots are located below the hazard curves and are deaggregations at the given return period for each of the analyses run (Figure 0-52).

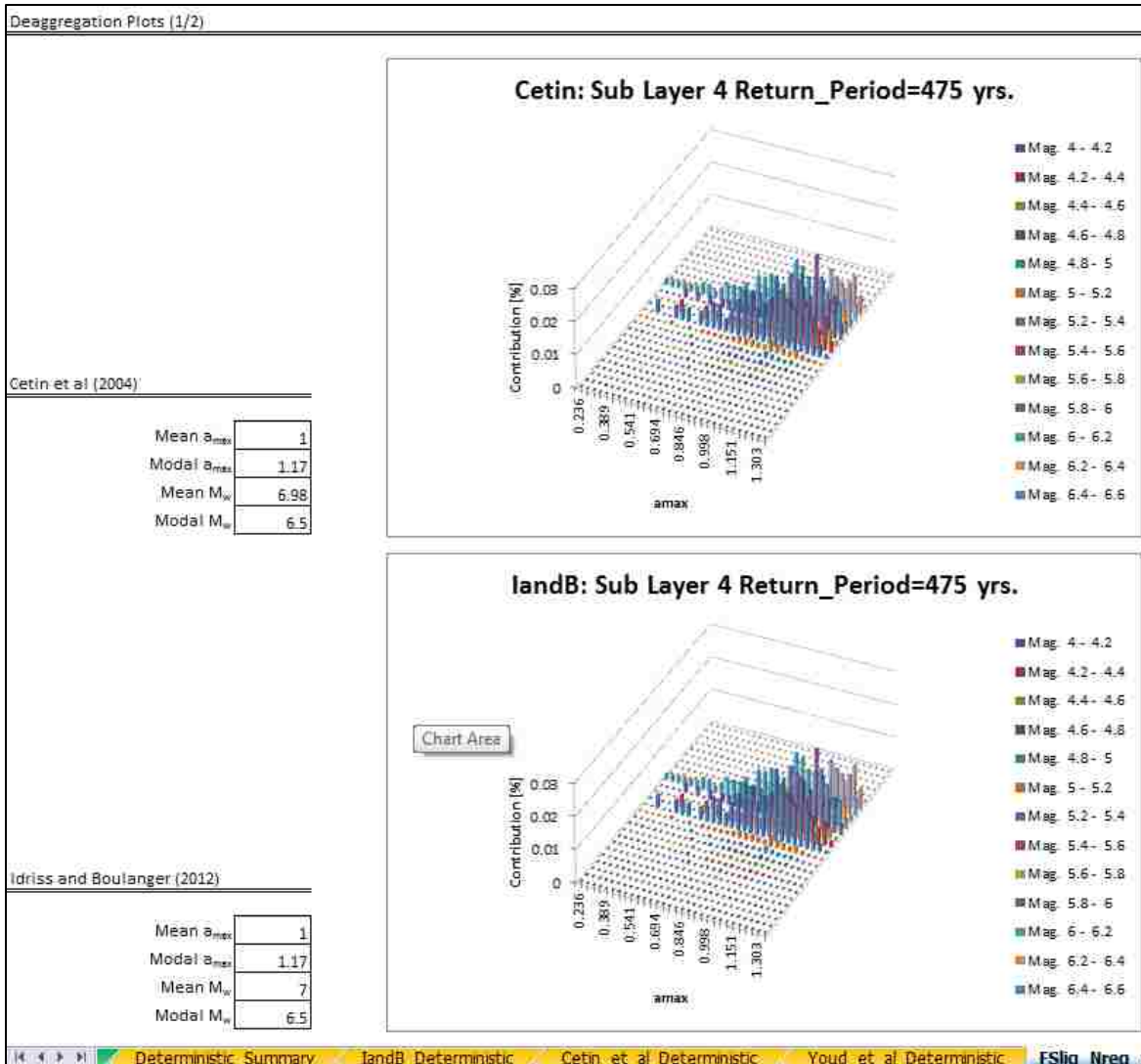


**Figure 0-52: Deaggregation plots for Cetin et al (2004) and Boulanger and Idriss (2012).**

These deaggregations show the contribution to the hazard curve for a given return period with acceleration on the x axis, magnitude on the y axis, and contribution on the z axis. From these graphs it is possible to see which hazards are contributing the most to the liquefaction hazard.

Located near the bottom left corner of each deaggregation are data values corresponding to that deaggregation and that return period. The program will generate values for the mean and modal acceleration ( $a_{max}$ ) and magnitude ( $M_w$ ) corresponding to the deaggregation they are near.

This page offers a comprehensive view of liquefaction initiation and as such enables the user to better understand the hazard. For further understanding of the needed ground improvement to achieve a factor of safety of 1.0 with regards to liquefaction triggering see the next section.

### **C.1.8 Analysis Options for Ground Improvement**

To assist the user in determining the ground improvement at a site for corresponding return periods a separate analysis was set up. Go to the flow chart and click on the ‘Ground Improvement Analysis’ hyperlink. This will take you to the ground improvement analysis page (Figure 0-53). On this page you will see a set of options similar to the options available on the previous analyses. There are two ways to use the options on this page. The two ways for the user to analyze the data: using return periods, and using pseudo return periods.

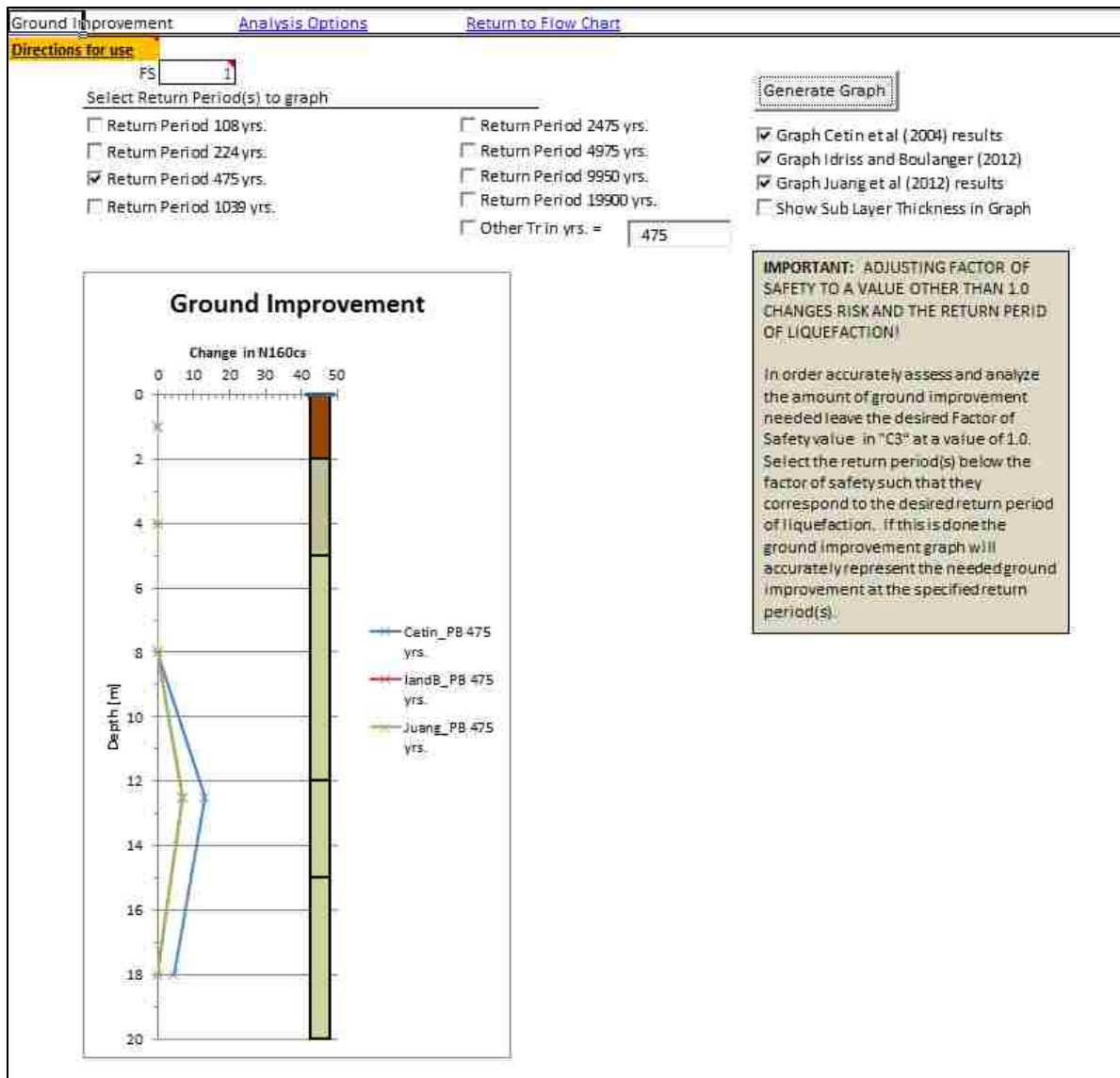
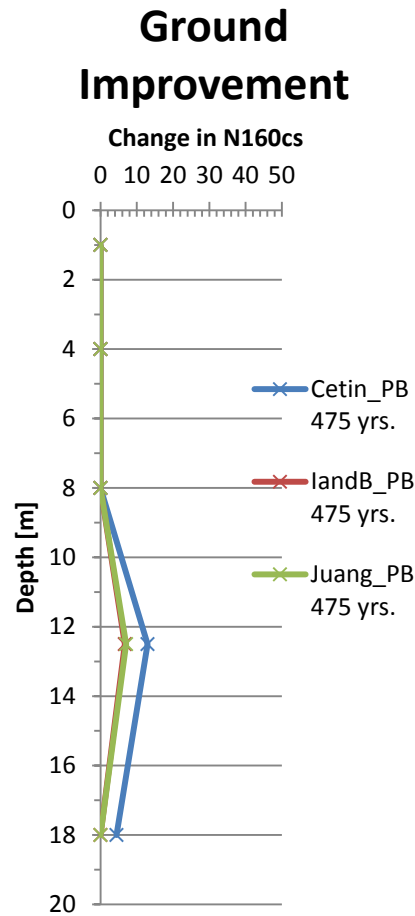


Figure 0-53: Ground improvement analysis page.

Using return periods for analysis is relatively straight forward and simple. Before beginning the user should ensure that the FS value at the top of the page is set to 1.0. This ensures that we are using return periods and not pseudo return periods. Then click on the return period of interest. In the example shown in Figure 0-54 a return period of 475 years was used. Other return periods can also be used either simultaneously or individually. The graphing

options work in a similar manner to the graphing options available in the previous analysis and more detailed instructions can be found in the ‘Analysis by Return Period’ section. Analysis by return period will yield a graph of needed improvement vs. depth (Figure 0-54).



**Figure 0-54: Ground improvement vs. depth in terms of  $\Delta(N_1)_{60cs}$ .**

The user will note that this graph is in terms of needed improvement based on a change in  $(N_1)_{60cs}$ . On this graph needed improvement begins at about 8 meters of depth and goes to 18 meters.

The second analysis option that is available on this page is the pseudo return period analysis. This method takes into account a factor of safety in the analysis. It is important to

note, however, that by changing the factor of safety from 1.0 to some other value, the user is in effect changing the return period of the results. A more correct method would be to change the desired return period instead to increase the return period of liquefaction.

The pseudo return period analysis allows the engineer to specify a factor of safety, for example 1.2, and see the needed ground improvement based on this factor of safety. To calculate the needed ground improvement at a given factor of safety for a Cetin et al (2004) analysis the equation first proposed by Mayfield, Kramer et al. (2010) is used.

$$FS^* = \exp\left(\frac{N_{site} - N_{req}}{13.79}\right) \quad (86)$$

This equation relates factor of safety (FS\*), the  $(N_1)_{60cs}$  value of the site ( $N_{site}$ ), and the required  $(N_1)_{60cs}$  value of the site calculated in the performance base analysis ( $N_{req}$ ).

$$\Delta N_{req} = N_{site} - N_{req} = 13.79 \ln(FS^*) \quad (87)$$

This equation is useful and allows the input of a value of factor of safety other than the value of 1 and a calculation of the change in the SPT blow count of the site to achieve the desired factor of safety at a given return period.

To calculate the ground improvement required from the Boulanger and Idriss (2012) and Juang et al (2012) analysis is a more complex process requiring iteration. In order to do so an equation relating factor of safety to  $N_{site}$  and  $N_{req}$  can be formed such that,

$$FS^* = \exp\left(\frac{N_{site} - N_{req}}{14.1} + \frac{N_{site}^2 - N_{req}^2}{126^2} - \frac{N_{site}^3 - N_{req}^3}{23.6^3} + \frac{N_{site}^4 - N_{req}^4}{25.4^4}\right) \quad (88)$$

Using this equation the  $N_{site}$  needed to achieve the given factor of safety can be found by iterating the formula using the value of  $N_{req}$  from the analysis and the FS specified by the user. The required N value to prevent liquefaction,  $N_{site}$ , will be found after multiple iterations.

An FS\* other than 1.0 should not be used in the ground improvement calculations. The use of an FS\* other than 1.0 results in unpredictable changes in the return period of the  $N_{req}$

value used. Rather than increasing FS\*, it is recommended that the engineer or researcher increase the return period used in the analysis instead. This will decrease the hazard and should increase the safety in a more predictable way.

Using these equations and methods the program determines the needed factor of safety. The preferred method is the return period method, due to its more precise nature and more technically sound implementation which lends itself to a more intuitive understanding of the return periods involved.

### **C.1.9 Using and Understanding the Performance-Based Summary Page**

The performance-based summary page allows the user a quick and easy view of all data and a collection of some of the graphs from previous pages. This page is set up to allow the user to both view and interact with the data selected on previous pages. To access this page select the 'Performance-Based Summary' hyperlink from the flow chart. This will take you to the performance-based summary page (Figure 0-55).

On this page is a summary of the graphs created on the other pages. The two graphs that will appear first are graphs of factor of safety vs. depth. The left graph shows the performance-based data only, while the right graph allows the user to modify the graph to show any combination of methods, and to compare the performance-based data to deterministic data. This is done using the controls located below the graph. One control which is unique to this page is the 'Graph Specified Return Periods Only' option. This option excludes the return periods specified on the other pages and only graphs the return periods visible on this page in the data table below the graphs.

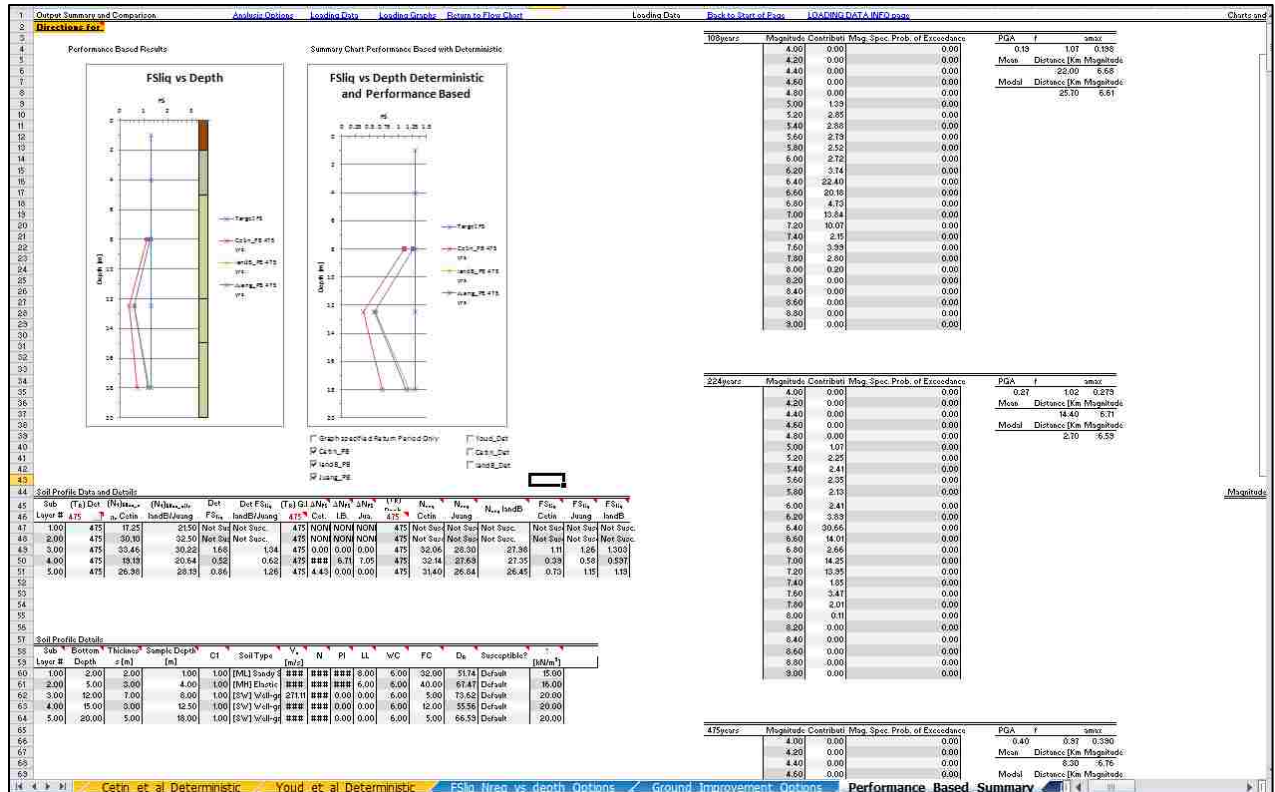


Figure 0-55: Performance-based summary page.

The data tables located below the graphs allow an interactive view of the results. The first table displays numerical results to the performance-based analysis, and will also display the results from the deterministic analysis if an analysis has been run. To change the data displayed in this table there are two options the user can use. The first is to go back to the previous tables and select a different set of options. The second and by far easier and more reliable way is to change the values for return periods shown in red. This enables the user to change the display to corresponding return periods. For example if the ground improvement return period is 475 (Figure 0-56) the data for ground improvement will correspond to this return period. We can change this by clicking on the cell and typing 500, which will result in a different set of data corresponding to this new return period.



Ground Improvement Return Period										Performance-Based Return Period							
Soil Profile Data and Details																	
Sub	(T <sub>s</sub> ) Det	(N <sub>1</sub> ) <sub>600,100</sub>	(N <sub>1</sub> ) <sub>600,100</sub>	Det FS <sub>liq</sub>	Det FS <sub>liq</sub>	G.I.	ΔN <sub>FE</sub>	ΔN <sub>FE</sub>	ΔN <sub>FE</sub>	(T <sub>s</sub> ) Prot	N <sub>req</sub>	N <sub>req</sub>	N <sub>req</sub> landB	FS <sub>liq</sub>	FS <sub>liq</sub>	FS <sub>liq</sub>	
Layer #	475	Cetin	landB/Juang	Cetin	landB/Juang	475	Cet.	I.B.	Jua.	475	Cetin	Juang	N <sub>req</sub> landB	Cetin	Juang	landB	
47	1.00	475	17.25	21.50	Not Susd	Not Susc.	475	NONE	NONE	NONE	475	Not Susc.	Not Susc.	Not Susc.	Not Susc.	Not Susc.	Not Susc.
48	2.00	475	30.10	32.50	Not Susd	Not Susc.	475	NONE	NONE	NONE	475	Not Susc.	Not Susc.	Not Susc.	Not Susc.	Not Susc.	Not Susc.
49	3.00	475	33.46	30.22	1.68	1.34	475	0.00	0.00	0.00	475	32.06	28.30	27.98	1.11	1.26	1.303
50	4.00	475	19.19	20.64	0.52	0.62	475	12.96	6.71	7.05	475	32.14	27.69	27.35	0.39	0.58	0.597
51	5.00	475	26.98	28.19	0.86	1.26	475	4.43	0.00	0.00	475	31.40	26.84	26.45	0.73	1.15	1.19

Figure 0-56: Summary data table.

To change the deterministic return period (also shown in red) it is necessary to click on the button to the right of this cell and fill out the requisite data in a similar fashion to the deterministic data approach shown previously. Keep in mind that this will rerun the deterministic data at the new values specified and will delete any previously run deterministic analyses. The data table located below this first data table is a copy of the data entered on the soil profile info page and is included for convenience.

Other data is also available on this page. To the right of the graphs mentioned above the numerical values for the magnitude contribution bins from the different return periods are included, and to the right of this are the magnitude specific hazard curves, and other graphs associated with the seismic data.

### C.1.10 PBliquefy – Theory, Assumptions, and Code

Most of the theory associated with this program is contained in the body of this project, however, some of the specific details were not discussed and for a detailed understanding of how the program works and what it is doing, the user of the program needs to understand the assumptions made in the writing of the program. These assumptions will be dealt with on a page by page basis in the order that the user would encounter them

### C.1.11 PBliquefY – Soils Profile Input Page

On the soils profile input page several assumptions must be made either for ease of calculation or for user convenience. Two locations where assumptions must be made are in the calculation of the shear wave velocity and the relative density.

In the calculation of the shear wave velocity using the Andrus and Stokoe, a value for the corrected SPT blow count is required. As the Andrus and Stokoe equation was derived from the same database as the NCEER procedure, the corrections applied by the NCEER workshop are used to find this value. Further modifications were made to the standard deviation (see Appendix A.)

A similar assumption is made in the calculation of the relative density. For this calculation a value for  $(N_1)_{60cs}$  is required. The relative densities seen on the main page are only approximations of the relative densities used in the program. On the main page the SPT blow count is corrected according to the NCEER procedure. However, in the body of the program the corrections are applied according to the procedure in which the relative density is being used. For example, in the case of the  $MSF_{PB}$  being used with the Idriss and Boulanger procedure, the corrected SPT blow count is found according to the Idriss and Boulanger procedure. The relative density equation used in the program is found using the form of the equation discussed by Idriss and Boulanger (2008) where,

$$D_R = 100 * \left( \frac{N_{160cs}}{C_d} \right)^{.5} \quad (89)$$

In this equation  $N_{160cs}$  is the corrected SPT blow count and  $C_d$  is a term that is input by the user. Typical values for  $C_d$  are shown in Table 0-6. This relationship can be overridden within the program, and user specified values used, simply by unselecting the auto calculation box and inputting values by hand.

**Table 0-6: Typical values of  $C_d$  from Idriss and Boulanger (2008).**

<b>Relationship</b>	<b><math>C_d</math> value</b>
Idriss and Boulanger (2010)	46
Meyerhof (1957)	41
Skempton (1986)	Recent fills - 40; natural deposits - 55
Cubrinovski and Ishihara (1999)	51

### **C.1.12 PBliquefY – Loading Data Input Page**

The loading information page also has some details and assumptions that are useful to understand in understanding how the program works. Several of these include the calculation of the amplification factor, binning, and how the program handles magnitude specific hazard curves that are not of the standard shape.

The amplification factor default is set to use Stewart et al. (2003) Quaternary alluvium values. This assumption was felt to be valid as other authors have used and recommended this value (Kramer and Mayfield 2007). It was also felt to be valid as most soils that engineers deal with, and on which liquefaction analysis will need to be conducted has been laid down recently on a geologic time scale and is well within the Quaternary time period, and is often in the late Holocene.

This is not the case in all places however, and there are some circumstance where the use of such a generalize relationship as the one proposed by Stewart et al (2003) is inappropriate. For these cases the other options associated with the selection of amplification factor are made available to the practicing engineer.

Engineers in practice use a variety of deaggregations and relationships. In order to accommodate as many practicing engineers as possible, and to enable the program to be used outside the continental United States where USGS deaggregations are not available, the program is set to be able to read two different file types, and has a file creator that enable users to create their own files from other data sources if necessary.

During the course of the creation of the program it was found that some deaggregations when broken down by magnitude did not follow the standard form of the hazard curve in shape. The program accounts for this by taking values at all point of intersection and adding together the cumulative contribution for a given probability of exceedance bin (Figure 0-57) from all values associated with that bin.

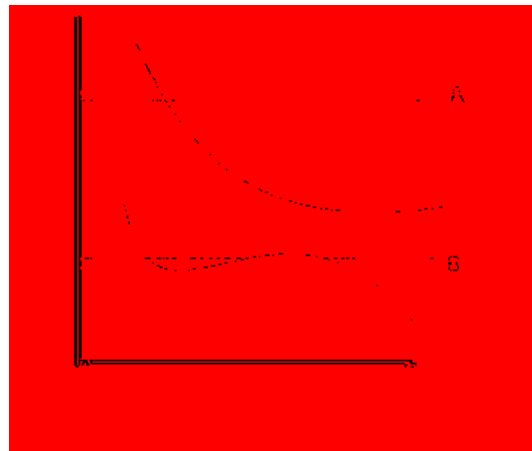


**Figure 0-57: Bin A intersects the line in one place as the line is of a normal form; Bin B intersects the line in three locations as the hazard curve is not of a normal form.**

Finally this page calculates and bins data by magnitude, creating a series of magnitude contribution charts, and deaggregation charts with the associated data. This is used later in the performance-based analysis of liquefaction initiation.

### **C.1.13 PBliquefY – Liquefaction Analysis Options Page**

There are two options available on the liquefaction analysis options page, and each of the options have several assumptions and a lot of theory behind them. For a detailed discussion of the theory behind the analysis the reader is referred to the body of the text.

The deterministic analysis options available allow the user to modify how the analysis is run. One of the available options allows the user to limit  $K_{\sigma}$  to the values given by Idriss and Boulanger (2010). However, Idriss and Boulanger have recognized that this is not always desirable, and there for the option is available to turn off this limit.

Another option available to the user is to use  $MSF_{PB}$  or not. For deterministic calculations only the median value from the Cetin and Bilge (2012) analysis are used. These values are used in the place of the values specified by the authors of the methods for MSF. For a more detailed understanding the reader is referred to the body of the text.

The performance-based options available to the user are similar to the deterministic options. The  $MSF_{PB}$  in the performance-based option is different from the deterministic approach as it will run the analysis using the low, median, and high values resulting from the variations in the  $m$  equations proposed by Cetin and Bilge (2012). Parameter estimation error can also be turned on and off. This allows the user to either include standard variation to the variation in parameter estimation, or to exclude this variation which runs the relationships with the parameter estimation error excluded, or in other words, the results only include epistemic uncertainty.

Boulanger and Idriss (2012) proposed a system to include standard deviation in the CRR, CSR, and N values. Their equation allows for the inclusion of these in the total standard deviation of their equations. The user can input values for these standard deviations for use in the Boulanger and Idriss equations using the advanced options available on this page. In the implementation of this equation it was found that using N values higher than about 30 resulted in the application of this equation resulting in incorrect values for  $FS_{liq}$ . This led to a limitation being applied to the N value such that N greater than 30 will be applied to this equation using an N value of 30.

#### **C.1.14 PBliquefY – $FS_{liq}$ and $N_{req}$ Analysis Options Page**

This page allows the user to view the results of the analysis. However, some understanding of the way it summarizes the results will help the user better understand what is available.

There are two sets of options included on this page. The top part of the page allows the user to view the FS and N values with depth. These values are obtained from the hazard curves developed during the analysis where available. However, if the return period specified by the user is outside the range of available data the program will return the last available value known from the curve. It will also inform the user that this has occurred, and for which analysis type and return period it was unable to find the data requested.

The second set of analysis options allows the user to view the data on a sub layer by sub layer basis. This allows the user to see the hazard curves, and deaggregations associated with that layer. Again, where the data is unavailable, the program uses the last available data point and informs the user which analysis this occurred for.

The deaggregations available at the bottom of this portion of the page inform the user of the way in which the hazard has been influenced by acceleration and magnitude. The deaggregations are created using the values obtained during the analysis. Also available in this section are the mean and modal  $a_{\max}$  and  $m_w$  which contributed to the hazard for each analysis type.